Gravitational Thermodynamics: From Black Holes to Holography

by

Fil Simovic

A thesis
presented to the University of Waterloo
in fulfilment of the
thesis requirement for the degree of
Doctor of Philosophy
in
Physics

Waterloo, Ontario, Canada, 2021

Examining Committee Membership

The following served on the Examining Committee for this thesis. The decision of the Examining Committee is by majority vote.

External Examiner:	Valeri P. Frolov Professor, University of Alberta
Supervisors:	Laurent Freidel Faculty Member, Perimeter Institute for Theoretical Physics
	Robert B. Mann Professor, University of Waterloo
Internal Members:	Richard J. Epp Instructor, University of Waterloo
	Niayesh Afshordi Associate Professor, University of Waterloo
Internal-External Member:	Florian Girelli Associate Professor, University of Waterloo

Author's Declaration

This thesis consists of material all of which I authored or co-authored: see Statement of Contributions included in the thesis. This is a true copy of the thesis, including any required final revisions, as accepted by my examiners

I understand that my thesis may be made electronically available to the public.

Statement of Contributions

This thesis is based on the following publications and forthcoming articles. I (Fil Simovic) was the primary researcher, sole author, and primary editor in all cases except those indicated with an asterisk (*) below. My co-authors provided guidance during the research and provided feedback on draft manuscripts.

Chapter 2 is based on:

Fil Simovic and Robert B. Mann, *Critical Phenomena of Charged de Sitter Black Holes in Cavities*, Classical and Quantum Gravity 36, 014002 (2019)
DOI: 10.1088/1361-6382/aaf445, arXiv:1807.11875

Chapter 3 is based on:

Fil Simovic and Robert B. Mann, *Critical Phenomena of Born-Infeld-de Sitter Black Holes in Cavities*, Journal of High Energy Physics 2019, 136 (2019)
DOI: 10.1007/JHEP05(2019)136, arXiv:1904.04871

Chapter 4 is based on:

Fil Simovic, Danny Fusco, and Robert B. Mann, *Thermodynamics of de Sitter black holes with conformally coupled scalar fields*, Journal of High Energy Physics 2021, 219 (2021)
DOI: 10.1007/JHEP02(2021)219, arXiv:2008.07593

Chapter 5 is based on:

Sumarna Haroon, Robie A. Hennigar, Robert B. Mann, and **Fil Simovic**, *Thermodynamics of Gauss-Bonnet-de Sitter Black Holes*, Physical Review D 101, 084051 (2020)
DOI: 10.1103/PhysRevD.101.084051, arXiv:2002.01567

**Section 5.1 of this thesis is adapted from Section 2 of the article above, to which Robie Hennigar provided a large written contribution.*

Chapter 6 and 7 are based on:

Fil Simovic, *Gravitational Screens*, Forthcoming.

Abstract

The subject of gravitational thermodynamics lies at the center of numerous fields of study, many of which may seem disconnected, yet have proven to be deeply entwined. This thesis examines two primary facets of this subject, the study of black hole thermodynamics, and the principle of bulk/boundary duality (or 'holography') as applied to gravitating systems.

In Part I of this thesis we explore thermodynamic aspects of a wide variety of black hole spacetimes. We focus on asymptotically de Sitter black holes, in an extended phase space where the cosmological constant is interpreted as a thermodynamic pressure. We begin with the prototypical classes, examining general relativistic Schwarzschild- and Reissner-Nordström-de Sitter black holes. We demonstrate the consistent formulation of their thermodynamics in the extended phase space using a Euclidean path integral approach, and uncover novel compact small-large black hole transitions not seen in asymptotically AdS spacetimes. We also consider a number of extensions of Einstein-Maxwell theory: Born-Infeld electrodynamics, conformally coupled scalar fields, and Gauss-Bonnet gravity. We study the thermodynamic properties and phase structure of black hole solutions in these theories, uncovering (among other things) a unique reentrant phase transition in the grand canonical ensemble, compact reentrant phase transitions, and isolated critical points. We also examine the analogy these systems make with ordinary fluid systems, showing that in contrast to asymptotically anti-de Sitter black holes, de Sitter black holes have nonlinear equations of state which forbid such an interpretation.

Part II of this thesis represents an attempt to understand the thermodynamic nature of gravity from a broader perspective. Here, we take a 'holographic' approach, promoting the gravitational screen formalism to a fully covariant mapping between bulk geometric quantities and those of a relativistic dissipative fluid system on the (arbitrary, timelike) boundary. We demonstrate the projection of the field equations onto the screen boundary, derive the corresponding fluid conservation equations, and explicitly construct the dictionary relating the two systems. We show how entropy production in the fluid is tied to gravitational wave propagation in the bulk, and discuss the role of the equation of state of the fluid in the correspondence. Finally, we explicitly construct several gravitational screens in spherically symmetric spacetimes. We determine the properties of the resulting holographic fluids, and use thermodynamical laws governing the fluid to assign a notion of temperature and entropy to the bulk geometry.

Acknowledgements

Thank you to my supervisors Laurent Freidel and Robert B. Mann, who have dramatically shaped my understanding of physics and the universe over the course of my degree (and even well before that). I will always be grateful for the inspiration, opportunities, and support that you have given me over the years.

Thank you to my friends, who whether near or far are always in my mind and memory. Alexander Smith, Hilary Snyder, Jack Davis, Flaminia Giacomini, Davide Racco, Adam Lewis, Robie Hennigar, Laura Henderson, Erickson Tjoa, Paul McGrath, Jake Dyck, Fiona McCarthy, Natacha Altamirano, and many others: you have all made me laugh, inspired me, and taught me something new.

Thank you to my brother Aleksandar and parents Ljiljana and Milorad, who have given immeasurable support throughout my life, always encouraged me to pursue my dreams, and have provided me a home like no other.

Thank you to my rock and my other half, Kathryn Miller. My world has been a far bigger and more wonderful place with you in it.

Dedication

To my parents, Ljiljana and Milorad. Without you, the endless wonder that is life and the universe would forever remain a mystery to me.

Table of Contents

List of Figures xi

Notation and Conventions xvi

The Structure of this Thesis xvii

Part I Black Hole Thermodynamics 1

Introduction 2

1 Aspects of General Relativity and Black Hole Thermodynamics 6
- 1.1 Manifolds, Metrics, and Curvature . . . 7
- 1.2 Einstein's Equations and the Action Principle . . . 9
- 1.3 Path Integrals . . . 12
- 1.4 Black Hole Thermodynamics . . . 14
  - 1.4.1 The First Law . . . 15
  - 1.4.2 Hawking Radiation and Black Hole Temperature . . . 19
  - 1.4.3 The Hawking-Page Transition . . . 23
  - 1.4.4 The Extended Phase Space and Variable Λ . . . 26
- 1.5 de Sitter and its Problems . . . 29

2 De Sitter Black Holes in Cavities 33
- 2.1 Thermodynamics of Black Holes in a Cavity . . . 34
- 2.2 Evaluating the Euclidean Action . . . 35
- 2.3 Thermodynamic Quantities and the First Law . . . 38
- 2.4 Schwarzschild-de Sitter Black Holes . . . 40
  - 2.4.1 The First Law . . . 42
  - 2.4.2 Helmholtz Free Energy and Phase Transitions . . . 44
- 2.5 Reissner-Nordström-de Sitter Black Holes . . . 45
  - 2.5.1 The First Law . . . 46
  - 2.5.2 Helmholtz Free Energy and Phase Transitions . . . 47
- 2.6 Summary . . . 50

3 Born-Infeld-de Sitter Black Holes 52
- 3.1 Thermodynamic Quantities and the First Law . . . 54
- 3.2 Born-Infeld-de Sitter Black Holes . . . 55

3.2.1 The First Law . . . 57
3.2.2 Vacuum Polarization and Metric . . . 58
3.2.3 Helmholtz Free Energy and Phase Transitions . . . 60
3.3 Free Energy at Fixed Potential . . . 64
3.3.1 Maxwell Theory . . . 64
3.3.2 Born-Infeld Theory . . . 65
3.4 Summary . . . 67

4 Black Holes with Scalar Fields **68**
4.1 Scalars in Gravitational Theories . . . 70
4.2 Self-Interacting Scalar Fields . . . 71
4.3 Evaluating the Euclidean Action . . . 73
4.4 Thermodynamics and Phase Structure . . . 75
4.4.1 The First Law . . . 75
4.4.2 Equilibrium Temperature . . . 76
4.4.3 MTZ Black Holes ($\xi = 0$) . . . 78
4.4.4 AC Black Holes ($\xi \neq 0$) . . . 79
4.5 Summary . . . 81

5 Gauss-Bonnet-de Sitter Black Holes **83**
5.1 Gauss-Bonnet Gravity . . . 84
5.1.1 Evaluating the Euclidean Action . . . 86
5.2 Uncharged Gauss-Bonnet Black Holes . . . 89
5.2.1 The First Law . . . 91
5.2.2 5 Dimensional Black Holes . . . 92
5.2.3 6+ Dimensional Black Holes . . . 95
5.3 Charged Gauss-Bonnet Black Holes . . . 96
5.3.1 The First Law . . . 97
5.3.2 Phase Structure . . . 98
5.4 Summary . . . 101

Part II Beyond Black Holes **103**

Introduction **104**

6 Gravitational Screens **107**
6.1 Gravity . . . 107
6.1.1 Screen Energy-Momentum . . . 110
6.1.2 Conservation of Energy . . . 111
6.1.3 Conservation of Momentum . . . 112
6.1.4 The Radial Constraint . . . 113
6.2 Relativistic Hydrodynamics . . . 114
6.2.1 Thermodynamical Laws . . . 116
6.2.2 Perfect Fluids . . . 118

6.2.3 Non-Perfect Fluids . . . 119
6.3 The Dictionary . . . 122
6.4 Summary . . . 124

7 Using the Dictionary **126**
7.1 Equations of State . . . 126
7.2 Entropy Production . . . 127
7.3 Static, Spherically Symmetric Screens . . . 129
7.3.1 Static Screens in Minkowski Space . . . 130
7.3.2 Accelerating Screens in Minkowski Space . . . 135
7.3.3 Schwarzschild Screens . . . 136
7.4 Summary . . . 140

Epilogue **143**

Letters of Copyright Permission **149**

References **151**

APPENDICES **169**
Appendix A - The Reduced Action . . . 169
Appendix B - Replacing Spacetime with Screens . . . 173

List of Figures

1.1 Penrose diagram of collapsing matter forming a black hole. **Left:** A classical black hole which forms through collapse but does not evaporate. Red and blue dashed lines represent (respectively) past and future Cauchy surfaces on which mode functions can be constructed. **Right:** A semi-classical black hole, which forms and later evaporates. The orange arrow represents the evaporation event, which appears instantaneous due to the conformal transformation. 21

1.2 The free energy F of the Schwarzschild black hole, demonstrating the presence of a Hawking-Page transition. **Left:** F as a function of temperature T. When $T < T_c$, empty space is thermodynamically preferred. When $T > T_c$, the large black hole phase minimizes F instead. **Right:** F as a function of horizon radius r_h. The free energy (and thus the action) changes sign when the black hole becomes large enough. 25

1.3 Representations of de Sitter space dS_d. **Left:** The hyperboloid defined by (1.86) embedded in $\mathcal{M}^{1,d}$ with $(d-1)$ coordinates suppressed. Static coordinates only cover the shaded region inside the de Sitter horizon (represented by the curved lines). **Right:** Penrose diagram of dS_d. Points in the interior are S^{d-2}, with future (past) timelike infinity represented by $\mathcal{I}_+$ ($\mathcal{I}_-$). The yellow region $\mathcal{O}^+$ represents the causal future of an observer sitting at the north pole, while their causal past $\mathcal{O}^-$ is represented by the blue region. . . 30

2.1 Regions of positivity (blue) for thermodynamic potentials associated with the Schwarzschild-de Sitter black hole as a function of $x = r_h/r_c$ and Λ, with fixed $r_c = \sqrt{3}$. **Left:** The thermodynamic volume V. **Right:** The surface tension λ. 43

2.2 Helmholtz free energy of the Schwarzschild-de Sitter black hole. **Left:** $F(T)$ for fixed cavity size ($r_c = 1$) and varying pressure. **Right:** $F(T)$ for fixed pressure ($P = -0.1$) and varying cavity size. The critical temperature T_c is indicated with a red dot. 44

2.3 Helmholtz free energy of the Schwarzschild-de Sitter black hole as a function of temperature and pressure for fixed cavity radius ($r_c = 0.5$). The $F = 0$ plane is indicated in blue. Hawking-Page transitions occur along the line of intersection. 45

2.4 Regions of positivity (colored) for thermodynamic potentials associated with the Reissner-Nordström-de Sitter black hole as a function of $x = r_h/r_c$ and Λ, with fixed cavity radius $r_c = \sqrt{3}$. **Left:** The thermodynamic volume V. **Right:** The surface tension λ. 47
2.5 Helmholtz free energy of the Reissner-Nordström-de Sitter black hole as a function of temperature. **Left:** Various pressures ($P = -0.08, -0.07, -0.01$) with fixed charge ($q = 0.08$) and cavity size ($r_c = 1$), showing clearly the formation of a swallowtail below the critical pressure, in this case $P_c \approx -0.82$. **Right:** Various cavity sizes ($r_c = 0.6, 0.8, 0.9$) with fixed charge charge ($q = 0.08$) and pressure ($P = -0.08$). The red dots indicate the location of the small-to-large black hole phase transition. 48
2.6 Helmholtz free energy of the Reissner-Nordström-de Sitter black hole as a function of temperature and pressure for fixed charge ($q = 0.08$), showing slices of constant pressure, and demonstrating the compact nature of the phase transition. 49
2.7 **Left:** Coexistence line for the charged dS black hole, along which the small and large black hole phases coexist. The line terminates at two ends where a second order phase transition occurs, indicated by a black dot. **Right:** Coexistence line for the charged AdS black hole. 50

3.1 Regions of positivity (colored) for the thermodynamic volume V as a function of $x = r_h/r_c$ and Λ, with fixed cavity radius $r_c = \sqrt{3}$. **Left:** Varying charge with $b = 0.1$. **Right:** Varying b with $q = 0.5$. 58
3.2 Regions of positivity for the surface tension λ as a function of x and Λ with fixed cavity radius $r_c = \sqrt{3}$. Shaded regions indicate positivity, where λ should be regarded as a surface pressure. **Left:** Varying charge with $b = 0.1$. **Right:** Varying b with $q = 0.7$. 59
3.3 The metric function $f(r)$ as a function of r for $q = 0.1$, $\Lambda = 1$, and $r_c = 0.6$; the cavity radius is indicated by the red dashed line. **Left:** Fixed vacuum polarization ($b = 10.22$) and varying mass parameter m. **Right:** Fixed mass ($m = 0.18$) and varying b. In both figures the marginal case appears in green. 59
3.4 Behaviour of the vacuum polarization for $q = 0.1$, $\Lambda = 1$, and $r_c = 0.6$; the cavity radius is indicated by the red dashed line. **Left:** $\mathcal{B}$ as a function of $x \equiv r_f/r_c$ for various b. The red dots indicate the marginal mass along each line. **Right:** $\mathcal{B}$ as a function of b for fixed $T = 0.5$ ($\mathcal{B} - b$ isotherms), with two branches. 60
3.5 Helmholtz free energy of the Born-Infeld-de Sitter black hole for fixed cavity size ($r_c = 0.6$), pressure ($P = -0.0025$), and charge ($q = 0.1$). **Left:** $b = 4$. **Right:** $b = 4.42$. 61
3.6 Helmholtz free energy of the Born-Infeld-de Sitter black hole for fixed cavity size ($r_c = 0.6$), pressure ($P = -0.0025$), and charge ($q = 0.1$). On the left we have $b = 4.57565$ and on the right $b = 4.65$. The red dashed lines mark the temperature at which phase transitions occur. 62

3.7 Helmholtz free energy of the Born-Infeld-de Sitter black hole for $q = 0.105$, $r_c = 0.6$, showing slices of fixed P. The red dots mark the small→large phase transition on each slice. The red line is the coexistence curve. **Left:** $b = 4.6$. A reentrant phase transition is present on the slices indicated with the black arrows. These slices resemble the left of Figure 3.6. The remaining slices resemble the right of Figure 3.6. **Right:** $b = 5$. There are no reentrant phase transitions present. Note the difference in small-T behaviour between the two figures: on the left, there is a minimum temperature at which the black hole phase exists, while on the right there is no minimum temperature (the lines extend to $T = 0$). 63
3.8 Free energy at fixed potential, with $r_c = 1.5$, $\Lambda = 0.001$. The temperatures at which phase transitions occur are indicated by the red dashed lines. The cavity radius r_c is indicated by a red dot. **Left:** The Reissner-Nordström-de Sitter black hole, with varying ϕ. **Right:** The Born-Infeld-de Sitter black hole with $b = 10$ for $\phi = 0.141$. 65
3.9 Free energy of the Born-Infeld-de Sitter black hole at fixed potential. The three lines overlap where they merge together in both figures. **Left:** $b = 0.5$, $r_c = 1.5$, and varying ϕ. The temperatures at which phase transitions occur are indicated by the red dashed lines. The cavity radius r_c is indicated by a red dot. **Right:** Fixed $\phi = 0.095$, $r_c = 1.5$, and varying b. 66

4.1 Equilibrium temperature T as a function of $x = r_+/r_c$ for fixed cavity radius $r_c = 2$, showing regions where r_h is multivalued at fixed temperature, signalling a possible phase transition. **Left:** Varying pressure Λ with $\xi = 0$. **Right:** Varying pressure Λ with $\xi = 0.2$. 77
4.2 Free energy of the MTZ ($\xi = 0$) black hole in the canonical ensemble, with varying Λ. The black $F = 0$ line corresponds to the radiation phase. Red dots mark the critical temperature at which the black hole begins to dominate the thermal ensemble and a first-order Hawking-Page-like phase transition occurs. 79
4.3 Free energy of the AC ($\xi \neq 0$) black hole in the canonical ensemble, with varying Λ. The black $F = 0$ line corresponds to the radiation phase. Red dots mark the critical temperature at which the black hole begins to dominate the thermal ensemble and a first-order Hawking-Page-like phase transition occurs. 80
4.4 Free energy F as a function of temperature T for fixed cavity radius $r_c = 2$ and varying ξ. For each curve, a Hawking-Page-like transition occurs at the critical temperature marked by a red point. **Left:** $\xi > 0$. **Right:** $\xi < 0$. Along the dashed portions of each curve, a naked singularity is present. The colored point on each curve indicates that equality in (4.28) has been reached. 81

5.1 Thermodynamic volume of the uncharged Gauss-Bonnet black hole in $d = 5$ with $\lambda_{GB} = 0.1$ and $\Lambda = 0.3$. The blue shaded region indicates positivity of the volume V. The diagonal and curved boundaries mark, respectively, where $r_c = r_h$ and $r_c = r_{\text{cosmo}}$. 93

5.2 Temperature T as a function of $x = r_h/r_c$ for fixed cavity radius $r_c = 2$ and $d = 5$, showing regions where r_h is multi-valued, signaling a possible phase transition. **Left:** Varying pressure with $\lambda_{GB} = 0.3$. The red dashed horizontal lines demarcate the region in which T is not a monotonically increasing function of x. **Right:** Varying Gauss-Bonnet coupling with $P = -0.02$. Above the red dashed line T is not a monotonically increasing function of x. 94
5.3 Free energy of the Gauss-Bonnet-de Sitter black hole in $d = 5$ with $r_c = 2$, showing a Hawking-Page phase transition from radiation to a large black hole, where the free energy crosses $F = 0$. **Left:** Varying pressure with $\lambda_{GB} = 0.3$. **Right:** Varying Gauss-Bonnet coupling with $P = -0.03$. For very small values of λ_{GB} the free energy limits to the Einstein case where there is a Hawking-Page phase transition with a minimum black hole temperature. 95
5.4 Free energy of the Gauss-Bonnet-de Sitter black hole with $d = 6$, $r_c = 2$, $P = -0.03$, and varying Gauss-Bonnet coupling. **Left:** With $\lambda_{GB} > 0$, there is a first-order phase transition from thermal de Sitter to a large black hole. **Right:** With $\lambda_{GB} < 0$, there is a first-order small-large black hole phase transition. Note the free energy of the small black hole branch is below that of radiation in this case. This behaviour is qualitatively the same in higher dimensions. 96
5.5 Thermodynamic volume of the charged Gauss-Bonnet black hole in $d = 5$ with $\lambda_{GB} = 0.1$, $\Lambda = 0.3$, and varying charge. The shaded regions indicate positivity of the volume V. The diagonal boundary marks where $r_c = r_h$. 98
5.6 Free energy of the charged Gauss-Bonnet-de Sitter black hole with $d = 5$ and $r_c = 2$, showing a first-order phase transition from a small black hole to a large black hole. **Left:** Varying pressure with $\lambda_{GB} = 0.3$. **Right:** Varying Gauss-Bonnet coupling with $P = -0.03$. In the $\lambda \to 0$ limit we have a small-large phase transition. 99
5.7 Free energy of the Gauss-Bonnet-de Sitter black hole in $d = 5$ with $r_c = 2$ and $\lambda_{GB} = 0.3$, showing the formation of a swallowtube corresponding to a compact region of first-order phase transitions from a small to large black hole. Each line corresponds to a constant-pressure slice, while red dots mark the location of the critical temperature within each slice. The red line is the coexistence line. 100
5.8 Coexistence curves for black holes, along which the small and large black hole phases coexist. **Left:** The uncharged Gauss-Bonnet black hole with $r_c = 2$ and varying λ_{GB}. The large dots mark the critical pressures P_{min} (P_{max}), above (below) which there is no phase transition. At these points a second order phase transition from small to large black hole transition occurs. **Right:** The uncharged AdS black hole, illustrating the difference when there is no cavity present. There is only one second order phase transition at the red dot P_{max}. 100

5.9 Free energy of the charged Gauss-Bonnet-de Sitter black hole with $d = 5$, $r_c = 2$, and $\Lambda = 0.3$, showing a first-order phase transition from a small black hole to a large black hole below a critical value of the charge q. In this case, $q_c \sim 0.8$. 101

6.1 A gravitational screen Σ and a spatial section $\mathcal{S}$. 108

7.1 Energy density e and pressure p of the static, flat screen. 132
7.2 Temperature T, entropy density e, and total entropy S as a function of screen radius r for the static, spherically symmetric screen in Minkowski space. 133
7.3 Total entropy S, entropy density s, and temperature T of a gravitational screen at fixed radius in flat space with $\mu n = -9$. The dashed line corresponds to the minimum supported screen radius, below which $T < 0$. e and T are rescaled to fit on the graph. 134
7.4 Energy density e, pressure p, and enthalpy $e + p$ for a gravitational screen at fixed radius outside of a Schwarzschild black hole of mass $m = 1$. The horizon is indicated by a red dashed line. 137
7.5 Equations of state $e_1(p)$ and $e_2(p)$ for the Schwarzschild screen, with $m = 1$. The first branch has a well-defined $m \to 0$ limit while the second does not. 138
7.6 Total entropy $S(r)$, entropy density $s(r)$ and temperature T of a gravitational screen at fixed areal radius r in a Schwarzschild background with $m = 1$ and $\mu n = -0.01$. T and S are rescaled to fit on the graph. The dashed red line corresponds to the event horizon $r_h = 2m$. 139

Notation and Conventions

Throughout this thesis, we adopt the following conventions. Indices are indexed beginning with 0, with coordinate ordering such that (proper) time is always listed first, so that $u_0 = u_\tau$ for example. Where appropriate, coordinate symbols (τ, r, θ, ϕ) are used in place of their corresponding numerical values $(0, 1, 2, 3)$. The Latin indices (a, b, c, d, e) are reserved for the bulk spacetime, and run from 0 to d where d is the dimension of the manifold $\mathcal{M}$ being considered. Latin indices (i, j, k, l) are used for quantities defined on any $(d-1)$-dimensional subspace of $\mathcal{M}$. We typically work in natural or *Planck* units, where $c = \hbar = G = 1$. This considerably simplifies the visual clutter of many expressions, yet leaves the scale of various quantities obscure at a glance. We restore the appropriate factors of $(c, \hbar, G)$ where connections to physical scales are to be made, or the presence of quantum effects is being highlighted. Following Wald, MTW, and many others, we adopt the 'mostly plus' convention $(-, +, +, +)$ for the metric signature, endowing spacelike hypersurfaces with a positive-definite metric. Partial derivatives with respect to a given index (or coordinate variable) are denoted ∂_a (or ∂_τ) while the covariant derivative is likewise denoted by ∇_a. One can always assume the dimension of the spacetime is $d = 4$ unless otherwise noted. Of course, the Einstein summation convention for repeated indices is assumed throughout.

The Structure of this Thesis

In presenting a large body of work such as this thesis, one must carefully balance how reflective the work is of the research journey against the quality of the reading experience for others. I have erred on the side of the reader, presenting the work not necessarily in chronological order, but rather in a way that is pedagogically ideal and allows concepts to be built naturally from one chapter to the next. The progress of theoretical research often possesses no such continuity!

I assume familiarity with classical Lagrangian and Hamiltonian mechanics, special relativity and basic aspects of quantum field theory. I further assume a working knowledge of general relativity. For the most part, the language of the relativists is used, though the languages of differential forms and symplectic geometry are occasionally employed when making connections between these subjects and the present work. In an effort to make this thesis relatively self-contained, I also give a brief review of some fundamentals of general relativity, path integral methods, and the most important aspects of black hole thermodynamics. Throughout, the reader is referred to the canonical texts (or other sources) for further details. With this, I hope that one who has never studied gravitational thermodynamics before can still appreciate the work and find inspiration for their own research (or learning).

The reader who is familiar with general relativity, but unfamiliar with the subject of black hole thermodynamics, is encouraged to start their journey in Section 1.3. Chapters 2-5 are largely self-contained, as is Part II of the thesis, though minor allusions to themes from earlier chapters appear throughout. Both Parts I and II include their own introductions and motivations.

Part I

Black Hole Thermodynamics

Introduction

Humanity's journey towards a scientific understanding of the fundamental nature of reality spans some six thousand years, culminating dramatically in our present day ability to reach out to the edges of the universe from a tiny rock in an endless void[1]. Along this journey, breakthroughs in our understanding of physics at all scales have precipitated countless advancements in technology, which have largely elevated humankind to a realm beyond that which evolution has brought any other species. Today, this understanding is encapsulated by the two pillars of modern theoretical physics: the Standard Model of particle physics, and the general theory of relativity. What remains elusive however is a unified, consistent merging of these two theories, due in part to difficulties intrinsic to quantizing the gravitational field. This 'problem of quantum gravity' represents perhaps the biggest open problem in theoretical physics today, requiring knowledge of gravity's behaviour at the microscopic scale, deep within the regime where quantum mechanics operates. Though the correct approach to this problem is often contested, what cannot be argued is the unique status the gravitational field has as the very architecture of reality, being a manifestation of the geometry of space and time itself. Of course, our motivations for studying the gravitational interaction extend beyond the theoretical realm. The fact that gravity underlies and connects all other processes in the universe has cemented its observation as a powerful lens through which we may come to understand astrophysical phenomena, physics beyond the standard model, and the evolution of the cosmos.

Understanding gravity is therefore essential if we are to discern Nature at the most fundamental level. Fortunately, a window into the microscopic structure of gravity is provided through its *thermodynamic* properties. For every system we know of in the universe, underlying its thermodynamic description is the statistical mechanics of its (fundamentally quantum) constituents. The remarkable discoveries of the early 1970's that black holes radiate and possess entropy demonstrate that gravity is no different [1, 2]. This has ignited an entire field of research into the thermodynamic properties of black holes, objects which live at the intersection of the infrared and the UV. Undoubtedly, the study of black hole thermodynamics has provided deep insights into aspects of not only quantum field theory in curved spacetime, but also string theory, information theory, and even condensed matter physics [3–6]. Concepts like the universality of black hole entropy, the Unruh and Hawking effects, soft charges and asymptotic symmetries, etc. have all played a role in shedding

[1]Tracing back to Mesopotamia and Ancient Egypt, though we necessarily loosen our definition of 'science' significantly as we reach further into the past.

light on gravity's thermodynamic nature [7–10], and though its microscopic degrees of freedom remain poorly understood, this thermodynamic nature continues to guide our efforts towards developing a quantum theory of gravity.

Like traditional thermodynamic systems, variations between equilibrium black hole configurations are captured by the first law of thermodynamics [11]. This similarity with ordinary substances extends beyond the first law, with analogues of the second and third laws of thermodynamics being readily available for black holes, and processes like evaporation occurring naturally. One of the most striking features of black holes arising from their thermodynamic properties is that they, like ordinary systems, can undergo phase transitions. This phenomenon, first discovered by Hawking and Page for anti-de Sitter (AdS) black holes [12], has since been shown to occur generically in a wide variety of black hole spacetimes, in higher dimensions, and in theories beyond Einstein-Hilbert gravity [13–16]. Much of the motivation for studying these 'Hawking-Page' transitions is rooted in the anti-de Sitter/conformal field theory (AdS/CFT) correspondence, which provides a map between a d-dimensional gravitational theory in bulk AdS to a $(d-1)$-dimensional CFT on its boundary [4]. The Hawking-Page transition has a natural interpretation in this context, where the transition between a black hole and thermal radiation in the bulk is dual to a deconfinement transition in the boundary CFT. This bulk/boundary duality has proven to be an extremely powerful theoretical tool, allowing us to study strongly coupled systems where perturbation theory fails, address issues related to information loss in black hole evaporation, and compute the fine-grained entropy of a black hole [17–21]. Moreover, modifications to the description of gravity in the bulk necessarily leads to corresponding modifications of the boundary theory. As a result, all of the aforementioned generalizations of the Hawking-Page transition, along with the more exotic transitions that have been discovered, are expected to have non-trivial interpretations in terms of the boundary CFT (though decidedly less attention has been given to this connection compared to the phase structure of the bulk).

The last decade has seen a resurgence of interest in the thermodynamics—and especially the phase structure—of black holes in the presence of a cosmological constant. This interest is due in large part to the observations of Kastor, Ray, and Traschen [22] that a new thermodynamic potential, the thermodynamic volume, enters into the derivation of the Smarr formula for non-zero Λ. The thermodynamic volume can be understood as the quantity conjugate to the cosmological constant, interpreted in this context as a pressure, and appears as such in the first law of thermodynamics when variations of Λ are included. There has since been considerable development of these ideas, including a proposed bound on the black hole entropy in terms of the thermodynamic volume [23], the notion of holographic heat engines [24], extensions to include acceleration, going beyond black holes to spacetimes with non-trivial topology [25–27], and connections with holography [27–30]. Perhaps most actively investigated has been the subject of black hole phase transitions, where examples of Van der Waals behaviour, triple points (like that of water), re-entrant phase transitions (like those occurring in certain gels), and even lambda transitions (like those marking the onset of superfluidity) have been observed [16, 31–33]. We refer the reader to the review [34] where a number of these developments are summarized.

Whereas a wealth of interesting phenomena in AdS spacetimes have been discovered thus far, the domain of asymptotically de Sitter (dS) spacetimes remains largely unexplored [34, 35]. This is despite recent measurements from a variety of sources indicating that we live in a de Sitter-like universe [36–38], giving significant astrophysical relevance to de Sitter black holes compared to their AdS counterparts. There have also been developments in the formulation of a de Sitter/conformal field theory (dS/CFT) correspondence [39], leading one to naturally wonder what the dual interpretation of dS phase transitions might be. More pragmatically, it is of interest to understand how generic the phase structure of anti-de Sitter black holes is: do the same types of phase transitions manifest for de Sitter black holes, or are there new examples? This is the focus of Part I of this thesis: an examination of the thermodynamics and phase structure of asymptotically de Sitter black holes.

With strong motivations available, the historic lack of progress concerning de Sitter black hole thermodynamics may be surprising. The reason however is simple: de Sitter black holes present unique challenges that their AdS counterparts do not possess. Perhaps the most salient is the presence of the cosmological horizon. With a temperate generally different from that of the black hole, the system is manifestly out of equilibrium. This is in stark contrast to anti-de Sitter space, which acts as a natural box that confines[2] radiation and allows equilibrium to be expressly achieved. Another issue with de Sitter is a lack of globally timelike Killing vector field with which to associate the mass, rendering the construction of conserved charges difficult [40–42]. The notion of a vacuum state is also problematic since the spacetime is essentially non-stationary [43–45], and there is no natural analogue of the Bondi news to characterize gravitational radiation in the full non-linear context [46].

Various approaches have been developed to circumvent these problems, each with their own issues and limitations. One is the *effective temperature* approach, where a single temperature (which depends on both the cosmological and event horizon) is assigned to the entire spacetime [47, 48]. Such a temperature however lacks a clear physical interpretation, and the system still appears out of equilibrium to a local observer. Another approach considers subsets of the parameter space where the two horizon temperatures are equal, allowing for a notion of equilibrium, but severely limiting the number of situations that can be explored [49]. In this thesis, we will adopt a Euclidean path integral approach, developed first by Gibbons and Hawking [50] and extended by York [51, 52] to allow for the definition of the canonical (and later, grand canonical) ensemble. In this approach, one considers an ensemble where the temperature is specified at a finite boundary, effectively enclosing the black hole in an isothermal 'cavity'. As a result, equilibrium is manifest and the meaning of the temperature is clear. This approach has seen some limited application, with Brown and collaborators [52] demonstrating the stability of such an ensemble, and later by Carlip and Vaidya, who found a Hawking-Page-like phase transition in both the asymptotically flat and de Sitter cases [53]. These investigations were rather limited in scope however, and did not consider the extended phase space in which we operate here.

[2] Asymptotically AdS spacetimes have a timelike boundary at infinity that radiation can reach in a finite time, as well as an attractive gravitational potential.

Part I of this thesis represents a dramatic extension of the themes explored in those cursory works. We will find that many new and interesting phenomena emerge, including 'swallowtubes' (compact regions in phase space outside of which transitions cannot occur), analogues of the familiar Hawking-Page, small-large, and reentrant phase transitions exhibited by AdS black holes, metastable reentrant transitions, and more. Throughout, we will develop techniques which can be applied to a wide variety of extensions of the present work, and discuss promising avenues for future research. The organization is as follows:

In Chapter 1, we provide a brief review of some essential aspects of general relativity, the action principle, and the relationship between the path integral and partition function. We also provide a detailed account of the most important aspects of black hole thermodynamics, including the first law, Hawking radiation, phase transitions, and the issues that arise in asymptotically de Sitter spacetimes.

In Chapter 2, we discuss the application of path integral methods to de Sitter spacetimes, demonstrating explicitly how thermodynamic quantities are derived from the Euclidean action. We study Schwarzschild and Reissner-Nordström-de Sitter black holes, examining the extended first law of thermodynamics and deriving expressions for various thermodynamic potentials that enter into the description. We further construct the free energy in the canonical ensemble, and study the phase structure of these black holes, finding analogues of the small-large transitions present in AdS black holes, though a lack of the Van der Waals-like transitions which occur generically in those systems.

In Chapter 3, we consider Schwarzschild and Reissner-Nordström-de Sitter black holes with a non-linear extension of the $U(1)$ sector á la Born-Infeld electrodynamics. We again discuss the extended first law, where a new potential appears through the Born-Infeld vacuum polarization. We study the behaviour of the metric function and vacuum polarization, and determine the relevant thermodynamic variables entering into the free energy. We consider ensembles where both the charge and electric potential are fixed, finding in the latter case the first known example of a reentrant radiation-black hole-radiation transition.

In Chapter 4, we consider a particular class of exact solutions to Einstein-Hilbert gravity with a conformally coupled scalar field, motivated to understand how matter coupling alters the thermodynamic description. We discuss subtleties involved in extending the first law to systems with secondary hair, and how to account for the properties of the scalar field in the thermodynamic analysis. We study the phase structure in the canonical ensemble, finding Hawking-Page-like transitions throughout the parameter space, though with the addition of a particular cosmic censorship bound arising from the scalar field profile.

In Chapter 5, we examine higher dimensional black holes in the context of Gauss-Bonnet gravity, a commonly studied higher curvature modification of general relativity. We discuss the construction of the Euclidean action and its corresponding reduction, and derive various thermodynamic potentials which enter into the description. We again study the free energy, finding the typical Hawking-Page and small-large black hole transitions. We also demonstrate a notable absence of the exotic triple points and reentrant transitions that occur in the 6-dimensional anti-de Sitter case.

Chapter 1

Aspects of General Relativity and Black Hole Thermodynamics

Having recently celebrated its 100 year anniversary, Einstein's general theory of relativity has enjoyed over a century of success in describing the universe around us. The insight that both gravitation, and our perception of time are manifestations of the very geometry of our reality has fundamentally changed how we view the world, and opened doors to a staggering number of advances both theoretical and practical. To date, general relativity has survived every conceived experimental test of its validity, and remains the only viable candidate metric theory of gravity in four dimensions[1]. Of course, many alternative theories of gravity have been developed over the decades, either to account for otherwise mysterious phenomena (such as dark matter, inflation, etc.) or for purely theoretical interest. There is indeed good motivation to study such theories, yet despite the wealth of alternatives available, none have measured close to general relativity in its combined observational successes and theoretical beauty.

In this chapter, we will review some fundamentals of the theory and provide some details regarding the various mathematical machinery that will be employed throughout the rest of this thesis. This includes a discussion about thermodynamic aspects of gravity, de Sitter space, and path integral methods. We refer the reader to a number of classic texts that provide significantly more detail than is given here. The book of Shutz [55] provides a differential-geometric view of relativity. Wald [56] and Weinberg [57] offer nice mathematical exposition from a physicist's perspective. Carrol [58] and Poisson [59] contain a large number of useful examples, the latter having also a nice review of the 3+1 formulation of general relativity. The book by Frolov [60] is specific to black hole physics, containing numerous astrophysically relevant examples, semi-classical aspects, and advanced topics such as quasinormal modes. The book by Will [61] provides a detailed overview of experimental and observational aspects of general relativity, while his book with Poisson [62] covers many applications of weak-field general relativity. One is left hardly devoid of evening reading material.

[1]The recently proposed 4D Gauss-Bonnet gravity may be a contender [54].

General relativity is distinguished from a wide variety of alternative theories of gravitation (which have been studied almost as long as general relativity itself) in that it is the unique theory in four spacetime dimensions that satisfies the following conditions:

1. It is a metric theory, with g being the only dynamical variable.
2. There are two degrees of freedom
3. Spacetime diffeomorphism invariance is explicit
4. The field equations are at most second-order

Relaxations of the conditions $(1)-(4)$ lead to various extensions or alternative theories, some of which are considered in later chapters. Numerous astrophysical observations, cosmological considerations, and technical difficulties have to various degrees constrained (sometimes severely) the extent to which these alternative theories can deviate from the dynamics of general relativity, firmly placing GR as the 'standard model' of gravitational physics and the ideal starting point for any investigation into gravitational phenomena.

1.1 Manifolds, Metrics, and Curvature

The basis of general relativity is the assumption that spacetime can be represented by a d-dimensional differentiable ($\mathcal{C}^\infty$) manifold $\mathcal{M}$. Such a manifold alone possesses insufficient structure to model gravitation as a geometric phenomenon. One must construct a tangent bundle on $\mathcal{M}$, endow it with an inner product structure, and then define a notion of parallel transport which can be used to define curvature.

Beginning with the tangent bundle, one constructs at each point $p \in \mathcal{M}$ a tangent space $T_p\mathcal{M}$ with dimension d. The tangent bundle $T\mathcal{M} = \bigcup_{p\in M} T_pM$ is the disjoint union of all tangent spaces on $\mathcal{M}$. The manifold is then equipped with an everywhere non-degenerate symmetric rank-two tensor called the metric g. The metric acts as a bilinear form that maps two vectors $u, v \in T_p\mathcal{M}$ at p to a real number, thus defining an inner product structure on $T\mathcal{M}$. The object g is the (only) fundamental variable of the theory, and satisfies:

1. $g:\ T_p\mathcal{M} \times T_p\mathcal{M} \to \mathbb{R}$
2. $g(u,v) = g(v,u)$
3. $g(Au+v,z) = Ag(u,z) + g(v,z) \quad \text{for } a \in \mathbb{R}$
4. $\forall u, v \in T_p\mathcal{M},\ \nexists u \notin \emptyset \,|\, g(u,v) = 0$

The second condition represents symmetry of g, the third represents bilinearity, and the final is nondegeneracy. The metric thus serves to endow the tangent space at each point

in the manifold with an inner product. In a coordinate basis, the metric can be expanded in terms of its components as

$$g = ds^2 = g_{ab} dx^a \otimes dx^b \tag{1.1}$$

where the metric g is often represented as ds^2 and referred to as the line element. It is standard practice to omit the tensor product symbol above. The metric defines a notion of distance within each tangent space, but does not suffice to meaningfully describe the geometry or curvature of $\mathcal{M}$, which requires that vectors at different points (elements of different tangent spaces) to be compared. This is accomplished by the covariant derivative, which can be used to determine how vectors are parallel-transported between tangent spaces. A notion of curvature can then be defined by the failure of a vector to return to its initial value when parallel transported around a closed curve in $\mathcal{M}$.

To define parallel transport of tensor fields on $\mathcal{M}$, one must first define a covariant derivative ∇. ∇ is a connection on the tangent bundle and generalizes the usual derivative operator to tensor fields. For an arbitrary tensor T of rank (r, s), its covariant derivative in a given coordinate basis is given by

$$\begin{aligned}
(\nabla_{e_c} T)^{a_1 \ldots a_r}{}_{b_1 \ldots b_s} &= \partial_c T^{a_1 \ldots a_r}{}_{b_1 \ldots b_s} && (1.2)\\
&+ \Gamma^{a_1}{}_{dc} T^{d a_2 \ldots a_r}{}_{b_1 \ldots b_s} + \cdots + \Gamma^{a_r}{}_{dc} T^{a_1 \ldots a_{r-1} d}{}_{b_1 \ldots b_s} && (1.3)\\
&- \Gamma^{d}{}_{b_1 c} T^{a_1 \ldots a_r}{}_{d b_2 \ldots b_s} - \cdots - \Gamma^{d}{}_{b_s c} T^{a_1 \ldots a_r}{}_{b_1 \ldots b_{s-1} d}. && (1.4)
\end{aligned}$$

In general relativity the connection ∇ is taken to be *torsion-free*, namely we have that

$$\nabla_a \nabla_b f = \nabla_b \nabla_a f \ . \tag{1.5}$$

This is equivalent to demanding that the torsion tensor defined by $\nabla_a \nabla_b f - \nabla_b \nabla_a f = -T^c_{ab} \nabla_c f$ vanishes. Note that while in differential geometry ∇ itself is referred to as the connection, in relativity the name 'connection' is often reserved for the pseudotensor Γ instead. As it stands, there are many possible choices of derivative operator on $\mathcal{M}$ owing to the large freedom in the components of Γ. One may worry that different definitions of derivative operator on the manifold may lead to inequivalent curvatures for the same manifold, and this is indeed the case, as the ordinary derivative operator is coordinate dependent and therefore cannot be associated with the manifold structure. Fortunately, a natural (and unique) choice of derivative operator can be selected by imposing the *metric compatibility* condition, $\nabla_e g_{ab} = 0$. This condition arises from the natural demand that the inner product of two vectors remain unchanged when parallel transported around a curve. With this condition, the following connection can be constructed:

$$\Gamma^e{}_{ab} = \tfrac{1}{2} g^{ed} \left(g_{da,b} + g_{db,a} - g_{ab,d} \right) \ . \tag{1.6}$$

This is the *Levi-Civita* connection, and is the *unique* torsion-free connection that satisfies the metric compatibility condition.

With the connection in hand, we can finally define the curvature of a manifold through

the path-dependence of parallel transport. We consider the parallel transport of a dual vector ω^a around a closed curve in $\mathcal{M}$, and compare the difference between the final value when transporting in opposing directions around the curve. An intrinsic notion of curvature is given by the failure of ω^a to return to its original value when parallel transported around a loop, and is captured fully by the *Riemann tensor* R_{abdc}, defined as a $(1,3)$ tensor field acting on ω^a as

$$R(u,v)w = \nabla_u \nabla_v w - \nabla_v \nabla_u w - \nabla_{[u,v]} w \ . \tag{1.7}$$

In a coordinate basis the Riemann tensor is given by

$$R_{abc}{}^{d}\omega_d = \nabla_a \nabla_b \omega_c - \nabla_b \nabla_a \omega_c \tag{1.8}$$

as the final term in (1.7) vanishes if (u,v) are coordinate vector fields. The Riemann tensor encodes not only the failure of dual vectors to parallel transport back to their initial values along closed loops, but also captures other innate properties one associates with curved manifolds, such as the failure of initially parallel lines to remain parallel. The Riemann tensor possesses $d^2(d^2-1)/12$ independent components by virtue of its skew symmetry, interchange symmetry, and Bianchi identities:

1. $R_{abcd} = -R_{abdc} = -R_{bacd}$
2. $R_{abcd} = R_{cdab}$
3. $R_{a[bcd]} = R_{abcd} + R_{acdb} + R_{adbc} = 0$
4. $\nabla_{[e|} R_{ab|cd]} = \nabla_e R_{abcd} + \nabla_c R_{abde} + \nabla_d R_{abec} = 0$

The form of the Bianchi identities above assumes a torsion-free connection. Contraction on the first and third index gives the symmetric Ricci tensor R_{ab}

$$R^a{}_b = R^e{}_{aeb} \ , \tag{1.9}$$

which in three dimensions or less contains all of the information encoded in the Riemann tensor (though not when $d > 3$). The trace of the Ricci tensor is called the Ricci scalar, or scalar curvature R:

$$R = g_{ab} R^{ab} = R_a{}^a \tag{1.10}$$

The Ricci scalar is a curvature invariant which measures the deviation in volume of a geodesic ball in curved space relative to Euclidean space. With these minimal ingredients one can understand the meaning of the field equations presented in the next section.

1.2 Einstein's Equations and the Action Principle

General relativity is much more than a prescription for defining the curvature of manifolds. It is a statement of the origin of that curvature, and provides a model for how a manifold's

curvature interacts with the fields that live on it (and vice versa). The fundamental insight made by Einstein is that the presence of matter (as described by quantum field theory through the Standard Model) curves the spacetime in which the matter lives. In turn, the curvature of spacetime dictates how matter moves throughout spacetime. Schematically this is represented as

$$\text{matter moves} \leftrightarrow \text{space curves} \tag{1.11}$$

or colloquially, "matter tells space how to curve; space tells matter how to move". This matter/curvature relationship is precisely captured by the Einstein field equations (EFEs). One can heuristically derive their form by attempting to generalize the Poisson equation for the Newtonian gravitational field

$$\nabla^2\Phi = 4\pi G\rho \ , \tag{1.12}$$

where Φ is the Newtonian gravitational potential and ρ is the mass density of the matter producing the gravitational field. The object that naturally generalizes mass density to the relativistic case is the energy-momentum (or stress-energy) tensor T_{ab}. Constrained by index rules, the simplest generalization of (1.12) is

$$G_{ab} = \kappa T_{ab} \tag{1.13}$$

Following the assumption that the gravitational field (and thus potential) is encoded in the curvature, one attempts to build the tensor G_{ab} out of suitable combinations/contractions of the Riemann tensor. Due to the equivalence principle[2], the simplest possible choice turns out to be

$$\underbrace{R_{ab} - \tfrac{1}{2}Rg_{ab}}_{G_{ab}} = \kappa T_{ab} \tag{1.14}$$

One can show that this equation exactly reduces to Newtonian gravity in the weak-field, slow moving, time-independent limit. From the Newtonian limit one can further establish that $\kappa = 8\pi G$. Equation (1.14) is the original equation proposed by Einstein that expresses the link between matter and the geometry of spacetime. It is a system of ten second-order partial differential equations that determine the evolution of the metric g_{ab} in the presence of stress-energy (matter). This equation can be generalized by including a constant Λ on the left-hand side:

$$G_{ab} + \Lambda g_{ab} = 8\pi G T_{ab} \ . \tag{1.15}$$

Λ is known as the *cosmological constant*, and its presence has wide-reaching implications in general relativity and our understanding of the universe. Originally introduced by Einstein to allow for static cosmological solutions in the presence of matter, it was soon rejected due to the discovery of Edwin Hubble that the universe is expanding[3]. In the coming decades,

[2]The equivalence principle dictates that $\nabla^a T_{ab} = 0$. Due to the Bianchi identity, choosing $G_{ab} = R_{ab}$ would imply that $T = const.$ everywhere in spacetime regardless of matter content, which is highly implausible.

[3]Einstein later deeply regretted the introduction of Λ into his field equations. According to Archibald Wheeler, he was heard lamenting that "[it] was my biggest blunder of my life." in the Institute for Advanced Study's Fuld Hall.

our understanding of quantum field theory would eventually see Einstein vindicated as it became clear that the vacuum itself possesses an energy density, which can be interpreted as the cosmological constant appearing in the field equations. By 1998, the accelerating expansion of the universe would be observed by the Supernova Cosmology Project and the High-z SN Search in perhaps the most important discovery of modern cosmology [63, 64], an observation whose accuracy has been significantly improved upon since then [65, 66]. However, the discrepancy between its predicted value from quantum field theory and the observed value of Λ is anywhere from 60 to 120 orders of magnitude depending on the model used, representing one of the biggest unresolved mysteries in physics (see [67] for a detailed discussion of these developments and issues). Despite its tangled history, the cosmological constant is now a cornerstone of the current ΛCDM model of the universe, and will take on a central role in our work.

More rigorously, one can derive the Einstein equations from an action principle, as one does in classical mechanics to arrive at Newton's laws. The principle of stationary action states that a system evolves from an initial state q_1 at time t_1 to a final state q_2 at t_2 along a path (in the configuration space of the generalized coordinates q_i) for which the action $I[q]$ is stationary to first-order, namely $\delta\mathcal{S} = 0$. The action itself is defined as the integral over time of the Lagrangian $L \equiv \int \mathcal{L}\, d^3x$ of the system, or (equivalently) the integral of the Lagrangian density $\mathcal{L}$ over the spacetime

$$I[q(\tau), \dot{q}(\tau)] = \int \mathcal{L}(q(\tau), \dot{q}(\tau))\ d\tau \tag{1.16}$$

The Lagrangian itself is a function of the generalized coordinates of the system and their time-derivatives, and contains all information about the dynamics of the system. In the non-relativistic case, the Lagrangian simply represents the difference between the kinetic and potential energy of the system. Varying the action with respect to the fields/coordinates and requiring that the variation vanishes ($\delta I = 0$) then gives the equations of motion of the system. For general relativity, it is the Einstein-Hilbert action that gives the EFEs when varied:

$$I_{\text{EH}} = \frac{1}{16\pi G} \int d^4x \sqrt{-g} \Big(R - 2\Lambda\Big) \tag{1.17}$$

Here, g is the determinant of the metric tensor giving the natural volume form on the manifold, R is the Ricci scalar, and Λ is the cosmological constant. This action is supplemented by a contribution from the matter content of the system, so that[4] $I_{\text{tot}} = I_{\text{EH}} + I_{\text{Matter}}$. Varying the action with respect to the inverse metric g^{ab} gives

$$\delta I_{\text{EH}} = \frac{1}{16\pi G} \int d^4x\ \delta\sqrt{-g} \Big(R - 2\Lambda\Big) + \frac{1}{16\pi G} \int d^4x\ \sqrt{-g}\, \delta\Big(R - 2\Lambda\Big) \tag{1.18}$$

[4]This is the minimal coupling prescription, where no individual terms involve both the curvature and matter fields.

where

$$\delta\sqrt{-g} = -\frac{1}{2\sqrt{-g}}\delta g = \frac{-g}{2\sqrt{-g}}\left(g^{ab}\delta g_{ab}\right) = -\tfrac{1}{2}\sqrt{-g}\left(g_{ab}\delta g^{ab}\right)$$

$$\delta\big(R-2\Lambda\big) = \delta(R_{ab}g^{ab}) = R_{ab}\delta g^{ab} + g^{ab}\delta R_{ab} = R_{ab}\delta g^{ab} + \underbrace{\nabla_d\big(g^{ab}\delta\Gamma^d_{ab} - g^{ad}\delta\Gamma^c_{ac}\big)}_{\text{Total derivative}} \,.$$

The total derivative term becomes a pure boundary term by Stokes' theorem, vanishing when $\mathcal{M}$ is closed (compact with no boundary). Combining the results above, and noting that the variation of $\mathcal{S}_{\text{matter}}$ with respect to the matter fields gives a stress-energy contribution T_{ab}, one arrives at

$$\delta I_{\text{tot}} = \frac{1}{16\pi G}\int d^4x\,\sqrt{-g}\Big(R_{ab} - \tfrac{1}{2}Rg_{ab} + \Lambda g_{ab} - 8\pi G T_{ab}\Big)\delta g^{ab} = 0\,, \quad T_{ab} \equiv \frac{-2}{\sqrt{-g}}\frac{\delta\left(\sqrt{-g}\mathcal{L}_{\text{M}}\right)}{\delta g^{ab}}$$

where it is clear that for any such variation to vanish, we must have

$$G_{ab} + \Lambda g_{ab} = 8\pi G T_{ab}$$

which are the Einstein field equations derived above. The above prescription for arriving at the field equations generalizes to arbitrary actions that have Lagrangians as functions of the generalized coordinates. This gives a powerful framework for studying many different candidate theories of gravity, since all of the kinematic and dynamical information is contained in the theory's action and general covariance is manifest. Note that in cases where $\mathcal{M}$ has a boundary $\partial\mathcal{M}$, the action (1.17) must be supplemented by the Gibbons-Hawking-York boundary term for the variational principle to be well-defined:

$$I_{\text{GHY}} = \frac{1}{8\pi G}\int_{\partial\mathcal{M}} \mathrm{d}^3x\,\sqrt{h}\,H \tag{1.19}$$

Here, h is the determinant of the induced metric h_{ab} on the boundary, and H is the trace of the extrinsic curvature of $\partial\mathcal{M}$.

1.3 Path Integrals

Though not without its technical issues, the path integral has proven to be an extremely useful tool in understanding gravity beyond the classical realm [68,69]. Aside from formally defining a quantum theory of gravity, the path integral further provides us with a powerful way to study gravitational thermodynamics when the spacetime under consideration does not admit a straightforward definition of temperature (this application is discussed in depth in Chapter 2). In this application, one exploits the fundamental relationship between the classical Euclidean action I_E and the quantum mechanical partition function $\mathcal{Z}$,

$$F = -T\log\mathcal{Z} \approx TI_E \tag{1.20}$$

where F is the free energy of the system and T is the temperature. The above relation holds in the semi-classical approximation and comes directly from the path integral. As the path integral underlies the 'cavity' approach we will use to study the thermodynamics of various spacetimes within this work, we provide here a review of its construction. Starting in Chapter 2, we will see explicitly how the path integral can be applied to asymptotically de Sitter spacetimes to formulate a thermodynamic description.

In quantum theory, the amplitude for a system to evolve from an initial state $|q_i, t_i\rangle$ to a final state $|q_f, t_f\rangle$ can be written in terms of the path integral as

$$\langle q_f, t_f | q_i, t_i \rangle = \langle q_f | \, e^{-iH(t_f - t_i)/\hbar} \, | q_i \rangle = \int_{q(t_i)=q_i}^{q(t_f)=q_f} \mathcal{D}[q] \; e^{-I[q]/\hbar} \; . \tag{1.21}$$

This is an integral over all field configurations that take on values q_i at t_i and q_f at t_f. Eventually, we will interpret this as the amplitude for a spacetime to transition from one state to another. The field q may be any quantum field: a scalar, Dirac field, spinor field, etc. A probabilistic interpretation requires that we move to the Euclidean sector of the theory under consideration, by analytically continuing t to imaginary values (sending $t \to -i\tau$). The signature of the metric then becomes Euclidean (instead of Lorentzian) which renders the kernel $K = \langle q_f | \, e^{-H\tau/\hbar} \, | q_i \rangle$ of the evolution operator positive, allowing for its interpretation as a probability density. The amplitude then becomes

$$\langle q_f | \, e^{-iH(t_f - t_i)/\hbar} \, | q_i \rangle \quad \to \quad \langle q_f | \, e^{-H\tau/\hbar} \, | q_i \rangle \; . \tag{1.22}$$

Recall now that the partition function for a thermal state in quantum theory can be written

$$\mathcal{Z} = \mathrm{Tr} \left(\exp -\beta H \right) \; , \tag{1.23}$$

where $\beta \equiv T^{-1}$ is the inverse temperature of the state. For a continuous spectrum of states, the trace can be expanded as

$$\mathrm{Tr} \left(\exp -\beta H \right) = \int dq \; \langle q | \, e^{-\beta H} \, | q \rangle \; . \tag{1.24}$$

Notice now that if we integrate only over paths that are periodic with periodicity τ in (1.21), then $q(0) = q(\tau) \implies q_i = q_f$, and the path integral becomes

$$\langle q | \, e^{-H\tau/\hbar} \, | q \rangle = \int_{q(0)}^{q(\tau)} \mathcal{D}[q] \; e^{-I_E[q]/\hbar} \; . \tag{1.25}$$

Comparing (1.24) and (1.25) we see that a path integral, when restricted to the Euclidean sector of the theory and to states periodic in imaginary time, is equal to the partition function of a thermal state in the theory, provided that we identify the periodicity with the inverse temperature $\beta = \tau/\hbar$. We thus have

$$\mathcal{Z} = \mathrm{Tr} \left(\exp -\beta H \right) = \int_{q(0)}^{q(\tau)} \mathcal{D}[q] \; e^{-I_E[q]/\hbar} \; , \tag{1.26}$$

where the integral over dq has been absorbed into the integration measure $\tilde{\mathcal{D}}[q]$.

In gravity, we are concerned with the interaction of (quantum) matter fields with the (presumably quantum) gravitational field. The path integral measure should thus include the metric g along with the fields q. However, to leading order in $\frac{m_p}{M}$ the matter fields do not contribute to the path integral, so the measure is simply $\mathcal{D}(g)$, where topologically distinct metrics may contribute. With this, the partition function can be approximated by

$$\mathcal{Z} = \int_{\text{metrics periodic with } \tau} \mathcal{D}[g]\ e^{-I_E[g]/\hbar}\ . \tag{1.27}$$

We can further approximate this quantity by considering only the leading contribution to the integral, which comes from metrics that are classical solutions to the equations of motion, namely those for which $\delta I_E[g_{cl}] = 0$. This is the saddle point approximation, in which

$$\int \mathcal{D}[g]\ e^{-I_E[g]/\hbar} \approx e^{-I_E[g_{cl}]/\hbar}\ , \tag{1.28}$$

where we denote by g_{cl} said classical metrics. Therefore we have that

$$\mathcal{Z} \approx e^{-I_E[g_{cl}]/\hbar} \qquad \rightarrow \qquad F \approx T I_E\ . \tag{1.29}$$

This can be regarded as the zero-loop approximation to the full partition function, which only includes the (dominant) contribution from the gravitational fields. The partition function can then be related to other thermodynamic quantities through the usual formulas from statistical mechanics

$$\langle E \rangle = \frac{\partial I_E}{\partial \beta}\ , \qquad S = \beta \frac{\partial I_E}{\partial \beta} - I_E\ . \tag{1.30}$$

Some care must be taken in the application of these formulas. It is really a variation of the action that is being done with certain parameters being held fixed, something we clarify further in Section 2.3. Loosely speaking then, determining the thermodynamic properties of quantum fields in a given spacetime (in a semi-classical setting) amounts to evaluating the on-shell Euclidean action I_E. Such path integral methods have been used as early as 1977 by Gibbons and Hawking [70] to compute the entropy and temperature associated with a black hole.

1.4 Black Hole Thermodynamics

To what extent can a black hole (and indeed, gravity itself) be understood as a thermodynamic system? This question has long been the subject of intense research, and is the basis for the studies at hand. Central to the discussion is the first law of thermodynamics, which expresses the relationship between equilibrium states of a system in terms of quasistatic variations of the extensive parameters x_i which characterize that system. In terms of the temperature T, entropy S, pressure P, volume V, and other thermodynamic potentials X_i

(these may be the charge, chemical potential, etc.), the first law states that the change in internal energy of the system U is given by

$$dU = T dS - P\, dV - \sum_i X_i dx_i \ . \tag{1.31}$$

The far-reaching consequences of this law are difficult to overstate. Arising from a coarse-graining of the fundamental microscopic description of matter, the laws of thermodynamics underlie the entirety of the modern world, being responsible for heat engines, transportation, our understanding of weather and the global climate, agriculture, and more. Given the power of the thermodynamic description, and its statistical mechanical underpinnings, one would be remiss to not attempt to describe gravity in the very same way. In this section, we describe how our understanding of black holes as thermodynamic objects has crystallized over the decades, along with the subtleties involved in applying (1.31) to gravitational systems. We also remark on the inclusion of the cosmological constant in the first law of thermodynamics for black holes, and define the *extended phase space* in which we will operate.

1.4.1 The First Law

Beginning in 1972 with the famous area theorem by Hawking [71], which states that the horizon area of a classical black hole can never decrease, it quickly became clear that many analogies could be drawn between black holes and ordinary thermodynamic systems. With the striking similarity between the area theorem and the second law of thermodynamics, Hawking, Bardeen and Carter [11] soon formulated the "four laws of black hole mechanics", which state that for an asymptotically flat, uncharged, stationary, axisymmetric black hole:

1. The surface gravity κ is constant over the event horizon of a black hole.
2. First-order variations in the charges M, Q, J are captured by

$$dM = \frac{\kappa}{8\pi G} dA_h + \Omega_h dJ \tag{1.32}$$

   where Ω_h is the angular velocity of the black hole.
3. The area of any individual event horizon cannot decrease, $dA_h \geq 0$.
4. No finite sequence of physical processes can reduce the surface gravity κ of a black hole to zero.

These neatly parallel the laws of thermodynamics for 'ordinary' systems, with the surface gravity κ playing the role of temperature, the horizon radius r_h appearing in place of the system's entropy, and the mass M being interpreted as the internal energy U. At the classical level the similarities between (1.31) and (1.32) are merely a coincidence, because the temperature of a black hole is identically zero and there is no mechanism by which two

black holes might exchange heat in order achieve thermal equilibrium. Various thought experiments by Bekenstein in 1972 led him to a convincing connection between black hole entropy and horizon area [2, 72], given by

$$S \sim \frac{A_h}{\hbar G} \ . \tag{1.33}$$

Just three years later, in one of the most significant theoretical papers ever written [1], Stephen Hawking would use arguments from quantum field theory in curved spacetime to show that black holes in fact radiate as blackbodies with a temperature proportional to their surface gravity,

$$T = \frac{\kappa}{2\pi} \ . \tag{1.34}$$

That black holes radiate has profound and far-reaching consequences for our understanding of gravity and quantum mechanics. For one, the existence of Hawking radiation cements black holes as true thermodynamic systems, by providing an equilibration mechanism and allowing their temperature to be non-zero. It also fixes the proportionality constant in (1.33) such that

$$S = \frac{A_h}{4\hbar G} \ , \tag{1.35}$$

giving an explicit relationship between the horizon area and black hole entropy. This relation has deep implications for information theory, providing a theoretical bound on the amount of information that can be contained in a region of spacetime. These discoveries also make clear the holographic nature of gravity, with the entropy scaling as the area of the bounded region rather than its volume (as it does for traditional systems). Most importantly, that gravity apparently possesses thermodynamic properties provides a window into its microscopic structure, as for every system we know of in the universe, coarse-grained thermodynamic properties arise from the underlying statistical mechanics of the constituent degrees of freedom.

Of course, while the origin of the black hole's apparent temperature is well understood, the nature of the entropy remains much more mysterious. Below, we see how a modern derivation of the first law hints at the origin of black hole entropy, but it should be noted that the relationship (1.35) has been calculated using a half-dozen or so completely disparate approaches [73–78], each of which provide a unique perspective on the state-counting interpretation of $S = A_h/4$. The universality of the Bekenstein-Hawking entropy, and lack of a complete quantum theory of gravity, make the origin of S one of the biggest open problems in theoretical physics today.

A historic derivation

As the first law is central to the study of black hole thermodynamics, we begin by outlining the original derivation of (1.32) by Bardeen and collaborators (for explicit details, see [11]). To arrive at the differential mass formula above, one uses the fact that a stationary, asymptotically flat spacetime possesses a unique timelike Killing vector field k_a which satisfies

$$\nabla_a \nabla_b k^b = -R_{ab} k^b \ . \tag{1.36}$$

In the axisymmetric case, there is also a unique rotational Killing vector $\tilde{k}_a$ satisfying the same constraint. One can integrate (1.36) over a spacelike hypersurface S and rewrite the left side as an integral over the boundary ∂S, giving

$$\int_{\partial S} \nabla^b k^a \, d\Sigma_{ab} = -\int_S R_a{}^b k^a \, d\Sigma_b \ . \tag{1.37}$$

By choosing S to intersect the event horizon, the boundary ∂S is made to contain the event horizon $\partial\mathcal{B}$ and a 2-surface at infinity. The integral at infinity is related to the ADM mass of the spacetime M, allowing one to rewrite this as

$$M = \int_S \left(2T_a{}^b - T\delta_a^b\right) k^a d\Sigma_b + \frac{1}{4\pi}\int_{\partial B} \nabla^b k^a d\Sigma_{ab} \tag{1.38}$$

where $T = T_a{}^a$. A similar integration can be performed for $\tilde{k}_a$, giving the angular momentum as measured at infinity:

$$J = -\int_S T_a{}^b \tilde{k}^a d\Sigma_b - \frac{1}{8\pi}\int_{\partial B} \nabla^b \tilde{k}^a d\Sigma_{ab} \ . \tag{1.39}$$

Expressing the null vector tangent to the horizon generators as $l^a = k^a + \Omega_h \tilde{k}^a$, and using the fact that Ω_h is constant over ∂B, we can combine (1.38) and (1.39) to get

$$M = \int_S \left(2T_a{}^b - T\delta_a^b\right) k^a d\Sigma_b + 2\Omega_H J_H + \frac{1}{4\pi}\int_{\partial B} \nabla^b l^a d\Sigma_{ab} \ , \tag{1.40}$$

where J_h is the horizon contribution of (1.39). The final term $\nabla^b l^a d\Sigma_{ab}$ can be rewritten in terms of the surface gravity and horizon area element as κdA. Then, using the fact that κ is constant over the event horizon one finally arrives at

$$M = \int_S \left(2T_a{}^b - T\delta_a^b\right) k^a d\Sigma_b + 2\Omega_h J_h + \frac{\kappa}{4\pi} A_h \ . \tag{1.41}$$

For vacuum spacetimes, $T_{ab} = 0$. The first-order variation of (1.41) gives the differential form of the second law as stated above, namely

$$dM = \frac{\kappa}{8\pi G}\, dA_h + \Omega_h dJ_h \ . \tag{1.42}$$

A modern derivation

Here we sketch out a modern derivation of the first law using the Iyer-Wald-Zoupas symplectic formalism, which has the advantage of being more broadly applicable and also reveals the origin of the black hole entropy S as the Noether charge associated with diffeomorphism invariance (for explicit details see [11]). Beginning with a generic Lagrangian $L = L(\phi, d\phi)$, its first-order variation with respect to the fields ϕ can be written as

$$\delta L = E\delta\phi + d\theta \ . \tag{1.43}$$

Here, the equations of motion (Euler-Lagrange equations) are $E = 0$ and $d\theta$ is a boundary term written as the differential of the symplectic potential θ. The (symmetry) variation of the field ϕ associated with a diffeomorphism-generating vector field ξ^a is given by[5]

$$\delta_\xi \phi = \mathcal{L}_\xi \phi \ , \tag{1.44}$$

where $\mathcal{L}_\xi$ is the Lie derivative along ξ. If there are no background fields, then the variation of L can be written in terms of the symmetry variations of ϕ, giving

$$\delta L = \mathcal{L}_\xi L = [i, d]L = i_\xi(dL) + d(i_\xi L) = d\, i_\xi L \ , \tag{1.45}$$

where d is the exterior derivative[6] and i is the interior product[7]. Subtracting (1.43) from (1.45) implies the existence of a current j that is conserved on-shell:

$$E\delta\phi + d\theta - d\, i_\xi L = 0 \qquad \rightarrow \qquad d(\underbrace{\theta - i_\xi L}_{j}) = -E\delta\phi \ . \tag{1.46}$$

If $E = 0$, the current j is closed and can be written in terms of a 2-form Q_ξ such that $j = dQ_\xi$, which when integrated over a spatial hypersurface gives the Noether charge. The variation of the Hamiltonian H_ξ generating the flow in phase space that corresponds to the diffeomorphism ξ gives Hamilton's equations

$$\delta H_\xi = \int_\Sigma \Omega(\phi, \delta\phi, \mathcal{L}_\xi\phi) \qquad \leftrightarrow \qquad i_{X_H}\omega + dH = 0 \ , \tag{1.47}$$

where Σ is a Cauchy surface and $\Omega \equiv \delta\theta(\phi, \mathcal{L}_\xi) - \mathcal{L}_\xi\theta(\phi, \delta\phi)$ is the symplectic current. Using (1.43)-(1.46) along with the definition of j and Ω, this variation can be expressed as

$$\delta H_\xi = \int_\Sigma \delta\theta - \mathcal{L}_\xi\theta = \int_{\partial\Sigma} \delta Q_\xi - \ i_\xi\theta = 0 \ , \tag{1.48}$$

where the last equality holds if ξ is a symmetry. Suppose we further consider an asymptotically flat black hole spacetime. If the boundaries of the hypersurface Σ are chosen to be spatial infinity and the event horizon $\partial\mathcal{B}$, then we have

$$\int_{\partial\mathcal{B}} \delta Q_\xi = \int_\infty \delta Q_\xi - \ i_\xi\theta \ , \tag{1.49}$$

where the surface normals are taken to be outward pointing. Defining a Killing vector field $\xi^a = t^a + \Omega_h\psi^a$ which vanishes on $\partial\mathcal{B}$, and defining the canonical energy (the ADM mass M in this case) and angular momentum J as

$$M = \int_\infty Q_t - i_t\theta \ , \quad J = -\int_\infty Q_\psi \ , \tag{1.50}$$

[5]Since generally, $\delta_s\phi = [\phi, C^a]\epsilon_a$ for a gauge symmetry.

[6]$d\omega = \frac{\partial a}{\partial x^i} dx^i \wedge dx^{i_1} \wedge \cdots \wedge dx^{i_k}$ for a k-form $\omega = a\, dx^{i_1} \wedge dx^{i_2} \wedge \cdots \wedge dx^{i_k}$

[7]The interior product relates the Lie and exterior derivatives of a form through the Cartan magic formula: $\mathcal{L}_X\omega = d\,(i_X\omega) + i_X d\omega$.

one can rewrite (1.49) as

$$\delta M = \int_{\partial \mathcal{B}} \delta Q_\xi + \Omega_h \delta J \ . \tag{1.51}$$

It remains to show that the integral term can be written in terms of the surface gravity and horizon area (or entropy). To proceed, one must recognize that Q_ξ is an algebraic function of ξ and its derivatives and use the relation $\nabla_a \xi^b = \kappa \sigma_a{}^b$ (with $\sigma_a{}^b$ being the normal 2-form to $\partial\mathcal{B}$). With this, Q_ξ can be rewritten entirely in terms of the surface gravity κ and horizon binormal σ, with no explicit reference to the killing field ξ. Defining the Noether charge $\tilde{Q}_\xi$ as the object obtained by these replacements, one has

$$\delta M = \frac{\kappa}{2\pi} \delta S + \Omega_h \delta J \ , \qquad S \equiv 2\pi \int_{\partial \mathcal{B}} \tilde{Q}_\xi \ , \tag{1.52}$$

where explicit integration of the entropy term gives the horizon area A (in the case of Einstein gravity). This derivation is much more powerful than the previous one in that it holds for any diffeomorphism invariant Lagrangian theory of gravity and for nonstationary perturbations of black hole spacetimes as well [79]. It is also more insightful, as the horizon entropy S can be clearly traced back to the Noether charge Q_ξ of the diffeomorphism ξ.

1.4.2 Hawking Radiation and Black Hole Temperature

As we have seen, underlying the concrete interpretation of (1.32) as the first law for a true thermodynamic system is the existence of Hawking radiation, which is absent in the purely classical description of the black hole geometry. Lacking this, we have only a formal analogy between black hole spacetimes and ordinary thermodynamic systems. As the concept of a black hole's temperature is central to the study at hand, we sketch out one of many derivations of Hawking radiation here, and also demonstrate the important connection between the surface gravity of a horizon and the temperature its associated radiation.

To understand Hawking radiation at a fundamental level, a quantum description of both matter and gravity would be required. Fortunately, it suffices to consider the behaviour of quantum fields on a fixed classical black hole background, which amounts to taking the limit $m_p/M \to 0$ while keeping $r_h = 2GM$ fixed. For a solar mass black hole, we have

$$\frac{m_p}{M} = \frac{\sqrt{\hbar c/G}}{M_\odot} \approx 10^{-38} \ , \tag{1.53}$$

while for a supermassive black hole the value is many orders of magnitude smaller. For this reason, the behaviour of quantum fields in curved spacetimes can be understood in a semi-classical approximation in all but the most extreme scenarios, and the back-reaction of the fields on the geometry can be safely neglected.

Hawking radiation is rooted in the fact that in curved spacetimes, there is in general no unique definition of the vacuum state $|0\rangle$. As a result, and especially in time-dependent spacetimes, the vacuum state in at some early time $|0_i\rangle$ may not be equivalent to the

vacuum state at a later time $|0_f\rangle$. This can be interpreted as particle production resulting from the time-dependence of the gravitational field. To see this, consider a 4d massless scalar field ϕ with conjugate momentum π^a which satisfies the Klein-Gordon equation and equal time canonical commutation relation

$$\Box\phi = 0 \ , \qquad [\phi(x_i), \pi(y_j)] = i\delta^{(3)}(x_i - y_j) \tag{1.54}$$

The field ϕ can be expanded in terms of a complete basis of solutions to the wave equation as

$$\phi(x) = \int \frac{d^3p}{(2\pi)^3} \frac{1}{\sqrt{2\omega_p}} \left(a_p e^{-ip\cdot x} + a_p^\dagger e^{ip\cdot x}\right) \tag{1.55}$$

where $\omega_p = \sqrt{|p|^2 + m^2}$. The creation and annihilation operators a_p and $a_q^\dagger$ satisfy $[a_p, a_q^\dagger] = (2\pi)^3\delta^{(3)}(p-q)$, and the vacuum state $|0\rangle$ is defined as the state for which

$$a_p\,|0\rangle = 0 \tag{1.56}$$

for all p. In the above, plane-wave solutions were chosen for the field expansion, but we could in principle use any other orthonormal basis $\{f_p, f_p^*\}$ as well. In the asymptotic region, the field can be expanded as

$$\phi = \int_p \left(f_p a_p + f_p^* a_p^\dagger\right) \ , \tag{1.57}$$

where $\Box f_p = 0$. The $\{f_p\}$ are chosen to contain only positive frequency solutions with respect to some preferred time coordinate, and are orthogonal with respect to the Klein-Gordon inner product

$$(\phi_i, \phi_j) = -i \int_c \sqrt{k} \left(\phi_i \nabla_a \phi_j^* - \phi_j^* \nabla_a \phi_i\right) n^a \, d^3x = \delta_{ij} \ , \tag{1.58}$$

where Σ is a Cauchy surface and n^a is its normal. For the case of Hawking radiation, we are concerned with the Penrose diagram shown on the left side of Figure 1.1, which represents the formation of a black hole from collapsing matter. In the asymptotic past, one can define particle states (on the blue line) by choosing a set $\{f_p\}$ which satisfy (1.58) on $c = \mathcal{I}^-$, such that the solutions have positive frequency with respect to the null generators of $\mathcal{I}^-$ and can be written as in (1.57). a_p and $a_p^\dagger$ are then the creation and annihilation operators associated with the ingoing particle states, and since $\mathcal{I}^-$ is a Cauchy surface, the field can be written as (1.57) everywhere.

However, an observer in the distant future (at $\mathcal{I}^+$) does not have access to the entire spacetime, owing to the presence of the event horizon. While the red line $\mathcal{H} \cup \mathcal{I}^+$ in Figure 1.1 is a Cauchy surface, $\mathcal{I}^+$ itself is not. Particle states for observers outside the black hole must be defined by combining data on $\mathcal{H}$ and $\mathcal{I}^+$:

$$\phi = \int_p \Big(\underbrace{g_p b_p + g_p^* b_p^\dagger}_{\mathcal{H}} + \underbrace{k_p c_p + k_p^* c_p^\dagger}_{\mathcal{I}^+} \Big) \ . \tag{1.59}$$

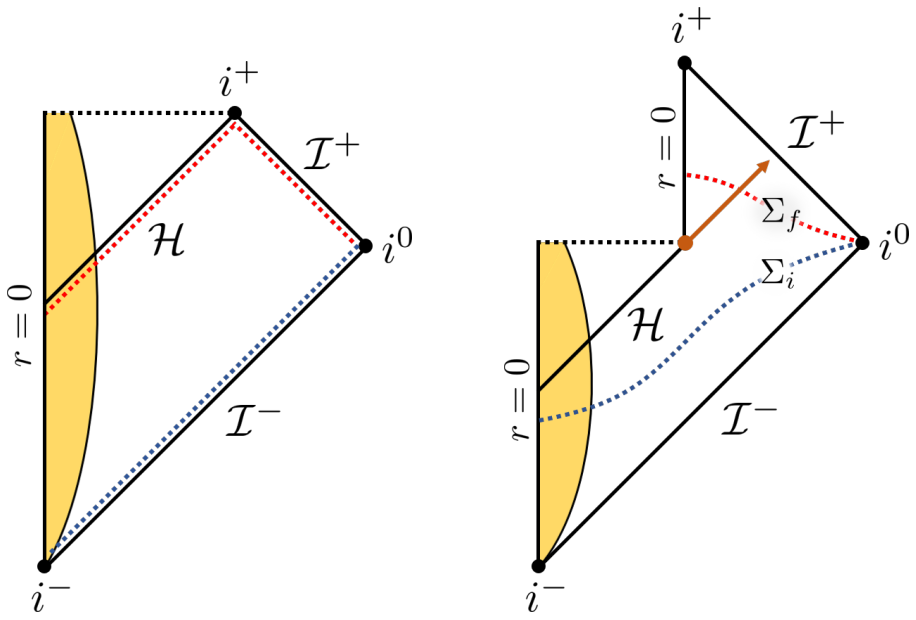

Figure 1.1: Penrose diagram of collapsing matter forming a black hole. **Left:** A classical black hole which forms through collapse but does not evaporate. Red and blue dashed lines represent (respectively) past and future Cauchy surfaces on which mode functions can be constructed. **Right:** A semi-classical black hole, which forms and later evaporates. The orange arrow represents the evaporation event, which appears instantaneous due to the conformal transformation.

The solutions $\{g_p\}$ are purely ingoing having support only on $\mathcal{H}$, while the $\{k_p\}$ are the outgoing modes with support on $\mathcal{I}^+$. Both sets of solutions independently satisfy (1.57) on their respective hypersurfaces. Finally, choosing $\{k_p\}$ to be positive frequency with respect to the generators on $\mathcal{I}^+$ allows for the interpretation of $\{c_p, c_p^\dagger\}$ as creation and annihilation operators for particle states in the asymptotic future. Since $\mathcal{I}^-$ is a Cauchy surface, one can express the solutions on $\mathcal{I}^+$ as a linear combination of the $\{f_p, f_p^*\}$, and the corresponding creation and annihilation operators as linear combinations of the a_p and $a_p^\dagger$'s. Explicitly, one has

$$c_i = \int_j \left(\alpha_{ij}^* a_j + \beta_{ij}^* a_j^\dagger\right) \ . \tag{1.60}$$

Since in general $\beta_{ij} \neq 0$, an initial vacuum state defined by $a_p \left|0\right\rangle = 0$ will not appear to be a vacuum state at $\mathcal{I}^+$. Using (1.60) one can write the expectation value for the number operator defined in the asymptotic future, where this becomes plain to see:

$$\langle N_p \rangle = \langle 0 \left| b_p^\dagger b_p \right| 0 \rangle = \int_q |\beta_{pq}|^2 \ . \tag{1.61}$$

Global analytic solutions to the wave equation for ϕ do not exist in the Schwarzschild spacetime, preventing an explicit calculation of β_{pq}. However, one can determine the asymptotic form of β_{pq} by recasting the Klein-Gordon equation as a 1-D scattering problem

with an effective potential due to the presence of the black hole (see [1] for explicit details). The result is that

$$\langle N_p \rangle = \Gamma_p \times \frac{1}{e^{\frac{2\pi\omega_p}{\hbar\kappa}} - 1} \tag{1.62}$$

where Γ_p is the classical absorption coefficient for the scattering of the field off the black hole, and κ is the surface gravity. This is just a thermal spectrum at a temperature

$$T = \frac{\kappa}{2\pi} \ . \tag{1.63}$$

Evidently there is a flux of energy escaping to infinity from the black hole, which one can show necessarily causes the mass of the black hole to decrease. This is evaporation via Hawking radiation. Though we only considered the presence of a massless scalar field here, similar calculations can be performed for fermions, linearized metric perturbations, and charged fields. All are found to have a blackbody spectrum as in (1.62). These results also hold for rotating black holes despite the initial stationarity assumption. For massive fields the frequency ω_p contains the rest mass of the corresponding particle, and so the black hole will only radiate such particles in an appreciable amount when $T > m$. Therefore, for the majority of the lifetime of a typical black hole the Hawking radiation consists of photons and gravitons.

The dramatic implications of the above extend beyond simply allowing for the interpretation of a black hole as a thermodynamic object. As the black hole evaporates, its mass will decrease until (presumably) the entire rest mass of the black hole escapes in the form of radiation, leaving again an asymptotically flat space as illustrated on the right side of Figure 1.1. The issue that arises here touches at the foundations of quantum mechanics. Evidently Σ_i is a Cauchy surface while Σ_f is not, the implication being that unitarity is violated by black hole evaporation, since the final state of the fields present is a thermal state and thus contains no information about the state of the matter which formed the black hole (or anything else which may have fallen into it during its lifetime). This is the famous *black hole information paradox*. Though no complete answer to the problem of information loss in black hole evaporation exists today, its attempted resolution has served as the inspiration for a great number of theoretical advances in physics [80].

The temperature in more general settings

As it happens, the relationship (1.63) between the temperature of Hawking radiation and the surface gravity of the event horizon is quite general. In the previous section we considered a static, spherically symmetric spacetime representing a Schwarzschild black hole. In fact, that the temperature of the thermal state in the asymptotic region of a black hole spacetime is proportional to the surface gravity of the event horizon is true for a wide class of black hole spacetimes, including charged Reissner-Nordström black holes and spinning Kerr black holes. Moreover, Gibbons and Hawking showed that similar arguments apply to other horizons as well, in particular the cosmological horizon associated with $\Lambda > 0$ (de Sitter) solutions to Einstein's equations [81]. They showed that an observer in de Sitter

space measures an isotropic background of thermal radiation with temperature

$$T = \frac{\kappa_{\text{cosmo}}}{2\pi} \ . \tag{1.64}$$

This temperature enters into a thermodynamic description of the cosmological horizon through the first law (1.32) the same way that the horizon temperature would, except the area A is now the proper area of the cosmological horizon. The entropy S can thus be regarded as a measure of the lack of knowledge about the universe beyond the cosmological horizon. The general relation (1.63) allows one to determine easily the temperature associated with a given horizon. Consider a general static, spherically symmetric metric of the form

$$ds^2 = -f(r)dt^2 + g(r)dr^2 + r^2 d\Omega^2 \ . \tag{1.65}$$

with the event horizon being located at $r = r_h$. Recall that the surface gravity for a Killing horizon with Killing vector k^a is defined as

$$\kappa^2 = -\tfrac{1}{2} \left(\nabla_a k_b\right) \left(\nabla^a k^b\right) \ . \tag{1.66}$$

The normalized time translation Killing vector associated with the metric above metric is simply $k^a = \delta^a_t$, so that on the event horizon

$$\kappa = \lim_{r \to r_h} \frac{1}{2} \frac{\partial_r f(r)}{\sqrt{f(r) g(r)}} \ . \tag{1.67}$$

As in the Schwarzschild spacetime, it will often be the case that $g(r) = f^{-1}(r)$, and so we simply have

$$\kappa = \tfrac{1}{2} f'(r)\big|_{r=r_h} \qquad \rightarrow \qquad T_h = \left.\frac{f'(r)}{4\pi}\right|_{r=r_h} \tag{1.68}$$

where the prime indicates a derivative with respect to the argument, and the result is evaluated at $r = r_h$. For the asymptotically flat Schwarzschild black hole, this gives the well-known result of $T_h = (8\pi M)^{-1}$. One could just as well apply (1.68) to the cosmological horizon (if it exists) to determine its temperature instead.

1.4.3 The Hawking-Page Transition

Having previously alluded to the Hawking-Page transition and remarked on its theoretical importance, we should be precise about what the transition represents and how it fits into the larger theoretical context. The Hawking-Page transition represents a phase transition from radiation to a 'large' black hole in asymptotically anti-de Sitter spacetimes (ones in which $\Lambda < 0$). Unlike flat space the (conformal) boundary of AdS is *timelike*, allowing massless particles to reach the boundary in finite proper time. Almost universally, reflecting boundary conditions are imposed at this boundary so that AdS can be treated as a closed system. As a result, massless particles are reflected back towards the center upon reaching $r = \infty$. Outgoing massive particles return to the center in similar fashion, owing to

the attractive nature of the potential when $\Lambda < 0$. This peculiar feature of AdS leads immediately to an interesting observation: while a small black hole may evaporate quickly (before any radiation reaches the boundary), a sufficiently large black hole may achieve a state where the rate of outgoing radiation matches that of the ingoing reflected radiation, rendering the black hole stable.

The two situations described above represent equilibrium states, with the entire spacetime being described by a single temperature T (either that of the radiation or of the large black hole). It should be clear that if one had a mechanism by which to vary the temperature of the spacetime, at some point a phase transition will occur between pure radiation (often called empty AdS) and a large black hole. This idea can be made precise by considering the contributions of both the radiation and large black hole to the partition function $\mathcal{Z}$. Using (1.29), one can evaluate the contribution to the partition function from both the AdS geometry and the black hole geometry. In Chapter 2 we will see the details of how such a calculation is performed. For now, we merely quote the result for the 4-dimensional case:

$$I_E\left[g_{AdS}\right] = -\frac{\beta\,\Omega_2}{4\pi G}\frac{1}{\sqrt{1+1/r_c^2}}\,r_c^2\left(1+r_c^2\right) \tag{1.69}$$

$$I_E\left[g_{sch}\right] = I_E\left[g_{ads}\right] + \frac{\beta\,\Omega_2}{16\pi G}\,r_h\left(1-r_h^2\right) + \mathcal{O}\left(1/r_c^2\right). \tag{1.70}$$

Here, r_h is the horizon radius, $\beta = 1/T$ is the inverse temperature, and r_c is some large but finite cutoff radius at which various subtraction terms should be matched to remove any divergences. It is clear from (1.70) that when $r_h > 1$, the dominant contribution to the partition function is $I_E[g_{sch}]$, while for $r_h < 1$ it is $I_E[g_{ads}]$. At $r_h = 1$, the quantity $I_E\left[g_{sch}\right] - I_E\left[g_{ads}\right]$ changes sign, and a transition occurs between the radiation and large black hole phases. This is the Hawking-Page transition.

In classical thermodynamic terms, this behaviour is typically captured by the free energy of the system. For an isolated system at constant temperature, the thermodynamic potential of interest is the Helmholtz free energy

$$F = E - TS\ . \tag{1.71}$$

The free energy is a useful quantity since the equilibrium state of a system at a given temperature always corresponds othe global minimum of F. Another way to see the Hawking-Page transition is to simply evaluate F given the appropriate definitions of E, T, and S for the AdS black hole, and compare it to the free energy of the radiation phase (which is always taken to be $F = 0$). Where the free energy of the black hole becomes lower than that of the radiation phase, the Hawking-Page transition occurs. This is shown in Figure 1.2.

As we have noted, there is extensive theoretical interest in the Hawking-Page transition. In the context of AdS/CFT, contributions from the bulk geometric states to the partition function have a clear interpretation in terms of boundary CFT states. In fact, the bulk partition function for the geometries exactly maps to the thermal partition function for

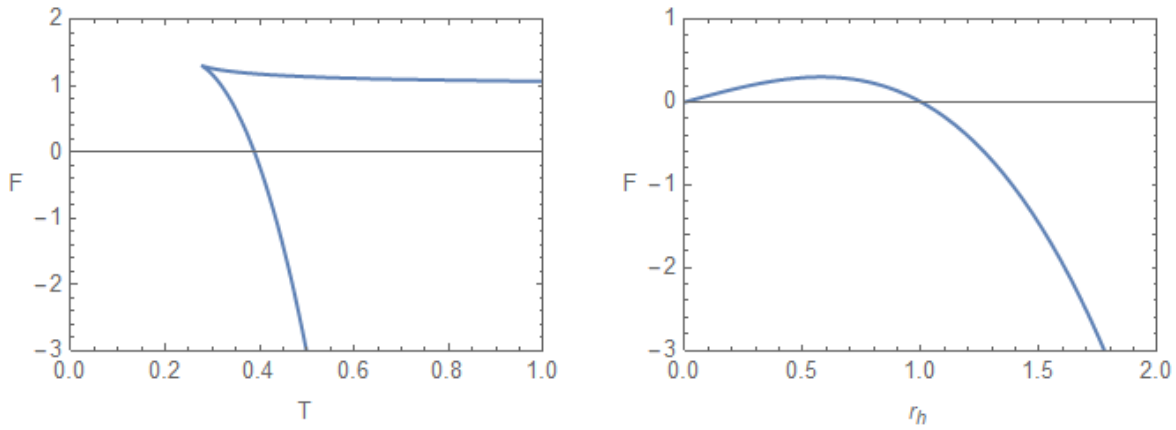

Figure 1.2: The free energy F of the Schwarzschild black hole, demonstrating the presence of a Hawking-Page transition. **Left:** F as a function of temperature T. When $T < T_c$, empty space is thermodynamically preferred. When $T > T_c$, the large black hole phase minimizes F instead. **Right:** F as a function of horizon radius r_h. The free energy (and thus the action) changes sign when the black hole becomes large enough.

the boundary CFT, the most well-known example being the map between type IIb string theory on $AdS_5 \times S^5$ and $\mathcal{N} = 4$ super Yang-Mills theory on the boundary of AdS_5 [4]. The bulk $I_E[g_{ads}]$ contribution represents a low temperature confining phase in the CFT, while the $I_E[g_{sch}]$ contribution represents a high temperature deconfined free gas phase. This is the often cited AdS/CFT interpretation of the bulk Hawking-Page transition as a boundary deconfinement transition (as occurs in a quark-gluon plasma for example).

The Hawking-Page transition provides a partial resolution to the black hole information paradox, as the transition between the black hole and radiation phase (which appears to not be unitary, at least without a quantum theory of gravity) has an expressly unitary description in terms of the boundary CFT. As a result, it is clear that information is preserved during the evaporation process.[8]

The theoretical power of the AdS/CFT correspondence has motivated a very large number of investigations into the phase structure of bulk gravitational theories, as any modifications to the description of the bulk transition (be it from the inclusion of charge, angular momentum, higher curvatures, etc.) will necessarily correspond to a modification of the boundary CFT description. More exotic phenomena beyond the simple radiation-black hole Hawking-Page transition are possible as well, each having a unique interpretation on the CFT side. The hope is that a complete understanding of the bulk phase structure of black holes in Einstein gravity and its extensions will allow for insights into strongly coupled CFT physics, and this has indeed proven to be the case [83].

These motivations extend to the asymptotically de Sitter cases we study here, owing to recent developments of the dS/CFT correspondence [39]. Though dS/CFT is still in its

[8]Computing exactly what happens at the transition remains an open problem, namely, the Page curve cannot be constructed in this way [82]. In this sense the issue is only partially resolved.

infancy compared to its anti-de Sitter counterpart, we expect that our understanding of the phase structure of asymptotically dS black holes will be widely applicable to the study of those boundary CFTs as well (once we have achieved a sufficient technical maturity concerning dS/CFT).

1.4.4 The Extended Phase Space and Variable Λ

In discussing the analogy between the first law of thermodynamics for traditional systems (1.31) and the first law of black hole thermodynamics (1.32), there is a notable absence of a pressure-volume term on the gravity side. In the asymptotically flat case considered in the early work of Bardeen and collaborators, there is indeed no variable in the black hole description that has a natural interpretation as a thermodynamic pressure, and so on the surface the absence of a pressure-volume term is perhaps expected.

This expectation changes when one considers solutions with non-zero cosmological constant, as Λ itself can be seen to act as a kind of pressure. Consider moving the contribution from the cosmological constant to the matter side of the field equations:

$$G_{ab} + \Lambda g_{ab} = 8\pi G T_{ab} \quad \rightarrow \quad G_{ab} = 8\pi G(T_{ab} - \underbrace{\tfrac{1}{8\pi G}\Lambda g_{ab}}_{T^{\Lambda}_{ab}}) \ . \tag{1.72}$$

What kind of stress energy tensor is this reminiscent of? A perfect fluid with energy density d and isotropic pressure p has a stress-energy tensor

$$T_{ab} = \mathrm{diag}[\rho, p, p, p] \ . \tag{1.73}$$

Therefore, the cosmological constant acts like an isotropic perfect fluid with

$$\rho_{\Lambda} = \frac{\Lambda}{8\pi G} \ , \qquad p_{\Lambda} = -\rho_{\Lambda} \ . \tag{1.74}$$

Motivated by the parallels between a non-zero cosmological constant and a universal fluid, it is natural to ask how Λ might enter into the first law. This occurs naturally when one considers variations of Λ, an idea that has been explored at least as early as 1985 by Teitelboim [84]. Since then there has been extensive study of this idea, notably in [22] where various scaling arguments were used to construct an *extended* first law for AdS black holes which accounts for variations in Λ. Previous work suggested that a pressure-volume term could be incorporated into the first law through explicit calculation of various quantities for a given spacetime [85–87], while the results of Kastor and collaborators showed that this can be achieved in the general case, without reference to a particular solution. In that work, a Hamiltonian perturbation analysis was used to show that variations in the cosmological constant $\delta\Lambda$ lead to an expression for the mass variation which reads

$$\delta M = \frac{\kappa}{8\pi G}\delta A + \frac{\Theta}{8\pi G}\delta\Lambda \ . \tag{1.75}$$

The quantity Θ is given by a Komar integral as

$$\Theta = -\left[\int_{\partial\Sigma_\infty} d\Sigma_{ab}\left(\omega^{ab} - \omega^{ab}_{AdS}\right) - \int_{\partial\Sigma_\mathcal{H}} d\Sigma_{ab}\omega^{ab}\right] . \tag{1.76}$$

where ω^{ab} is the Killing potential (satisfying $\xi^b = \nabla_a\omega^{ab}$) and $\partial\Sigma$ is the codimension-2 surface representing the boundary of a suitably chosen hypersurface Σ, with volume element $d\Sigma_{ab}$. The quantity $\omega^{ab}_{\rm AdS}$ serves to renormalize the Killing potential which formally diverges in AdS. The Killing vector k^a is chosen to be the horizon generator, which approaches $\partial/\partial t$ in the asymptotic region given an appropriate choice of coordinates. Σ is taken to extend from the bifurcation surface $\partial\Sigma_\mathcal{H}$ to a boundary at infinity $\partial\Sigma_\infty$, whose unit normal vector is $n^a = f\nabla_a t$. If Σ is further orthogonal to k^a, then $k^a = fn^a$ and the integral above can be written

$$\int_{\partial\Sigma} dS_{ab}\omega^{ab} = -\int_\Sigma d^{D-1}x\sqrt{-g^{(D)}} . \tag{1.77}$$

which is just the negative of the volume of the surface Σ between the horizon and infinity. The second integral can be written in a similar way, giving

$$-\Theta = V_{AdS} - V_{bh} \equiv V \tag{1.78}$$

so the potential Θ entering in the first law has the interpretation of the (negative of the) volume excluded from the spacetime by the presence of the black hole. We saw previously that Λ could further be interpreted as a fluid with pressure given by

$$P = -\frac{\Lambda}{8\pi G} \qquad (\text{in } d = 4) . \tag{1.79}$$

Therefore, $\Theta\delta\Lambda/8\pi G = V\delta P$, and (1.75) becomes the extended first law of thermodynamics

$$\delta M = T\delta S + V\delta P , \tag{1.80}$$

where the thermodynamic volume V appears as the quantity conjugate to the pressure,

$$V \equiv \left(\frac{\partial M}{\partial P}\right)_{S,Q,J} . \tag{1.81}$$

An important distinction between this law and the first law without variable Λ is that the right hand side now represents the variation of the *enthalpy* $H = U + PV$ of the system. We therefore identify the mass M with H rather than the internal energy U as is the case in (1.32). The relation (1.80) can be suitably generalized to include charge and angular momentum, which enter in the same way here as they do in the regular phase space. In the case of asymptotically de Sitter ($\Lambda > 0$) spacetimes, the Killing field k^a becomes spacelike outside of the cosmological horizon, and so the conserved charge one would construct at infinity cannot have the interpretation as a mass as it is now 'conserved in space' rather than in time. Of course if one does not integrate past the cosmological horizon, no such issue arises, a fact that will be useful later in this work.

The remainder of our work will take place in this *extended phase space*, where in general the cosmological constant is related to the thermodynamic pressure through

$$P = -\frac{\Lambda}{8\pi} = -\frac{(d-1)(d-2)}{16\pi l^2} \ , \tag{1.82}$$

where l is the de Sitter length scale (see Section 1.5). In de Sitter space, the cosmological constant is positive, so the variable P is better thought of as a *tension* rather than a pressure. The extended phase space is the natural context in which to study the phase structure of black hole spacetimes with non-zero Λ, where many interesting thermodynamic phenomena have been uncovered including triple points, re-entrant phase transitions, superfluid transitions, and more [16, 33, 88]. These phenomena are not only interesting in their own right, drawing parallels between some of the most exotic objects that appear in our universe and everyday thermodynamic processes like the liquid-gas phase transition of ordinary water, but also have implications for gauge theories through gauge/gravity duality, each example having a non-trivial dual description in terms of the boundary CFT [28, 30, 89].

One common feature in the extended phase space is a striking analogy between the liquid-gas transition of a Van der Waals fluid and a small-large black hole phase transition in AdS spacetimes. A Van der Waals fluid is characterized by an equation of state

$$P(T, v) = \frac{T}{v-b} - \frac{a}{v^2} \tag{1.83}$$

where a accounts for the attractive forces between constituent particles and b accounts for their finite size. This equation of state accurately models the behaviour of fluids above their critical temperature and also captures the behaviour of fluids at the liquid-gas transition. Interestingly, the equation of state for AdS black holes in the extended phase space displays similar qualitative behaviour. For a 4D charged AdS black hole one has [90]

$$P(T, v) = \frac{T}{v} - \frac{1}{2\pi v^2} + \frac{2Q^2}{\pi v^4} \ . \tag{1.84}$$

There is a critical point $\{P_c, T_c, v_c\}$ at which the phase transition becomes second-order, which occurs when

$$\frac{\partial P}{\partial v} = \frac{\partial^2 P}{\partial v^2} = 0 \ . \tag{1.85}$$

For the black hole equation of state, the critical ratio $P_c T_c / v_c = 3/8$ is identical to that of the Van der Waals fluid, as are the associated critical exponents which govern the scaling behaviour of various quantities near this point. This remarkable similarity between fluid phases and black hole phases extends to many other cases [91]. We will see a departure from this behaviour for asymptotically de Sitter black holes, where the presence of the isothermal cavity leads to an equation of state that is nonlinear in T and does not support Van der Waals-like transitions. These de Sitter transitions are thus of a decidedly different character than their AdS counterparts, at least as far as this 'universal' behaviour is concerned.

1.5 de Sitter and its Problems

Much of the studies herein concern asymptotically de Sitter spacetimes for the motivations discussed in the introduction. In this section we define de Sitter spacetimes and their asymptotically related variants, describe some of their properties, and discuss the difficulties associated with providing a thermodynamic description of these spaces.

The d-dimensional de Sitter space, denoted dS_d, is a maximally symmetric solution to Einstein's equations with positive cosmological constant ($\Lambda > 0$). It can be understood as a hyperbolic submanifold of $d+1$ dimensional Minkowski space $\mathcal{M}^{1,d}$ satisfying the constraint

$$-x_0^2 + x_1^2 + \cdots + x_d^2 = l^2 \ . \tag{1.86}$$

Here, x_i are coordinates on $\mathcal{M}^{1,d}$ and l is the de Sitter length scale. Through the Einstein equations (1.15) the de Sitter length can be related to the cosmological constant Λ and scalar curvature R as

$$\Lambda = \frac{(d-1)(d-2)}{2l^2} = \frac{(d-2)}{2d}R \ , \tag{1.87}$$

from which we see that dS_d is a constant curvature space. If desired, l can always be set to unity by a Weyl rescaling. De Sitter space has a cylindrical topology $\mathcal{R} \times S^{d-1}$, and inherits its symmetry group $SO(1,d)$ from its embedding space (a Lorentzian manifold of dimension $d+1$). In static coordinates, the metric takes the form

$$ds^2 = -\left(1 - \frac{r^2}{l^2}\right) dt^2 + \left(1 - \frac{r^2}{l^2}\right)^{-1} dr^2 + r^2 d\Omega_{d-2}^2 \ , \tag{1.88}$$

where $d\Omega_{d-2}^2$ is the metric on the unit $(d-2)$ sphere. It is clear from (1.88) that the vacuum spacetime possesses a horizon at $r = l$, the *cosmological horizon*. In Figure 1.3 we show two convenient representations of dS_d, using static coordinates and Kruskal coordinates.

It should be clear from the Penrose diagram in Figure 1.3 that the causal structure of dS_d does not allow any single observer to access the entire spacetime. This is contrary to the experience of observers in Minkowski space, whose past lightcones will eventually contain the entire spacetime. In de Sitter, an observer sitting at the north pole lives in a causal patch defined by $\mathcal{O}^+ \cap \mathcal{O}^-$ whose diagonal boundaries represent the cosmological horizon. Furthermore, while there exists a well-defined future directed timelike killing vector field $\partial/\partial t$ in the left causal patch, this vector field becomes spacelike in the upper and lower patches, and is past-directed in the right patch. As a result, Hamiltonian time evolution cannot be properly defined for the entire spacetime, and we have issues defining thermodynamic quantities like energy or mass even before considering the presence of a black hole.

Further difficulties arise when we generalize to asymptotically de Sitter black hole

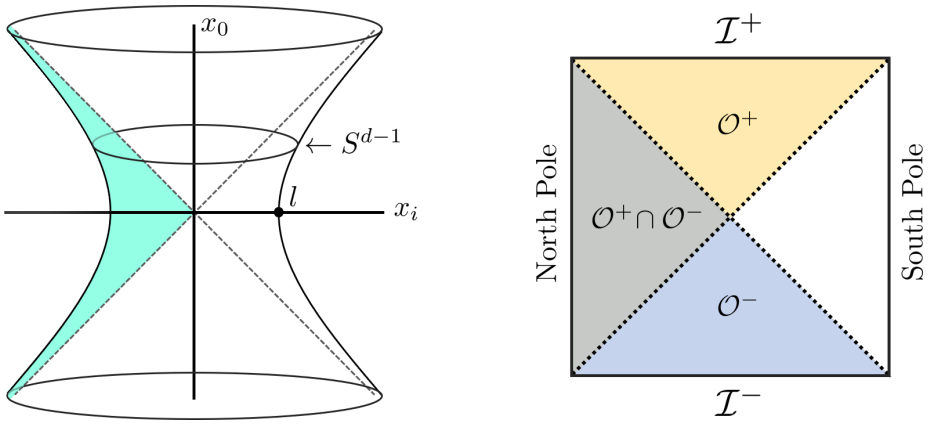

Figure 1.3: Representations of de Sitter space dS_d. **Left:** The hyperboloid defined by (1.86) embedded in $\mathcal{M}^{1,d}$ with $(d-1)$ coordinates suppressed. Static coordinates only cover the shaded region inside the de Sitter horizon (represented by the curved lines). **Right:** Penrose diagram of dS_d. Points in the interior are S^{d-2}, with future (past) timelike infinity represented by $\mathcal{I}_+$ ($\mathcal{I}_-$). The yellow region $\mathcal{O}^+$ represents the causal future of an observer sitting at the north pole, while their causal past $\mathcal{O}^-$ is represented by the blue region.

spacetimes. The simplest example is the Schwarzschild-de Sitter metric:

$$ds^2 = -\left(1 - \frac{2m}{r} - \frac{r^2}{l^2}\right) dt^2 + \left(1 - \frac{2m}{r} - \frac{r^2}{l^2}\right)^{-1} dr^2 + r^2 d\Omega_{d-2}^2 \,, \tag{1.89}$$

This metric represents a static, uncharged black hole in de Sitter space. The study of the thermodynamic properties of such a spacetime faces an immediate problem due to the presence of the cosmological horizon: with a temperature generically different from the black hole horizon, the system is manifestly out of equilibrium. To see this, consider the definition of temperature given by (1.63). For the metric (1.89), the temperature associated with the event horizon is

$$T_h = \left.\frac{f'(r)}{4\pi}\right|_{r=r_h} = \frac{\kappa_h}{2\pi} = \frac{1 - \Lambda r_h^2}{4\pi r_h} \tag{1.90}$$

where κ_h is the surface gravity of the bifurcate horizon, r_h is the location of the event horizon (given by the smallest positive real root of $f(r) = 0$), and the relation (1.87) has been used. For $\Lambda \to 0$, this gives the Hawking temperature of a Schwarzchild black hole as observed from infinity. Of course, no such observer exists in SdS_d due to the presence of the cosmological horizon. Rather, one should consider an observer situated between both horizons, $r_h < r < r_{\text{cosmo}}$. As we have noted however, such an observer will observe isotropic thermal radiation from the cosmological horizon as well, with a temperature of

$$T_{\text{cosmo}} = \left.\frac{f'(r)}{4\pi}\right|_{r=r_{\text{cosmo}}} = -\frac{\kappa_{\text{cosmo}}}{2\pi} = -\frac{1 - \Lambda r_{\text{cosmo}}^2}{4\pi r_{\text{cosmo}}} \tag{1.91}$$

which is in general different from the temperature of the black hole (1.90). Therefore, and observer in the region between the two horizons will never see an equilibrium state, as there will always be an apparent heat flux from one horizon to the other (except for in the Nariai limit, where $r_h = r_{\text{cosmo}}$). Furthermore, there is no single coordinate system that can be analytically extended from one horizon to the other. These are perhaps the most salient difficulties associated with applying the usual techniques for understanding AdS black hole thermodynamics—how can one achieve equilibrium?

A number of approaches have been pursued over the years which avoid the issues raised here in various ways, though each with their own difficulties or limitations.[9] One method is to assign a single equilibrium temperature to the system which accounts for both the event and cosmological horizon temperatures. This 'effective temperature' approach relies on enforcing the first law to hold for the system, and then *defining* the effective temperature to be the coefficient of the entropy variation dS [47, 48]. The issue with this is twofold: for one, the resulting effective temperature T_{eff} is in general not the temperature experienced by any observer in the spacetime (and can sometimes be negative). For two, while indeed a single temperature has been assigned to the spacetime, no mechanism has actually been employed to keep the system at equilibrium, and one is forced to question the application of equilibrium thermodynamics to the situation.

Another method involves fixing certain parameters of the system to set the two horizon temperatures to be equal, as was done in [49]. In that example, 5-dimensional charged Gauss-Bonnet black holes in asymptotically de Sitter space are considered, which are conformally coupled to a scalar field. We omit the details of the theory, noting only that the metric function for that class of black hole solutions takes the form

$$f(r) = 1 - \frac{8m}{3\pi r^2} + \frac{4\pi q^2}{3r^4} - \frac{\Lambda r^2}{6} - \frac{H}{r^3} \ , \tag{1.92}$$

where H is a parameter associated with the scalar field. As it happens, there is enough freedom in the choice of parameters in (1.92) to make the temperature associated with the event horizon (1.90) equal to that of the cosmological horizon (1.91) for certain values of $\{m, q, H, \Lambda\}$, so that there is no heat flux in the region between the two. While the advantage here compared to the effective temperature approach is that equilibrium is expressly achieved, one is limited to studying choices of parameters for which the horizon temperatures coincide, which is often not possible in a given theory if there are insufficient degrees of freedom to work with.

In order to make progress in the largely unexplored realm of de Sitter black hole thermodynamics, we will use a Euclidean path integral approach that surmounts the difficulties presented above. As described in Section 1.3, the thermal partition function $\mathcal{Z}$ for a system at temperature $T = \hbar/k_b\beta$ can be related to a functional integral over the Euclidean section of the theory. When applied to gravitating systems, a series of approximations allows one to evaluate the contribution of a given classical metric to the full partition function, and various thermodynamic quantities associated with the metric can be readily extracted.

[9] See also [92, 93] for other recent developments on this subject.

This approach was first used by Gibbons and Hawking [50] to compute the entropy of a Schwarzschild black hole from a statistical mechanical description of the gravitational field.

The advantages of the Euclidean approach over those previously mentioned are numerous. First, a clear semi-classical description of the origin of black hole entropy is available, with the added advantage that we know exactly what the equilibrium temperature T means. Second, our analysis is rooted in a much more fundamental description of the gravitational field, as the Euclidean path integral formally defines a quantum theory of gravity [94]. Third (and perhaps most relevant for our purposes) is that one is free to fix boundary-value data as appropriate for the problem at hand. Physically, this will be interpreted as a mechanism by which thermal equilibrium is ensured. In the following chapter, we will describe the application of Euclidean path integral methods to the problem of asymptotically de Sitter spacetimes, and clarify the advantages over previously used methods.

Chapter 2

De Sitter Black Holes in Cavities

Having laid the groundwork for the explorations to come, we now move into the main body of this thesis: the study of the thermodynamic properties of a variety of asymptotically de sitter black hole spacetimes. In this chapter we present an analysis of the simplest examples, namely the Schwarzschild-de Sitter and Reissner-Nordström-de Sitter black holes. We use a Euclidean action (or 'cavity') approach, where boundary value data is fixed on a finite radius cavity around the black hole. This imposes a condition for thermodynamic equilibrium for these otherwise out of equilibrium systems. Using similar methods, a cursory exploration of de Sitter black holes was done by Carlip and Vaidya [53], representing at the time the only known attempt at understanding de Sitter black hole thermodynamics in this way (aside from the seminal work of Brown and collaborators [52, 95]). However, these early attempts suffer from a number of issues, including a counter-intuitive choice of reference spacetime for the energy, and the lack of an explicit check of the first law. Furthermore, variations of Λ are not taken into account (indeed, the work in [52] considers only asymptotically flat black holes), adn attention is not given to the construction of a Smarr-like relation. In this chapter, we will resolve many of these issues, and explore to a much greater extent the phase structure of these black holes. We demonstrate new thermodynamic features not previously seen in this realm, discuss the extent to which the analogy between black holes and Van der Waals fluids persists in the de Sitter case, and examine the impact the presence of a cosmological horizon has on the thermodynamics.

We work in the extended phase space outlined in Section 1.4.4 for the reasons mentioned there, and also to make contact with a wealth of previous work in asymptotically AdS spacetimes. In AdS black holes, an extended phase space analysis reveals interesting connections between black hole phase transitions and those of ordinary fluid systems. We will find that de Sitter black holes exhibit behaviour in many ways analogous to that of their AdS counterparts, with a Hawking-Page phase transition appearing for uncharged black holes, and a small/large black hole phase transition appearing in the charged case. Despite this similarity, we show that the equation of state for these black holes has a non-linear temperature dependence and therefore cannot support behaviour characteristic of a Van der Waals fluid the way that AdS black holes do. Finally, we find a new type of

compact first-order phase transition in charged de Sitter black holes, which exists within a finite pressure range and is unlike any phase transition seen thus far in asymptotically AdS black holes. This manifests as a 'swallowtube' in the phase diagram, whose character differs dramatically from the swallowtails seen in AdS due to the cosmological horizon.

This chapter is organized as follows: In Section 2.1, we introduce the 'cavity' approach, outlining the general procedure we will use throughout this work to study the critical phenomena of asymptotically de Sitter black holes. We further comment on how the issues raised in Section 1.5 are resolved by this method. In Section 2.2, we show explicitly how the Euclidean path integral is evaluated. In Section 2.4 we examine in detail the Schwarzschild-de Sitter (uncharged) case, finding that black holes undergo a standard Hawking-Page phase transition despite the inclusion of the pressure-volume term in the first law. In Section 2.5 we examine Reissner-Nordström-de Sitter (charged) black holes, finding a number of new phenomena including a small to large black hole phase transition analogous to those found in AdS spacetimes, and a pressure-dependent compact phase transition.

2.1 Thermodynamics of Black Holes in a Cavity

Our treatment of black hole thermodynamics is inspired by methods used by Braden, Brown, Whiting, and York [52], where equilibrium is achieved by fixing boundary value data on a finite-radius surface within the spacetime (the cavity). By imposing reflecting boundary conditions on the surface of the cavity, equilibrium is guaranteed. There is also a flexibility in the choice of ensemble, which simply depends on which data is chosen at the cavity. We work in the canonical ensemble, where the temperature and charge are fixed on the boundary. In de Sitter spacetime, the backreaction of radiation near the event horizon will tend to *lower* the temperature of the spacetime [96]. We ignore such backreaction effects in the present analysis, assuming that the evaporation timescale is small compared to the typical timescale of the phase transitions in the system. Unlike previous work in this area, we will also interpret the cosmological constant as a thermodynamic pressure according to the discussion in Section 1.4.4, using the relation

$$P = -\frac{\Lambda}{8\pi} \tag{2.1}$$

where $P < 0$ when Λ is positive. As noted previously, although the physical interpretation of negative P is a *tension*, we shall continue to refer to it as pressure for the sake of clarity. The identification above will allow us to study the equation of state of these black holes in the extended phase space, where the analogy between the first law of thermodynamics and black hole thermodynamics is complete [34].

Let us first outline the general procedure for studying the thermodynamic properties and phase structure of a given spacetime/theory using the cavity approach. The steps involved are as follows:

1. Evaluate the (on-shell) Euclidean action I_E for the given theory/spacetime, with suitable choice of boundary conditions at finite radius.

2. Using I_E, determine the thermodynamic quantities relevant to the chosen ensemble (such as the mass M, entropy S, temperature T, or energy E).

3. Construct the free energy appropriate to the ensemble (Gibbs or Helmholtz). This quantity will be minimized by the thermodynamically preferred state and can thus be used to study the phase structure.

The above represents a minimal procedure for studying the phase structure of a given theory or spacetime. One may be interested in more than just the presence of phase transitions within a given system, and though many of our discussions will center around phase structure, indeed we will consider other thermodynamic properties as well. For example, one can study the (extended) first law and Smarr relation for these systems, and use them to determine other thermodynamic potentials involved in the description such as the volume V, surface tension λ, or electric potential Φ. One can also determine the equation of state $P(T, V)$ for a given spacetime and examine the extent to which the phase transitions are analogous to the Van der Waals phase transitions that occur in everyday fluids (as seen in asymptotically AdS examples). We will do all of the above. In the next section, we will give an explicit demonstration of step 1 for the simplest possible spacetime where this cavity approach is applicable, the asymptotically flat Schwarzschild black hole.

2.2 Evaluating the Euclidean Action

As described in Section 1.3, various thermodynamic quantities of interest for a given spacetime can be obtained through the Euclidean path integral. Here, we wish to clarify the technical details involved in the explicit computation of the Euclidean action, a procedure we will use repeatedly in the investigations to come. The example here will be for an asymptotically flat Schwarzschild black hole. The Euclidean action I_{Total} for the black hole with boundary $\partial\mathcal{M}$ is given by the Einstein-Hilbert action with the Gibbons-Hawking boundary term:

$$\begin{aligned} I_{\text{Total}} &= I_E - I_0 \\ &= -\frac{1}{16\pi}\int_{\mathcal{M}} d^4x\sqrt{g}\,R + \frac{1}{8\pi G}\int_{\partial\mathcal{M}} d^3x\sqrt{k}\,K - I_0 \end{aligned} \tag{2.2}$$

The definitions follow those of Section 1.2, where g is the bulk (Euclideanized) metric, R is the Ricci scalar, K is the trace of the extrinsic curvature of the boundary $\partial\mathcal{M}$, k is the boundary metric, and we have set $G = 1$. I_0 is a subtraction term that is chosen to properly normalize the action. One way to understand how this subtraction term arises is the following. Recall from Section 1.3 that in the semiclassical approximation the partition

function is related to the Euclidean action by

$$\mathcal{Z} = \int \mathcal{D}g\, e^{-I_E} \sim \sum_{g_{cl}} e^{-I_E[g_{cl}]} \tag{2.3}$$

where the second equality follows from the saddle-point approximation and I_E is given by (2.2). In the present case, the classical metrics g_{cl} that contribute to I_E are the Schwarzschild and Minkowski metrics, g_{sch} and g_{flat}. What we would like to do is isolate the contribution to the partition function $\mathcal{Z}$ coming from just the black hole. However, merely evaluating the contribution to $\mathcal{Z}$ coming from $I_E[g_{sch}]$ does not accomplish this, as the Euclidean action for the Schwarzschild metric also contains a large flat space contribution[1]. By subtracting from $I_E[g_{sch}]$ the same action evaluated for the Minkowski metric $I_E[g_{flat}]$ (with the metrics matched at the boundary), we are effectively removing the 'non-black hole' part of the Schwarzschild metric's contribution to the partition function. With this subtraction in mind, the total action becomes

$$I_{\text{Total}} = \underbrace{-\frac{1}{16\pi}\int\sqrt{g}\ R\ d^4x + \frac{1}{8\pi}\int\sqrt{k}\ K\ d^3x}_{\text{Schwarzschild contribution}} + \underbrace{\frac{1}{16\pi}\int\sqrt{g_0}\ R_0\ d^4x - \frac{1}{8\pi}\int\sqrt{k_0}\ K_0\ d^3x}_{\text{Flat space subtraction}}$$

$$ds^2 = f(r)d\tau^2 + \frac{dr^2}{f(r)} + r^2\Big(d\theta^2 + \sin^2(\theta)d\phi^2\Big)\ , \qquad f(r) = 1 - \frac{r_h}{r} \tag{2.4}$$

where R_0 and K_0 are the Ricci scalar and boundary extrinsic curvature in the reference spacetime, and ds^2 is the metric for both spacetimes (the horizon radius r_h is simply zero for Minkowski space). We specify boundary value data at a finite radius $r = r_c$, effectively surrounding the black hole in an isothermal cavity, so the boundary terms should be evaluated at this radius rather than spatial infinity. For the Schwarzschild and Minkowski spacetimes, the bulk action vanishes ($R = R_0 = 0$), so we are left with

$$I_{\text{Total}} = \frac{1}{8\pi}\int_0^{\beta_h}\!\!\int_0^{2\pi}\!\!\int_0^{\pi}\sqrt{k}\ \big(K\big)d\theta\, d\phi\, d\tau\ \Bigg|_{r=r_c} - \frac{1}{8\pi}\int_0^{\beta_0}\!\!\int_0^{2\pi}\!\!\int_0^{\pi}\sqrt{k_0}\ \big(K_0\big)d\theta\, d\phi\, d\tau_0\ \Bigg|_{r=r_c} \tag{2.5}$$

The two integrals are done in different spacetimes, so care must be taken that the time coordinates and their periodicities are chosen appropriately so that the metrics match at r_c. The matching condition is:

$$\Big(1 - \tfrac{r_h}{r_c}\Big)\, d\tau^2 = (1)\, d\tau_0^2 \qquad \rightarrow \qquad \sqrt{1 - \tfrac{r_h}{r_c}}\,\beta_h = \beta_0\ , \quad \sqrt{1 - \tfrac{r_h}{r_c}}\, d\tau = d\tau_0 \tag{2.6}$$

[1]The Schwarzschild geometry contains large contributions to the partition function coming from thermal excitations of gravitons far away from the black hole, which are removed by subtracting the flat space action.

We thus have

$$I_{\text{Total}} = \frac{\beta_h}{8\pi}\int_0^{2\pi}\!\!\int_0^{\pi}\sqrt{k}\,\big(K\big)d\theta\,d\phi\,\Big|_{r=r_c} - \frac{\beta_h}{8\pi}\sqrt{1-\tfrac{r_h}{r_c}}\int_0^{2\pi}\!\!\int_0^{\pi}\sqrt{k_0}\,\big(K_0\big)\,d\theta\,d\phi\,\Big|_{r=r_c}, \qquad (2.7)$$

where β_h is the periodicity in imaginary time τ in the *Schwarzschild* spacetime. This periodicity should be chosen to eliminate the conical singularity in the $\tau - r$ plane at the horizon. To see this, consider expanding near the horizon, where $r = r_h + \epsilon$. The metric there becomes

$$ds^2 = \frac{\epsilon}{r_h}\,d\tau^2 + \frac{r_h}{\epsilon}\,d\epsilon^2 + r^2 d\Omega^2 \qquad (2.8)$$

The metric factors into an $\mathcal{S}^2$ and a two-dimensional $\mathcal{S}^1 \times \mathbb{R}$ part:

$$ds_2^2 = \frac{\epsilon}{r_h}\,d\tau^2 + \frac{r_h}{\epsilon}\,d\epsilon^2 \qquad (2.9)$$

Making the substitutions $\rho = 2\sqrt{r_h\epsilon}$ and $\chi = \frac{\tau}{2r_h}$ reveals the metric

$$ds_2^2 = \rho^2 d\chi^2 + d\rho^2 \qquad (2.10)$$

which resembles polar coordinates ($ds^2 = r^2 d\phi^2 + dr^2$) but χ is not necessarily 2π-periodic, so in general this metric is that of a cone[2]. The singularity at $\rho = 0$ is a true metric singularity and not just the coordinate singularity at $r = 0$ in polar coordinates. To eliminate the conical singularity we impose that the period of χ is indeed 2π. Then τ has period $4\pi r_h$, which is the inverse Hawking temperature for the Schwarzschild black hole. More generally the periodicity required will be

$$\beta_h = \frac{2\pi}{\kappa} = \frac{4\pi}{f'(r)}\Big|_{r_h} \qquad (2.11)$$

where κ is the surface gravity[3]. This is what is meant by choosing the periodicity in imaginary time to eliminate the conical singularity. The whole spacetime is foliated by leaves of topology $\mathcal{S}^1 \times \mathcal{S}^2$, and β_h gives the periodicity required at the horizon so that the proper length of the $\mathcal{S}^1$ shrinks smoothly to zero at $r = r_h$. At the boundary $r = r_c$, the periodicity in the *local* time t is $\beta = \beta_h\sqrt{f(r_c)}$. The periodicity in the global time τ is β_h in the whole spacetime. Quantum fields in the spacetime inherit this periodicity and therefore the temperature of a thermal state is seen to be redshifted by a factor $\sqrt{f(r_c)}$ at the cavity.

Returning to the evaluation of (2.7), we construct the extrinsic curvature and boundary metric by choosing an *inward pointing* spacelike unit vector to the boundary, $s_a =$

[2]This is only true of the Euclidean section. In the Lorentzian section the near-horizon metric has the same form but with $(-,+)$ signature, and is actually the Rindler metric written in obscure coordinates.

[3]One can see this explicitly by using the general near-horizon expansion $r = r_h + \epsilon$ for any metric of the form (2.4) and following the same procedure, choosing the coordinate transformations for ρ and χ such that the metric is forced into the form (2.10).

$[0, -f^{-1/2}, 0, 0]$, giving:

$$K = -\frac{2\sqrt{f(r)}}{r} - \frac{f'(r)}{2\sqrt{f(r)}} \ , \qquad \sqrt{k} = f(r)\, r^2 \sin(\theta) \tag{2.12}$$

For the reference spacetime, we choose flat empty space, where $f(r) = 1$, so that the extrinsic curvature and metric there are

$$K_0 = -\frac{2}{r} \ , \qquad \sqrt{k_0} = r^2 \sin(\theta) \tag{2.13}$$

Performing the integrations over (θ, ϕ) then gives the reduced action

$$I_r = \left(\tfrac{3}{4} r_h - r_c + \sqrt{(r_c - r_h) r_c}\right) \beta_h \tag{2.14}$$

By direct substitution of the relation between periodicities $\beta = \beta_h \sqrt{f(r)}$ one can show that this is exactly the expected result of

$$I_r = \beta r_c \left(1 - \sqrt{1 - \frac{r_h}{r_c}}\right) - \pi r_h^2 \ . \tag{2.15}$$

The procedure described above can be followed almost identically to determine the Euclidean action for a large class of theories and/or black hole metrics, and is used in the remainder of this work to evaluate such actions. We refer to I_r as the *reduced* action to differentiate it from the corresponding general form (before any integration is done). We emphasize however that the integrations required may be highly non-trivial. In this example the bulk action vanishes for both the Schwarzschild and flat space metrics, so no radial integration is required in (2.7). This will not be the case in general. Alternatively, one could have arrived at the same result through repeated use of integration by parts and product rule to recast (2.4) as a total derivative (as was originally done in [52]). In this way the integration becomes trivial and one can immediate arrive at (2.15). However, in more complicated theories/spacetimes it may be difficult or impossible to rewrite the bulk action as a total derivative, necessitating the direct integration of the action as was done here.

2.3 Thermodynamic Quantities and the First Law

In this section we summarize how the relevant various thermodynamic quantities will be determined for the Schwarzschild and Reissner-Nordström-de Sitter black holes, and discuss where generalizations of the results in Section 1.4 are required. Recall from Section 1.3 that determining the relevant thermodynamic quantities becomes relatively straightforward once the (reduced) Euclidean action I_r has been determined. Varying the reduced action with respect to the physical degrees of freedom at the stationary points gives the energy

and entropy in this ensemble:

$$E = \frac{\partial I_r}{\partial \beta}, \qquad S = \beta\left(\frac{\partial I_r}{\partial \beta}\right) - I_r \tag{2.16}$$

The variations above are performed with all other parameters held fixed, possibly necessitating the inclusion of extra terms to account for the dependency of β on those parameters[4]. The energy as defined is the mean thermal energy of the black hole with respect to the empty de Sitter spacetime, which can be related (at least in the AdS and flat case) to the ADM mass of the spacetime after accounting for the gravitational and electrostatic binding energy[5].

We have established that fixing boundary value data on a finite radius reflecting cavity allows the black hole to be in equilibrium, but what is the associated temperature? In the path integral, the periodicity β corresponds to the inverse of the equilibrium temperature, $T = 1/\beta$. To determine β, one can simply extremize the reduced action with respect to r_h and solve for β. The expression will in general depend on the other physical degrees of freedom present:

$$\frac{\partial I_r(\beta, r_h, r_c, q, \Lambda)}{\partial r_h} = 0 \quad \rightarrow \quad \beta(r_h, r_c, q, \Lambda) \implies T(r_h, r_c, q, \Lambda) \tag{2.17}$$

E, T, and S will enter the thermodynamic description through the extended first law described in Section 1.4.4, which for the case at hand reads

$$dE = TdS - \lambda dA_c + VdP + \phi dQ \tag{2.18}$$

where κ is the surface gravity of the black hole, A is the horizon area, J is the angular momentum, Ω is the angular velocity, ϕ is the electrostatic potential, and Q is the electric charge. λdA_c is a work term arising from the presence of the cavity, where $A_c = 4\pi r_c^2$ is the cavity surface area and λ is the surface tension/pressure. For asymptotically AdS black holes in the extended phase space, one usually identifies the mass variation of the black hole dM with a variation of the enthalpy $H = E + PV$ rather than the internal energy U. In the case of these de Sitter black holes a similar statement holds true: the variation of the mean thermal energy dE is analogous to a variation of an ordinary thermodynamic enthalpy H.

The action allows us to directly determine the temperature T, entropy S, and energy E of the system. To determine the thermodynamic volume and surface tension, we evaluate the differentials dE, dS, dA_c, and dP, and enforce that (2.18) holds. The resulting ther-

[4]This is necessary if, for example, $\beta = \beta(r_h)$, since this imposes a constraint that does not allow the action to vary with respect to r_h while keeping β fixed.

[5]The thermal energy E is related to a conserved mass quantity M through $dM = dE\sqrt{\left(1 - \frac{r_h}{r_c}\right)\left(1 - \frac{\Lambda}{3}\left(r_c^2 + r_c r_h + r_h^2\right)\right)}$. In asymptotically AdS and flat spacetime M is the ADM mass. In de Sitter it has a different interpretation since it is not conserved in time.

modynamic volume will in general be different from the geometric volume $V = \frac{4}{3}\pi r_h^3$ (that appears for charged AdS black holes [31]) as we will see. Since we have included pressure in the thermodynamic ensemble, we will also be able to study the equation of state $P(T, v)$ of our system. Once the thermodynamic volume V has been determined from the first law, the equation of state follows by inverting the temperature for Λ and substituting into (2.1). The expression to be solved is generally quadratic in Λ, leading to two possible equations of state, though only one is physical in our case. The construction of the equation of state will allow us to determine the extent to which various analogies between black holes and fluid systems (common in AdS spacetimes) extend to the de Sitter case.

The inclusion of Λ and the isothermal cavity in the thermodynamic description also leads to a modified Smarr relation which in four dimensions is

$$E = 2(TS - \lambda A_c - PV) + \Phi Q \tag{2.19}$$

and can be derived from various scaling arguments [97]. In the absence of the isothermal cavity, the λdA_c term vanishes and we recover the usual form of the Smarr relation. This relation has played an important role in black hole thermodynamics both as a consistency check and through its broad applicability, as it holds for both asymptotically AdS and dS spacetimes, is valid in any dimension, and is satisfied by more exotic objects like black rings and black branes [22].

Finally, we wish to examine the phase structure of the Schwarzschild-de Sitter and Reissner-Nordström-de Sitter black hole. In the discussion of phase transitions, the thermodynamic potential of interest is the Helmholtz free energy F, which is globally minimized when a thermodynamic system reaches equilibrium at constant temperature. In the canonical ensemble, F is defined by $F = E - TS$ and can therefore be deduced directly from (2.16) and (2.17). Plotting $F(T)$ with the appropriate parameters held fixed (as determined by the chosen ensemble) can then reveal the character of any phase transitions present.

2.4 Schwarzschild-de Sitter Black Holes

In this section, we consider explicitly the (uncharged) Schwarzschild-de Sitter black hole. The action is

$$I_{\text{Total}} = -\frac{1}{16\pi}\int_{\mathcal{M}} d^4x\sqrt{g}\left(R - 2\Lambda\right) + \frac{1}{8\pi}\int_{\partial\mathcal{M}} d^3x\sqrt{k}\,K - \int_{\partial\mathcal{M}} d^3x\sqrt{k}\,F^{ab}n_a A_b - I_0 \tag{2.20}$$

where we have added an electromagnetic boundary term for the charged case, with n_a being normal to the cavity and the electromagnetic field strength tensor defined in terms of the potential as $F_{ab} = \partial_a A_b - \partial_b A_a$. We shall choose a subtraction term I_0 for the action such that $I_{\text{Total}} = 0$ when the mass of the black hole vanishes. This will just be the action for the empty de Sitter spacetime whose metric is matched to the black hole spacetime on the boundary. In this way, we are using empty de Sitter space as the reference point

from which energy is measured, as opposed to the topologically distinct Minkowski space. This is in contrast to the early work of Carlip and Vaidya [53], where the latter choice for reference spacetime was chosen, so that their action vanishes for flat space. Each choice results in different values for most thermodynamic quantities and changes the location of the critical points, but we will find that they produce the same qualitative behaviour. We emphasize however that ours is the intuitively correct choice, as one should not be altering the asymptotic structure of the spacetime when comparing its energy in the presence of a black hole vs. radiation. We take a spherically symmetric ansatz for the metric,

$$ds^2 = f(y)d\tau^2 + \alpha(y)dy^2 + r(y)^2 d\Omega^2 \tag{2.21}$$

where $y \in [0,1]$ is a compactified radial coordinate with $y = 0$ corresponding to the black hole horizon ($r(0) = r_h$) and $y = 1$ corresponding to the cavity wall ($r(1) = r_c$). The boundary at $y = 1$ has topology $S^1 \times S^2$ with S^2 having area $4\pi r_c^2$. Heat flux through the cavity wall is chosen such that its temperature $T = \beta^{-1}$ remains fixed. The inverse temperature β is related to the proper length of the boundary S^1 by $\beta = 2\pi f(1)$, where the periodicity in imaginary time τ is 2π.

Thermodynamic quantities can be derived from the action (2.20) after the integrations are carried out and the various constraints imposed to arrive at the reduced action I_r. For the case at hand, one proceeds by solving the Hamiltonian constraint to determine the metric function,

$$f(r) = 1 - \frac{2m}{r} - \frac{\Lambda r^2}{3} \ . \tag{2.22}$$

The horizons are located at the real and positive roots of $f(r) = 0$, of which there are two for the parameter range $0 < 9\Lambda m^2 < 1$. The smaller root r_h gives the location of the event horizon, while the larger root r_{cosmo} is the cosmological horizon. The limit where the horizons coincide is known as the Nariai limit, where $9\Lambda m^2 \to 1$ and thus $r_h \to r_{\text{cosmo}}$.

One can proceed in two equivalent ways, either by following the procedure detailed in Section 2.2 to explicitly evaluate the action using (2.22), or by inserting the ansatz (2.21) into the action and rewriting the integrand as a total derivative (thus bypassing the need for explicit radial integration). This alternative method is demonstrated in Appendix A for the case at hand. Either way, the integrations in (2.20) are performed and we arrive at the reduced action:

$$I_r = \beta r_c \left[\sqrt{1 - \frac{\Lambda r_c^2}{3}} - \sqrt{\left(1 - \frac{r_h}{r_c}\right)\left(1 - \frac{\Lambda}{3}\left(r_c^2 + r_c r_h + r_h^2\right)\right)} \ \right] - \pi r_h^2 \tag{2.23}$$

The inverse temperature is found by extremizing the action with respect to r_h and solving for β, giving

$$\beta = \frac{4\pi r_h \sqrt{\left(1 - \frac{r_h}{r_c}\right)\left(1 - \frac{\Lambda}{3}\left(r_c^2 + r_c r_h + r_h^2\right)\right)}}{1 - \Lambda r_h^2} \tag{2.24}$$

from which the temperature is simply

$$T = \frac{1 - \Lambda r_h^2}{4\pi r_h \sqrt{\left(1 - \frac{r_h}{r_c}\right)\left(1 - \frac{\Lambda}{3}\left(r_c^2 + r_c r_h + r_h^2\right)\right)}} \ . \tag{2.25}$$

In the limit $\Lambda \to 0,\ r_c \to \infty$, this reduces to the familiar result of $T = 1/4\pi r_h = 1/8\pi M$. The entropy is

$$S = \beta \frac{\partial I_r}{\partial \beta} - I_r = \pi r_h^2 \tag{2.26}$$

and finally the energy is

$$E = \frac{\partial I_r}{\partial \beta} = r_c \left[\sqrt{1 - \frac{\Lambda r_c^2}{3}} - \sqrt{\left(1 - \frac{r_h}{r_c}\right)\left(1 - \frac{\Lambda}{3}\left(r_c^2 + r_c r_h + r_h^2\right)\right)} \ \right] \tag{2.27}$$

2.4.1 The First Law

With the energy E, temperature T, and entropy S as defined above, we can determine the thermodynamic volume V and surface tension λ from the first law (2.18). Direct evaluation reveals that the surface tension is given by

$$\lambda = \frac{\left(4\Lambda r_c^3 - 6r_c\right)(X - Y) + r_h(\Lambda r_h^2 - 3)Y}{48\pi r_c^2 XY} \ , \tag{2.28}$$

and the thermodynamic volume is

$$V = \frac{4\pi}{3} \frac{r_c^3 (Y - X) - r_h^3 Y}{XY} \ , \tag{2.29}$$

where we have defined the quantities

$$X = X(\Lambda) \equiv \sqrt{\left(1 - \frac{r_h}{r_c}\right)\left(1 - \frac{\Lambda}{3}\left(r_c^2 + r_c r_h + r_h^2\right)\right)} \ , \quad Y = Y(\Lambda) \equiv \sqrt{1 - \frac{\Lambda r_c^2}{3}} \ . \tag{2.30}$$

With these definitions it is straightforward to verify that

$$dE = TdS - \lambda dA_c + VdP \ , \tag{2.31}$$

Unlike V (which should be positive to retain its interpretation as a physical volume) the sign of λ is free to be negative since this simply corresponds to a surface pressure. Figure 2.1 shows regions in parameter space where V and λ are positive, in terms of the dimensionless ratio $x \equiv r_h/r_c \in [0, 1]$.

There are two limits of interest here. The first is the asymptotically flat limit $\Lambda \to 0$.

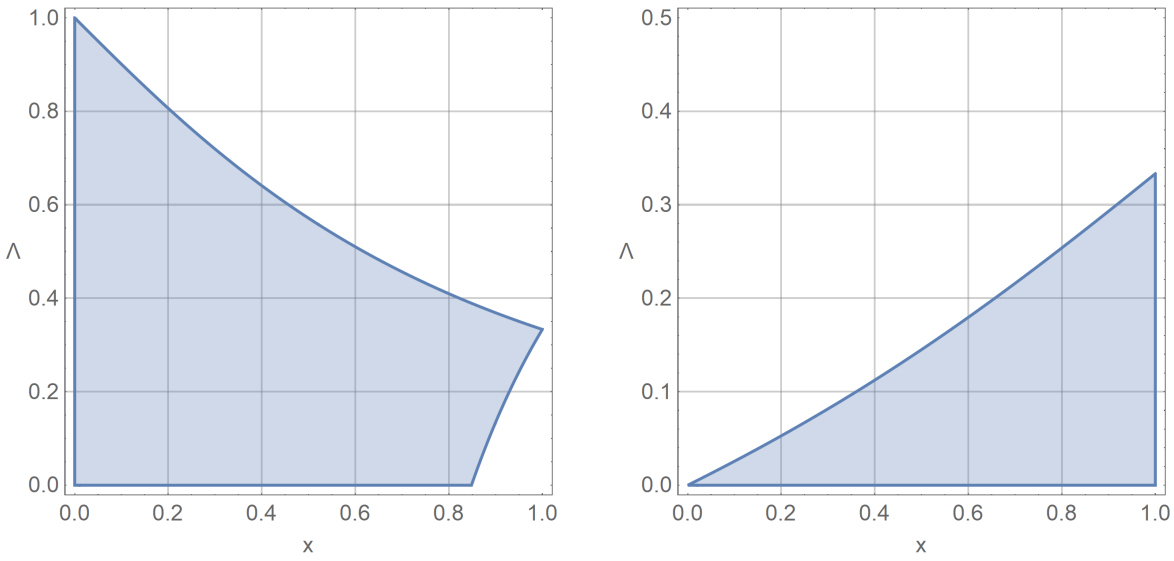

Figure 2.1: Regions of positivity (blue) for thermodynamic potentials associated with the Schwarzschild-de Sitter black hole as a function of $x = r_h/r_c$ and Λ, with fixed $r_c = \sqrt{3}$. **Left:** The thermodynamic volume V. **Right:** The surface tension λ.

In this case we have $X \to \sqrt{1 - r_h/r_c}$ and $Y \to 1$, giving

$$\lambda = \frac{2r_c\left(1 - \sqrt{1 - \dfrac{r_h}{r_c}}\right) - r_h}{16\pi r_c^2\sqrt{1 - \dfrac{r_h}{r_c}}}, \qquad V = \frac{4\pi}{3}\frac{r_c^3\left(1 - \sqrt{1 - \dfrac{r_h}{r_c}}\right) - r_h^3}{\sqrt{1 - \dfrac{r_h}{r_c}}} \tag{2.32}$$

which agrees with the results of [52]. Note that in this limit, $V > 0$ provided that $r_h < 0.84837 r_c$, as demonstrated in Figure 2.1. Since there is no longer a cosmological horizon in this limit, we can further take the large cavity limit $r_c \to \infty$, which results in $\lambda \to 0$ and $V \to \infty$, as expected.

We can also take the small black hole limit $r_h \to 0$, where $\lambda \to 0$ and $V \to 0$. In this case we let $r_h = x\, r_c$ and expand around $x = 0$ to find

$$\lambda \approx -\frac{\sqrt{3}r_c\Lambda}{16\pi(3 - \Lambda r_c^2)^{3/2}}\, x + \mathcal{O}(x^2)\,, \qquad V \approx \frac{6\pi r_c^3 x}{(3 - \Lambda r_c^2)\sqrt{9 - 3\Lambda r_c^2}}\left(1 - \frac{9x}{4(3 - \Lambda r_c^2)}\right) + \mathcal{O}(x^3) \tag{2.33}$$

Both the thermodynamic volume and surface tension vanish in the small black hole limit for fixed cavity size. Of course, we cannot take the large cavity limit here because the cavity size is bounded by the cosmological horizon.

2.4.2 Helmholtz Free Energy and Phase Transitions

We can now examine the phase structure of the uncharged Schwarzschild-de Sitter black hole. To do so, we consider the Helmholtz free energy ($F = E - TS$) whose global minimum corresponds to the equilibrium state of the system at fixed temperature. A plot of F as a function of T and P for fixed r_c reveals the presence of any phase transitions in the system. Using (2.25), (2.26) and (2.27) we have

$$F(r_h, r_c, P) = \frac{\Lambda r_h^3}{A} - r_c X + \frac{r_c Y}{\sqrt{3}} - \frac{r_h}{4A} \tag{2.34}$$

$$T(r_h, r_c, P) = \frac{1 - \Lambda r_h^2}{4\pi r_h A} \tag{2.35}$$

where F and T are understood to be functions of P through the definitions (2.30) of X and Y and the identification $\Lambda = -8\pi P$. We plot $F(T)$ parametrically for fixed P and r_c using r_h as the parameter. This is shown in Figure 2.2 and Figure 2.3, which reveal the presence of a standard Hawking-Page phase transition from pure radiation to a black hole, whose size increases with increasing temperature. The $F = 0$ line corresponds to the radiation phase, with the transition to a black hole occurring at the temperature T_c where the blue line crosses $F = 0$. Above this critical temperature the black hole phase has lower free energy and is thermodynamically preferred. The value of T_c is the solution to a fifth-degree polynomial and therefore must be found numerically. The kink in the $F - T$ curve corresponds to T_{min}, the lowest temperature at which a locally stable (supercooled) small black hole can exist at the given pressure and cavity size. This point occurs where $\partial F/\partial T$ becomes undefined, and can be found analytically. The expression for T_{min} is long and without much insight, so we omit it.

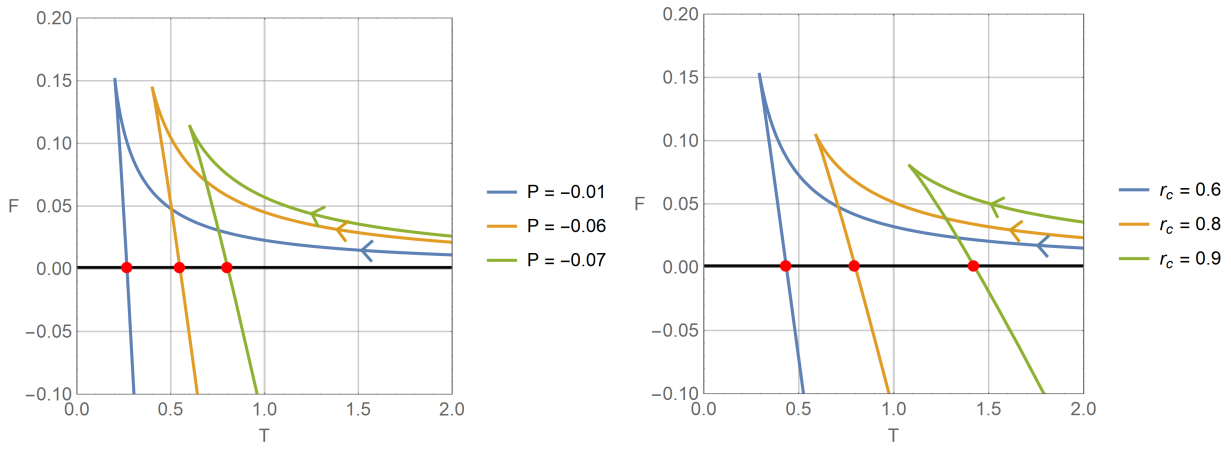

Figure 2.2: Helmholtz free energy of the Schwarzschild-de Sitter black hole. **Left:** $F(T)$ for fixed cavity size ($r_c = 1$) and varying pressure. **Right:** $F(T)$ for fixed pressure ($P = -0.1$) and varying cavity size. The critical temperature T_c is indicated with a red dot.

One can also verify that the heat capacity $C_v = -\beta(\partial S/\partial\beta)$ is positive above the transition temperature, demonstrating the stability of the black hole phase. Varying either

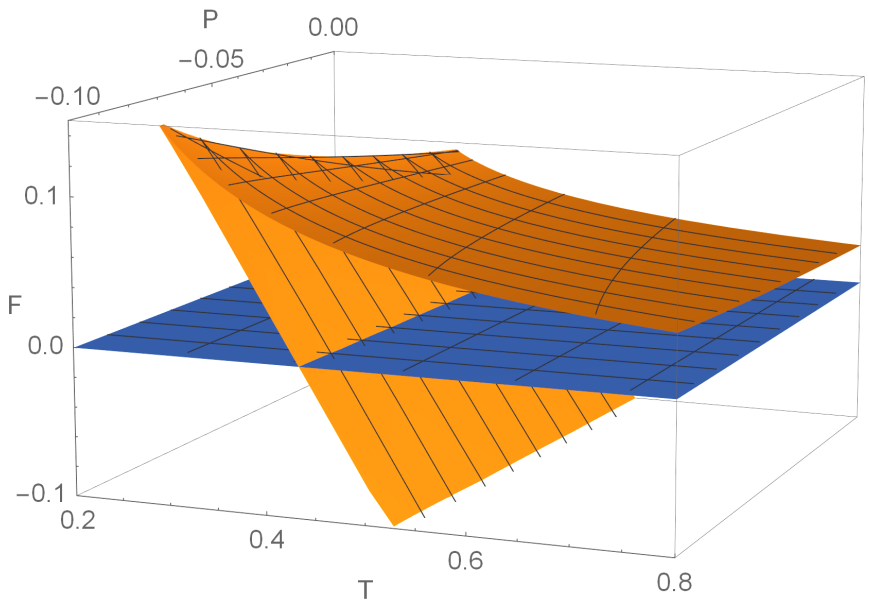

Figure 2.3: Helmholtz free energy of the Schwarzschild-de Sitter black hole as a function of temperature and pressure for fixed cavity radius ($r_c = 0.5$). The $F = 0$ plane is indicated in blue. Hawking-Page transitions occur along the line of intersection.

the cosmological constant Λ or the cavity size r_c simply moves the location of the critical temperature, but does not qualitatively change the behaviour of the phase transition. This agrees with the results of Carlip and Vaidya [53]; the flat-background choice of normalization for the action simply moves the location of the critical point but does not introduce new thermodynamic features.

As outlined in Section 1.4.4, working in the extended phase space allows us to examine the equation of state for these uncharged de Sitter black holes. The equation of state can be cast as a relationship between the pressure P, temperature T, and volume V, which we take to be the thermodynamic volume divided by the number of degrees of freedom associated with the horizon [34]. In AdS space the volume $V \sim r_h^3$ and the specific volume (the volume per horizon degrees of freedom) $v \sim r_h$ [31]. However in dS space, (2.35) means that the pressure is a non-linear function of (T, r_h), and (2.32) in turn implies that r_h is a highly non-linear function of V. As a result, the equation of state cannot be expressed in closed form. Implicitly plotting $P(V)$ at fixed T reveals an absence of the oscillations characteristic of the Van der Waals fluid. We omit the plot here for lack of insight.

2.5 Reissner-Nordström-de Sitter Black Holes

We now turn to the (charged) Reissner-Nordström-de Sitter black hole. In AdS, the presence of charge allows for small-to-large black hole phase transitions in the canonical ensemble [31]. Some of the thermodynamic properties of charged de Sitter black holes in a cavity have already been investigated by Carlip and Vaidya [53]. Here we explore their

phase structure further, working in the extended phase space, and examine more closely the nature of the phase transitions present.

As before, the Hamiltonian constraint determines the metric function for the 4-dimensional charged de Sitter black hole:

$$f(r) = 1 - \frac{2m}{r} + \frac{q^2}{r^2} - \frac{\Lambda r^2}{3} \ . \tag{2.36}$$

The reduced action in this case becomes

$$I = \beta r_c \left[\sqrt{1 - \frac{\Lambda r_c^2}{3}} - \sqrt{\left(1 - \frac{r_h}{r_c}\right)\left(1 - \frac{q^2}{r_h r_c} - \frac{\Lambda}{3}\left(r_c^2 + r_c r_h + r_h^2\right)\right)} \ \right] - \pi r_h^2 \ . \tag{2.37}$$

The expression (2.36) for $r^2 f$ is now a quartic polynomial in r, and we must restrict ourselves to regions where $f(r) > 0$ for the path integral to be well defined. An analysis of these allowed regions can be found in [53].

The temperature is found again by extremizing the action with respect to r_h and solving for β, giving

$$T = \frac{1}{\beta} = \frac{1 - \frac{q^2}{r_h r_c} - \frac{\Lambda}{3}\left(r_c^2 + r_c r_h + r_h^2\right) + \left(1 - \frac{r_h}{r_c}\right)\left(\frac{\Lambda}{3}(r_c^2 + 2 r_h r_c) - \frac{q^2}{r_h^2}\right)}{4\pi r_h \sqrt{\left(1 - \frac{r_h}{r_c}\right)\left(1 - \frac{q^2}{r_h r_c} - \frac{\Lambda}{3}\left(r_c^2 + r_c r_h + r_h^2\right)\right)}}. \tag{2.38}$$

The entropy is again

$$S = \beta \frac{\partial I_r}{\partial \beta} - I_r = \pi r_h^2 \tag{2.39}$$

and the energy is

$$E = \frac{\partial I_r}{\partial \beta} = r_c \left[\sqrt{1 - \frac{\Lambda r_c^2}{3}} - \sqrt{\left(1 - \frac{r_h}{r_c}\right)\left(1 - \frac{q^2}{r_h r_c} - \frac{\Lambda}{3}\left(r_c^2 + r_c r_h + r_h^2\right)\right)} \ \right]. \tag{2.40}$$

2.5.1 The First Law

As in Section 2.4, we use the first law to find the thermodynamic volume V and surface tension/pressure λ. The first law must be supplemented by an additional term ΦdQ to account for the presence of charge. We find that

$$\lambda = \frac{(4\Lambda r_c^3 - 6 r_c)\left(\tilde{X} - \tilde{Y}\right) + r_h(\Lambda r_h^2 - 3)\tilde{Y} - \dfrac{3q^2\tilde{Y}}{r_h}}{48\pi r_c^2 \tilde{X}\tilde{Y}} \tag{2.41}$$

$$V = \frac{4\pi}{3}\frac{r_c^3(\tilde{Y}-\tilde{X}) - r_h^3\tilde{Y}}{\tilde{X}\tilde{Y}}, \qquad \Phi = \frac{(r_c - r_h)q}{r_h r_c \tilde{X}} \tag{2.42}$$

where we have now defined the quantities

$$\tilde{X}(\Lambda) \equiv \sqrt{\left(1-\frac{r_h}{r_c}\right)\left(1-\frac{q^2}{r_h r_c}-\frac{\Lambda}{3}\left(r_c^2+r_c r_h+r_h^2\right)\right)}\,, \quad \tilde{Y}(\Lambda) \equiv \sqrt{1-\frac{\Lambda r_c^2}{3}}\,. \tag{2.43}$$

With these definitions we have that both the first law,

$$dE = TdS - \lambda dA_c + VdP + \Phi dQ. \tag{2.44}$$

and Smarr relation,

$$E = 2(TS - \lambda A_c - PV) + \Phi Q \tag{2.45}$$

are satisfied. We again depict the regions of positivity for V and λ in Figure 2.4. Note that as charge increases the region of positivity shrinks.

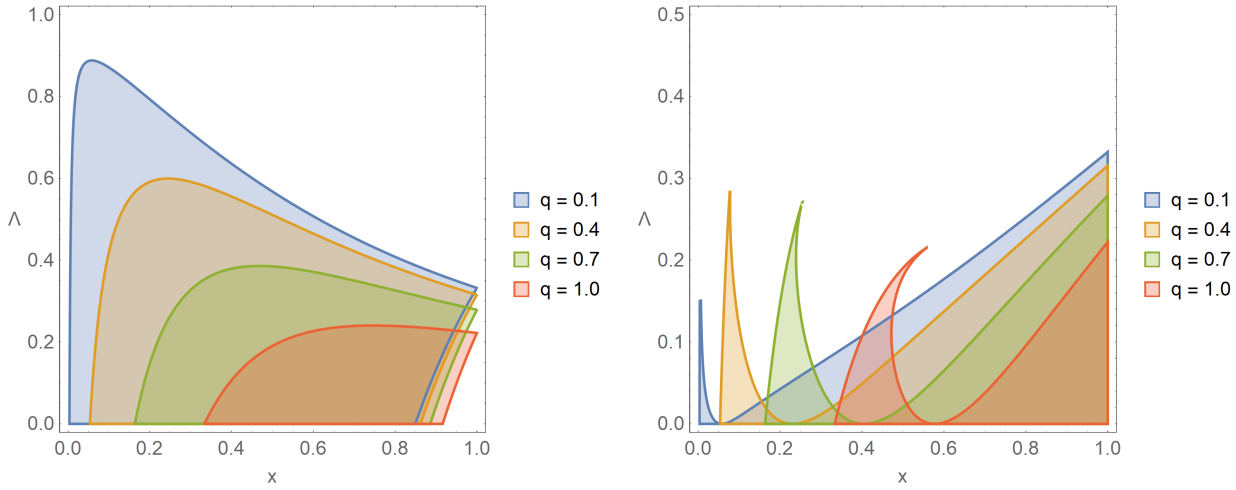

Figure 2.4: Regions of positivity (colored) for thermodynamic potentials associated with the Reissner-Nordström-de Sitter black hole as a function of $x = r_h/r_c$ and Λ, with fixed cavity radius $r_c = \sqrt{3}$. **Left:** The thermodynamic volume V. **Right:** The surface tension λ.

2.5.2 Helmholtz Free Energy and Phase Transitions

We turn once again to the Helmholtz free energy to examine the phase structure of the system. Using (2.38), (2.39) and (2.40) we have

$$F(r_h, r_c, P) = \frac{\Lambda r_h^3}{\tilde{X}} - r_c\tilde{X} + \frac{r_c B}{\sqrt{3}} - \frac{r_h}{4\tilde{X}} \tag{2.46}$$

$$T(r_h, r_c, P) = \frac{1-\Lambda r_h^2}{4\pi r_h \tilde{X}}\,, \tag{2.47}$$

which is identical to the uncharged case aside from the extra q-dependent term appearing in $\tilde{X}$. We plot $F(T)$ parametrically for fixed P and r_c using r_h as the parameter. This is shown in Figure 2.5.

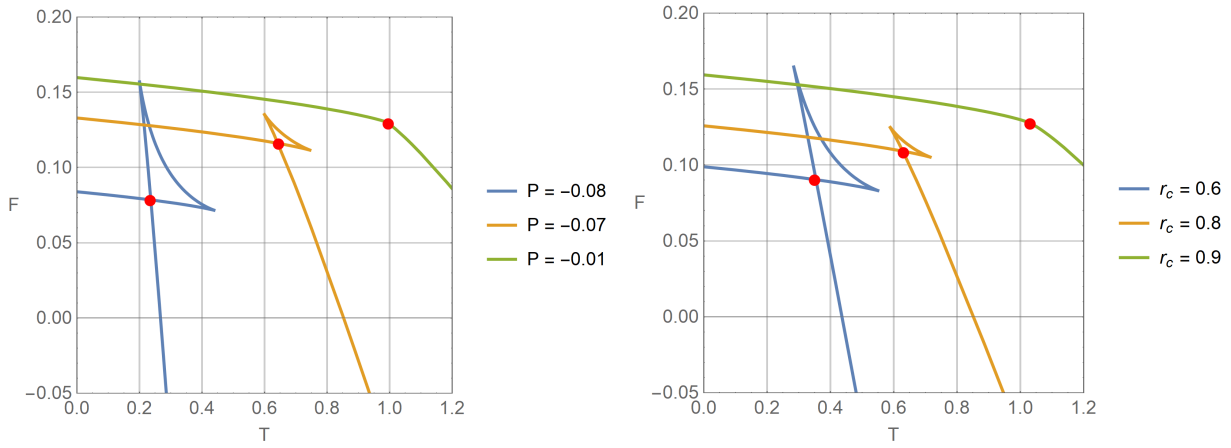

Figure 2.5: Helmholtz free energy of the Reissner-Nordström-de Sitter black hole as a function of temperature. **Left:** Various pressures ($P = -0.08, -0.07, -0.01$) with fixed charge ($q = 0.08$) and cavity size ($r_c = 1$), showing clearly the formation of a swallowtail below the critical pressure, in this case $P_c \approx -0.82$. **Right:** Various cavity sizes ($r_c = 0.6, 0.8, 0.9$) with fixed charge charge ($q = 0.08$) and pressure ($P = -0.08$). The red dots indicate the location of the small-to-large black hole phase transition.

Though the free energy is largely similar to that of (2.34), the presence of charge significantly alters the phase structure. Below a certain critical pressure P_c, the free energy develops a kink which in the $F-T-P$ space forms a swallowtail. The swallowtail indicates the presence of a first-order phase transition from a small black hole to a large black hole, which occurs at the crossing where the critical temperature T_c is reached. The horizon radius r_h increases along the near-horizontal line at the left (in the direction indicated by the arrow), which is the same as the direction of increasing temperature. Eventually a crossover point (where $T = T_c$) is reached, beyond which the free energy is minimized by moving downward along the steeper line instead of forward along the near-horizontal line. At $T = T_c$ there is a discontinuity in the horizon radius r_h. Note that for charged black holes, the $F = 0$ line is inaccessible to the system, as we have chosen an ensemble where q is fixed. To leading order in small-Λ, analyticity of $f(r)$ requires that $m^2 > q^2$, which cannot be satisfied by a black hole with fixed charge that evaporates to pure radiation.

This swallowtail behaviour appears also in charged and rotating AdS black holes, though we note a significant departure from the behaviour of previously studied examples in our case. Normally, as the magnitude of the pressure increases, the swallowtail grows without bound, indicating the presence of a phase transition for all pressures above the critical pressure P_c where the swallowtail first forms. In our case however, the swallowtail closes past a certain maximum pressure P_{max}, creating the *swallowtube* shown in Figure 2.6. The phase transition from a small to large black hole is then *compact* in the sense that it exists only in a finite domain in P. For sufficiently large r_c or small q, the

swallowtube intersects the $P = 0$ plane and is cut off (since we are in de Sitter space, P must be negative), though it still closes off at P_{max}. This is qualitatively different from the reentrant phase transitions found in, for example, higher dimensional rotating AdS black holes, where lowering the temperature of the black hole results in a small-large-small phase transition [32].

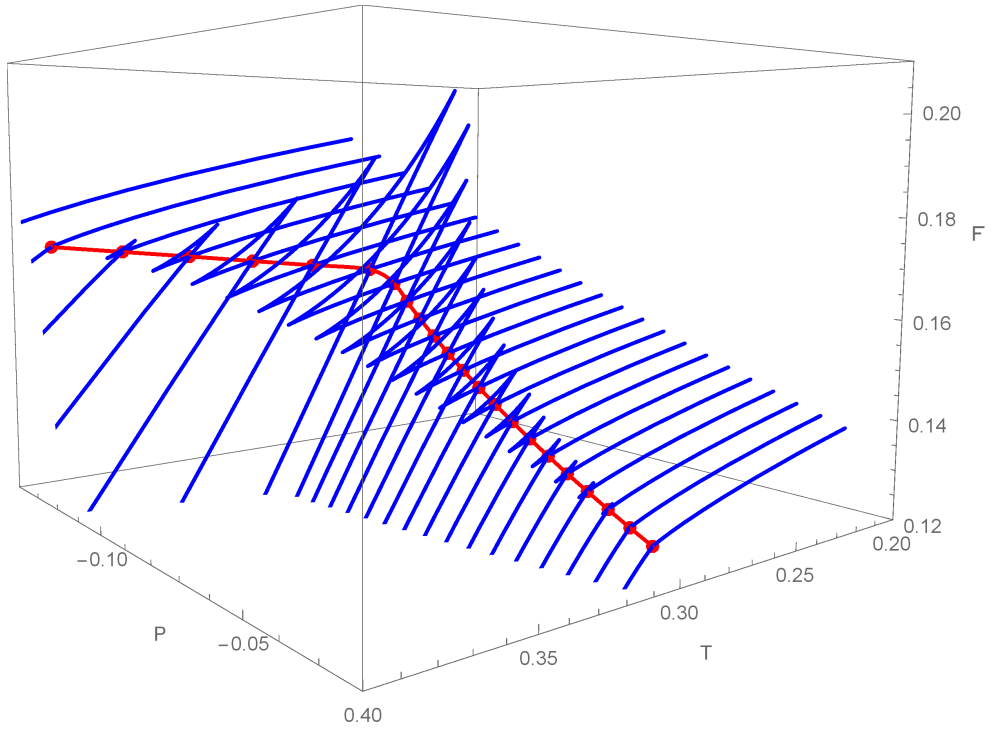

Figure 2.6: Helmholtz free energy of the Reissner-Nordström-de Sitter black hole as a function of temperature and pressure for fixed charge ($q = 0.08$), showing slices of constant pressure, and demonstrating the compact nature of the phase transition.

It is also interesting to examine the coexistence curve for this system, which we show in Figure 2.7. Here also we see a departure from the behaviour of AdS black holes, where the coexistence line increases monotonically and terminates at one end at a second order phase transition. Instead, the compact region that comprises the swallowtube is represented by a line segment in $P - T$ space along which the small and large black hole phase coexist, terminating at either end with a second order phase transition at the two critical pressures where the two ends of the swallowtube first form.

The two distinctly different branches correspond to two regimes where a separation of scales occurs. In the upper branch, the cosmological horizon is always farther from the black hole than the cavity is, namely $\max(r_c - r_h) < \max(r_{\text{cosmo}} - r_c)$. The influence of the cosmological horizon on the thermodynamic features is largely screened, and the upper portion of the coexistence line can be seen to resemble the case of the charged AdS black hole. For the lower branch, the cosmological horizon is always closer to the cavity than the event horizon, and so the thermodynamic behaviour deviates sharply from the AdS case. The transition region is marked by the bend in the coexistence line, which occurs when

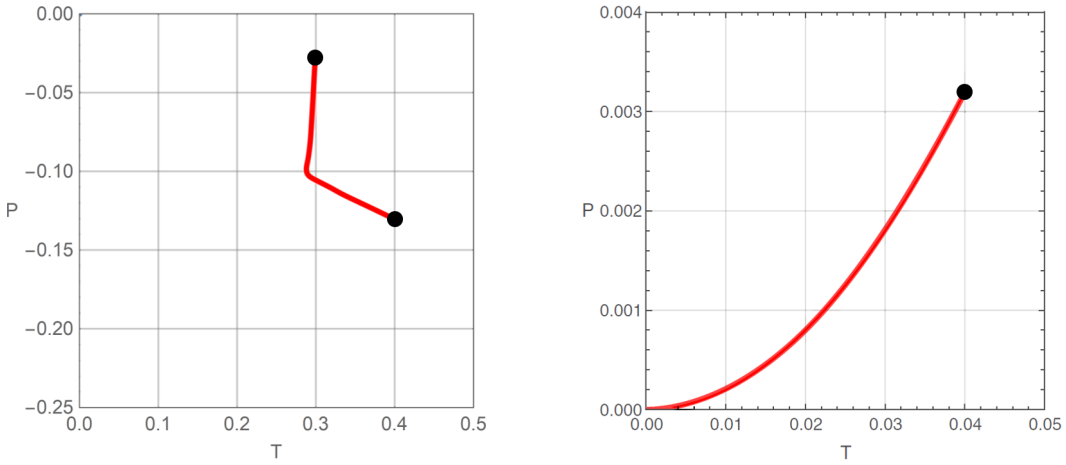

Figure 2.7: Left: Coexistence line for the charged dS black hole, along which the small and large black hole phases coexist. The line terminates at two ends where a second order phase transition occurs, indicated by a black dot. **Right:** Coexistence line for the charged AdS black hole.

the Nariai limit is achieved at exactly the cavity radius $r_{\text{Nariai}} = r_c$.

To close this section, we remark on the equation of state of the system. Finding the pressure $P(T, V)$ by eliminating r_h now requires solving $T = T(P, r_h, r_c, q)$, which is now a ninth-degree polynomial in r_h. Again, one must proceed by plotting P and T implicitly using r_h as the parameter. As in the uncharged case, implicitly plotting $P(V)$ for fixed T reveals an absence of the oscillations characteristic of the Van der Waals fluid.

2.6 Summary

The extended phase space thermodynamics of de Sitter black holes in an isothermal cavity is simultaneously quite similar and strikingly different from that of asymptotically flat and AdS black holes. Of immediate note is the fact that there is no simple equation of state relating the pressure to the thermodynamic volume. This is because in both the uncharged and charged cases the presence of a cavity necessarily introduces a complicated non-linear relationship between these quantities, and the presence of standard Van der Waals oscillations is no longer present. Despite this, the free energy indicates clear and interesting phase behaviour for both cases.

For the uncharged case, the identification of the cosmological constant with the thermodynamic pressure does not change the phase structure considerably; we still note a first-order Hawking-Page phase transition from hot gas to a black hole, with a locally stable supercooled region. This is not surprising since the extended phase space Helmholtz free energy is identical to the 'regular' phase space free energy. We also considered the analogy that these phase transitions make with Van der Waals systems, and concluded that

the equation of state does not support any liquid-gas type phase transition. Distinct from the usual AdS case however is the fact that that the equation of state is highly non-linear in T.

The charged de Sitter black hole presents novel features. We find a small-to-large black hole phase transition which occurs for pressures more negative than a certain critical pressure and above a certain critical charge. This structure is similar to the type seen in asymptotically AdS black holes. However this phase transition is compact in the sense that there is a second, more negative critical pressure P_{max} below which the phase transition disappears. This is in stark contrast to what occurs in AdS black holes, where above the (positive) critical pressure the phase transition is always absent, and below this pressure the phase transition is always present. For a large enough choice of cavity size, the phase transition is present even when $P \to 0$, but there is always a maximum pressure $|P_{max}|$ beyond which the small-large transition disappears, regardless of the choice of q and r_c. This swallowtube phenomenon results from the presence of the cosmological horizon and is unique to de Sitter, rather than arising from the presence of the cavity (swallowtubes do not exist for asymptotically flat or AdS black holes in cavities).

As a final remark we note that that the results we obtain and the existence of black hole phase transitions in general is largely dependent on the scaling properties of the basic thermodynamic variables in (2.19). These differ from the situation in standard thermodynamics, where the entropy is a homogeneous function of degree 1 of the total energy E, the volume V, and particle number N [98]. Whether or not such a requirement can be self-consistently imposed in black hole thermodynamics is not clear. There are many avenues to explore beyond the work presented here. It will be particularly interesting to see if the reentrant phase transitions and triple points typical of higher dimensional AdS black holes manifest themselves in the presence of an isothermal cavity for other types of de Sitter black holes. In the next few chapters, we will explore these questions by considering various extensions of the 4D Einstein-Maxwell black holes considered here.

Chapter 3

Born-Infeld-de Sitter Black Holes

In Chapter 2 we demonstrated the utility of the Euclidean path integral (or 'cavity') approach when considering spacetimes where no obvious notion of thermodynamic equilibrium is available. In the remaining chapters, we will show that this approach enjoys broad applicability not only to a wide variety of asymptotically de Sitter black hole spacetimes, but also to extensions of the traditional Einstein-Maxwell theory considered in Chapter 2. Our purpose in Chapter 3 will be to demonstrate this, by extending the $U(1)$ sector in our study of Reissner-Nordström-de Sitter black holes to Born-Infeld electrodynamics.

Named after its progenitors Max and Leopold, Born-Infeld theory is a nonlinear (still abelian) extension of Maxwell electrodynamics, proposed in 1934 to address the electron's self-energy divergence [99]. At the time, our understanding of quantum electrodynamics was still in its infancy, and two opposing views on the fundamental nature of particles persisted: the dualistic and unitarian standpoints. The dualistic view, which was prevailing at the time, supposed that matter and fields are fundamentally distinct entities. This implies in the electromagnetic case that electrons are entirely separate from the electromagnetic field (E, H); they source and are influenced by (E, H) yet are not part of them. The unitarian view on the other hand, was that particles such as the electron do not exist as entities separate from fields but are rather manifestations of (in the classical setting) singularities of the fields themselves, consistent with the divergence of (E, H) in the classical field theory description of the electron.

Adopting the unitarian point of view, Born and Infeld sought to write down a theory of classical electromagnetism that allowed for solutions that could have particle interpretations yet be divergence-free, the inspiration being drawn from the development of special relativity, where a finite bound on the speed of light proved to be an essential ingredient. Their idea was a nonlinear modification to the classical action of the electromagnetic field that would allow for soliton solutions to the field equations. These solitons would have finite self-energy and be able to persist on their own, providing an intriguing model for the electron as an electromagnetic field configuration, which is also free from the issues plaguing the Maxwellian description of an electron as a point particle. Born-Infeld theory also enjoys a unique status among nonlinear electromagnetic theories in that it alone is

absent of vacuum birefringence [100]. This effect appears generically in nonlinear electromagnetic theories, but is severely constrained by observational tests and also manifests in a pathological way as deformities in the lightcone structure of spacetime [101]. That Born-Infeld theory is free of these issues makes it an intriguing extension to study.

Decades after its introduction, interest in Born-Infeld theory would see a resurgence owing to the discovery of Fradkin and Tseytlin that the effective Lagrangian for abelian gauge fields coupled to open strings is given exactly by the Born-Infeld Lagrangian (3.2) [102], which extends to the supersymmetric case as well [103]. The parallels drawn by Born and Infeld between the finite electric field and speed of light would also see themselves validated by the discovery that the maximal electric field strength arises directly from the fact that brane propagation cannot exceed c [104]. For these reasons, there is great theoretical interest in Born-Infeld theory as an alternative to traditional Maxwellian electrodynamics. In the context of black hole thermodynamics, we are naturally led to ask what implications this type of modification to Einstein-Maxwell gravity might have for their thermodynamic properties, and in particular their phase transitions. That these phase transitions are also studied extensively in the context of string theory neatly ties the theoretical origins of Born-Infeld theory back to the present investigation.

The Born-Infeld Lagrangian stands in contrast to the Maxwell Lagrangian as follows:

$$\mathcal{L}_{\text{Maxwell}} = \frac{1}{4} F_{ab} F^{ab} \ , \qquad F_{ab} \equiv \partial_a A_b - \partial_b A_a \tag{3.1}$$

$$\mathcal{L}_{\text{Born-Infeld}} = 4b^2 \left(1 - \sqrt{1 + \frac{F^{ab} F_{ab}}{2b^2}} \right) \ . \tag{3.2}$$

Here, F_{ab} is the usual field strength tensor and b is the Born-Infeld parameter, with the limit $b \to \infty$ corresponding to Maxwell electrodynamics. b can also be related to the string tension $\alpha = (2\pi b)^{-1}$ in string theory, in which stretched open strings are created dynamically to suppress the electric field to a maximal value [105]. One can show that soliton solutions exist in this theory, and that the maximal allowed value of the electric field is finite and determined by the parameter b. Given the experimental constraints on the electron 'size' at the time, the original theory predicted a maximal value for the electric field (given by the Born-Infeld parameter) of

$$E_{\text{Max}} = 1.187 \times 10^{20} \text{ V/m} \tag{3.3}$$

Today, this value is lower-bounded by hydrogen ionization experiments and $\gamma\gamma$-scattering at the LHC such that $E_{\text{Max}} \geq 10^{28}$ V/m, corresponding to a lower bound on the brane–mass scale of $M \gtrsim 100$ GeV [106, 107]. In anti-de Sitter spacetimes, it is known that this non-linearity introduces interesting new features beyond the Einstein-Maxwell case [108]: the Gibbs free energy becomes discontinuous in a certain temperature range, indicating a new kind of phase transition between small and intermediate sized black holes.

In this Chapter, we will demonstrate that a similar type of phase transition occurs in de Sitter space, finding also a reentrant small→large→small black hole phase transition

previously unseen in Born-Infeld black holes. We find that the character of these phase transitions depends critically on the value of the maximal electric field strength in the Born-Infeld theory. We also examine the free energy in an ensemble where the potential is fixed, and find not only metastable reentrant phase transitions (where the radiation phase globally minimizes the free energy), but also a reentrant radiation→black hole→radiation transition, the first time such a phase transition has been observed to our knowledge.

This chapter is organized as follows: In the next section, we discuss what modifications one should make to the thermodynamic description for a proper treatment of Born-Infeld black holes. In Section 3.2 we examine the thermodynamic properties of Born-Infeld-de Sitter black holes, including a discussion of the first law, the phase structure that arises, and an analysis of the vacuum polarization and metric function. Finally, in Section 4 we examine the free energy of charged de Sitter black holes both in the Maxwell and Born-Infeld theories in an ensemble where the potential is fixed, and discuss the phase behaviour present there.

3.1 Thermodynamic Quantities and the First Law

With the appearance of a new coupling constant b in the Born-Infeld Lagrangian, we must suitably generalize the extended first law for Born-Infeld black holes, as the mass parameter M is now also a function of the Born-Infeld parameter b. Specifically, we may define a new quantity

$$\mathcal{B} \equiv \left(\frac{\partial M}{\partial b}\right) \tag{3.4}$$

known as the 'Born-Infeld vacuum polarization'. This quantity has units of an electric polarization and is required for consistency of the first law and associated Smarr relation [108]. With this new potential the first law becomes

$$dE = TdS + VdP - \lambda dA_c + \phi dQ + \mathcal{B}\, db \ . \tag{3.5}$$

As before, λ is the surface tension associated with the cavity, A_c is the cavity area, ϕ is the electrostatic potential, and Q is the electric charge. The identification (2.1) of the thermodynamic pressure with the cosmological constant persists from before. We can again determine the temperature T, entropy S, and energy E of the system from the Euclidean action, while the thermodynamic volume, surface tension, and vacuum polarization are determined from the first law (3.5).

We also have a modified Smarr relation for Born-Infeld black holes, which in four dimensions reads

$$E = 2(TS - \lambda A_c - PV) + \Phi Q - \mathcal{B}b \ . \tag{3.6}$$

As (a version of) the Smarr relation appears to hold for every known black hole system and can be derived using very general arguments, it serves as an important consistency check for our thermodynamic description.

3.2 Born-Infeld-de Sitter Black Holes

In this chapter, we focus our attention on asymptotically de Sitter solutions in Einstein-Born-Infeld theory. We follow the same general procedure as before, evaluating the on-shell Euclidean action, using the result to determine the energy, temperature, and entropy of the spacetime, then constructing the free energy to examing the phase structure. Einstein-Born-Infeld theory is described by the following bulk action and boundary term:

$$I_{\text{total}} = -\frac{1}{16\pi}\int_{\mathcal{M}} d^4x\sqrt{g}\left(R - 2\Lambda + \mathcal{L}_{\text{BI}}\right) + \frac{1}{8\pi}\int_{\partial\mathcal{M}} d^3x\sqrt{k}\left(K - K_0\right) . \tag{3.7}$$

R is the Ricci scalar, Λ is the cosmological constant (positive for de Sitter space), K is the trace of the extrinsic curvature of the boundary, and $\mathcal{L}_{\text{BI}}$ is the Born-Infeld Lagrangian given by (3.2).

Like before, we choose the subtraction term K_0 such that the action is normalized to $I = 0$ when the mass (and therefore charge) of the black hole vanishes, making 'empty' (actually radiation filled) de Sitter space the reference point for the energy. As in the Einstein-Maxwell case examined in Chapter 1, this choice does not change the qualitative behaviour of the critical phenomena, only the numerical values of various quantities and critical points. Nonetheless it is still the more natural choice of reference since empty de Sitter space has the same asymptotics and topology near the boundary as the corresponding black hole spacetime.

In Schwarzschild coordinates, the metric function takes the form

$$ds^2 = -f(r)dt^2 + \frac{dr^2}{f(r)} + r^2 d\Omega^2 \tag{3.8}$$

where $f(r)$ is determined by the Hamiltonian constraint and is given by

$$f(r) = 1 - \frac{m}{r} - \frac{\Lambda r^2}{3} + \frac{2b^2}{r}\int_r^\infty \left(\sqrt{r^4 + \frac{q^2}{b^2}} - r^2\right) dr . \tag{3.9}$$

The boundary will be placed between the two largest real (positive) roots of $f(r) = 0$, so that $r_h < r_c < r_{\text{cosmo}}$. In these coordinates, we can also write the gauge field as

$$A_t = \frac{q}{r}\ {}_2F_1\left(\frac{1}{4}, \frac{1}{2}, \frac{5}{4}, \frac{-q^2}{b^2 r^4}\right) , \tag{3.10}$$

which generates a finite radial electric field

$$E(r) = \frac{q}{\sqrt{r^4 + \frac{q^2}{r^2}}} , \tag{3.11}$$

where ${}_2F_1(a, b, c, z)$ is the Gaussian hypergeometric function. The 'integral' form of the

metric function (3.9) is valid for all Λ, b, q and $r > 0$. It can also be written in terms of ${}_2F_1$ as

$$f(r) = 1 - \frac{m}{r} - \frac{\Lambda r^2}{3} + \frac{2b^2r^2}{3}\left(1 - \sqrt{1 + \frac{q^2}{b^2r^4}}\right) + \frac{4q^2}{3r^2}\,{}_2F_1\left(\frac{1}{4}, \frac{1}{2}, \frac{5}{4}, \frac{-q^2}{b^2r^4}\right) \ , \tag{3.12}$$

where the series expansion of ${}_2F_1(a, b, c, z)$ is convergent for $|z| > 1$, i.e. $r > \sqrt{q/b}$. The reduced action for this spacetime can then be determined explicitly using methods discussed previously. We find that

$$\begin{aligned} I_r =& \beta r_c \left[\left(1 - \frac{\Lambda r_c^2}{3}\right)^{1/2} - \left(\frac{(2b^2 - \Lambda)(r_c^3 - r_h^3) + 3(r_c - r_h) - 2br_c\sqrt{b^2r_c^4 + q^2}}{3r_c}\right.\right. \\ & \left.\left. \frac{+2br_h\sqrt{b^2r_h^4 + q^2}}{3r_c} - \frac{4q^2\left({}_2F_1\left(\frac{1}{4}, \frac{1}{2}, \frac{5}{4}, \frac{-q^2}{b^2r_h^4}\right) r_c - \,{}_2F_1\left(\frac{1}{4}, \frac{1}{2}, \frac{5}{4}, \frac{-q^2}{b^2r_c^4}\right) r_h\right)}{3r_c^2 r_h}\right)^{1/2}\right] - \pi r_h^2 \end{aligned} \tag{3.13}$$

The temperature is found by extremizing the action with respect to r_h and solving for β, giving

$$\beta^{-1} = T = \frac{\sqrt{3}\, r_c \left(1 + r_h^2\,(2b^2 - \Lambda) - 2\,b\sqrt{b^2r_h^4 + q^2}\right)}{4\pi\sqrt{r_h}\, X} \tag{3.14}$$

where we have defined

$$X \equiv \sqrt{r_c\, r_h\left(3(r_c - r_h) + (2b^2 - \Lambda)\,(r_c^3 - r_h^3) - 2b\left(r_c\sqrt{b^2r_c^4 + q^2} - r_h\sqrt{b^2r_h^4 + q^2}\right)\right) - \mathsf{F}} \tag{3.15}$$

and

$$\mathsf{F} \equiv 4q^2\left[{}_2F_1\left(\frac{1}{4}, \frac{1}{2}, \frac{5}{4}, \frac{-q^2}{b^2r_h^4}\right) r_c - \,{}_2F_1\left(\frac{1}{4}, \frac{1}{2}, \frac{5}{4}, \frac{-q^2}{b^2r_c^4}\right) r_h\right] \ . \tag{3.16}$$

In the limit $b \to \infty$, this reduces to the Maxwell case discussed in Chapter 2,

$$T = \frac{1 - \frac{q^2}{r_h r_c} - \frac{\Lambda}{3}\left(r_c^2 + r_c r_h + r_h^2\right) + \left(1 - \frac{r_h}{r_c}\right)\left(\frac{\Lambda}{3}(r_c^2 + 2r_h r_c) - \frac{q^2}{r_h^2}\right)}{4\pi r_h\sqrt{\left(1 - \frac{r_h}{r_c}\right)\left(1 - \frac{q^2}{r_h r_c} - \frac{\Lambda}{3}\left(r_c^2 + r_c r_h + r_h^2\right)\right)}} \ , \tag{3.17}$$

and taking further the limits $\Lambda \to 0$, $q \to 0$, and $r_c \to \infty$ gives the familiar result $T = 1/4\pi r_h$ for the asymptotically flat Schwarzschild black hole. The entropy is

$$S = \beta\frac{\partial I_r}{\partial\beta} - I_r = \pi r_h^2 \tag{3.18}$$

and finally the energy is

$$E = \frac{\partial I_r}{\partial \beta} = r_c \left[\left(1 - \frac{\Lambda r_c^2}{3}\right)^{1/2} - \left(\frac{2b(r_c^3 - r_h^3)^2 - \Lambda(r_c^3 - r_h^3) + 3(r_c - r_h) - 2br_c\sqrt{b^2 r_c^4 + q^2}}{3r_c} \right.\right.$$
$$\left.\left. \frac{+2br_h\sqrt{b^2 r_h^4 + q^2}}{3r_c} - \frac{4q^2 \left({}_2F_1\left(\frac{1}{4}, \frac{1}{2}, \frac{5}{4}, \frac{-q^2}{b^2 r_h^4}\right) r_c - {}_2F_1\left(\frac{1}{4}, \frac{1}{2}, \frac{5}{4}, \frac{-q^2}{b^2 r_c^4}\right) r_h \right)}{3r_c^2 r_h} \right)^{1/2} \right]$$
$$= \frac{1}{3}\left(r_c\sqrt{9 - 3\Lambda r_c^2} - X\sqrt{3/r_h} \right) \ . \tag{3.19}$$

One can check that in the limit $b \to \infty$ these quantities also reduce to those obtained in Chapter 2.

3.2.1 The First Law

With the energy E, temperature T, and entropy S as defined above, we can determine the thermodynamic volume V, surface tension λ, and vacuum polarization $\mathcal{B}$ from the first law. In order for (3.5) to hold, the surface tension must be

$$\lambda = \frac{1}{8\pi r_c} \left(\frac{3 - 2\Lambda r_c^2}{\sqrt{9 - 3\Lambda r_c^2}} + \frac{\mathsf{F} - r_c r_h \left((2b^2 - \Lambda)\left(4r_c^3 - r_+^3\right) + 3(2r_c - r_h) \right)}{2\sqrt{3} r_c \sqrt{r_h} X} \right.$$
$$\left. - \frac{2b\left(4r_c\sqrt{b^2 r_c^4 + q^2} - r_h\sqrt{b^2 r_+^4 + q^2}\right)}{2\sqrt{3} r_c \sqrt{r_h} X} \right) \ , \tag{3.20}$$

the thermodynamic volume is

$$V = \frac{4\pi r_c \left(r_c^3\sqrt{r_h} - \frac{r_c^2 X}{\sqrt{3 - \Lambda r_c^2}} - r_h^{7/2} \right)}{\sqrt{3}\, X} \ , \tag{3.21}$$

the electric potential is

$$\phi = \frac{\sqrt{3}\,\mathsf{F}}{4q\sqrt{r_h} X} \ , \tag{3.22}$$

and the vacuum polarization is

$$\mathcal{B} = \frac{2r_c r_h \left[q^2 \left(\frac{r_c}{\sqrt{b^2 r_c^4 + q^2}} - \frac{r_h}{\sqrt{b^2 r_h^4 + q^2}} \right) + b^2 \left(\frac{r_c^5}{\sqrt{b^2 r_c^4 + q^2}} - \frac{r_h^5}{\sqrt{b^2 r_h^4 + q^2}} \right) - b\left(r_c^3 - r_h^3\right) \right] + \frac{\mathsf{F}}{4b}}{\sqrt{3 r_h}\, X} \ . \tag{3.23}$$

With these definitions it is straightforward to verify that

$$dE = TdS - \lambda dA_c + VdP + \phi dQ + \mathcal{B}db \ . \tag{3.24}$$

As an important check, direct substitution of the above quantities also reveals that the modified Smarr relation (3.6) is also satisfied.

Figure 3.1 shows regions in parameter space where V is positive, in terms of the dimensionless ratio $x \equiv r_h/r_c \in [0,1]$ and the cosmological constant (i.e. pressure) Λ. We have implicitly restricted our analysis to regions where $r_h < r_c < r_{\text{cosmo}}$. Outside the shaded regions one cannot interpret (3.21) as a volume in the traditional sense. One can see on the right side of Figure 3.1 that as b becomes large, the volume behaves as it does in the Maxwell case depicted in Figure 2.4, as expected.

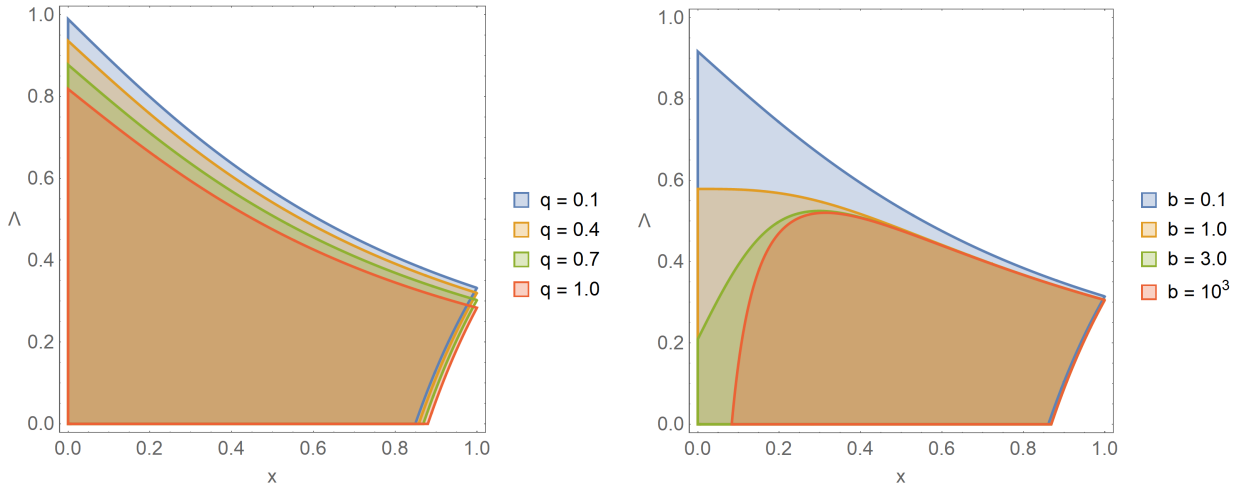

Figure 3.1: Regions of positivity (colored) for the thermodynamic volume V as a function of $x = r_h/r_c$ and Λ, with fixed cavity radius $r_c = \sqrt{3}$. **Left:** Varying charge with $b = 0.1$. **Right:** Varying b with $q = 0.5$.

Figure 3.2 depicts regions where the cavity tension λ is positive. Outside of the shaded regions (some of which overlap with $V > 0$ regions) λ is negative and should be thought of as a surface pressure. Within the shaded regions λ can be regarded as a surface tension. There is therefore a critical line along which $\lambda = 0$ where the work required to create the cavity vanishes.

3.2.2 Vacuum Polarization and Metric

Born-Infeld theory has the feature that two distinct types of black hole solutions exist, depending on the values of b and q. This is demonstrated in Figure 3.3, where we plot the metric function (3.12) for fixed mass and varying b, as well as fixed b and varying mass. There is a *marginal* case (indicated in green) separating the two types of solutions, which occurs when $f(r)$ attains a finite value at the origin. At this point, the black hole is completely regular. The condition for this to occur is

$$m_m = \frac{\sqrt{b\,q^3}\,\Gamma\left(\frac{1}{4}\right)^2}{3\sqrt{\pi}}\ . \tag{3.25}$$

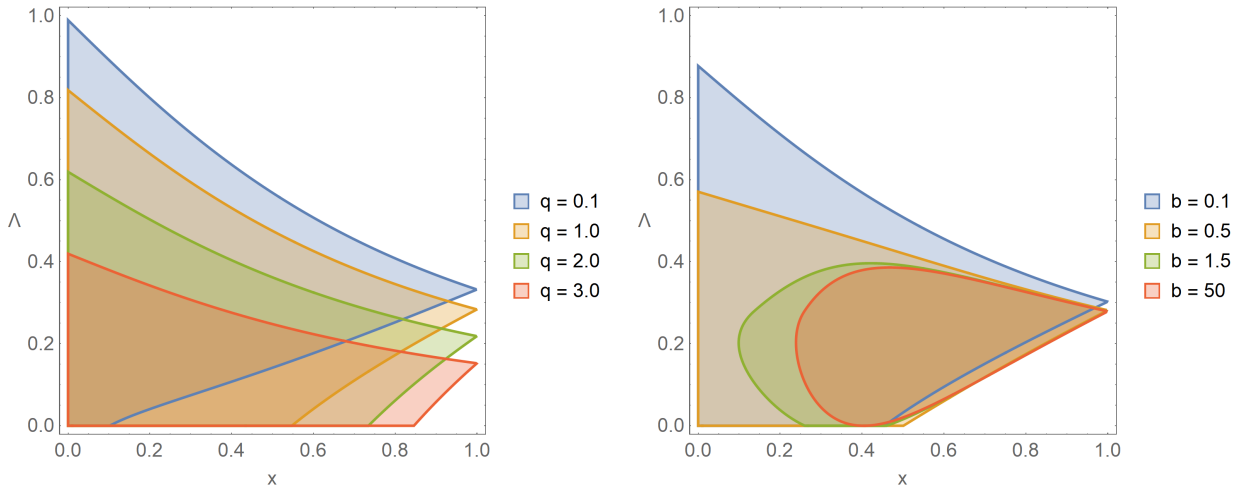

Figure 3.2: Regions of positivity for the surface tension λ as a function of x and Λ with fixed cavity radius $r_c = \sqrt{3}$. Shaded regions indicate positivity, where λ should be regarded as a surface pressure. **Left:** Varying charge with $b = 0.1$. **Right:** Varying b with $q = 0.7$.

Spacetimes with $m > m_m$ are Schwarzschild-de Sitter-like, having a singularity at $r = 0$, a black hole horizon at $r = r_h$, and a cosmological horizon at $r = r_{\text{cosmo}}$ (beyond the cavity radius r_c). Spacetimes with $m < m_m$ are Reissner-Nordström-de Sitter-like (and approach this solution as $b \to \infty$), with up to three distinct horizons: the inner horizon at $r = r_i$, the outer black hole horizon at $r = r_h$, and the cosmological horizon at $r = r_{\text{cosmo}}$. The small-r behaviour is similar to that of the Born-Infeld-AdS case examined in [108]. However the positive cosmological constant changes the large-r behaviour; even though the cosmological horizon is 'hidden' behind the cavity, spacetime is still de Sitter-like up to the cavity radius.

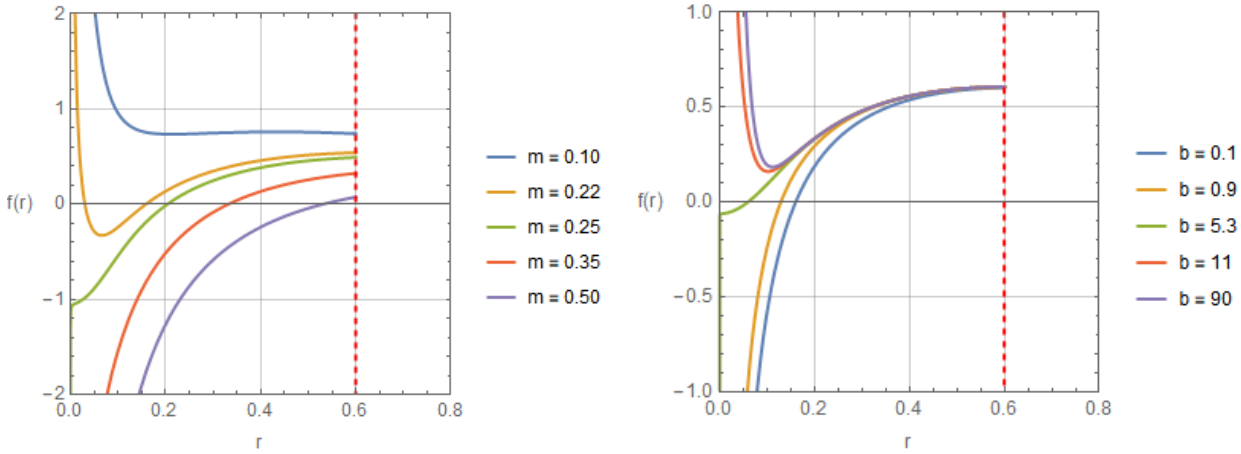

Figure 3.3: The metric function $f(r)$ as a function of r for $q = 0.1$, $\Lambda = 1$, and $r_c = 0.6$; the cavity radius is indicated by the red dashed line. **Left:** Fixed vacuum polarization ($b = 10.22$) and varying mass parameter m. **Right:** Fixed mass ($m = 0.18$) and varying b. In both figures the marginal case appears in green.

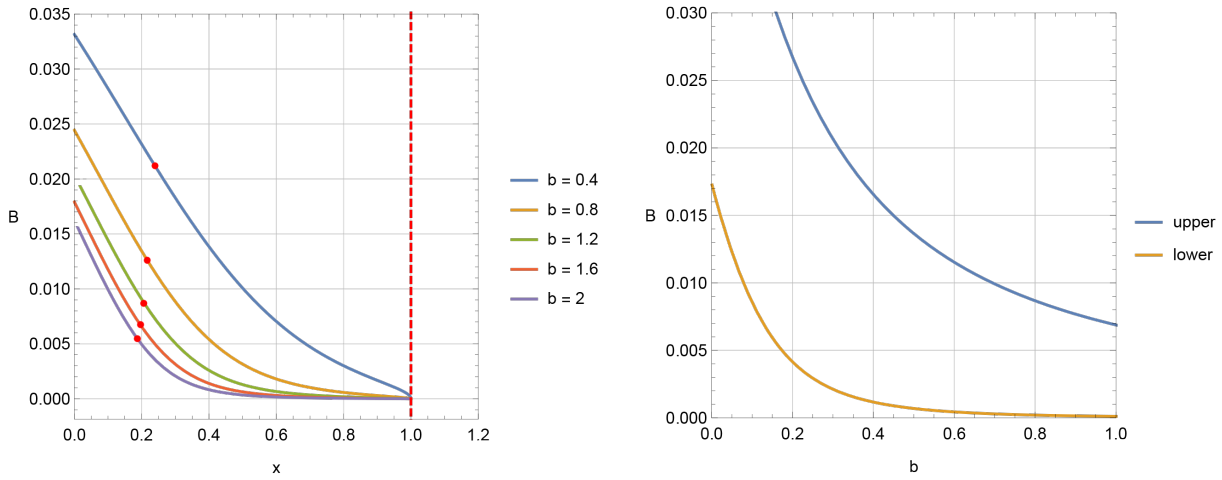

Figure 3.4: Behaviour of the vacuum polarization for $q = 0.1$, $\Lambda = 1$, and $r_c = 0.6$; the cavity radius is indicated by the red dashed line. **Left:** $\mathcal{B}$ as a function of $x \equiv r_f/r_c$ for various b. The red dots indicate the marginal mass along each line. **Right:** $\mathcal{B}$ as a function of b for fixed $T = 0.5$ ($\mathcal{B} - b$ isotherms), with two branches.

The conjugate $\mathcal{B}$ to the maximal electric field strength b in the first law has units of polarization per unit volume, and is referred to as the *Born-Infeld vacuum polarization*. Its behaviour is shown in Figure 3.4. On the left, we see that for any $r < r_c$, the vacuum polarization approaches zero as b increases (corresponding to the Maxwell limit), and appears to reach a finite value at the origin. However we cannot draw conclusions about the small-r behaviour since (3.12) restricts us to working in regions where $r > \sqrt{q/b}$. The red dots on each line mark where the marginal mass (3.25) is achieved; to the left of this dot the solution is Reissner-Nordström-de Sitter-like and to the right it is Schwarzschild-de Sitter-like.

Also of note is the fact that $\mathcal{B}$ vanishes at r_c for any value of b, implying that the cavity itself does not support a vacuum polarization. Looking at the right diagram in Figure 3.4, we see that there are two branches of $\mathcal{B} - b$ isotherms. The upper branch corresponds to a negative thermodynamic volume V, while the lower branch has $V > 0$, so we take the lower branch to be the 'physical' one. In both branches the vacuum polarization approaches zero as we approach the Maxwell limit $b \to \infty$.

3.2.3 Helmholtz Free Energy and Phase Transitions

We now turn to the phase structure of the Born-Infeld-de Sitter black hole. The quantity of interest is the Helmholtz free energy, $F = E - TS$, which is minimized by the equilibrium state of the system. Plotting F as a function of T for fixed P (or Λ) will reveal the presence of any phase transitions in the system, generally indicated by discontinuities in the free

energy. Using (5.34), (3.18), and (3.19) we have

$$F(r_h,\Lambda)=r_c\sqrt{1-\frac{\Lambda r_c^2}{3}}+\frac{\sqrt{3}\,r_c\,r_h^{3/2}\left(1+(2b^2-\Lambda)\,r_h^2-2b\sqrt{q^2+b^2r_h^4}\right)}{4X}-\frac{X}{\sqrt{3r_h}} \tag{3.26}$$

where F is understood to also depend on q, b, and r_c, which are fixed. In Figure 3.5, Figure 3.6, and Figure 3.7, we plot $F(T)$ parametrically using r_h as the parameter.

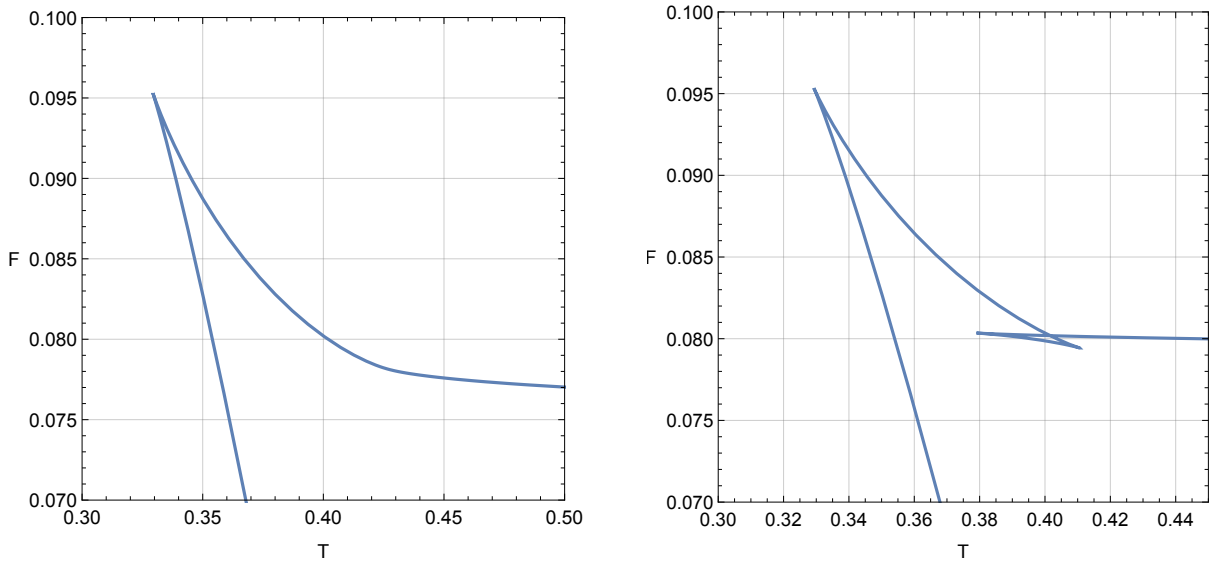

Figure 3.5: Helmholtz free energy of the Born-Infeld-de Sitter black hole for fixed cavity size ($r_c = 0.6$), pressure ($P = -0.0025$), and charge ($q = 0.1$). **Left:** $b = 4$. **Right:** $b = 4.42$.

There are a total of 4 distinct critical values of b marking points where qualitative differences in the phase behaviour occur. We refer to these as $\{b_{c1}, b_{c2}, b_{c3}, b_{c4}\}$ and note that the exact values depend on q, r_c, and Λ and must be found numerically. On the left of Figure 3.5, we see that for 'small' values of the maximal electric field strength ($b < b_{c1}$), the free energy resembles that of an uncharged AdS black hole, where a Hawking-Page phase transition normally occurs. In this case however, we have chosen an ensemble where the charge is fixed, so there can be no transition from a black hole to empty space, and only a large black hole exists above the minimum temperature where the leftmost cusp is. To see a possible phase transition, we must plot the free energy at fixed potential, $G = M - TS - \Phi q$, which we do in Section 4. Above the critical value b_{c1} (in this case $b_{c1} \approx 4.38$) a kink forms in the free energy, which traces out an inverted swallowtail in $F-T-P$ space, similar to the one observed in [108]. This is shown in the right-hand figure in Figure 3.5. However, for values of b in the range (b_{c1}, b_{c2}) this kink does not intersect the lower large black hole branch, which still minimizes the free energy, and therefore does not indicate the presence of a phase transition.

In Figure 3.6, we see that when b exceeds the second critical value ($b > b_{c2}$), a 'star' pattern characteristic of a reentrant phase transition forms. Examining the figure on

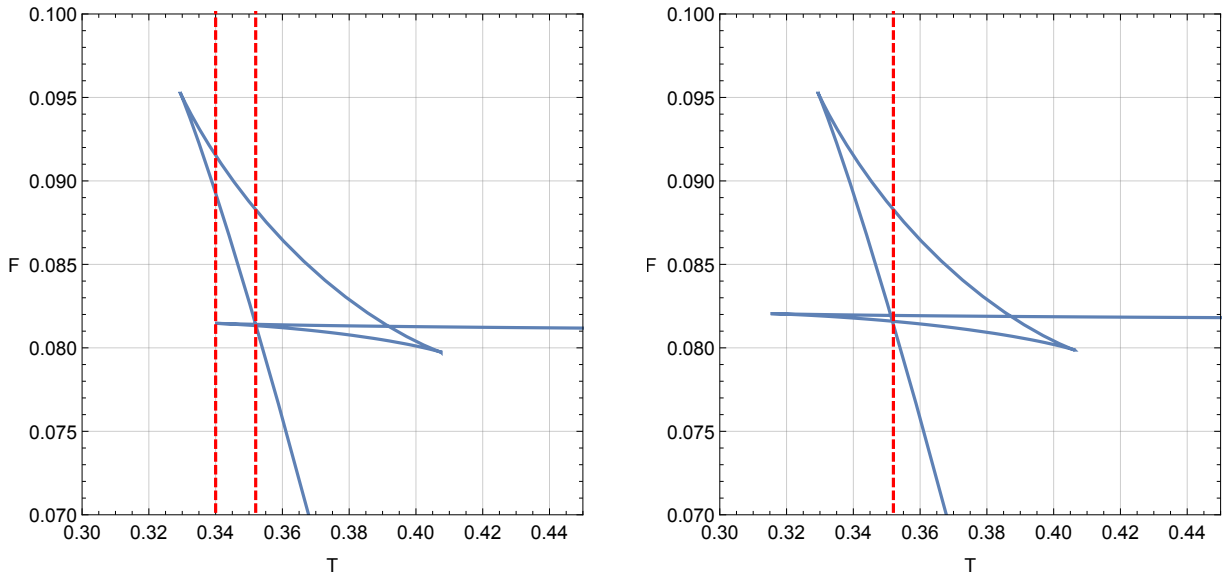

Figure 3.6: Helmholtz free energy of the Born-Infeld-de Sitter black hole for fixed cavity size ($r_c = 0.6$), pressure ($P = -0.0025$), and charge ($q = 0.1$). On the left we have $b = 4.57565$ and on the right $b = 4.65$. The red dashed lines mark the temperature at which phase transitions occur.

the left, as the temperature increases the first dashed line corresponds to a zeroth-order large→small black hole phase transition, whereas the second dashed line corresponds to the usual first-order small→large transition. When $b > b_{c3}$ (as in the right side of Figure 3.6), the small black hole branch always has lower free energy than the upper large black hole branch, so the first phase transition is washed out and only the small→large black hole transition at the second dashed line remains. Finally, when b is above the fourth critical value $b > b_{c4}$, the phase structure of a charged Schwarzschild-de Sitter black hole emerges, as expected since the limit $b \to \infty$ corresponds to the usual Einstein-Maxwell action. Indeed in this limit we recover all of the phenomena and qualitative behaviour seen in the previous chapter, with only small quantitative changes to the various critical values when b is very large but finite. To summarize, there are five regions separated by four critical values of b:

$0 < b < b_{c1}$:	No phase transitions. Large black hole phase globally minimizes F.
$b_{c1} < b < b_{c2}$:	No phase transitions. Unstable inverted swallowtail region forms.
$b_{c2} < b < b_{c3}$:	Reentrant phase transition from large → small → large black hole.
$b_{c3} < b < b_{c4}$:	Small → large transition with a minimum temperature.
$b_{c4} < b < \infty$:	Small → large transition with no minimum temperature.

In the Maxwell case examined in Chapter 2, we demonstrated the presence of a unique 'swallowtube' structure in phase space which results from the presence of the isothermal

cavity. This tube represented a compact region in phase space where a small/large black hole phase transition occurs, the pressure being bounded by an upper and lower critical value $P \in \{P_{\min}, P_{\max}\}$ outside of which the phase transition disappears. A similar, albeit more complicated structure appears when Born-Infeld electrodynamics is introduced. For large values of b we recover the swallowtube seen in the Maxwell case, with a slightly modified shape (the identical shape being achieved in the limit $b \to \infty$). However once b falls below a critical value, the shape of this tube qualitatively changes, such that each constant-pressure slice resembles one of the two cases shown in Figure 3.5. Depending on the exact choice of parameters, these slices may contain a reentrant phase transition (as in the left side), or a regular small→large transition (as in the right side), and always have the property that there are no black holes with $T \approx 0$, unlike in the Maxwell case where black holes exist down to $T = 0$. This difference is shown in Figure 3.7, with the tube structure being represented as a series of constant pressure slices in $F - T - P$ space. Furthermore, for any choice of q, r_c, and b where a reentrant phase transition is present in one of the slices, the tube terminates at $P = 0$. If there is no reentrant phase transition, one can always choose parameters such that the tube pinches off at a non-zero pressure as it does in the Maxwell case. Note finally that if b is small enough, then for no choice of q, r_c, and Λ is the swallowtube present.

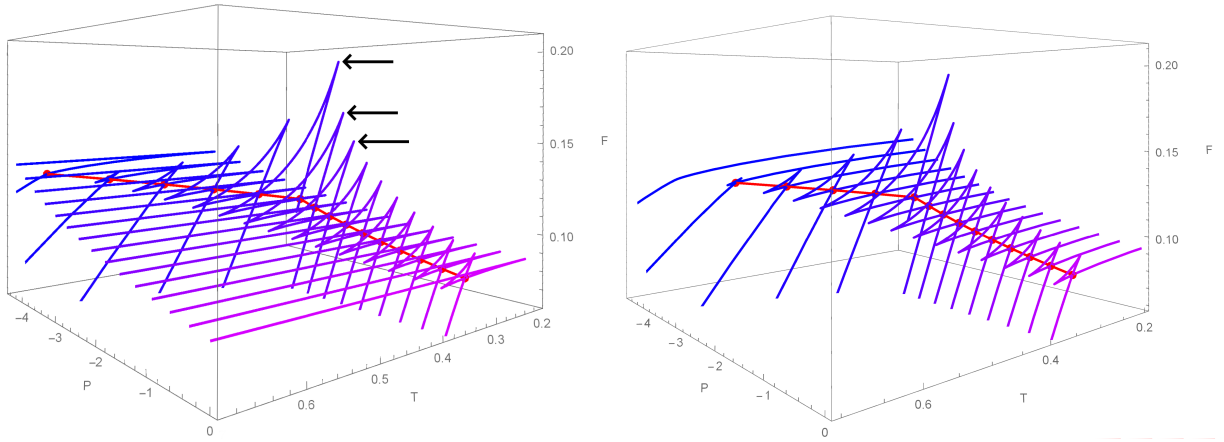

Figure 3.7: Helmholtz free energy of the Born-Infeld-de Sitter black hole for $q = 0.105$, $r_c = 0.6$, showing slices of fixed P. The red dots mark the small→large phase transition on each slice. The red line is the coexistence curve. **Left:** $b = 4.6$. A reentrant phase transition is present on the slices indicated with the black arrows. These slices resemble the left of Figure 3.6. The remaining slices resemble the right of Figure 3.6. **Right:** $b = 5$. There are no reentrant phase transitions present. Note the difference in small-T behaviour between the two figures: on the left, there is a minimum temperature at which the black hole phase exists, while on the right there is no minimum temperature (the lines extend to $T = 0$).

Working in the extended phase space also allows us to determine the equation of state for these Born-Infeld-de Sitter black holes. This is a relationship between the pressure P, temperature T, and volume V (the thermodynamic volume divided by the number of degrees of horizon degrees of freedom) [34]. In AdS space the volume $V \sim r_h^3$ and the

specific volume (the volume per horizon degrees of freedom) $v \sim r_h$ [31]. However in dS space, (5.34) means that the pressure is a non-linear function of (T, r_h), and (3.21) in turn implies that r_h is a highly non-linear function of V. As a result, the equation of state cannot be expressed in closed form. We can plot $P(V)$ at fixed T numerically; however doing so shows an absence of the oscillations characteristic of the van der Waals fluid. We omit the plot here for lack of insight. These oscillations *are* present in the Born-Infeld-AdS case examined in [108]; it remains to be determined whether the analogy with van der Waals fluids in the extended phase space breaks down because of the presence of the cavity, or due to the fact that we are working in asymptotically de Sitter spacetime.

3.3 Free Energy at Fixed Potential

As noted above, we should not expect to see a Hawking-Page-like phase transition when examining the free energy as defined by (3.26). This is because the ensemble considered there is one where the total charge q is fixed. However, a black hole cannot dissolve into pure radiation and conserve charge at the same time. Instead, one must consider what happens when the potential is fixed at the cavity while the charge is allowed to vary. With these boundary conditions the free energy becomes $G = M - TS - \Phi q$. We examine first the Maxwell limit $b = \infty$, followed by the Born-Infeld case.

3.3.1 Maxwell Theory

In the Maxwell limit, the free energy at fixed potential is:

$$G = r_h + \frac{q^2}{r_h} - \frac{\Lambda r_h^3}{3} - \frac{\sqrt{3}q^2(r_c - r_h)}{\sqrt{r_h(r_h - r_c)\left(r_c r_h\left(\Lambda\left(r_c^2 + r_c r_h + r_h^2\right) - 3\right) + 3q^2\right)}}$$

$$+ \frac{r_h^3\left(\left(8\pi\sqrt{\frac{r_c}{r_h^2}}\sqrt{(r_c - r_h)\left(r_c r_h\left(\Lambda\left(r_c^2 + r_c r_h + r_h^2\right) - 3\right) + 3q^2\right)} + \sqrt{3}(\Lambda r_c^2 - 1)\right) + \frac{\sqrt{3}q^2}{r_c^2}\right)}{4\sqrt{r_c(r_c - r_h)\left(r_c r_h\left(\Lambda\left(r_c^2 + r_c r_h + r_h^2\right) - 3\right) + 3q^2\right)}} \tag{3.27}$$

We plot (3.27) as a function of temperature T for fixed ϕ, r_c, b, and Λ in Figure 3.8, along with the free energy of the Born-Infeld-de Sitter black hole for large b. Examining the figure on the left, as one follows the branches from $T = \infty$ (where they overlap) the black hole increases in size towards the maximal value r_c, which is achieved at the red dots. The yellow line in Figure 3.8 represents a reentrant phase transition, with a small→large transition occurring at the leftmost red line, followed by a large→small transition at the

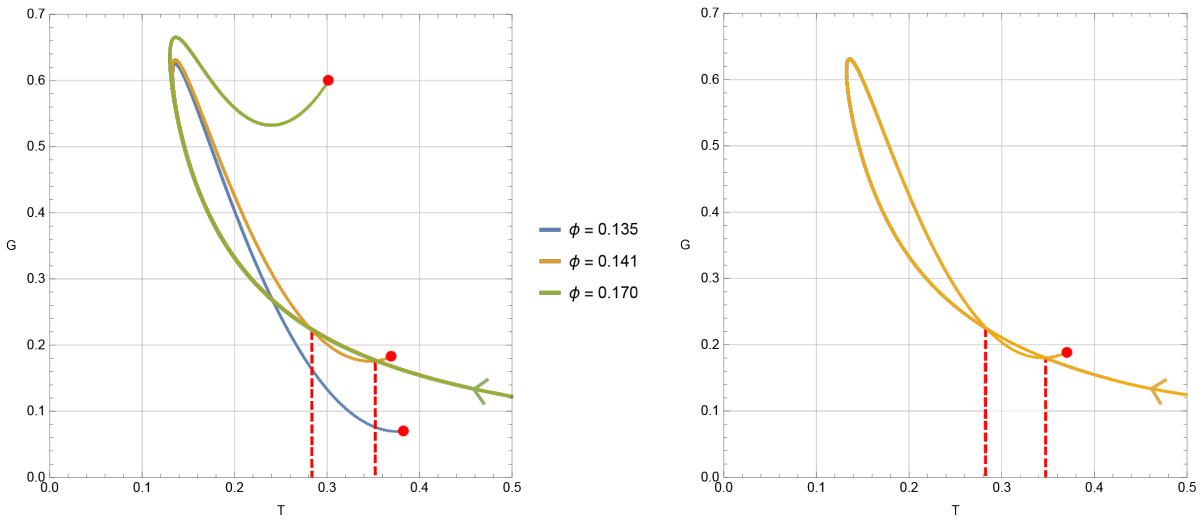

Figure 3.8: Free energy at fixed potential, with $r_c = 1.5$, $\Lambda = 0.001$. The temperatures at which phase transitions occur are indicated by the red dashed lines. The cavity radius r_c is indicated by a red dot. **Left:** The Reissner-Nordström-de Sitter black hole, with varying ϕ. **Right:** The Born-Infeld-de Sitter black hole with $b = 10$ for $\phi = 0.141$.

second line. For values of ϕ above a certain critical value ϕ_c, the branches no longer intersect (as in the green case), and the small black hole globally minimizes the free energy for all temperatures. This value depends on the choice of r_c, b, and Λ and must be found numerically. Below ϕ_c (as in the blue curve) there is only a small→large transition, as the free energy terminates at r_c before intersecting the small black hole branch again. Critically, these transitions are all *metastable*, as the free energy is in all cases above the $G = 0$ line corresponding to the radiation phase.

3.3.2 Born-Infeld Theory

In the Born-Infeld case, the free energy at fixed potential is:

$$G = \frac{4q^2\,{}_2F_1\left(\frac{1}{4},\frac{1}{2},\frac{5}{4},-\frac{q^2}{b^2r_h^4}\right) - r_h^2\left(2b\sqrt{b^2r_h^4+q^2} - 2b^2r_h^2 + \Lambda r_h^2 - 3\right)}{3r_h} - \frac{\sqrt{3\,r_+^3}\,r_c\left(1 + r_h^2\,(2b^2-\Lambda) - 2\,b\sqrt{b^2r_h^4+q^2}\right)}{4\sqrt{r_h}\,X} - \frac{\sqrt{3}\,\mathsf{F}}{4\sqrt{r_h}X} \tag{3.28}$$

Figure 3.9 displays the free energy (3.28) of the Born-Infeld-de Sitter black hole at fixed potential. On the left, we plot G for fixed b and varying ϕ. Just like in the Maxwell case, there is a critical value of ϕ for which the large black hole branch begins to intersect the small branch (as in the blue line) and gives rise to a (metastable) reentrant small→large→small phase transition. The exact value of ϕ at which this occurs again

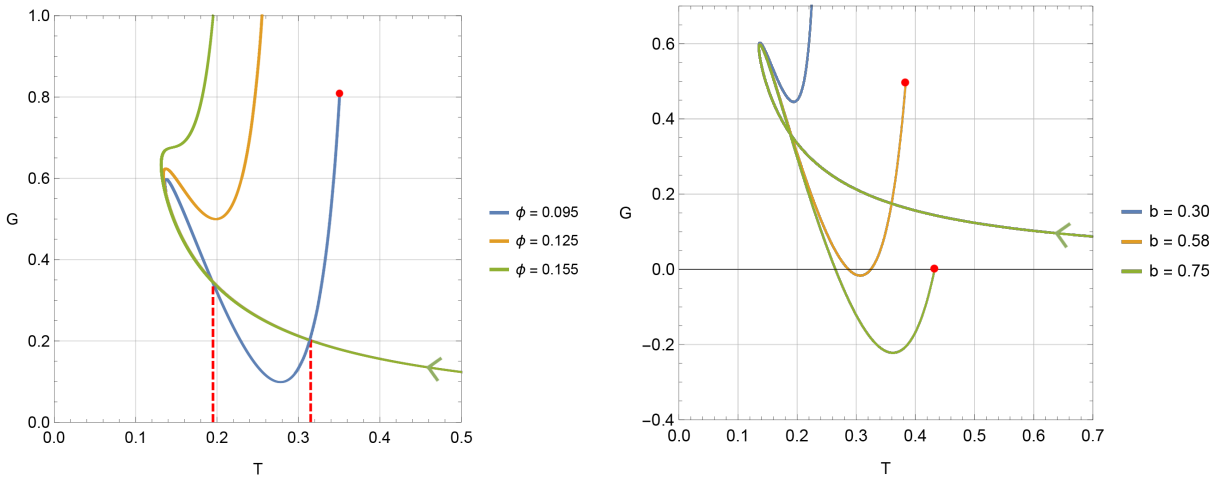

Figure 3.9: Free energy of the Born-Infeld-de Sitter black hole at fixed potential. The three lines overlap where they merge together in both figures. **Left:** $b = 0.5$, $r_c = 1.5$, and varying ϕ. The temperatures at which phase transitions occur are indicated by the red dashed lines. The cavity radius r_c is indicated by a red dot. **Right:** Fixed $\phi = 0.095$, $r_c = 1.5$, and varying b.

depends on the value of r_c, ϕ and Λ, and must be found numerically. In the given example, this occurs at approximately $\phi_c \sim 0.08$. We emphasize again that the radiation phase globally minimizes the free energy here. For comparison, we plot the same free energy for the Born-Infeld-de Sitter black hole for $b = 10$ and $\phi = 0.141$ on the right side of Figure 3.8, demonstrating that for large enough values of b the two cases are identical.

On the right of Figure 3.9, we plot G for fixed ϕ and varying b. Here we see that a true reentrant phase transition emerges within a small range of values for the maximal electric field strength b. In the given example, for $b \in (0.57, 0.75)$ the large black hole branch crosses the $G = 0$ line, giving rise to a reentrant phase transition from radiation to an intermediate black hole, and back to radiation as the temperature increases. The thermodynamically stable state is pure radiation at both small and large temperatures, with a charged black hole as the stable state at intermediate values. Above $b = 0.75$, the cavity radius r_c is reached before the large black hole branch crosses the $G = 0$ line, and we have a zeroth order phase transition from a large size black hole to radiation. To our knowledge this is the first time these particular types of reentrant phase transitions from black holes to radiation have been observed. The fact that a black hole exists within an intermediate temperature range while radiation is the preferred state at both low and high temperatures is a curiosity that is so far only seen when an isothermal cavity and Born-Infeld gauge field are present.

3.4 Summary

The introduction of an isothermal cavity as an equilibrating mechanism allows for the study of a wealth of thermodynamic phenomena in various asymptotically de Sitter spacetimes. We have shown that Born-Infeld-de Sitter spacetimes admit interesting new phase structures that are not present in either traditional Maxwell theories or in asymptotically AdS spacetimes, namely the existence of a tube-like structure in $F - T - P$ space analogous to the swallowtail typically seen in AdS spacetimes, but which is compact in the sense that there is an upper and lower bound of pressures for which a small/large black hole phase transition occurs. In the Maxwell case studied in Chapter 2, this *swallowtube* represented a series of first-order small→large black hole phase transitions. The non-linearities of Born-Infeld theory significantly alter this structure, so that each slice of the tube instead represents a *reentrant* phase transition when b is small enough. Notable is the fact that the boundedness of the electric field strength means that the swallowtube is cut off at $P = 0$ for a wide range of values for r_c and q (i.e. the phase transition survives in the $P \to 0$ limit). This is in contrast to the Maxwell case where the tube pinches off at both ends at non-zero pressure, and the phase transition disappears as $P \to 0$.

We have also observed for the first time reentrant phase transitions between charged black holes and pure radiation in the Gibbs ensemble where the potential is fixed. We find that for a certain range of ϕ, Born-Infeld black holes are stable at intermediate values of the temperature, provided the parameter b is in an intermediate range of values. Otherwise either cold radiation or hot radiation is the more stable state. Finally, we note that the isothermal cavity necessarily introduces non-linearities in the equation of state $P(T, V)$ that prevent the oscillations associated with Van der Waals-like phase transitions (typically seen in asymptotically AdS spacetimes) from occurring. This was seen in Chapter 2 in the Einstein-Maxwell case, and remains true even with the inclusion of Born-Infeld electrodynamics. It seems that the equilibrating mechanism (isothermal cavity in dS vs. reflecting boundary conditions in AdS) plays a larger role in determining the nature of the equation of state than does the inclusion of field non-linearity. It remains to be seen if this is still true in higher dimensions, when angular momentum is considered, or when considering other modifications to Einstein-Maxwell theory. Some of these possibilities will be explored in the chapters to follow.

Chapter 4

Black Holes with Scalar Fields

Having studied the effect of gauge fields (both in the context of Maxwellian electrodynamics and its non-linear extension), we now turn our attention to generalizations of the Einstein-Hilbert action which include a scalar field ϕ, and the effect such inclusions have on the thermodynamic description of black holes. There is an obvious motivation to consider such extensions coming from our desire to eventually understand the thermodynamic properties of astrophysical black holes. These are never of the idealized, isolated variety described by the standard metrics. Rather, they reside in environments where other matter fields are constantly interacting with the black hole, the simplest model for which is a scalar field. Though there is a rich history in examining the interplay between scalar fields and the gravitational interaction, there has been comparatively little interest in the thermodynamic aspects of black holes endowed with scalar fields, despite the strong motivations available from cosmology, field theory, and particle physics. Among these are the recent discovery of a fundamental scalar in nature (the Higgs boson), as well as the ubiquity of scalar fields in cosmology, where they are used to model dark matter, neutron stars, the early universe, and more [109–112]. Indeed, scalar fields arise quite generally in effective field theory descriptions of fundamental fields after coarse-graining, and also underlie the mechanism of inflation [113, 114]. Examining their role in black hole thermodynamics therefore is essential if we are to eventually understand the thermodynamic properties of astrophysical black holes.

Some attempts at understanding this interplay have already been made, notably with the Bronnikov-Melnikov-Bocharova-Bekenstein (BMBB), the Martinez-Troncoso-Zanelli (MTZ) and the Achucarro-Gregory-Kuijken (AGK) pierced black hole solutions [115–118]. These early examples, originally the only known exceptions to the "black holes have no (scalar) hair" theorem [119] have now given way to a large number of solutions of Einstein gravity and its extensions [120]. However in the context of black hole thermodynamics, particularly for asymptotically de Sitter black holes, they have received relatively little attention. The BMBB black hole has been shown to lack any sensible thermodynamic interpretation [121], owing to the divergence of the scalar field at the horizon, while also being generically unstable [122]. However the situation for the MTZ black hole, which

is the analogous solution for $\Lambda > 0$, is somewhat more promising. There, the entropy and temperature are both found to be finite, and there appears to exist non-trivial phase structure when charge is present [123]. However, these preliminary investigations (the ones with $\Lambda \neq 0$ in particular) are not formulated in the extended phase space as we will do here.

Another motivation for including a scalar field in the action comes from alternative theories of gravity, a large class of which are *scalar-tensor theories*. These theories generically contain a scalar field and have proven to be very resistant to exclusion by observational tests. They also possess a substantial phenomenology and have significant theoretical interest due to the ubiquity of scalar field–gravity coupling in unifying theories and cosmology [124]. These are metric theories of gravity (as defined in Section 1.1.1) which contain an extra scalar 'gravitational field' ϕ coupled directly to the metric g (the basic aspects of which are presented in the subsequent section). The earliest and most well-known example of a scalar-tensor theory is Jordan-Brans-Dicke theory, in which the gravitational coupling G is allowed to vary in spacetime and is encoded in the scalar field profile. The theory is, like general relativity, in agreement with all current astrophysical observations, though it contains a tunable parameter, which can be used to ensure the theory falls within experimental constraints. Nonetheless, more general scalar-tensor theories remain extremely interesting as they are equivalent in many cases to some counterpart $f(r)$ theory of gravity, which are often used to model dark matter in cosmology [125].

With these motivations in mind, a number of open questions concerning the role that scalar fields play in the context of black hole thermodynamics naturally arise. Can sensible thermodynamics be formulated with conformal coupling, or are more complicated couplings required? Which classes of scalar-tensor theories admit reasonable thermodynamic descriptions of black holes, and how do boundary conditions imposed on the scalar field affect or constrain the allowed phenomena? Do general features seen in the phase structure of de Sitter black holes (Hawking-Page transitions, swallowtubes, etc.) survive when a scalar field is introduced, or do new features appear? In order to shed some light on these questions, we consider a more general class of solutions recently reported by Anabalon and Cisterna [126]. There, a large class of analytic (asymptotically de Sitter) solutions to Einstein gravity with a conformally coupled scalar field were discovered, a subclass of which are the well-known MTZ and BMBB solutions. In this chapter we will examine the thermodynamic aspects of these Anabalon-Cisterna (AC) black holes, in an effort to answer some of the questions posed above, and towards a better understanding of black hole thermodynamics with matter fields at play. We emphasize that these AC black holes are solutions to Einstein gravity with a non-minimally coupled scalar field, rather than the scalar-tensor theories described above (a sometimes subtle distinction which we clarify in Section 4.1). Even still, there are good motivations for studying non-minimally coupled scalar fields, and given the close parallels between these two classes at the level of the action we expect that at least some qualitative features of the thermodynamic aspects will be transferable.

This chapter is organized as follows. In Section 4.1, we discuss the inclusion of scalar fields in the gravitational action, and clarify the distinction between scalar-tensor theories

and scalar fields coupled to gravity. In Section 4.2 we describe the theory being considered, defining the relevant quantities and commenting on various limits being considered. In Section 4.3, we calculate the on-shell Euclidean action for these conformally coupled de Sitter black holes, and determine the free energy of the spacetime. In Section 4.4, we examine the phase structure of these black holes, using the temperature to determine regions where interesting phase structure may be present, and demonstrate the presence of Hawking-Page-like transitions through the free energy. Finally, we summarize the main results and comment on future avenues of research.

4.1 Scalars in Gravitational Theories

We have discussed two different ways in which a scalar field might arise in the action for a given gravitational theory. One is as a fundamental geometric field as occurs in generic scalar-tensor theories. These theories have gravitational actions of the form

$$I = \frac{1}{16\pi}\int \sqrt{-g}\left[\phi R - \frac{\omega(\phi)}{\phi} g^{ab}\partial_a\phi\partial_b\phi - V(\phi)\right] d^4x + I_{\text{matter}} \tag{4.1}$$

where $\omega(\phi)$ is a coupling function, $V(\phi)$ is the potential of the scalar field, and I_{matter} is the action of any matter fields present. Variation of the action with respect to the metric g and scalar field ϕ gives the equations of motion for the fields,

$$G_{ab} = \frac{8\pi}{\phi}T_{ab} + \frac{\omega(\phi)}{\phi^2}\left(\partial_a\phi\partial_b\phi - \frac{1}{2}g_{ab}(\partial\phi)^2\right) + \frac{1}{\phi}\left(\nabla_a\nabla_b\phi - g_{ab}\Box_g\phi\right) \tag{4.2}$$

$$\Box_g\phi = \frac{1}{3+2\omega(\phi)}\left(8\pi T - \frac{d\omega}{d\phi}(\partial\phi)^2 + \frac{d}{d\phi}\left(\phi^2 V\right)\right) \tag{4.3}$$

where $\Box_g$ is the D'Alembertian associated with the metric g, and T is the trace of the matter stress-energy tensor. The well-known Brans-Dicke theory is recovered in the limit where $\omega(\phi) = \text{const.}$ and the potential $V(\phi)$ vanishes.

Similar structure at the level of the action emerges when one considers the scalar field to be part of the matter content of the theory (rather than a geometric field) when a non-trivial coupling is assigned between the matter and curvature. Historically, and indeed in the ΛCDM description of the universe (whose bases are general relativity and the Standard Model), the gravitational and matter sectors factorize as

$$I_{\text{Total}} = I_{\text{EH}} + I_{\text{matter}} \tag{4.4}$$

where I_{EH} is the Einstein-Hilbert action and I_{matter} is the action of any matter fields present. This prescription for describing matter in the presence of gravity is known as the *minimal coupling* prescription. In quantum field theory, the minimal coupling prescription means that fields only couple through their charge distributions, rather than higher multipoles of the distributions. In the context of gravity, it means that matter fields only couple to

gravity through the measure $\sqrt{-g}\,d^4x$, and not directly to the curvature R.

Despite minimal coupling underlying the ΛCDM description of matter and gravity, there is good reason to consider instead a non-minimally coupled prescription, which involves the appearance of a $\frac{1}{2}\varepsilon R\phi^2$ term in the action. For one, inflationary theories generically contain non-minimally coupled ($\varepsilon \neq 0$) scalar fields, and their viability is highly sensitive to the choice of ε [127,128]. Furthermore, non-minimal couplings generically arise in quantum corrections to a given action even if no such coupling exists in the classical theory [129]. The value $\varepsilon = 1/6$ is particularly significant, and is known as the *conformal coupling* prescription, so named because it renders the action invariant under a conformal rescaling of the metric $g_{ab} \to \Omega^2(x)g_{ab}$. Conformal coupling allows one to circumvent early 'no-hair' theorems formulated either in asymptotically flat spacetimes or with minimally coupled scalar fields (for reviews see [120, 130]). $\varepsilon = 1/6$ is also the unique choice for which the Green's functions of the field reduce locally to their Minkowski space counterparts, and propagation of massive particles on the light cone is avoided [131]. All said, we have motivations along a number of axes for considering the implications that scalar fields have for black hole thermodynamics, especially with the conformal coupling prescription[1].

4.2 Self-Interacting Scalar Fields

In light of the preceding discussion, we will consider the AC class of exact solutions to Einstein's equations with non-zero cosmological constant and a conformally coupled, self-interacting scalar field [126]. This large class of solutions describes a variety of topologically distinct spacetimes, including everywhere-regular black holes and wormholes, which further have everywhere regular scalar field configurations. The general theory is described by the following bulk action I, potential $V(\phi)$, and equation of motion for ϕ,

$$I = \int\sqrt{-g}\left[\frac{R-2\Lambda}{16\pi} - \frac{1}{2}(\partial\phi)^2 - \frac{1}{12}\phi^2 R - V(\phi)\right]d^4x\ , \tag{4.5}$$

$$V(\phi) = \alpha_1\phi + \alpha_3\phi^3 + \alpha_4\phi^4\ , \qquad \Box\phi = \frac{1}{6}R\phi + \frac{\partial V}{\partial\phi}\ ,$$

$$\frac{1}{8\pi}(G_{ab} + \Lambda g_{ab}) = \partial_a\phi\partial_b\phi - \frac{1}{2}g_{ab}(\partial\phi)^2 - g_{ab}V(\phi) + \frac{1}{6}\left(g_{ab}\Box - \nabla_a\nabla_b + G_{ab}\right)\phi^2\ ,$$

where we have set $G = 1$, and the cosmological constant determines the de Sitter length scale through $\Lambda = 3/l^2$. With the choices $\alpha_1 = -\frac{3}{4\pi}\,\alpha_3$, $\alpha_3 = -\Lambda\sqrt{\frac{16\pi}{27}}\frac{\xi}{\xi^2+1}$, and $\alpha_4 = -\frac{2\pi\Lambda}{9}$, the equations of motion have an exact solution given by

$$\phi(r) = \left(\frac{3}{4\pi}\right)^{1/2}\frac{m(\xi-1)-\xi r}{m(\xi-1)+r}\ , \tag{4.6}$$

[1]Einstein gravity with a non-minimally coupled scalar field is subsumed by the so-called *generalized scalar-tensor gravity* (GSTG) theories. In that context, the two seemly different cases discussed above are in fact one and the same.

while the Euclidean[2] metric for the spacetime is

$$ds^2 = \Omega(r)\left[f(r)\,d\tau^2 + \frac{dr^2}{f(r)} + r^2 d\Omega_2^2\right] \tag{4.7}$$

$$\Omega(r) = \frac{(r+(\xi-1)m)^2}{(r-m)^2}\ , \qquad f(r) = \left(1-\frac{m}{r}\right)^2 - \Sigma^2 r^2\ , \qquad \Sigma \equiv \sqrt{\frac{\Lambda\,(\xi^2-1)^2}{3\,(\xi^2+1)}}\ .$$

Here, ξ is an arbitrary dimensionless parameter yielding the MTZ solution when equal to zero, m is the mass parameter, Λ is the cosmological constant, and $d\Omega_2^2$ is the metric on $\mathcal{S}^2$. We have also defined $\Sigma = \Sigma(\Lambda)$ for convenience. Note that the above solution can actually be seen to arise from the MTZ solution through a conformal transformation and field redefinition, as shown in [132]. However, even though the two solutions are related in this way, it has been shown that such a relationship does not imply the thermodynamic properties of the solution are the same. Rather, such transformations can significantly affect the thermodynamics, warranting the investigation of the system defined by (4.5) [133, 134].

Though a number of geometrically distinct solutions arise in various limits of the general theory defined above (detailed in [135]), we focus mainly on the case where $\Lambda > 0$ and $0 \leq \xi < 1$. This gives rise to a black hole spacetime with the conformal structure of the Schwarzschild-de Sitter solution, with a new asymptotic region replacing the inner singularity, and an everywhere finite value for the scalar field (as long as $r > m$). The focus on positive ξ arises from the fact that the spacetime possesses a curvature singularity at $r = m(1-\xi)$ due to the divergence of the scalar field there. When $\xi \geq 0$, this singularity is always hidden behind the event horizon, while for $\xi < 0$ one can have a naked singularity for certain values of $\{m, \xi, \Lambda\}$. There is also a curvature singularity at $r = 0$. Note that the conformal factor Ω diverges on the horizon in the limit $m \to 0$, unless the limit $\xi \to 0$ is taken first.

The spacetime possesses three distinct horizons: a cosmological, an event, and an inner horizon. The cosmological and event horizons are located at

$$r_h = \frac{1-\sqrt{1-4m\Sigma}}{2\Sigma}\ , \qquad r_{\text{cosmo}} = \frac{1+\sqrt{1-4m\Sigma}}{2\Sigma}\ . \tag{4.8}$$

The Nariai limit, where the event horizon and cosmological horizon coincide, is achieved if

$$m_{\text{Nariai}} = \frac{1}{4\Sigma} = \frac{\sqrt{3\,(\xi^2+1)}}{4\sqrt{\Lambda}\,(\xi^2-1)}\ . \tag{4.9}$$

In the Nariai limit, the only possible location for the cavity is at $r_c = r_{\text{Nariai}}$, where both the entropy and energy (as determined by (5.33)) diverge. However they diverge in such a way that the temperature acquires a finite value.

[2]The Lorentzian counterpart is easily obtained via Wick rotation $\tau \to it$.

4.3 Evaluating the Euclidean Action

In this section, we evaluate the on-shell Euclidean action for the theory defined above. As before, we must supplement the action (4.5) with a Gibbons-Hawking-York-type boundary term for the action to be stationary and to have the correct composition properties for the path integral [50, 136]. In the case of the scalar-tensor theory defined above, the required boundary term gives a total action

$$I_E = \int\sqrt{g}\left[\frac{\Lambda}{8\pi} + V(\phi) - \frac{1}{4}\Box\phi^2\right] d^4x - 2\int\sqrt{k}\left[\frac{1}{16\pi} + \frac{1}{12}\phi^2\right] K\ d^3x\ , \tag{4.10}$$

where the equations of motion have been used to simplify the bulk part. In the boundary part, k_{ab} is the metric on the boundary (with determinant k), and K is the trace of the extrinsic curvature of the boundary defined by an inward pointing normal vector s^a as $K = \frac{1}{2}\mathcal{L}_s k_a{}^a$. As always, the requirement that the $\mathcal{S}^2$ corresponding to the event horizon be non-degenerate further requires that the periodicity in τ be fixed to

$$\beta_h = \left.\frac{4\pi}{f'(r)}\right|_{r_h} = \frac{2\pi}{\Sigma\left(1 - 2\,\Sigma\, r_h\right)}\ . \tag{4.11}$$

This is the inverse Hawking temperature of the black hole (and is invariant under conformal rescaling of the metric), which reduces to the known temperature of the MTZ solution when $\xi = 0$. Equilibrium in the system is achieved by fixing the temperature at the cavity β^{-1} to simply be the Hawking temperature redshifted to the cavity radius, thus determining the periodicity in locally observed time for quantum fields at r_c, namely

$$\beta = \beta_h\sqrt{f(r_c)\,\Omega(r_c)}\ . \tag{4.12}$$

The contributions to the Euclidean action (4.10) are

$$V(\phi) = \frac{\Lambda\xi}{\sqrt{3\pi}\,(\xi^2+1)}\phi - \frac{\Lambda\sqrt{16\pi}}{27}\frac{\xi}{\xi^2+1}\phi^3 - \frac{2\pi\Lambda}{9}\phi^4\ , \tag{4.13}$$

$$\Box\phi^2 = \frac{4f\phi\,\phi'}{\Omega}\left(\frac{1}{r} + \Omega'\Omega\right) + \left(\frac{2f\phi\,\phi'}{\Omega}\right)^2\ , \tag{4.14}$$

$$K = \frac{r\,\Omega f' + 3\,r f\Omega' + 4\,\Omega f}{\Omega^2\, r}\sqrt{\frac{\Omega}{f}}\ , \tag{4.15}$$

where primes indicate derivatives with respect to r. Performing the integrations gives the on-shell Euclidean action for the black hole spacetime

$$
\begin{aligned}
I_E =& \frac{\beta\, r_c}{6}\left(1-\xi^2\right)\Big[\Lambda\,(r_c-r_h)\,\big(\,(r_c+r_h)\,\Sigma-1\big)\Big(\Sigma^2 r_c^4+(3\,\Sigma\,\Xi+1)\,(\Xi+r_c)\,\big(\Sigma\,r_c^2+\Xi+r_c\big)\Big) \\
&\times\big(r_c+\Xi(1-\xi)\big)\left(\xi^2-1\right)^2-3\,\Sigma^3\left(\xi^2+1\right)\Big(2\,r_c^5-3\,r_c^7\,\Sigma^2+\Xi^5\,(\xi-1)+r_c\,\Xi^4\,(2+9\,\xi) \\
&+\Xi^3 r_c^2\left(14+3\,r_c^2\,\Sigma^2\,(\xi-1)+19\,\xi\right)+\Xi\,r_c^4\left(11+4\,\xi-3\,r_c^2\,\Sigma^2\,(\xi+4)\right) \\
&+\Xi^2 r_c^3\left(20+15\,\xi-3\,r_c^2\Sigma^2\,(\xi+4)\right)\Big)\Big]
\end{aligned}
\tag{4.16}
$$

where $\Xi \equiv r_h(\Sigma\, r_h - 1)$. In the semi-classical approximation, equation (1.29) is justified by observing that the dominant contributions to the path integral come from metrics that are classical solutions to the equations of motion. In our case, there are two distinct ones[3]: the Schwarzschild-de Sitter-like solution given by (4.7), and the "empty" de Sitter-like solution where $m = 0$. The path integral over (4.7) contains contributions from graviton fluctuations far away from the black hole. In order to isolate the contribution to the partition function coming from the black hole itself, we subtract from the black hole action the same action evaluated for $m = 0$, matching the metrics on the boundary $\partial\mathcal{M}$. Despite a lack of divergences in the Euclidean action with finite boundary (the usual motivation for including a subtraction term being to regulate them), in our case this subtraction still serves to set the reference point for the free energy to be the empty de Sitter spacetime. We will often refer to this phase as the 'radiation phase' or 'thermal de Sitter'. Note that even when $m = 0$, the scalar field does not vanish, though it does achieve a constant value.

Hawking-Page-like transitions are sometimes insensitive to the choice of background subtraction, such as in charged black holes in the canonical ensemble, because the pure radiation phase is inaccessible to black holes with fixed non-zero charge. However, in our case performing this subtraction correctly is critical, since a shift in the free energy above/below the $F = 0$ line (which corresponds to the radiation phase) may wash out any Hawking-Page-like phase transitions present. One cannot naively take the $r_h \to 0$ limit of (4.16) to obtain this subtraction term. Rather, the Euclidean action must be re-evaluated for the $m = 0$ solution, taking care to match the metrics between this and the $m \neq 0$ action on the boundary. The Euclidean action for the reference spacetime is

$$
I_0 = \frac{\beta_c\, r_c\Big[\left(1-\xi^4\right)\left(9\,\Sigma^2 r_c^2-6\right)-\Lambda\, r_c^2\left(\xi^2-1\right)^3\Big]\big(r_c+r_h\,(\Sigma\, r_h-1)\,\big)}{6\big(\xi^2+1\big)\sqrt{1-\Sigma^2 r_c^2}\,\big[r_c-r_h\,(\Sigma\, r_h-1)\,(\xi-1)\,\big]}\ . \tag{4.17}
$$

With these considerations the Euclidean action for the Schwarzschild-de Sitter black hole with conformally coupled scalar field is simply

$$
I_{\text{Total}} = I_E - I_0\ . \tag{4.18}
$$

This is in contrast to the Euclidean action obtained in [137], where instead of the canonical

[3]Note that Minkowski space is not a solution to the classical equations of motion when $\Lambda \neq 0$, and so it does not contribute to the path integral. This justifies the use of the empty de Sitter space as the "background subtraction" instead of the commonly employed flat space.

ensemble considered here, a microcanonical ensemble without boundary is used for the MTZ black hole. One can obtain this result by taking the limit $r_c \to r_{\text{cosmo}}$ in (4.16), which gives

$$I_{\text{Total}} = 0 \ . \tag{4.19}$$

The action in this case identically vanishes as there is no charge for the scalar field, in agreement with Equation (22) of [137]. Our result is more general though, since we have not set $\xi = 0$. Even in this more general case the action vanishes without charge when no cavity is present. Of course, when the action vanishes one cannot obtain a sensible notion of energy and entropy for the spacetime through the canonical relations (1.30), further motivating the inclusion of the cavity.

4.4 Thermodynamics and Phase Structure

The action (4.18) allows us to calculate all thermodynamic quantities of interest using (1.30). In particular, we will be interested in examining the equilibrium temperature (4.12) and free energy F to look for possible phase transitions within the spacetime. We remind the reader that we work in units where $\hbar = C = G = 1$ unless otherwise specified.

4.4.1 The First Law

Before analyzing the phase structure, we should discuss the first law of thermodynamics for these black holes. As stated, we have

$$dE = TdS + VdP - \lambda dA_c \ . \tag{4.20}$$

where we are working in the extended phase space where

$$P = -\frac{\Lambda}{8\pi} \ . \tag{4.21}$$

The natural question to ask is whether a suitable generalization of the first law is required in the presence of the scalar field, as it was in Chapter 3 for Born-Infeld theory. Formally, we may consider adding a term representing the variation of the scalar charge along with its conjugate potential, so that

$$dE = TdS + VdP - \lambda dA \ + \Phi d\phi \ , \qquad \Phi \equiv \left(\frac{\partial E}{\partial \phi}\right) \ . \tag{4.22}$$

In the context of string theory [138], such a first law appears generically for black holes as both their mass and area depend on the values of the moduli fields ϕ_∞ at spatial infinity. These moduli label different ground states of the theory, as the string coupling g_s is related to the vacuum expectation value of the dilaton ϕ at infinity. The moduli do not correspond to new conserved charges however, as they are not associated with a new

integration constant [139]. The question of whether or not an inclusion of the form (4.22) is warranted is thus subtle. This issue was recently explored in [140], where black holes in Einstein-Maxwell-dilaton gravity were considered. In that work, it was shown that neither the Smarr formula nor the first law require the addition of a scalar charge term. For our purposes, we can therefore take the extended first law to read

$$dE = TdS + VdP - \lambda dA_c \ , \tag{4.23}$$

where the quantities have their usual meaning from the previous chapters.

4.4.2 Equilibrium Temperature

Working in the regime of equilibrium thermodynamics requires the assignment of a single equilibrium temperature to the system under consideration. As we have seen, the cavity approach is particularly well suited to de Sitter spacetimes, where the differing temperatures associated with the event and cosmological horizons drive the system out of equilibrium. Fixing the temperature at the surface of the cavity circumvents this issue by forcing the spacetime to equilibrate to the cavity temperature. The spacetime considered here, in contrast to the previous cases, is unique in that the event and cosmological horizons are actually at the same temperature, namely,

$$T_\Delta = \left.\frac{f'(r)}{4\pi}\right|_{r_\Delta} = \frac{\Sigma\,(1-2\,\Sigma\,r_\Delta)}{2\pi} \ , \tag{4.24}$$

where $\Delta = \{h, \text{cosmo}\}$. However, this is not the temperature that an observer between the two horizons (at $r = r_c$ for example) would experience, who instead sees the black hole radiating at a redshifted temperature of

$$T = \frac{T_h}{\sqrt{\Omega(r_c) f(r_c)}} \ . \tag{4.25}$$

Thus, even though equilibrium in terms of particle flux is already manifest between the two horizons (as the surface gravities are equal), equilibrium as understood by observers in the spacetime is still achieved by fixing the temperature at the cavity to be equal to T. In this case, the temperature at the cavity required for equilibrium is

$$T = \frac{\Sigma\ (1-2\,\Sigma\,r_h)\left(r_c - r_h\ (1-\Sigma\,r_h)\right)}{2\pi\big(r_c + r_h\ (1-\Sigma\,r_h)\,(\xi-1)\big)\sqrt{\left(\Sigma\,r_h^2 + r_c - r_h\right)^2 - \Sigma^2 {r_c}^4}} \ . \tag{4.26}$$

With this in mind, we begin with a study of the equilibrium temperature (4.26) of the spacetime under consideration. A necessary (but not sufficient) condition for the existence of complex phase structure is the multivalued nature of the horizon radius r_h as a function of temperature. This is because the existence of multiple black hole phases at a given temperature is manifest in the multiple (real, positive) values of the horizon radius r_h,

which correspond to the different sizes of black holes that exist at that temperature for a given set of fixed parameters $\{\Lambda, \xi\}$. The horizon radius thus plays the role of the order parameter for the system. These phases may be unphysical for other reasons, or otherwise be inaccessible through quasistatic transformations, so ultimately the free energy F must be evaluated to determine whether a phase transition actually occurs at the given temperature, but an examination of $T(r_h)$ nonetheless provides useful insight as to where in parameter space such transitions might exist. For example, one can immediately rule out the presence of small-large phase transitions if the temperature is a monotonic function of the horizon radius. Note that even if $T(r_h)$ is monotonic, Hawking-Page-like phase transitions may still occur.

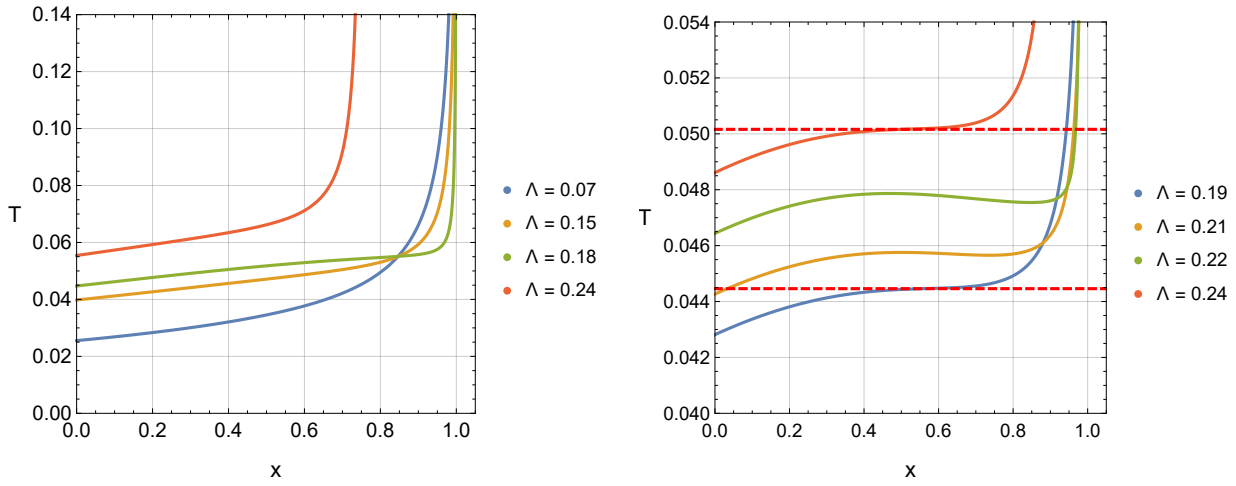

Figure 4.1: Equilibrium temperature T as a function of $x = r_+/r_c$ for fixed cavity radius $r_c = 2$, showing regions where r_h is multivalued at fixed temperature, signalling a possible phase transition. **Left:** Varying pressure Λ with $\xi = 0$. **Right:** Varying pressure Λ with $\xi = 0.2$.

In Figure 4.1, we plot the equilibrium temperature $T(r_h)$ of the black hole spacetime for various choices of Λ and ξ. For convenience, the function is written in terms of the relative size of the black hole with respect to the cavity, $x \equiv r_h/r_c$. On the left of Figure 4.1, we consider different values of Λ with $\xi = 0$, corresponding to the MTZ black hole. We observe that the temperature is always positive and monotonically increasing with respect to the size of the black hole[4], eventually diverging as the black hole fills the cavity entirely ($r_h \to r_c$). For large enough Λ (as in the red curve) the temperature asymptotes before r_h reaches r_c. This corresponds to a black hole whose mass is large enough to pull the cosmological horizon inside the cavity for the given value of Λ. Since we require $r_h < r_c < r_{\text{cosmo}}$, this places an upper limit on the black hole size. Despite the apparent jump in the figure, the new maximum moves smoothly from $x = 1$ as Λ increases. When $\Lambda < \Lambda_{\text{max}}$, the cosmological horizon always lies outside of the cavity regardless of the size of the black hole. This maximal value, below which the entire spacetime is available to the

[4]The apparent crossings near $x = 0.8$ are coincidental.

black hole, occurs at

$$\Lambda_{\max} = \frac{3\,(\xi^2+1)}{4\,r_c^2\big(\xi^2-1\big)^2}\ . \tag{4.27}$$

In the case of the MTZ black hole, we therefore expect to only see a Hawking-Page-like phase transition, which we will confirm by examining the free energy.

The case for non-zero ξ is markedly different. On the right of Figure 4.1, we again plot $T(r_h)$ for varying Λ, this time with $\xi = 0.2$. In this case, there is a region bounded by a minimum and maximum pressure (indicated by the red horizontal lines) where r_h is multivalued for fixed T. The three distinct values of r_h that exist at a particular equilibrium temperature in this region represent (up to) three coexistent black hole phases. Further analysis is required to assess whether these phases are accessible to the system. For example, the divergence of the scalar field $\phi(r)$ and the vanishing of the conformal factor $\Omega(r)$ (which leads to a singular inverse metric) place further constraints on the valid parameter space. Both of these occur at $r = m(1-\xi)$, requiring that $r_h > m(1-\xi)$. From (4.8) this places a constraint on ξ such that

$$(1-\Sigma\, r_h)(1-\xi) < 1 \tag{4.28}$$

for non-zero r_h in order for the divergence to be hidden behind the event horizon. This 'cosmic censorship bound' is always satisfied for $\xi \geq 0$, while for $\xi < 0$ it can be violated.

4.4.3 MTZ Black Holes ($\xi = 0$)

We consider first the case where $\xi = 0$, corresponding to the de Sitter MTZ black hole [117]. In this limit, the metric and scalar field simplify in the following ways:

$$\phi(r) = \sqrt{\frac{3}{4\pi}}\,\frac{m}{r-m}\ , \qquad V(\phi) = \alpha_4\phi^4 \tag{4.29}$$

$$\Omega(r) = 1\ , \qquad f(r) = \Big(1-\frac{m}{r}\Big)^2 - \frac{\Lambda r^2}{3}\ . \tag{4.30}$$

The spacetime has the geometry of the lukewarm Reissner-Nordstrom-de Sitter black hole [141, 142]

In Figure 4.2, we plot the free energy $F(T)$ of the MTZ black hole as a function of the cavity temperature (parametrically using r_h). The black line, where $F = 0$, corresponds to the free energy of the empty[5] de Sitter spacetime (the radiation phase). For each colored curve, the black hole size increases from left to right, with the leftmost end terminating where $m = 0$. For low temperature, the radiation phase globally minimizes the free energy. As the temperature increases, eventually a critical point is reached (marked by a red dot) where the free energy of the black hole becomes lower than that of the radiation phase, and

[5]Empty in the sense there is no black hole. There is still a scalar field present in the spacetime.

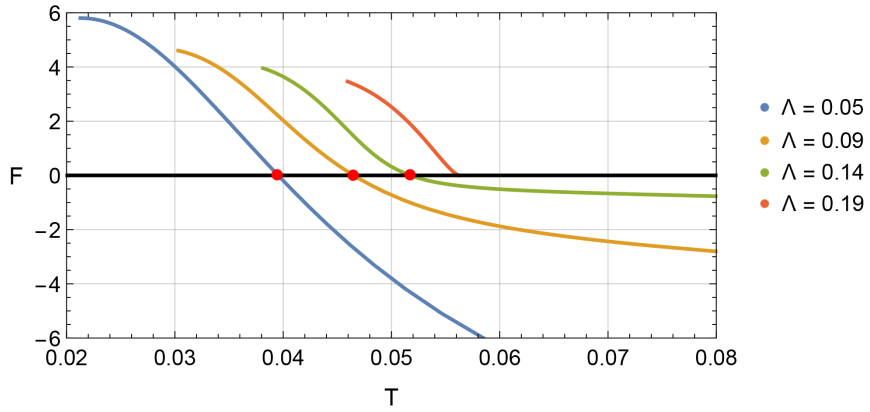

Figure 4.2: Free energy of the MTZ ($\xi = 0$) black hole in the canonical ensemble, with varying Λ. The black $F = 0$ line corresponds to the radiation phase. Red dots mark the critical temperature at which the black hole begins to dominate the thermal ensemble and a first-order Hawking-Page-like phase transition occurs.

a Hawking-Page-like first-order phase transition occurs. As the black hole size increases further, the free energy monotonically decreases until the cavity radius is reached, where the temperature diverges. When Λ becomes large enough (as in the red curve, where $\Lambda = \Lambda_{\text{max}}$) the Nariai limit is achieved at exactly the cavity radius, so that the line terminates on the right side at $r_h = r_c = r_{\text{cosmo}}$.

4.4.4 AC Black Holes ($\xi \neq 0$)

Next we consider the more general class of solutions given by $\xi \neq 0$. In this case the scalar field and metric functions are given by (4.7), with the total Euclidean action still being (4.10). In Figure 4.3 we plot $F(T)$ as before, with $\xi = 0.2$ and various choices of Λ. The results are qualitatively similar to that of the MTZ black hole, with Hawking-Page-like phase transitions from radiation to a large black hole occurring at a critical temperature that depends on the cavity size and cosmological constant. As before, the black hole size r_h increases from left to right along each curve, terminating at the left where $r_h = 0$. There is again a maximal value for Λ given by (4.27) where the cavity radius coincides with the Nariai limit, as in the red curve of Figure 4.3. Below this limit, we always have $r_h \leq r_c < r_{\text{cosmo}}$, and the temperature diverges as the black hole horizon approaches the cavity. At exactly $\Lambda = \Lambda_{\text{max}}$, the system exists at a finite temperature whose free energy is equal to that of radiation, however both the energy and entropy diverge. Despite Figure 4.1 suggesting otherwise, there are no small-large black hole phase transitions present, even though for some choices of Λ and ξ, $T(r_h)$ has three real roots. In all cases where this is true, only one of the roots turns out to satisfy (4.28).

In Figure 4.4 we again plot the free energy, this time for various ξ at fixed Λ. On the left, we show positive values of the scalar parameter, while on the right we show negative values. When $\xi > 0$, the behaviour is again similar to the MTZ case, where a Hawking-

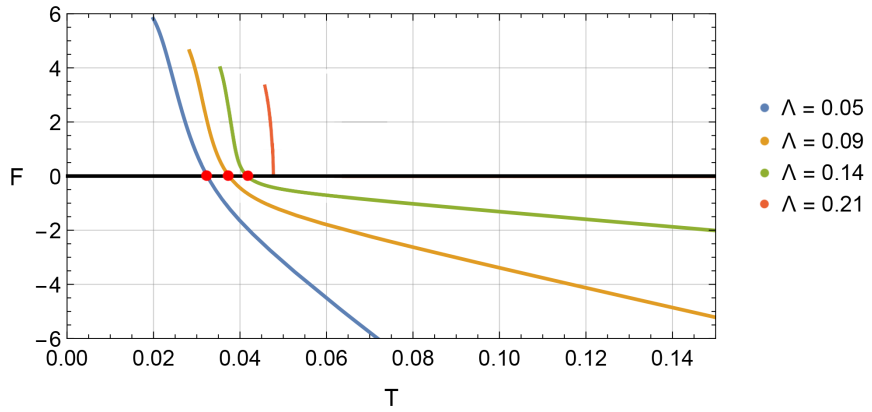

Figure 4.3: Free energy of the AC ($\xi \neq 0$) black hole in the canonical ensemble, with varying Λ. The black $F = 0$ line corresponds to the radiation phase. Red dots mark the critical temperature at which the black hole begins to dominate the thermal ensemble and a first-order Hawking-Page-like phase transition occurs.

Page-like phase transition occurs at a critical temperature whose exact value depends on the value of ξ and Λ. Again there is a minimum temperature for the spacetime, achieved when $m = 0$, and the temperature diverges as the cavity is approached.

On the other hand when $\xi < 0$, qualitatively different behaviour emerges. In this case it is possible for (4.28) to be violated, so even though the free energy of the black hole crosses the $F = 0$ line as it would for a Hawking-Page-like phase transition, the transition itself does not necessarily occur. On the right of Figure 4.4 we plot the free energy for various negative values of ξ. Marked with a circle on each curve is the minimal value of r_h that satisfies (4.28), below which there is a naked singularity. The dashed portions of the curves indicate that the bound has been violated. When ξ is sufficiently negative, no black hole of any size can exist within the cavity, as in the red curve where $\xi = -0.4$. For intermediate values (as in the yellow curve where $\xi = -0.2$) there is a branch of black holes that are regular outside the horizon. However, as the temperature decreases, a naked singularity forms (the Kretschmann scalar diverges) before the black hole can reach a free energy that is lower than radiation, so no transition occurs. The blue curve demonstrates a scenario where ξ is sufficiently small so that the critical temperature is reached before a naked singularity forms, and a Hawking-Page transition occurs. This is the case for a given (fixed) cavity radius. It is always possible to *choose* the location of the cavity to ensure that the HP transition occurs before a naked singularity forms. In other words, for a given value of Λ and ξ, one can always choose an appropriate value for r_c such that a curve similar to the blue one is obtained, as opposed to the yellow one. In this way, the correct choice of boundary location is essential for the avoidance of naked singularities and the persistence of the HP transition.

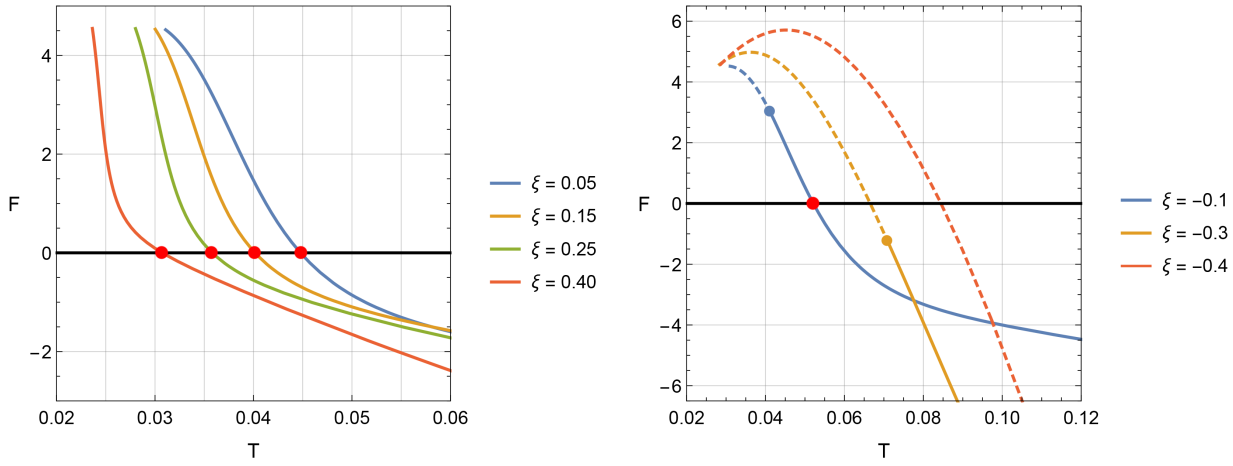

Figure 4.4: Free energy F as a function of temperature T for fixed cavity radius $r_c = 2$ and varying ξ. For each curve, a Hawking-Page-like transition occurs at the critical temperature marked by a red point. **Left:** $\xi > 0$. **Right:** $\xi < 0$. Along the dashed portions of each curve, a naked singularity is present. The colored point on each curve indicates that equality in (4.28) has been reached.

4.5 Summary

We have studied the phase structure of a new class of asymptotically de Sitter black holes, conformally coupled to a real scalar field. The presence of an isothermal cavity, equivalent to fixing boundary value data on a finite surface in the spacetime, allows us to establish a notion of thermodynamic equilibrium in these asymptotically de Sitter spacetimes, which normally are not in equilibrium due to the two horizons present. What we have shown is that the Hawking-Page-like transition from a black hole spacetime to one filled with radiation occurs generically for these black holes. In the limit where the scalar field parameter ξ tends to zero, corresponding to the MTZ black hole, the HP transition is present throughout most of the parameter space, except in the special case where the event and cosmological horizons simultaneously asymptote to the boundary at r_c when the Nariai limit is approached. In this case, the black hole phase is unstable and always has a higher free energy than the empty spacetime.

When $\xi < 0$, the situation is more complex. There is now a cosmic censorship bound that must be satisfied due to the divergence of the scalar field ϕ and vanishing of the conformal transformation Ω. This means that while HP transitions are possible, ξ must be sufficiently small for the given values of Λ and r_c in order for the phase transition to occur before a naked singularity forms in the spacetime.

Of note is the distinct absence of the 'swallowtube' behaviour seen in previous examples of asymptotically de Sitter black holes. Indeed, even the typical small-large black hole phase transition does not occur for this class of black holes. This is not surprising insofar as the geometry here is that of the lukewarm Reissner-Nordstrom-de Sitter black hole [141, 142], which represents a measure-zero element of the parameter space for those black holes. It is possible that the consideration of a charged scalar field would produce some of these more exotic transitions that are common to AdS black holes. What is significant is the fact that the Hawking-Page phase transition appears to persist even when the geometry is coupled to matter, in this case a scalar field. Though the class of solutions considered here represents a special choice of potential for the scalar field for which exact solutions exist, we expect that similar results will hold for more 'realistic' potentials. Eventually, we would like to be able to understand the thermodynamic properties of astrophysical black holes, which may well couple to scalar fields in the form of dark matter or as effective descriptions of other fields. This work is a step in this direction.

Chapter 5

Gauss-Bonnet-de Sitter Black Holes

Having studied the prototypical case of Einstein-Maxwell gravity in Chapter 2, a well-motivated example of a modification to ordinary electrodynamics in Chapter 3, and the effect of matter content in Chapter 4, we now turn our attention to modifications of the gravitational sector itself. Since its inception, General Relativity has largely stood on its own as the unique metric theory of gravity in four dimensions that obeys the strong equivalence principle. It has also enjoyed unparalleled success in its agreement with just about every conceived experimental test and observation, the historic examples being the perihelion precession of Mercury (known as early as 1859 through the work of Le Verrier), gravitational lensing around massive objects (measured in the famous Eddington experiment during an eclipse in 1919), and gravitational redshift (the first confirmations being astrophysical measurements by Popper in 1954 and terrestrial ones by Pound, Rebka, and Snyder in 1959) [143–146].

Despite its historic success, which mounted over the coming decades as experimental technology quickly evolved, there has been interest in alternative theories of gravitation as early as general relativity itself. These include Whitehead's quasilinear theory of gravity, the torsional Einstein-Cartan theory, and Fierz-Pauli's massive graviton theory, to name a few [147–149]. Many such alternatives were quickly excluded, as even the early weak-field experiments would severely constrain how much a theory could deviate from the predictions of general relativity. Today, strong field tests of general relativity from binary black hole mergers and a wealth of cosmological considerations including structure formation and the CMB constrain alternative theories even further [150–152]. However, there remains significant interest in the study of alternative theories of gravity, as it is known that general relativity is merely an effective, low-energy description of some more fundamental theory. As a result we are motivated to consider not only observational consequences of alternatives to GR, but also theoretical ones, as we do in the present chapter.

One such class of alternatives are the popular scalar-tensor theories described in Chapter 4. In those theories, auxiliary fields are added to the gravitational action that encode the geometry of spacetime alongside the metric g. Rather than including new fields in the description, one can instead consider modifications to the Einstein-Hilbert action in

the form of additional metric-dependent terms only. Though there are many categories of such theories, the majority fall into the so-called $f(r)$ theories[1], and higher-curvature (or higher derivative) theories. In this chapter, we will focus on higher-curvature corrections to Einstein gravity, and consider their implications for de Sitter black hole thermodynamics. Such corrections are ubiquitous in approaches to quantum gravity where they arise as quantum corrections to the Einstein-Hilbert action, and are expected to occur quite generally in high-energy regimes [153]. In this chapter we will consider one such correction in the form of Gauss-Bonnet gravity. Gauss-Bonnet theory arises from the leading correction to the Einstein-Hilbert action contained in the Lovelock class of theories [154]. Lovelock gravity is in many ways the natural generalization of Einstein gravity to higher dimensions, providing the most general possible prescription for adding higher curvature corrections to the action while maintaining second-order equations of motion (thus being ghost-free). Moreover, the boundary terms for Lovelock theory have long been known [155–157], which is advantageous for the present study. In the years following the work contained in this chapter, further theoretical developments have even led to a formulation of Gauss-Bonnet gravity in four dimensions [54, 158], making the present studies even more interesting. In the realm of AdS black holes, higher-curvature theories have resulted in a number of interesting observations [24, 28, 30, 159–175], the most notable being the existence of multiple re-entrant phase transitions, triple points, and λ-type superfluid transitions [16, 33]. One of our goals here is to explore to what extent these interesting features carry over to the de Sitter case. Additionally, older [176] and more recent [177] work has considered the thermodynamics of asymptotically flat Gauss-Bonnet black holes in cavities; our work can be considered the natural generalization of these studies to de Sitter space.

This chapter is organized as follows: In Section 5.1, we present the Gauss-Bonnet theory of gravity, defining the action, metric function, and relevant boundary terms. In Section 5.2, we consider uncharged black holes. The on-shell action is evaluated and all relevant thermodynamic quantities are calculated. We use the first law to derive the conjugate variables. We also construct the free energy of the spacetime and study its phase structure. In Section 5.3, we repeat this analysis for charged black holes. We conclude with a summary of the results.

5.1 Gauss-Bonnet Gravity

As noted, Gauss-Bonnet gravity can be understood as a modification of Einstein gravity through the addition of a term to the Einstein-Hilbert action that is quadratic in the curvature. Such a term is only non-trivial in $d \geq 5$: due to the Chern theorem it is a pure boundary term in $d = 4$ and identically vanishes in lower dimensions. As a result, the black holes we consider here are necessarily higher dimensional[2]. The (Euclidean) action

[1] These can often be recast in the form of a scalar-tensor theory.

[2] As mentioned in the previous section, recent work indicates that a non-trivial formulation is possible in $d = 4$, though at the time this was not known.

for the theory is

$$
\begin{aligned}
I_{\rm E} = &-\int_{\mathcal{M}} d^dx\sqrt{g}\left\{\frac{1}{16\pi}\left[R-2\Lambda+\frac{\lambda_{\rm GB}\mathcal{X}_4}{(d-3)(d-4)}\right]-\frac{1}{4}F_{ab}F^{ab}\right\}\\
&-\frac{1}{8\pi}\int_{\partial\mathcal{M}} d^{d-1}x\sqrt{\gamma}\left[K+\frac{2\lambda_{\rm GB}}{(d-3)(d-4)}\left[\mathcal{J}-2\mathcal{G}_{ij}K^{ij}\right]\right]\\
&-\int_{\partial\mathcal{M}} d^{d-1}x\sqrt{\gamma}F^{ij}n_iA_j\,,
\end{aligned}
\tag{5.1}
$$

where we have included a Maxwell field in addition to the gravitational terms. Here, R is the Ricci scalar, Λ is the cosmological constant, λ_{GB} is the Gauss-Bonnet coupling (which has units of inverse length squared), $\mathcal{X}_4$ is the Euler density, and F_{ab} is the electromagnetic field strength tensor. The terms appearing in the first line are the usual bulk terms from which the equations of motion are derived. The boundary terms ensuring a well-posed Dirichlet problem appear in the second line. Finally, the third line contains the relevant boundary term for the Maxwell field to ensure that the system is in the fixed charge ensemble. Here g_{ab} is the full spacetime metric, while γ_{ij} is the induced metric on the boundary. The vector n_μ is the outward pointing normal to the constant r hypersurface. For a constant r surface in a (Euclidean) spherically symmetric geometry, this boundary metric takes the form

$$
\gamma_{ij}dx^idx^j = f(r)dt_{\rm E}^2+r^2d\Sigma_{k,d-2}\,. \tag{5.2}
$$

The object $\sqrt{\gamma}$ that appears in the boundary action is the square root of the determinant of this metric. $\mathcal{J}$ is the trace of the boundary tensor,

$$
\mathcal{J}_{ij} = \frac{1}{3}\left(2KK_{ik}K^k_j+K_{kl}K^{kl}K_{ij}-2K_{ik}K^{kl}K_{lj}-K^2K_{ij}\right)\,, \tag{5.3}
$$

with K_{ij} the extrinsic curvature and $K = h^{ij}K_{ij}$ its trace, $\mathcal{G}_{ij}$ is the Einstein tensor computed for the boundary metric γ_{ij}, and the Euler density $\mathcal{X}_4$ is given by

$$
\mathcal{X}_4 = R_{abcd}R^{abcd}-4R_{ab}R^{ab}+R^2\,. \tag{5.4}
$$

For the (Lorentzian) metric and gauge field we have that[3]

$$
ds^2 = -f(r)dt^2+\frac{dr^2}{f(r)}+r^2d\Omega^2\,, \tag{5.5}
$$

$$
A_a = -\frac{1}{2\sqrt{2\pi G}}\sqrt{\frac{d-2}{d-3}}\left[\frac{q}{r^{d-3}}-\frac{q}{r_h^{d-3}}\right]dt = \left[\phi(r)-\phi(r_h)\right]dt\,, \tag{5.6}
$$

and the field equations reduce to a polynomial equation that determines the metric function $f(r)$,

$$
h\left(\frac{(f(r)-1)}{r^2}\right) = \frac{\omega_{d-3}}{r^{d-1}}-\frac{q^2}{r^{2(d-2)}}\,, \tag{5.7}
$$

[3]Note that the one-form dt diverges on the horizon. We have chosen a gauge for A such that this divergence does not lead to an ill-defined gauge field on the horizon.

with $h(x)$ given by the polynomial function

$$h(x) = -\frac{2\Lambda}{(d-1)(d-2)} - x + \lambda_{\rm GB} x^2 \,. \tag{5.8}$$

In these expressions, q and ω are two integration constants that are related to the mass M and charge Q of the black hole according to

$$\omega_{d-3} = \frac{16\pi m}{(d-2)\Omega_{d-2}} \,, \tag{5.9}$$

$$q = \frac{Q}{\Omega_{d-2}} \sqrt{\frac{8\pi G}{(d-2)(d-3)}} \,. \tag{5.10}$$

Note that when $\lambda_{\rm GB} = 0$ we get

$$f(r) = 1 - \frac{\omega_{d-3}}{r^{d-3}} + \frac{q^2}{r^{2(d-3)}} - \frac{2\Lambda r^2}{(d-1)(d-2)} \,, \tag{5.11}$$

which is the ordinary charged (A)dS black hole solution in Einstein gravity. However, here we will be interested in the case where $\lambda_{\rm GB} \neq 0$ and will work with $d \geq 5$. In this case the metric function is the solution of a quadratic equation, and we pick the root that has a smooth limit as $\lambda_{\rm GB} \to 0$.

Our aim is to study the phase structure of de Sitter black holes including higher-curvature corrections to the action. As usual, the phase structure will be obtained via an analysis of the free energy which can in turn is obtained from the Euclidean on-shell action for the theory. As in the previous chapters, equilibrium is ensured by placing the black hole in a perfectly reflecting finite cavity, which necessitates a Dirichlet boundary condition at the location of the cavity, whose temperature is held fixed.

5.1.1 Evaluating the Euclidean Action

In this section we will compute the on-shell action. The action (5.1) is decidedly more complex than the cases considers thus far. A number of simplifications will allow us to determine a remarkably simple analytic form for the reduced action, as we will show. Working quite generally, we consider a metric of the Euclidean form

$$ds^2 = f(r)dt^2 + \frac{dr^2}{f(r)} + r^2 d\Sigma_{k,d-2} \,, \tag{5.12}$$

where $d\Sigma$ is the line element on a space of constant curvature with $k \in \{-1, 0, 1\}$ denoting negative, zero, and positive curvature. The specific form of the line element can be found, for example, in equation (4) of [168]. Using the methods of [178], it is quite straight-forward to perform a direct computation of the on-shell action in any spacetime dimension. The

following terms contribute to the bulk action:

$$\begin{aligned}
R &= -\left[f'' + \frac{2(d-2)f'}{r} - \frac{(d-2)(d-3)(k-f)}{r^2}\right], \\
R^2 &= \left[f'' + \frac{2(d-2)f'}{r} - \frac{(d-2)(d-3)(k-f)}{r^2}\right]^2, \\
R_{ab}R^{ab} &= \frac{1}{2}\left(f'' + \frac{(d-2)f'}{r}\right)^2 + (d-2)\left(-\frac{f'}{r} + \frac{(d-3)(k-f)}{r^2}\right)^2, \\
R_{abcd}R^{abcd} &= (f'')^2 + 2(d-2)\left(\frac{f'}{r}\right)^2 + 2(d-2)(d-3)\left(\frac{k-f}{r^2}\right)^2 .
\end{aligned} \tag{5.13}$$

Rather than pursue a direct integration of the action (as we did in the previous chapters) it turns out that some algebra allows us to recognize that the bulk gravitational action is a total derivative:

$$I_{\rm E}^{\rm bulk} = -\frac{\Omega_{d-2}\beta_h}{16\pi}\frac{d}{dr}\left[-\frac{2(d-2)q^2}{r^{d-3}} + (d-2)\omega_{d-3} - r^{d-2}f'\left(1 - \frac{2(d-2)\lambda_{\rm GB}}{D-4}\frac{(f-k)}{r^2}\right)\right], \tag{5.14}$$

In producing this expression we have made use of the field equations. Specifically, we have replaced the appearance of a $r^{d-1}h$ term with the corresponding factors of ω and q. Note that, in the above, β_h is the periodicity of the Euclidean time enforced by demanding no conical singularities at the zero of f.

Let us now focus on computing the boundary term. The Euclidean solution is a smooth manifold at the horizon with topology $\mathbb{R}^2 \times \mathcal{S}^{d-2}$. We therefore consider a boundary term only at the location of the cavity. To compute the boundary term, we use the convenient notation of [178] which introduces the orthonormal projectors

$$\tau_a{}^b = \delta_a{}^t\delta_t{}^b \qquad \rho_a{}^b = \delta_a{}^r\delta_r{}^b \qquad \sigma_a{}^b = \sum_{i=1}^{d-2}\delta_a{}^i\delta_i{}^b \tag{5.15}$$

to decompose the curvature into temporal, radial, and angular parts (in the last term the sum extends over the angular directions). These orthogonal projectors satisfy the following relations:

$$\tau_a{}^c\tau_c{}^b = \tau_a{}^b\,, \quad \rho_a{}^c\rho_c{}^b = \rho_a{}^b\,, \quad \sigma_a{}^c\sigma_c{}^b = \sigma_a{}^b\,, \tag{5.16}$$

and

$$\tau_a{}^b\tau_b{}^a = \rho_a{}^b\rho_b{}^a = 1\,, \quad \sigma_a{}^b\sigma_b{}^a = d-2\,. \tag{5.17}$$

The boundary term is composed of various traces and contractions of the extrinsic curvature tensor K_{ij}. For a constant r surface, the extrinsic curvature computed for the outward-pointing unit normal vector is

$$K_i{}^j = \frac{f'}{2\sqrt{f}}\tau_i{}^j + \frac{\sqrt{f}}{r}\sigma_i{}^j\,, \tag{5.18}$$

and the curvature tensor of the boundary is

$$\mathcal{R}_{ij}{}^{kl} = \frac{2k}{r^2}\sigma^k_{[i}\sigma^l_{j]}\,, \tag{5.19}$$

where k characterizes the curvature of the constant time slices of the boundary, as mentioned above. From the Riemann tensor we compute the Ricci tensor and Ricci scalar of the boundary to be

$$\mathcal{R}_i{}^j = \frac{(d-3)k}{r^2}\sigma_i{}^j\,, \quad \mathcal{R} = \frac{(d-3)(d-2)k}{r^2}\,. \tag{5.20}$$

We then note that the Einstein tensor of the boundary geometry is just given by

$$\mathcal{G}_i{}^j = \mathcal{R}_i{}^j - \frac{1}{2}\delta_i{}^j\mathcal{R} = \frac{(d-3)k}{r^2}\left[\sigma_i{}^j - \frac{d-2}{2}\delta_i{}^j\right]\,. \tag{5.21}$$

Using these results, some simple manipulations yield the following results

$$\begin{aligned} K &= \frac{1}{2\sqrt{f}}\left[f' + \frac{2(d-2)}{r}f\right]\,, \\ K_i{}^jK_j{}^i &= \left(\frac{f'}{2\sqrt{f}}\right)^2 + (d-2)\left(\frac{\sqrt{f}}{r}\right)^2\,, \\ K_i{}^jK_j{}^lK_l{}^i &= \left(\frac{f'}{2\sqrt{f}}\right)^3 + (d-2)\left(\frac{\sqrt{f}}{r}\right)^3\,. \end{aligned} \tag{5.22}$$

Putting these together we obtain

$$\begin{aligned} \mathcal{J} = \frac{1}{3}\Bigg\{ &\frac{3}{2\sqrt{f}}\left[f' + \frac{2(d-2)}{r}f\right]\left[\left(\frac{f'}{2\sqrt{f}}\right)^2 + (d-2)\left(\frac{\sqrt{f}}{r}\right)^2\right] \\ &-2\left[\left(\frac{f'}{2\sqrt{f}}\right)^3 + (d-2)\left(\frac{\sqrt{f}}{r}\right)^3\right] - \left(\frac{1}{2\sqrt{f}}\left[f' + \frac{2(d-2)}{r}f\right]\right)^3\Bigg\} \end{aligned} \tag{5.23}$$

and

$$\mathcal{G}_{ij}K^{ij} = -\frac{(d-2)(d-3)k}{2r^2}\left[(d-4)\left(\frac{\sqrt{f}}{r}\right) + \frac{f'}{2\sqrt{f}}\right]\,, \tag{5.24}$$

where primes denote derivatives with respect to r. With this in place, we can calculate explicitly the on-shell action for the Gauss-Bonnet black hole.

In the following sections we will consider the uncharged case and the charged cases separately. We will work in the fixed charge ensemble, which requires the addition of the Maxwell boundary term appearing in the last line of Eq. (5.1). Noting that the outward pointing normal one-form is

$$n_a dx^a = \frac{dr}{\sqrt{f(r)}} \tag{5.25}$$

and taking care to work with the Euclideanized gauge potential[4] it can easily be shown that

$$\int_{\partial\mathcal{M}} \sqrt{\gamma}\, F^{ij} n_i A_j = \frac{(d-2)\beta_h \Omega_{d-2}}{8\pi}\left[\frac{q^2}{r_c^{d-3}} - \frac{q^2}{r_h^{d-3}}\right] = \frac{(d-2)\beta_h \Omega_{d-2}}{8\pi G}\left[\frac{q^2}{r^{d-3}}\right]_{r=r_h}^{r=r_c} . \quad (5.26)$$

From the expression for the bulk action in (5.14) it is then obvious that when this term is subtracted from the bulk action the explicit charge dependence completely drops out. In the fixed charge ensemble, the charge appears in the action only through its appearance in $f(r)$.

5.2 Uncharged Gauss-Bonnet Black Holes

We begin with a study of the thermodynamic properties of D-dimensional uncharged Gauss-Bonnet-de Sitter black holes. Computing the full on-shell Euclidean action is straightforward since the bulk action is a total derivative. Upon integration it gives two contributions: one at the horizon r_h, and one at the location of the cavity, r_c. We will also specialize to the case $k = 1$, so that the transverse sections are spheres. The boundary term contributes only at the cavity. Performing the action calculation, followed by some simplification, we arrive at the following general result:

$$\begin{aligned} I_{\rm E} = {} & \frac{(d-2)\Omega_{d-2}\beta_h f(r_c) r_c^{d-5}}{24\pi}\left(-3r_c^2 + 2\lambda_{\rm GB}(f(r_c)-3)\right) \\ & - \frac{\Omega_{d-2} r_h^{d-2}}{4}\left[1 + \frac{2(d-2)\lambda_{\rm GB}}{(d-4)r_h^2}\right] . \end{aligned} \quad (5.27)$$

Here β_h is the periodicity of the Euclidean time, which is redshifted to a value $\sqrt{f(r_c)}\beta_h$ at the cavity. We wish to physically fix the temperature of the boundary to be this value, so that $\beta = \sqrt{f(r_c)}\beta_h$, thereby ensuring thermodynamic equilibrium within the cavity.

The answer above is not quite complete. It is customary to normalize the action such that flat, empty spacetime has zero action and energy. To achieve this, we must subtract from the action the boundary term evaluated for an identical cavity in flat spacetime. This subtraction term has the form

$$I_0 = -\frac{(d-2)\Omega_{d-2}\beta_c\, r_c^{d-5}}{8\pi}\left[r_c^2 + \frac{4}{3}\lambda_{\rm GB}\right] , \quad (5.28)$$

and the complete action is then $I_{\rm E} - I_0$. In the present work, especially in the context of uncharged black holes, we will be interested in comparing the free energy of the black hole solutions with the free energy of an identical cavity filled with radiation. The free energy of the latter configuration is obtained from setting the metric function $f(r)$ to be the one

[4] In other words, requiring that $q \to iq$ so that $A_t dt = A_{t_E} dt_E$ — see, e.g., [52] for additional details.

for a pure de Sitter solution in $I_{\rm E}-I_0$.[5] For convenience, we then consider the difference between these two actions which is equal to

$$I_r \equiv \Delta(I_{\rm E}-I_0)=\frac{(d-2)\Omega_{d-2}\beta_c r_c^{d-5}}{24\pi}\Big[\sqrt{f(r_c)}\left(-3r_c^2+2\lambda_{\rm GB}(f(r_c)-3)\right) \\ -\sqrt{f_0(r_c)}\left(-3r_c^2+2\lambda_{\rm GB}(f_0(r_c)-3)\right)\Big]-\frac{\Omega_{d-2}r_h^{d-2}}{4}\left[1+\frac{2(d-2)\lambda_{\rm GB}}{(d-4)r_h^2}\right], \tag{5.29}$$

where $f_0(r)$ denotes the metric function with the mass parameter set to zero and $f(r)$ is the full solution for the physical Gauss-Bonnet-de Sitter black hole

$$f(r)=1+\frac{r^2}{2\lambda_{\rm GB}}-\frac{r^{2-d/2}\sqrt{r^d+4\,\lambda_{\rm GB}\big(r\,\omega_{d-3}+\,r^d/l^2\big)}}{2\lambda_{\rm GB}} \tag{5.30}$$

where we have defined

$$\Lambda\equiv\frac{(d-1)(d-2)}{2l^2} \tag{5.31}$$

in the above. It is this branch that reduces appropriately to the Einstein gravity solution when the Gauss-Bonnet coupling is turned off. However note also that when the mass parameter is set to zero the metric function becomes

$$f_0(r)=1+\left(\frac{1-\sqrt{1+4\lambda_{\rm GB}/l^2}}{2\lambda_{\rm GB}}\right)r^2 \tag{5.32}$$

which corresponds to the pure dS vacuum of the theory. Note that the higher-curvature corrections 'renormalize' the cosmological constant. The asymptotics will be sensible provided that $\lambda_{\rm GB}/l^2>-1/4$. This will be the case in the bulk of this work where we focus primarily on positive coupling. If this bound is violated then the solution will terminate at some value of r and will not extend all the way $r\to\infty$.

From the above it is now possible to compute the entropy and energy of the solutions in the standard way. We find

$$E=\frac{\partial I_r}{\partial\beta}=\frac{(d-2)\Omega_{d-2}r_c^{d-5}}{24\pi}\Big[\sqrt{f(r_c)}\left(-3r_c^2+2\lambda_{\rm GB}(f(r_c)-3)\right) \\ -\sqrt{f_0(r_c)}\left(-3r_c^2+2\lambda_{\rm GB}(f_0(r_c)-3)\right)\Big], \\ S=\beta\frac{\partial I_r}{\partial\beta}-I_r=\frac{\Omega_{d-2}r_h^{d-2}}{4}\left[1+\frac{2(d-2)\lambda_{\rm GB}}{(d-4)r_h^2}\right], \tag{5.33}$$

[5]Note that, in the case of flat asymptotics, the action and energy for an empty cavity are set to zero simply by subtracting a boundary term for an identical cavity embedded in flat spacetime. However, in the dS case, a subtraction of the boundary term for an identical cavity in pure dS will not accomplish this — the reason is that when the cosmological constant is nonzero the bulk action contributes also to the total action.

where we note that, since I_r is the difference in actions of the black holes and the cavity filled with thermal gas, E here corresponds to difference in energies between those solutions. Note also that since we are working on-shell, the computation of these quantities needs to account for the fact that ω is not independent of β. The entropy here is exactly the Iyer-Wald entropy computed for Gauss-Bonnet black holes with spherical horizons. The energy has received "self energy" corrections due to the presence of the cavity.[6] Note that the energy implicitly depends on r_h due to the appearance of the mass parameter ω_{d-3} in the metric function.

As usual, the temperature $T = \beta^{-1}$ is obtained by demanding that the variation of I_r with respect to r_h vanish. This is accomplished by first rewriting $f(r_c)$ in terms of r_h, by isolating for M in $f(r = r_h) = 0$ and substituting back into f. We find that

$$\frac{\partial I_r}{\partial r_h} = 0 \quad \rightarrow \quad \beta^{-1} = T = \frac{f'(r)\big|_{r_h}}{4\pi\sqrt{f(r_c)}}\,, \tag{5.34}$$

where again the prime indicates a derivative with respect to r. This result is consistent with our expectation that the temperature required for equilibrium in the cavity should coincide with the redshifted Hawking temperature at the location of the cavity.

5.2.1 The First Law

The (extended) first law of thermodynamics for uncharged Gauss-Bonnet black holes reads:

$$dE = TdS + VdP - \lambda dA_c + \Phi_{GB}\lambda_{GB}\ , \tag{5.35}$$

where the usual work term λdA_c associated with changes in the cavity area A is present, and a $\Phi_{GB}\lambda_{GB}$ term is now included to account for variations in the Gauss-Bonnet coupling. Having determined the energy E, temperature T, and entropy S, we can determine the form of the conjugate variables $\{V, \lambda, \Phi_{GB}\}$ entering the first law. For convenience, we define

$$\gamma = \frac{-2\Lambda}{(d-1)(d-2)}\ , \tag{5.36}$$

and let $f(r) \rightarrow f$ and $f_0(r) \rightarrow f_0$, though note that these functions depend on $(r_+, r_c, \gamma, \lambda_{GB}, q)$.

[6] In the case where $\Lambda = 0$ we can easily see that, in the limit $r_c \rightarrow \infty$

$$\lim_{r_c\rightarrow\infty} E = \frac{(d-2)\Omega_{d-2}\omega_{d-3}}{16\pi G} = M$$

which matches precisely our expectations.

Using (3.7)–(3.8) we find the following:

$$V = \frac{2\,\Omega_{d-3}\left[\left(\lambda_{GB}\,(f_0-1)\,r_c^D - \frac{1}{2}\,r_c^{D+2}\right)\frac{\partial f_0}{\partial\gamma}\sqrt{f} - \left(r_c^D\lambda_{GB}(f-1) - \frac{1}{2}\,r_c^{D+2}\right)\frac{\partial f}{\partial\gamma}\sqrt{f_0}\right]}{r_c^5\sqrt{f_0\,f}\,(D-1)} \tag{5.37}$$

$$\begin{aligned}\lambda = \frac{(d-2)\,\Omega_{d-3}}{96\pi^2\sqrt{f_0\,f}\,r_c^7}\Bigg[&r_c^D\sqrt{f_0}\left(f\left(\lambda_{GB}\,(d-5)\,f + \tfrac{3}{2}\,(3-D)\,r_c^2 - 3\lambda_{GB}\,(D-5)\right)\right.\\ &\left.+\tfrac{3}{2}\left(\lambda_{GB}f - \tfrac{1}{2}r_c^2 - \lambda_{GB}\right)r_c\,\frac{\partial f}{\partial r_c}\right) + \sqrt{f}\left(r_c^{D+2}\left(\tfrac{3}{4}\left(\frac{\partial f_0}{\partial r_c}\right)r_c + \tfrac{3}{2}\,f_0\,(D-3)\right)\right)\\ &- r_c^D\left(\tfrac{3}{2}\,r_c\,(f_0-1)\,\frac{\partial f_0}{\partial r_c} + f_0\,(D-5)\,(f_0-3)\right)\lambda_{GB}\Bigg]\end{aligned} \tag{5.38}$$

$$\begin{aligned}\Phi_{GB} = \frac{(d-2)\,\Omega_{d-3}}{12\pi\sqrt{f_0\,f}\,r_c^5}\Bigg[&\left(\tfrac{3}{2}\left(r_c^D\lambda_{GB}(1-f_0) + \tfrac{1}{2}\,r_c^{D+2}\right)\frac{\partial f_0}{\partial\lambda_{GB}} - r_c^D\,f_0\,(f_0-3)\right)\sqrt{f}\\ &+\left(\tfrac{3}{2}\left(f\,\lambda_{GB} - \tfrac{1}{2}\,r_c^2 - \lambda_{GB}\right)\frac{\partial f}{\partial\lambda_{GB}} + f^2 - 3\,f\right)r_c^{d-5}\sqrt{f_0}\,r_c^5\Bigg]\end{aligned} \tag{5.39}$$

$$\phi = \frac{(D-2)\,\Omega_{d-3}\,r_c^{d-5}\left(\lambda_{GB}\,(f-1) - \frac{1}{2}\,r_c^2\right)\frac{\partial f}{\partial q}}{8\pi\sqrt{f}} \tag{5.40}$$

The uncharged case differs from the charged case only in the functional forms of f and f_0 that appear in these expressions, as well as the lack of ϕdQ term in the first law. One can also show through explicit substitution that these variables satisfy the modified Smarr relation, which in this case reads

$$(d-3)E = (d-2)TS - 2(PV + \lambda A_c) + 2\Phi_{GB}\lambda_{GB}\ . \tag{5.41}$$

In Figure 5.1 we plot regions where the thermodynamic volume is positive, as a function of r_h and r_c with Λ and λ_{GB} held fixed. The volume is positive in the blue shaded region. There are two boundaries enclosing this region. The diagonal line marks the boundary where $r_c > r_h$; since we are restricting the cavity to lie outside the event horizon, we are automatically on the upper-left side of this line. The second, curved boundary represents the line along which $r_c = r_{\rm cosmo}$. Again we are restricting our cavity to lie within the cosmological horizon, therefore the thermodynamic volume is positive in all regions of interest. This picture is qualitatively identical in higher dimensions.

5.2.2 5 Dimensional Black Holes

Having derived the general results for the uncharged Gauss-Bonnet black holes, we turn to the study of their phase structure, starting with $d = 5$. The quantity of interest is the

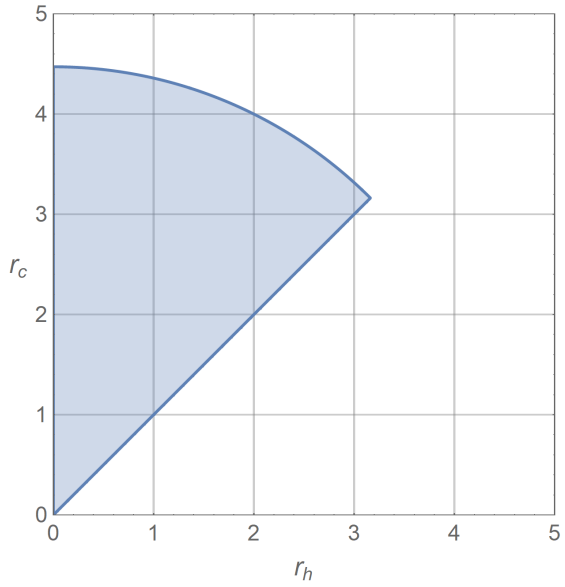

Figure 5.1: Thermodynamic volume of the uncharged Gauss-Bonnet black hole in $d = 5$ with $\lambda_{GB} = 0.1$ and $\Lambda = 0.3$. The blue shaded region indicates positivity of the volume V. The diagonal and curved boundaries mark, respectively, where $r_c = r_h$ and $r_c = r_{\text{cosmo}}$.

free energy $F = E - TS$, the quantity that is minimized by the equilibrium state of the system.

One way to examine the behaviour of this system is to realize that for a phase transition to occur at a given temperature T, the function $r_h(T)$ with fixed $\{r_c, \lambda_{GB}, P\}$ must be multi-valued.[7] The interpretation of this is the existence of multiple thermodynamically competing states with equal temperature but different horizon radii r_h, which will in general have different free energies. The transition of the horizon radius being a single valued function of the temperature to multi-valued thus (typically) corresponds to the free energy becoming multi-valued at fixed temperature. This will not, however, tell us about the stability of the phases or nature of the transition, which must be determined from the free energy itself. An analytic study of the roots of $T(r_h)$ is not possible in this case since the expression does not admit a closed form solution for r_h. In Figure 5.2 we plot the temperature as a function of $x \equiv r_h/r_c$ for fixed coupling λ_{GB} and varying pressure P, as well as fixed P and varying λ_{GB}, showing the transition from the single to multi-valued regime.

On the left of Figure 5.2, one can see that at fixed coupling there is a compact region $[P_{min}, P_{max}]$ between the red dashed lines where T is not a monotonically increasing function of x, in which case the horizon radius is a multi-valued function of the temperature. Below the minimum and above the maximum pressure, there is only one thermodynamically allowed state. In contrast, on the right we see that at fixed pressure, there is a maximum value of the Gauss-Bonnet coupling below which the horizon radius is multi-

[7] This is true throughout most of the parameter space, however there are some points where the temperature may be single-valued but at an inflection point, signalling a second-order phase transition.

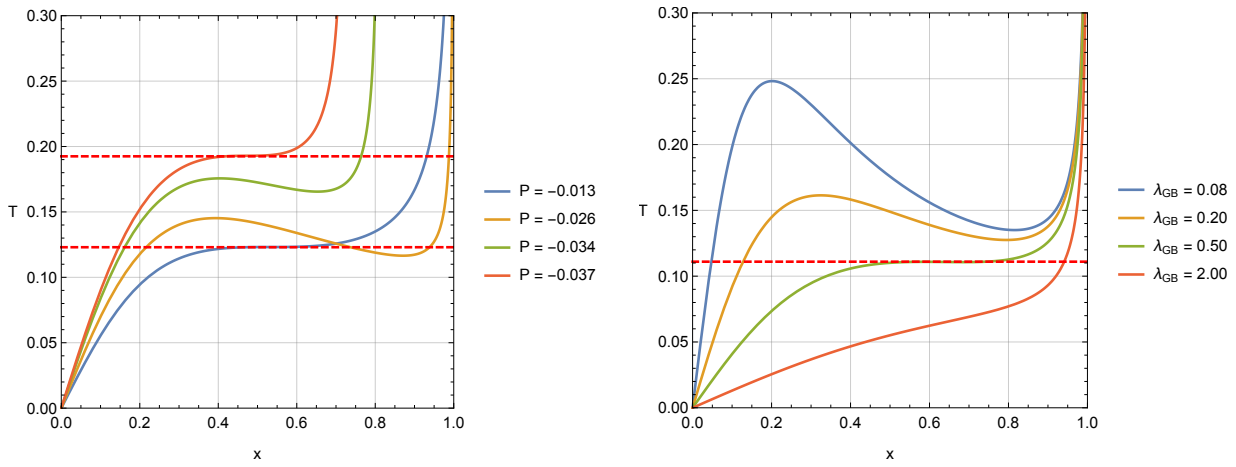

Figure 5.2: Temperature T as a function of $x = r_h/r_c$ for fixed cavity radius $r_c = 2$ and $d = 5$, showing regions where r_h is multi-valued, signaling a possible phase transition. **Left:** Varying pressure with $\lambda_{GB} = 0.3$. The red dashed horizontal lines demarcate the region in which T is not a monotonically increasing function of x. **Right:** Varying Gauss-Bonnet coupling with $P = -0.02$. Above the red dashed line T is not a monotonically increasing function of x.

valued. However there is no minimum and the phase transition (if it exists for a given choice of parameters at fixed pressure) always persists in the limit $\lambda_{GB} \to 0$. This type of analysis gives hints as to which regions in parameter space may have multiple competing phases, but only the free energy F can tell the whole story. The free energy of empty de Sitter space is $F = 0$, so even if multiple black hole phases exist, they may not be thermodynamically preferred, as we will see.

In Figure 5.3 we plot the free energy $F = E - TS$ parametrically as a function of T with r_h as the parameter. The thermodynamically preferred state is the one that globally minimizes the free energy. As the temperature of the system increases, the system will follow the line with lowest free energy whenever a crossing is reached. On the left of Figure 5.3, we plot the free energy at fixed value of the Gauss-Bonnet coupling and varying pressure. There is a crossing of the black hole free energy with itself, corresponding to a first order small-to-large black hole phase transition. However, since this crossing is above the free energy of thermal de Sitter space ($F = 0$), the relevant transition occurs at the red dots where the black hole free energy line crosses $F = 0$. This represents a Hawking-Page phase transition from radiation, or thermal de Sitter space, to a large black hole, and is generically seen in asymptotically AdS black holes.

We briefly clarify the notion of the Hawking-Page transition in de Sitter space. Here the transition is between a thermal gas confined to the cavity (this is what we mean by 'thermal de Sitter') and a black hole confined to the cavity. The temperature of both the gas and the black hole will generically be different from the temperature associated with the cosmological horizon. This is justified by the presence of the cavity: the boundary conditions imposed by the cavity allow for the control of the temperature of the cavity and

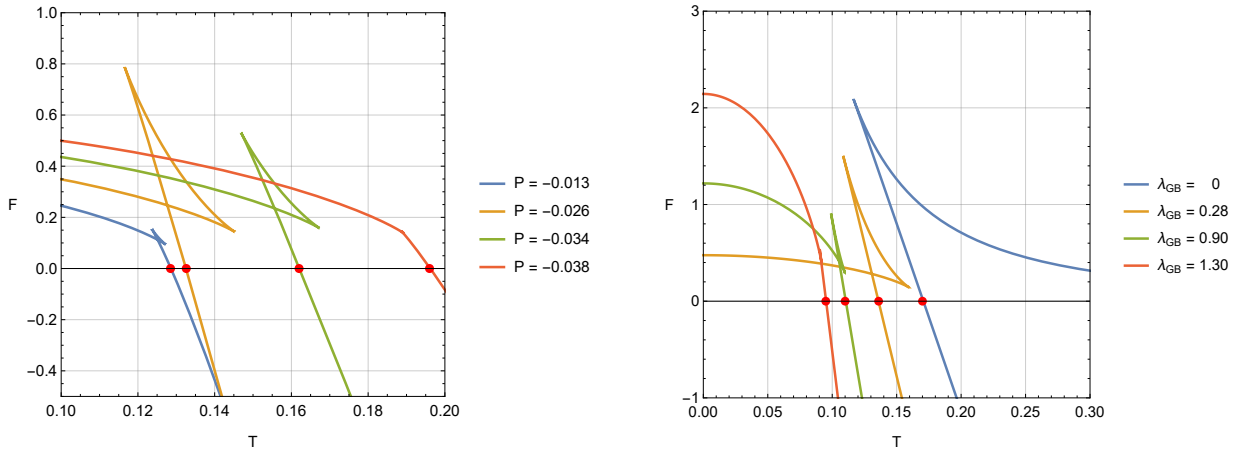

Figure 5.3: Free energy of the Gauss-Bonnet-de Sitter black hole in $d = 5$ with $r_c = 2$, showing a Hawking-Page phase transition from radiation to a large black hole, where the free energy crosses $F = 0$. **Left:** Varying pressure with $\lambda_{GB} = 0.3$. **Right:** Varying Gauss-Bonnet coupling with $P = -0.03$. For very small values of λ_{GB} the free energy limits to the Einstein case where there is a Hawking-Page phase transition with a minimum black hole temperature.

its contents independently of the cosmological horizon.

On the right side of Figure 5.3, we plot the free energy at fixed pressure for varying coupling λ_{GB}. Here we see that below a critical value of the coupling (in this case $\lambda_{GB} \sim 1.3$), a crossing forms in the black hole free energy, though because it is always above $F = 0$, we again only have a Hawking-Page phase transition where the large black hole branch crosses $F = 0$. In the limit $\lambda_{GB} \to 0$, corresponding to Einstein gravity, we recover the results presented in Chapter 2. Note that while the Hawking-Page transition is present for any choice of λ_{GB}, three situations are distinguished by the number of unstable phases available to the system. When $\lambda_{GB} = 0$, there are two black hole phases, when $0 < \lambda_{GB} < 1.3$ there are three black hole phases, and when $\lambda_{GB} > 1.3$ there is only one. The presence of the Gauss-Bonnet correction also gives rise to unstable black hole phases down to $T = 0$, while in the Einstein limit $\lambda_{GB} \to 0$ there is a minimum temperature black hole where the free energy reaches a point.

5.2.3 6+ Dimensional Black Holes

When $d > 5$, there are two cases of interest. When $\lambda_{GB} > 0$, there is again only a Hawking-Page transition from thermal de Sitter space to a large black hole, with a minimum black hole temperature as in the Einstein limit of the $d = 5$ case. This is encoded in the fact that the temperature is never more than double-valued as a function of $x = r_h/r_c$. When $\lambda_{GB} < 0$ however, we observe a small-large black hole phase transition, since the small black hole branch now has lower free energy than the radiation phase, and is the preferred state of the system at low temperatures. We demonstrate this in Figure 5.4, plotting the

free energy for fixed pressure and varying coupling for $d = 6$. Note that unlike in the $d = 5$ cases, when the coupling is negative, the small black hole branch (represented by the near-horizontal lines) has free energy less than that of radiation, and is not continuously connected to the large black hole branch. The phase structure is qualitatively identical for higher dimensions, with only the precise value of the critical temperature differing for a given choice of cavity size, pressure, and coupling.

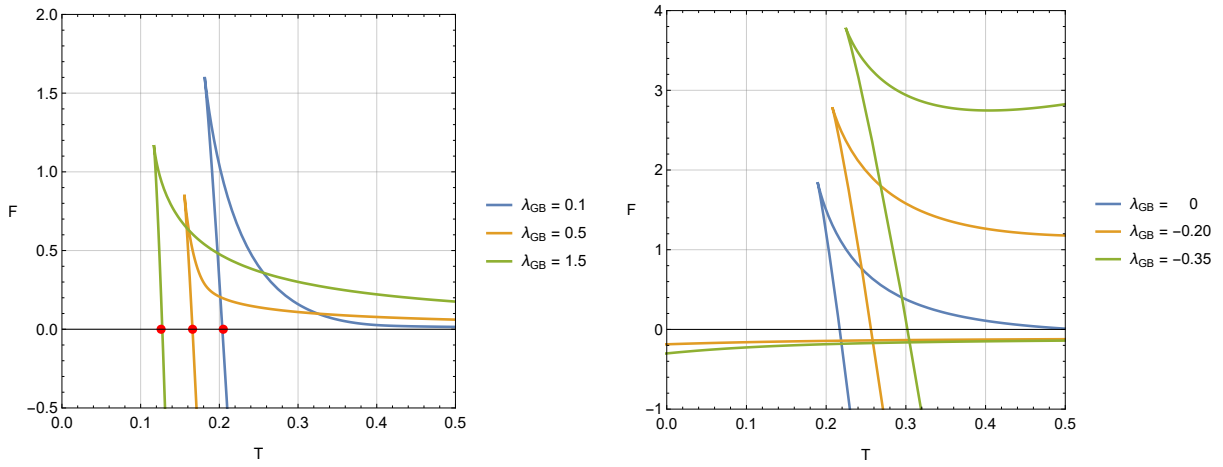

Figure 5.4: Free energy of the Gauss-Bonnet-de Sitter black hole with $d = 6$, $r_c = 2$, $P = -0.03$, and varying Gauss-Bonnet coupling. **Left:** With $\lambda_{GB} > 0$, there is a first-order phase transition from thermal de Sitter to a large black hole. **Right:** With $\lambda_{GB} < 0$, there is a first-order small-large black hole phase transition. Note the free energy of the small black hole branch is below that of radiation in this case. This behaviour is qualitatively the same in higher dimensions.

As is well-known, at sufficiently negative coupling Gauss-Bonnet gravity exhibits pathological behaviour such as naked singularities or negative string tension (if viewed as arising from α corrections in string theory) [179]. However, small negative couplings cannot be completely ruled out via analysis of physicality conditions [180]. Note also that when one considers the dynamical stability of these black holes, the coupling is further constrained [181], and that these black holes will be dynamically unstable in higher dimensions [182]. These constrained merit further investigation, especially in light of our results here where a change in sign of the coupling leads to very different phase structure.

5.3 Charged Gauss-Bonnet Black Holes

We next consider the inclusion of a $U(1)$ gauge field in the action (5.1), and study the resulting thermodynamics. In general, the presence of a Maxwell-like field leads to reentrant phase transitions and van der Waals-like behaviour. This is tied to the r^{6-2D} falloff of the charge term that appears in the metric function when such a field is present,

leading to additional roots in the temperature. The action is the same as before,

$$I_r = \frac{(d-2)\Omega_{d-2}\beta r_c^{d-5}}{24\pi}\Big[\sqrt{f(r_c)}\left(-3r_c^2+2\lambda_{\rm GB}(f(r_c)-3)\right) \\ -\sqrt{f_0(r_c)}\left(-3r_c^2+2\lambda_{\rm GB}(f_0(r_c)-3)\right)\Big] - \frac{\Omega_{d-2}r_h^{d-2}}{4}\left[1+\frac{2(d-2)\lambda_{\rm GB}}{(d-4)r_h^2}\right], \tag{5.42}$$

however now the metric function takes the form

$$f(r) = 1+\frac{r^2}{2\lambda_{GB}} - \frac{r^{2-d/2}\sqrt{r^d+4\,\lambda_{GB}\left(r\,\omega_{d-3}-q^2\,r^{4-d}-r^d/l^2\right)}}{2\lambda_{GB}}\,. \tag{5.43}$$

The energy E, temperature T, and entropy S therefore take the same functional form as in the uncharged case, namely (5.32)–(5.34), differing only by the form of the metric function $f(r)$. The free energy $F = E - TS$ thus also takes the same general form as in the uncharged case.

5.3.1 The First Law

When charge is present, the first law must be supplemented by an additional $\phi\, dQ$ term, with ϕ representing the electric potential of the spacetime measured at the cavity, and Q the total charge:

$$dE = TdS + VdP + \lambda dA_c + \phi\, dQ + \Phi_{GB}d\lambda_{GB} \tag{5.44}$$

We can again derive the conjugate quantities $\{V, \phi, \lambda, \lambda_{GB}\}$ from the first law. We omit the expressions here as they are structurally identical to those in Section 5.2.1 with the appropriate replacement of the metric function with the charge-dependent one. One can again verify through direct substitution that the Smarr relation holds for these quantities, which in the presence of charge reads

$$(d-3)E = (d-2)TS + (d-3)\phi\, Q - 2PV + 2\Phi_{GB}\lambda_{GB}\,. \tag{5.45}$$

As before, we examine the thermodynamic volume to check for positivity. In Figure 5.5, we plot regions where $V > 0$ for varying charge q.

When $q = 0$ we reproduce Figure 5.1. With non-zero q, regions where the thermodynamic volume is positive are smaller than in the uncharged case. The inner boundary of the shaded regions correspond to the location of the inner horizon r_- of the charged black hole. Outside of these regions, the volume is not negative, but rather imaginary. Since we are restricting the cavity to lie within $r_- < r_c < r_{\rm cosmo}$, we have an everywhere positive thermodynamic volume as in the uncharged case.

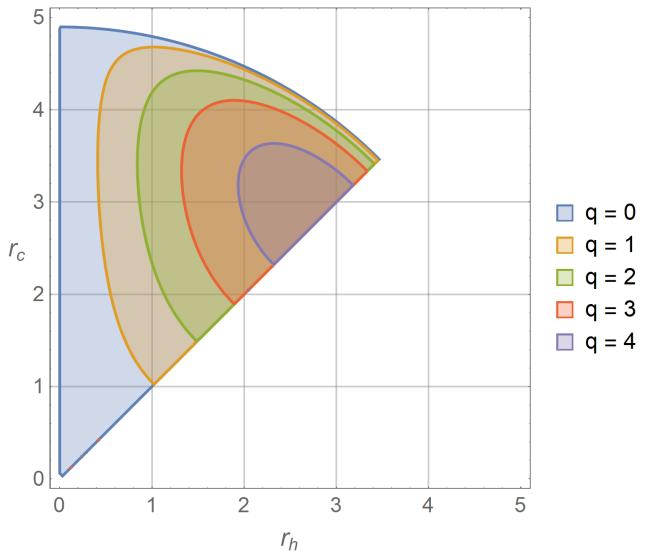

Figure 5.5: Thermodynamic volume of the charged Gauss-Bonnet black hole in $d = 5$ with $\lambda_{GB} = 0.1$, $\Lambda = 0.3$, and varying charge. The shaded regions indicate positivity of the volume V. The diagonal boundary marks where $r_c = r_h$.

5.3.2 Phase Structure

We again turn to an analysis of the free energy $F = E - TS$ to uncover the phase structure, this time for charged Gauss-Bonnet-de Sitter black holes. Figure 5.6 shows a plot of the free energy of the black hole both for varying pressure and varying coupling.

While the free energy in Figure 5.6 looks identical to the uncharged case, the interpretation is different in an important way. Since we are working in the canonical ensemble, the charge q of the black hole is fixed. This means that there is no Hawking-Page phase transition at the crossing of the black hole free energy with the $F = 0$ line, because a black hole cannot fully evaporate while its charge is held fixed. Instead, we have a small-large black hole phase transition where the black hole free energy line crosses itself. The system will follow the branch with lowest free energy, so the black hole suffers a jump from small r_h to large r_h at the crossing. With the cavity present, there is not only a minimum critical pressure P_{min} below which a kink forms in the free energy, but also a maximum pressure P_{max}. These critical pressures coincide with the values of $[P_{min}, P_{max}]$ at which x becomes multi-valued at a given temperature. At these critical pressures, a cusp forms in the free energy where a second order phase transition occurs, as in the red curves of Figure 5.6. Outside of the range $[P_{min}, P_{max}]$, the free energy is monotonic and there is no phase transition.

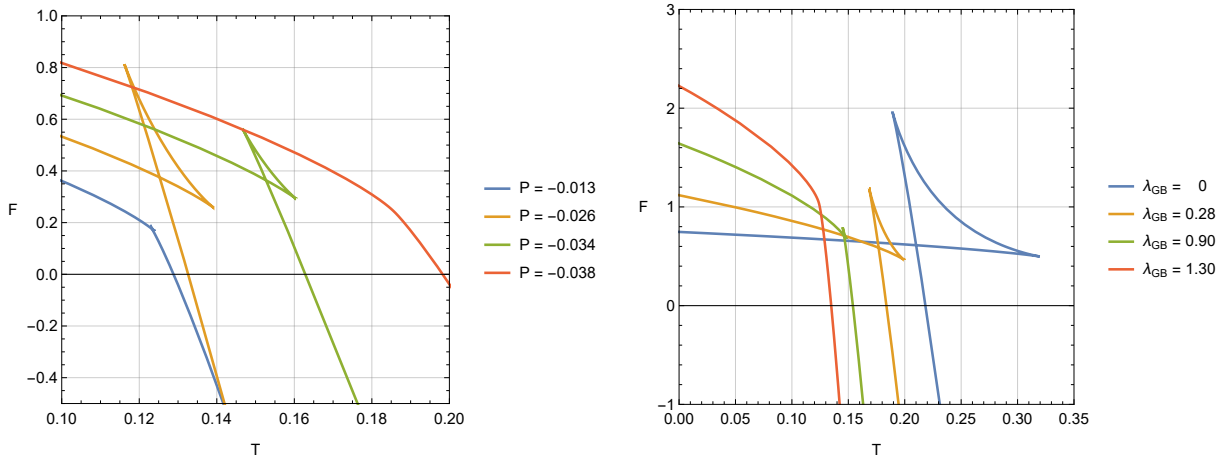

Figure 5.6: Free energy of the charged Gauss-Bonnet-de Sitter black hole with $d = 5$ and $r_c = 2$, showing a first-order phase transition from a small black hole to a large black hole. **Left:** Varying pressure with $\lambda_{GB} = 0.3$. **Right:** Varying Gauss-Bonnet coupling with $P = -0.03$. In the $\lambda \to 0$ limit we have a small-large phase transition.

On the right side of Figure 5.6, we vary instead the Gauss-Bonnet coupling with pressure held fixed. For couplings above a certain value (in this case $\lambda_{GB} = 1.3$) there is only one phase. Below this value, a crossing forms and we have a small-large phase transition. Notably, in the Einstein limit $\lambda_{GB} \to 0$ this small-large transition persists, unlike in the uncharged case considered previously. Unlike the uncharged case, when charge is present all of the qualitative features of the $d = 5$ black hole remain the same in higher dimensions; only the precise values of the free energy and critical points change, but all other phase structure and limiting behaviour is identical.

Unlike the typical 'swallowtail' behaviour seen in asymptotically AdS black holes (see for example [31]), the free energy here forms a tube in $F - T - P$ space, as shown in Figure 5.7. This 'swallowtube' behaviour, first observed in Chapter 2, is in stark contrast to the swallowtails that arise in black hole systems without cavities. In those systems, there is only a maximum pressure P_{max} below which the phase transition is present. Here, there is also a minimum pressure $|P_{min}| > 0$ that is reached where another second-order phase transition occurs, and only between these two pressures is there a small-large black hole phase transition. In Figure 5.8, we plot the coexistence curve for the black hole and compare it to a typical AdS black hole. These curves are lines in $P - T$ space along which the small and large black hole phases simultaneously exist and have equal free energy. Note the striking difference: when a cavity is present, the coexistence line terminates at two second-order phase transitions as opposed to one. One can also vary the charge q at fixed values of the pressure and coupling, as shown in Figure 5.9. Here we see a single critical value of the charge q_c for a given choice of Λ and λ_{GB}, below which there exists a small-large black hole phase transition, persisting down to $q = 0$. Notice that swallowtubes only exist in $F-T-P$ space: both in $F-T-q$ and $F-T-\lambda_{GB}$ space we see a swallowtail instead, with just one critical value of the respective parameters q or λ_{GB}.

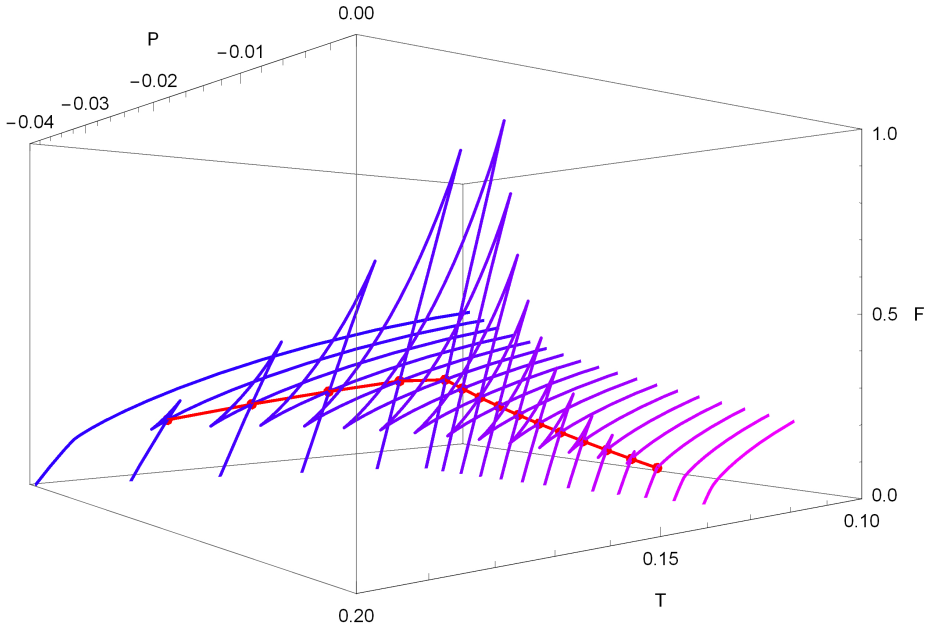

Figure 5.7: Free energy of the Gauss-Bonnet-de Sitter black hole in $d = 5$ with $r_c = 2$ and $\lambda_{GB} = 0.3$, showing the formation of a swallowtube corresponding to a compact region of first-order phase transitions from a small to large black hole. Each line corresponds to a constant-pressure slice, while red dots mark the location of the critical temperature within each slice. The red line is the coexistence line.

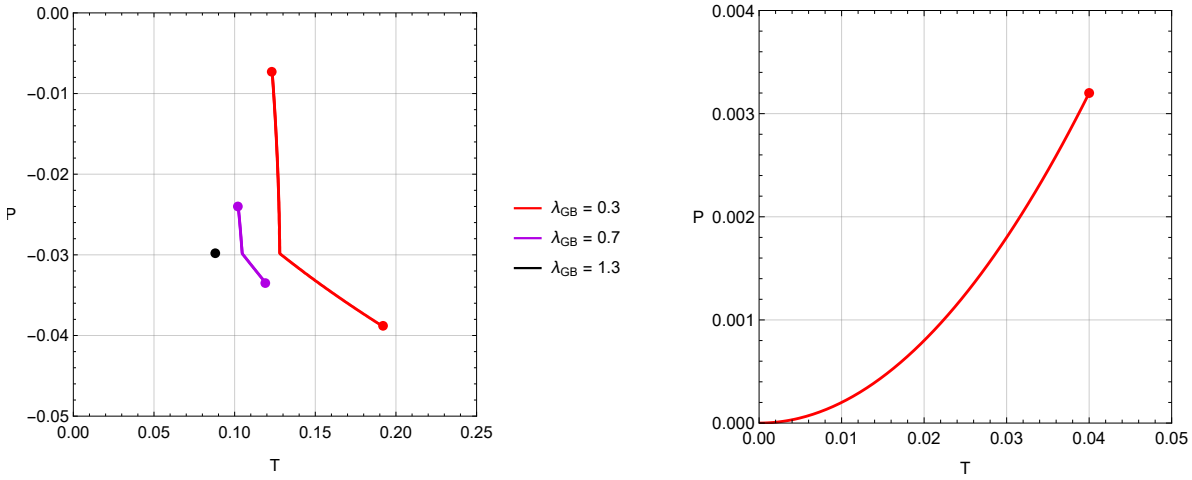

Figure 5.8: Coexistence curves for black holes, along which the small and large black hole phases coexist. **Left:** The uncharged Gauss-Bonnet black hole with $r_c = 2$ and varying λ_{GB}. The large dots mark the critical pressures P_{min} (P_{max}), above (below) which there is no phase transition. At these points a second order phase transition from small to large black hole transition occurs. **Right:** The uncharged AdS black hole, illustrating the difference when there is no cavity present. There is only one second order phase transition at the red dot P_{max}.

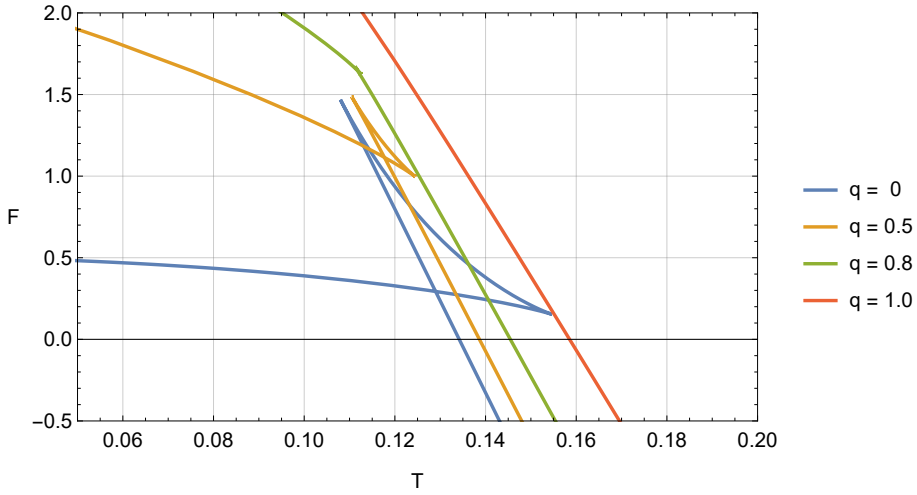

Figure 5.9: Free energy of the charged Gauss-Bonnet-de Sitter black hole with $d = 5$, $r_c = 2$, and $\Lambda = 0.3$, showing a first-order phase transition from a small black hole to a large black hole below a critical value of the charge q. In this case, $q_c \sim 0.8$.

5.4 Summary

We have studied the phase structure of both charged and uncharged de Sitter black holes in Gauss-Bonnet gravity, in the canonical ensemble. The presence of an isothermal cavity, equivalent to fixing boundary value data on a finite surface in the spacetime, allows us to have a notion of thermodynamic equilibrium in these asymptotically de Sitter spacetimes, which normally are not in equilibrium due to the two horizons present. What we have seen is a host of interesting phenomena. In the uncharged case, there exist Hawking-Page-like phase transitions throughout most of the parameter space, with a number of unstable black hole phases present. In the special case of $\lambda_{GB} < 0$, we find a region of first order small-large black hole phase transitions, where the free energy of the small black hole branch becomes smaller than that of radiation. Interestingly, while exotic re-entrant phase transitions and triple points are seen in 6-dimensional uncharged Gauss-Bonnet black holes in AdS spacetimes, here we see only a Hawking-Page phase transition in the 6-dimensional case. This touches on an important point: that while anti-de Sitter space acts like a 'box' that confines radiation much like a cavity does (allowing the black hole to reach thermodynamic equilibrium), these two methods of achieving equilibrium leave their imprint on the phase structure. One cannot understand the thermodynamic behaviour of a black hole without also considering how it is being maintained at equilibrium, for the exact method by which this is achieved affects significantly the resulting behaviour, even if the mechanisms seem qualitatively alike.

When charge is present, the story is considerably different. We generically see first order small-large black hole phase transitions encoded in the presence of a swallowtube in the $F - T - P$ space, with second order phase transitions at the minimum and maximum

pressures representing the end points of the tube. This swallowtube behaviour appears to be a characteristic feature of black holes embedded in isothermal cavities, as we have seen throughout Part I. Interestingly, such tubes only exist in $F - T - P$ space. When either the charge q or coupling λ_{GB} are varied, only a swallowtail emerges. These parameters do however control the size of the swallowtube in $F - T - P$ space, and for any particular choice of P for which a tube exists, one can find values of q and λ_{GB} such that the two ends of the tube (corresponding to a second order phase transition) meet. Based on previous work [166] we would expect that the merging of two critical exponents would yield novel critical exponents. However, the investigation of this expectation is difficult here as there is no first-order phase transition present in the case where the 'merged' critical exponent occurs — it is a truly isolated second-order phase transition. It is an open question as to whether different critical exponents emerge at this point, and how universal such behaviour is when a cavity is present.

Finally, recent developments [54, 158, 183] indicate that Gauss-Bonnet gravity (or a version of it) can in fact be formulated in $D = 4$, in such a way that the Gauss-Bonnet term (5.4) contributes nontrivially to the dynamics. The resulting theory is a Horndeski-type scalar-tensor theory that contains, among others, spherical black hole solutions for both positive and negative cosmological constant. Despite unanswered questions regarding the space of solutions and the nature of divergences which occur in the asymptotic region, significant attention has been given to the theory as it contests general relativity in its uniqueness as a four-dimensional, ghost-free metric theory of gravity. Our studies here should certainly be extended to this four-dimensional case.

This concludes our foray into the extended phase space thermodynamics of asymptotically de Sitter black holes. At the end of each chapter we have attempted to summarize important results and possible extensions of the work contained therein. Nonetheless, the reader should look to the Epilogue where we provide a summary of the main results of each chapter, the broad lessons one should take away from this work, as well as a discussion of the most important avenues to explore in the future. In Part II of this thesis, we will make strides towards understanding gravitational thermodynamics in more general settings (where convenient boundaries like the event horizon are unavailable) through a holographic approach rooted in relativistic hydrodynamics.

Part II

Beyond Black Holes

Introduction

The task of understanding the microscopic degrees of freedom of the gravitational field has a long history[8], one which has led to significant advances in our understanding of physics and mathematics across dozens of often disparate fields. As we have emphasized in Part I, a key observation guiding our exploration has been that gravity appears to possess thermodynamic properties, most readily manifest in Hawking radiation and the laws of thermodynamics for black holes. Undoubtedly, significant progress has been made in uncovering the structure of gravity at the microscopic scale, yet a fundamental understanding is still lacking. How do we answer the questions that seem to naturally arise in the discussions, namely, "What is the energy of gravity?" and "What does the entropy count?". Black hole thermodynamics appears to provide at least partial answers, but there is still much work to be done towards resolving them in full.

There is a sense in which the subject of black hole thermodynamics seems rather contrived. We are in principle making statements about the thermodynamic properties associated with the very geometry of space, yet binding ourselves to the existence of the event horizon, a surface that is teleological, null, and frankly bizarre. We are of course being disingenuous in adopting such a viewpoint. Black holes provide a extremely convenient environment where the connection between thermodynamics and geometry is readily apparent[9], and the insight gained from their study has been profound. Still, one is left wondering why it is so difficult to discuss thermodynamics in the absence of such boundaries — after all, gravitation hardly requires the presence of a black hole. Can we somehow understand the thermodynamic properties of the gravitational field in more general settings? This question is not new, and the answer is likely contained in a particularly exceptional property of gravity.

Unique to the gravitational interaction is its *holographic* nature [3,185,186], captured by both the universality of the Bekenstein-Hawking entropy (being related to various entropy bounds [40, 187]), as well as the vanishing of the Hamiltonian of general relativity (a consequence of diffeomorphism invariance). As a result of this property, the notion of a boundary plays a central role in the discussion of gravitational thermodynamics. We have already mentioned several examples of frameworks which could be reasonably called 'holographic'. In perhaps the most well-known realization of this principle, AdS/CFT,

[8]See [184] for a brief history of quantum gravity research.

[9]In the derivation of the first law presented in Section 1.4.1, one can choose a boundary other than $\mathcal{H}$, but in so doing the resulting quantities lose their simple interpretations as temperature, entropy, etc.

bulk degrees of freedom in supergravity can be mapped to gauge theory degrees of freedom on the conformal boundary of AdS [188]. Another notable example is the membrane paradigm, where one effectively replaces the interior of a black hole with a fluid living on the stretched horizon, the two being indistinguishable to an external observer [189]. This in some ways resembles also the fluid/gravity correspondence [190], where a long-wavelength limit of Einstein's equations is mapped to the boundary of AdS in the form of a classical fluid, though there the fluid is relativistic and the boundary is at infinity, rather than the black hole[10]. Of course, the relationship between bulk and boundary degrees of freedom is not unique to black holes and string theory; it is a general property of gauge theories that transformations which are pure gauge in the bulk can (when bounded regions are considered) give rise to physical symmetries, and thus non-trivial degrees of freedom, on the boundary [191–193]. This is a theme that is prevalent not only in quantum gravity, but condensed matter as well [83]. Though the holographic principle takes on many guises, these are all in essence statements of the fundamental idea that the information contained in a bulk region of space-time can be encoded purely in the boundary of that region.

Each of these examples of bulk/boundary correspondence come with their own limitations. In AdS/CFT, the duality critically relies on the asymptotic properties of anti-de Sitter space, whose boundary is timelike and can be reached with finite affine parameter. The boundary CFT correlators live only at $\mathcal{I}$, where the asymptotic symmetry group $SO(2,d)$ underlies also the d-dimensional CFT. Our understanding of situations where $\Lambda = 0$ is still rather incomplete [194, 195], but in this flat space holography the boundary is still at (null) infinity. In the membrane paradigm, the stretched horizon is confined to within epsilon of the event horizon $\mathcal{H}$, a surface that is teleological and null. The canonical examples of holography thus offer a limited perspective, because one is constrained to situations where knowledge of the boundary of space or the end of time is required. From a practical point of view this is unsatisfactory; as local observers we generally lack the ability to access these types of boundaries. From a theoretical point of view, given the holographic nature of the gravitational interaction, and the fact that gravity is something we observe not just globally, but also (quasi-)locally, there is no a priori reason to discount the formulation of a bulk/boundary relation for more general surfaces.

Recent developments in addressing these issues has led to the concept of using a *gravitational screen* as a quasi-local observer [196, 197]. A gravitational screen represents the time evolution of a two dimensional space-like hypersurface, which serves as the boundary of a bulk region of spacetime. Projecting Einstein's equations onto the screen yields the incompressible Navier-Stokes equations for a viscous fluid, allowing for a mapping between bulk geometric degrees of freedom and boundary fluid degrees of freedom. However, unlike in the membrane paradigm or AdS/CFT, the boundary is not restricted to the event horizon of a black hole or to spatial infinity. This approach is in some ways reminiscent of other quasi-local approaches to gravity, such as the original work of Brown and York [198], rigid quasilocal frames [199], and other 2+2 formulations of general relativity [200–202], though no fluid interpretation is given in those constructions.

[10]Even black hole thermodynamics is in a sense a holographic approach, with thermodynamic quantities being defined in terms of the event horizon, whose entropy scales with its area rather than its volume.

Our goal in Part II of this thesis will be to extend the concept of the gravitational screen to the relativistic regime, drawing a connection between two manifestly covariant frameworks: general relativity in the bulk, and non-equilibrium relativistic hydrodynamics on the boundary. In so doing, we make steps towards the resolution of many of the issues presented above. The bulk and boundary theories are placed on an equal footing, and non-Newtonian phenomena can be properly incorporated into the fluid description. We will draw much inspiration from both the membrane paradigm and fluid/gravity correspondence—indeed those examples should in principle arise as various limits of appropriately chosen screens. Beyond demonstrating the construction of the formalism, we further clarify the interpretation of the fluid pressure as the screen's normal acceleration, finding that the correct bulk/viscous splitting must include an expansion-dependent term. We also explicitly construct several examples of gravitational screens both in Minkowski and Schwarzschild spacetimes and examine the properties of the corresponding holographic fluids. Finally, we examine how the fluid entropy is linked to the curvature of spacetime, and remark on the salient features of the correspondence. The organization is as follows:

In Chapter 6 we present the gravitational screen formalism. We detail both the geometric construction of the screen and all of the elements that enter into the description of the boundary hydrodynamic system. We show how to relate the screen variables to those of the fluid system, and derive various conservation laws. Finally, we establish the dictionary that maps the geometric quantities to the hydrodynamic ones.

In Chapter 7, we present some explicit examples of our dictionary in action. We show how phenomena like entropy production can be interpreted geometrically, and construct several examples of screens in various backgrounds. We derive the equation of state of the screen fluids, along with other relevant thermodynamic quantities, and discuss various subtleties involved in the fluid interpretation. Finally, we close by commenting on a number of open questions and applications.

Chapter 6

Gravitational Screens

In this chapter, we will develop the relativistic gravitational screen framework, and construct the dictionary we will use to relate the screen geometry to a hydrodynamic system. We begin in Section 6.1 by presenting the geometric construction of a gravitational screen, and demonstrate how conservation of energy and momentum arises from various projections of the Einstein equations onto the boundary. In Section 6.2 we review important features of relativistic hydrodynamics, and derive conservation of energy/momentum equations for the boundary fluid. We treat separately the case of the equilibrium (perfect) and non-equilibrium (dissipative) fluids, and further discuss the thermodynamical laws governing quasistatic evolutions of the system. Finally in Section 6.3, we construct the mapping between the bulk geometric variables describing the screen and the boundary variables describing the relativistic hydrodynamic system. We comment on the interpretation of the mapping, and discuss some of the limitations and open questions that arise.

6.1 Gravity

We begin with a discussion of the geometry of the gravitational screen, and define all of the relevant quantities we will use in describing its features and evolution. A gravitational screen Σ is a 2+1 dimensional timelike hypersurface, which is viewed as the time evolution of a 2-dimensional boundary $\mathcal{S}$ of some 3-dimensional bulk (connected) region of spacetime. For the time being we consider spherically symmetric boundaries only, though the geometry can in principle be more complex. The screen is characterized by s^a, the outward pointing spacelike unit vector normal to $\mathcal{S}$, and u^a, the timelike unit vector tangent to Σ. By construction we have that $s_a s^a = 1$, $u_a u^a = -1$, and $s_a u^a = 0$. Throughout, Latin indices are used for vector and tensor components, where their dimension is made clear from their definition. Figure 6.1 illustrates the construction.

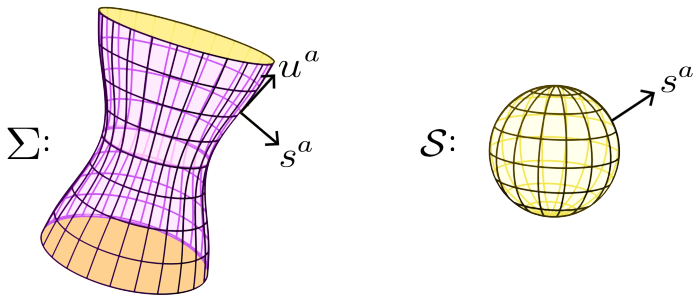

Figure 6.1: A gravitational screen Σ and a spatial section $\mathcal{S}$.

From the bulk metric g_{ab} we can construct the metrics on Σ and $\mathcal{S}$ as:

$$\Sigma: \qquad h_{ab} = g_{ab} - s_a s_b \tag{6.1}$$

$$\mathcal{S}: \qquad q_{ab} = h_{ab} + u_a u_b \tag{6.2}$$

Here, h_{ab} projects into the space orthogonal to s^a and encodes the intrinsic geometry of Σ. Likewise, q_{ab} further projects into the space orthogonal to u^a. The screen is topologically $\mathbb{R} \times S^2$, admitting a smooth codimension-one foliation by the leaves $\mathcal{S}$, which are level sets of some time function $t(x)$ inherited from the bulk foliation.

The extrinsic curvature of Σ is given by

$$H_{ab} = h_a{}^c h_b{}^d \nabla_c s_d \ . \tag{6.3}$$

while the geometry of the boundary surface $\mathcal{S}$ is encoded in the extrinsic curvature tensors

$$\Theta_{\mathbf{s}ab} \equiv q_a{}^c q_b{}^d \nabla_c s_d \ , \quad \Theta_{\mathbf{u}ab} \equiv q_a{}^c q_b{}^d \nabla_c u_d \ , \tag{6.4}$$

the normal one-form

$$\omega_a \equiv q_a{}^b (s_c \nabla_b u^c) \ , \tag{6.5}$$

and the normal accelerations,

$$\gamma_{\mathbf{u}} \equiv s_b u^a \nabla_a u^b \ , \quad \gamma_{\mathbf{s}} \equiv -u_b s^a \nabla_a s^b \ . \tag{6.6}$$

Together these quantities completely characterize the geometry of $\mathcal{S}$ and its embedding in $\mathcal{M}$. The quantity $\gamma_{\mathbf{u}}$ is the radial acceleration of a screen observer and will play an important role in our work. In the case where u_a is not hypersurface orthogonal, there will also be a non-zero *twist* vector

$$\epsilon^a \equiv u^b \nabla_b s^a - s^b \nabla_b u^a \ , \tag{6.7}$$

which measures the deviation from orthogonality of the congruence u^a to the spacelike hypersurfaces which foliate Σ.

The extrinsic curvature H_{ab} and projector h_{ab} can be used to construct the surface stress-energy tensor on Σ, given by

$$\tilde{S}_{ab} = \frac{1}{8\pi G} S_{ab} = \frac{1}{8\pi G}\Big([H]h_{ab} - [H_{ab}]\Big) \ , \qquad H \equiv h^{ab}H_{ab} \ . \tag{6.8}$$

Square brackets represent the discontinuity of a quantity across the boundary between the regions exterior ($\mathcal{V}_+$) and interior ($\mathcal{V}_-$) to the boundary, so that $[A] \equiv A|_{\mathcal{V}_+} - A|_{\mathcal{V}_-}$. This is the Brown-York stress-energy tensor for a hypersurface embedded in spacetime and is justified by Israel's junction conditions [198, 203]. The form of S_{ab} arises from the requirement that Einstein's equations are consistent in the distributional sense in the presence of singular surface stress-energy. It expresses the intuitive notion that if a closed surface has non-zero stress-energy, the extrinsic curvature and metric necessarily differ on either side of the surface (see [203] for details).

Eventually we will interpret (6.8) as the stress-energy tensor of a relativistic fluid living on the surface Σ. We adopt a holographic point of view, where the fluid stress-energy tensor (supported entirely on Σ) and the equations governing its evolution map to the gravitational dynamics and geometry within the screen. To this end, we require $[H_{ab}] \to H_{ab}$ and $[H] \to H$, so that the screen becomes the boundary[1] of our spacetime. In our case, this can be accomplished concretely by imposing a $\mathbb{Z}_2$ identification at Σ so that the screen acts like a mirror. The interior region is thereby replaced entirely by a surface stress-energy tensor

$$S_{ab} = Hh_{ab} - H_{ab} \ , \tag{6.9}$$

This is in the same spirit as the membrane paradigm [189], where the stretched horizon is taken to be the boundary of the spacetime, and boundary conditions for the fields present are chosen on the stretched horizon such that an external observer cannot distinguish the membrane from the 'real' black hole. A few conceptual points are worth addressing here. In the membrane paradigm, the stretched horizon is placed very close to the event horizon, such that crossing it and returning would require Planckian accelerations [204]. In this paradigm, we consider arbitrary timelike screens and so in principle an observer could pass through the screen and communicate her/his findings to the outside world. Moreover, the apparent location of the screen differs for different external observers, unlike the event horizon which is a global property of the spacetime. The former issue is one of interpretation: the claim is not that the universe is filled with fluid bubbles inside of which spacetime vanishes, rather, that any observer external to some region $\mathcal{V}_-$ can understand its gravitational features in terms of a relativistic boundary fluid[2]. The latter issue is resolved by the fact that the different observers are related simply by various boosts, and so can consistently map their observed screen variables to one another.

[1] This is markedly different from merely considering a surface within a spacetime. See Appendix B for more details.

[2] Of course, the extent to which this is possible is not known, and is one of the primary aims of this investigation.

6.1.1 Screen Energy-Momentum

With the definitions above and the general form of the surface stress-energy tensor (6.9), we can already see how the screen geometry might be recast in hydrodynamic terms. We begin by evaluating H_{ab} explicitly:

$$\begin{aligned}
H_{ab} &= h_a{}^c h_b{}^d \nabla_c s_d \\
&= (q_a{}^c - u_a u^c)(q_b{}^d - u_b u^d)\nabla_c s_d \\
&= q_a{}^c q_b{}^d \nabla_c s_d - q_a{}^c u_b u^d \nabla_c s_d - q_b{}^d u_a u^c \nabla_c s_d + u_a u_b u^c u^d \nabla_c s_d \\
&= \Theta_{\mathbf{s}ab} + q_a{}^c u_b s^d \nabla_c u_d - q_b{}^d u_a u^c (\nabla_{[c} s_{d]} + \nabla_d s_c) - u_a u_b u^c s^d \nabla_c u_d \\
H_{ab} &= \Theta_{\mathbf{s}ab} + \omega_a u_b + u_a \omega_b - \gamma_{\mathbf{u}} u_a u_b
\end{aligned} \tag{6.10}$$

We can then determine $\tilde{S}_{ab}$ using :

$$\begin{aligned}
\tilde{S}_{ab} &= H h_{ab} - H_{ab} \\
&= (\gamma_{\mathbf{u}} + \theta_{\mathbf{s}})(q_{ab} - u_a u_b) + \gamma_{\mathbf{u}} u_a u_b - \omega_a u_b - u_a \omega_b - \Theta_{\mathbf{s}ab} \\
&= \gamma_{\mathbf{u}} q_{ab} - \gamma_{\mathbf{u}} u_a u_b + \theta_{\mathbf{s}} q_{ab} - \theta_{\mathbf{s}} u_a u_b + \gamma_{\mathbf{u}} u_a u_b - \omega_a u_b - u_a \omega_b - \Theta_{\mathbf{s}ab} \\
&= -\theta_{\mathbf{s}} u_a u_b - \omega_a u_b - u_a \omega_b + (\gamma_{\mathbf{u}} + \tfrac{1}{2}\theta_{\mathbf{s}}) q_{ab} - (\Theta_{\mathbf{s}ab} - \tfrac{1}{2}\theta_{\mathbf{s}} q_{ab}) \\
&= -\theta_{\mathbf{s}} u_a u_b - \omega_a u_b - u_a \omega_b + (\gamma_{\mathbf{u}} + \tfrac{1}{2}\theta_{\mathbf{s}}) q_{ab} - \tilde{\Theta}_{\mathbf{s}ab}
\end{aligned} \tag{6.11}$$

where $\theta_{\mathbf{s}} \equiv q^{ab}\Theta_{\mathbf{s}ab}$ is the expansion and $\tilde{\Theta}_{\mathbf{s}ab} \equiv \Theta_{\mathbf{s}ab} - \frac{1}{2}\theta_{\mathbf{s}} q_{ab}$ is the trace-free part of $\Theta_{\mathbf{s}ab}$. Note that the form of (6.11) does not depend on u_a being hypersurface orthogonal. This expression for the surface stress-energy is already suggestive of a mapping between the screen geometry and a hydrodynamic counterpart. Consider a fluid living on a 2+1 dimensional timelike hypersurface defined by a timelike unit tangent vector u_a and 2D projector q_{ab}. Such a fluid has a stress-energy tensor

$$S_{ab} = e u_a u_b + \pi_a u_b + u_a \pi_b + p q_{ab} + \Pi_{ab} \ , \tag{6.12}$$

where e is the fluid energy density, π_a is the momentum density, p is the isotropic pressure, and Π_{ab} is the spatial stress tensor, given by

$$e \equiv u^a u^b S_{ab} \quad \pi_a \equiv -q^b{}_a u^c S_{bc} \quad \tilde{\Pi}_{ab} \equiv q^c{}_a q^d{}_b S_{cd} - p q_{ab} \ . \tag{6.13}$$

The stress-energy tensor (6.11) on the boundary Σ can seemingly be interpreted as a *fluid* stress-energy tensor provided we make the following identifications:

$$e = -\frac{\theta_{\mathbf{s}}}{8\pi G} \ , \qquad p = \frac{\gamma_{\mathbf{u}} + \frac{1}{2}\theta_{\mathbf{s}}}{8\pi G} \ , \qquad \pi_a = -\frac{\omega_a}{8\pi G} \ , \qquad \Pi_{ab} = -\frac{\tilde{\Theta}_{\mathbf{s}ab}}{8\pi G} \ . \tag{6.14}$$

This mapping from geometric variables describing the screen and thermodynamic variables describing a fluid formally suggests that we can understand at least part of the bulk gravitational physics inside of Σ in terms of a relativistic boundary fluid. What remains to be shown however, is that these identifications can derived consistently through Einstein's

equations and satisfy the necessary constraints, and to examine the conditions under which the quantities in (6.14) result in a system that obeys the known laws of thermodynamics and hydrodynamics. We would also like to determine the extent to which the screen is 'holographic', in the sense that it preserves information about the bulk despite being lower dimensional. In the remainder of this chapter, we make steps towards these goals.

6.1.2 Conservation of Energy

The identifications (6.14) demonstrate that at least a partial mapping is possible between variables describing the screen and those describing a fluid system. To make the correspondence more precise, we will examine Einstein's equations projected onto the screen, and compare them to their hydrodynamic counterparts. Einstein's equations with zero cosmological constant are $G_{ab} \equiv R - \frac{1}{2}Rg_{ab} = T_{ab}$. Their projection onto the hypersurface Σ is given by the Gauss-Codazzi equations,

$$D_b S^{ba} = -T_{cb} s^c h^{ba} \ , \tag{6.15}$$

where $D_a V_b = h_a{}^c h_b{}^d \nabla_c V_d$ is the covariant derivative on Σ. Equation (6.15) can further be projected along the timelike direction as

$$D_b S^{ba} u_a = -T_{\mathbf{su}} \tag{6.16}$$

where $T_{\mathbf{su}} \equiv s^a u^b T_{ab}$ represents the energy flux density flowing across the screen. This is the conservation of energy equation for the screen. Using (6.11) we have that

$$-T_{\mathbf{su}} = \underset{①}{-D_b(\theta_{\mathbf{s}} u^a u^b)u_a} \underset{②}{- D_b(\omega^a u^b)u_a} \underset{③}{- D_b(u^a \omega^b)u_a} \underset{④}{+ D_b[(\gamma_{\mathbf{u}} + \tfrac{1}{2}\theta_{\mathbf{s}})q^{ab}]u_a} \underset{⑤}{- D_b(\tilde{\Theta}^{ab}_{\mathbf{s}})u_a}$$

Evaluating the terms individually:

$$\begin{aligned}
① &= -D_b(\theta_{\mathbf{s}} u^b u^a)u_a \\
&= -D_b(\theta_{\mathbf{s}})u^b u^a u_a - \theta_{\mathbf{s}} D_b(u^b u^a)u_a \\
&= u^b D_b \theta_{\mathbf{s}} - u^a u_a \theta_{\mathbf{s}} D_b u^b - \theta_{\mathbf{s}} u^b u_a D_b u^a \\
&= D_{\mathbf{u}}\theta_{\mathbf{s}} + \theta_{\mathbf{s}}\theta_{\mathbf{u}} - u_b u^c D_c u^b \theta_{\mathbf{s}} \\
&= D_{\mathbf{u}}\theta_{\mathbf{s}} + \theta_{\mathbf{s}}\theta_{\mathbf{u}} \\
② &= -D_b(\omega^a u^b)u_a \\
&= -u_a u^b D_b \omega^a - u_a \omega^a D_b u^b \\
&= -u_a D_{\mathbf{u}} \omega^a - u^a \omega_a \theta_{\mathbf{s}} \\
&= \omega_a \mathrm{a}^a_{\mathbf{u}}
\end{aligned}$$

$$
\begin{aligned}
\textcircled{3} &= -D_b(u^a\omega^b)u_a \\
&= -u_a u^a D_b\omega^b - u_a\omega^b D_b u^a \\
&= D_b\omega^b - u_b\,\omega^c D_c u^b \\
&= D_b\omega^b \\
\textcircled{4} &= D_b[(\gamma_{\mathbf{u}} + \tfrac{1}{2}\theta_{\mathbf{s}})q^{ab}]u_a \\
&= u_a q^{ab} D_b(\gamma_{\mathbf{u}} + \tfrac{1}{2}\theta_{\mathbf{s}}) + u_a(\gamma_{\mathbf{u}} + \tfrac{1}{2}\theta_{\mathbf{s}})D_b q^{ab} \\
&= (\gamma_{\mathbf{u}} + \tfrac{1}{2}\theta_{\mathbf{s}})\theta_{\mathbf{u}} \\
\textcircled{5} &= -D_b(\tilde{\Theta}^{ab}_{\mathbf{s}})u_a \\
&= -D_b(\tilde{\Theta}^{ab}_{\mathbf{s}}u_a) + \tilde{\Theta}^{ab}_{\mathbf{s}}D_b u_a \\
&= \tilde{\Theta}^{ab}_{\mathbf{s}}\Theta_{\mathbf{u}ab}
\end{aligned}
$$

All together we have

$$
(D_{\mathbf{u}} + \theta_{\mathbf{u}})\theta_{\mathbf{s}} = -(8\pi G)T_{\mathbf{su}} + (\gamma_{\mathbf{u}} + \tfrac{1}{2}\theta_{\mathbf{s}})\theta_{\mathbf{u}} + \tilde{\Theta}^{ab}_{\mathbf{s}}\Theta_{\mathbf{u}ab} - (\mathrm{d}_a + 2\mathrm{a}_{\mathbf{u}a})\omega^a \tag{6.17}
$$

where we have used the fact that $u^a\omega_a = u_b u^c D_c u^b = u_b\,\omega^c D_c u^b = 0$ and $D_a V^a = \mathrm{d}_a V^a + \mathrm{a}_{\mathbf{u}a}V^a$ for a vector V^a which is tangent to $\mathcal{S}$.

6.1.3 Conservation of Momentum

The conservation of momentum equation is found by instead projecting (6.15) in the spatial direction as

$$
(D_b S^{ba})q_{ac} = -T_{\mathbf{s}c} \tag{6.18}
$$

where $T_{\mathbf{s}c} \equiv s^a T_{ac}$ and it is understood that the index c represents components tangent to $\mathcal{S}$. $T_{\mathbf{s}c}$ represents the momentum flux density across the screen. Again using (6.11) we can expand (6.18) as

$$
\underset{\textcircled{1}}{T_{\mathbf{s}c} = D_b(\theta_{\mathbf{s}}u^b u^a)q_{ac}} + \underset{\textcircled{2}}{D_b(\omega^b u^a)q_{ac}} + \underset{\textcircled{3}}{D_b(u^b\omega^a)q_{ac}} - \underset{\textcircled{4}}{D_b[(\gamma_{\mathbf{u}} + \tfrac{1}{2}\theta_{\mathbf{s}})q^{ba}]q_{ac}} + \underset{\textcircled{5}}{D_b(\tilde{\Theta}^{ba}_{\mathbf{s}})q_{ac}}
$$

Evaluating the terms individually:

$$
\begin{aligned}
\textcircled{1} &= D_b(\theta_{\mathbf{s}}u^b u^a)q_{ac} \\
&= q_{ac}(u^b u^a D_b\theta_{\mathbf{s}} + \theta_{\mathbf{s}}u^a D_b u^b + \theta_{\mathbf{s}}u^b D_b u^a) \\
&= \theta_{\mathbf{s}}\mathrm{a}_{\mathbf{u}c}
\end{aligned}
$$

$$
\begin{aligned}
\textcircled{2} &= D_b(\omega^b u^a) q_{ac} \\
&= q_{ac}\omega^b D_a u^b + q_{ac} u^a D_b \omega^b \\
&= \omega_b \Theta^b_{\mathbf{u}c} \\
&= \omega^b (\tfrac{1}{2}\theta_{\mathbf{u}} q_{bc} + \tilde{\Theta}_{\mathbf{u}bc} + \epsilon_{bc}) \\
\textcircled{3} &= D_b(u^b \omega^a) q_{ac} \\
&= q_{ac} u^b D_b \omega^a + q_{ac}\omega^a D_b u^b \\
&= \mathrm{d}_{\mathbf{u}}\omega_c + \theta_{\mathbf{u}}\omega_c \\
\textcircled{4} &= -D_b[(\gamma_{\mathbf{u}} + \tfrac{1}{2}\theta_{\mathbf{s}}) q^{ba}] q_{ac} \\
&= -q_{ac} q^{ba} D_b(\gamma_{\mathbf{u}} + \tfrac{1}{2}\theta_{\mathbf{s}}) - q_{ac}(\gamma_{\mathbf{u}} + \tfrac{1}{2}\theta_{\mathbf{s}}) D_b q^{ba} \\
&= -\mathrm{d}_c(\gamma_{\mathbf{u}} + \tfrac{1}{2}\theta_{\mathbf{s}}) - \mathrm{a}_{\mathbf{u}c} \\
\textcircled{5} &= D_b(\tilde{\Theta}^{ba}_{\mathbf{s}}) q_{ac} \\
&= D_b(\tilde{\Theta}^{ba}_{\mathbf{s}} q_{ac}) - \tilde{\Theta}^{ba}_{\mathbf{s}} D_b q_{ac} \\
&= D_b \tilde{\Theta}^b_{\mathbf{s}c}
\end{aligned}
$$

where ϵ_{ab} is the antisymmetric part of $\Theta_{\mathbf{u}ab}$. All together we have that

$$
(8\pi G) T_{\mathbf{s}c} = \theta_{\mathbf{s}} \mathrm{a}_{\mathbf{u}c} + (\tfrac{3}{2}\theta_{\mathbf{u}} q_{bc} + \tilde{\Theta}_{\mathbf{u}bc} + \epsilon_{bc})\omega^b + \mathrm{d}_{\mathbf{u}}\omega_c - (\mathrm{d}_c + \mathrm{a}_{\mathbf{u}c})(\gamma_{\mathbf{u}} + \tfrac{1}{2}\theta_{\mathbf{s}}) + D_b \tilde{\Theta}^b_{\mathbf{s}c} \ . \quad (6.19)
$$

6.1.4 The Radial Constraint

We also have a constraint equation for the rr component of the Einstein tensor coming from the Gauss-Codazzi equations. The constraint is:

$$
-2T_{ab} s^a s^b = {}^3R + H_{ab} H^{ab} - H^2 \ . \quad (6.20)
$$

Using (6.10) and the fact that $\omega_a u^a = 0$ we find that this reduces to the following condition:

$$
\begin{aligned}
-2T_{ab} s^a s^b &= {}^3R + (\Theta_{\mathbf{s}ab} + \omega_a u_b + \omega_b u_a - \gamma_{\mathbf{u}} u_a u_b)(\theta^{ab}_{\mathbf{s}} + \omega^a u^b + \omega^b u^a - \gamma_{\mathbf{u}} u^a u^b) - (\gamma_{\mathbf{u}} + \theta_{\mathbf{s}})^2 \\
&= {}^3R + \Theta_{\mathbf{s}ab}\theta^{ab}_{\mathbf{s}} - 2\omega^2 + \gamma^2_{\mathbf{u}} - \gamma^2_{\mathbf{u}} - 2\gamma_{\mathbf{u}}\theta_{\mathbf{s}} - \theta^2_{\mathbf{s}} \\
&= {}^3R + \tilde{\Theta}_{\mathbf{s}ab}\theta^{ab}_{\mathbf{s}} - 2\omega^2 - 2\gamma_{\mathbf{u}}\theta_{\mathbf{s}} - \tfrac{1}{2}\theta^2_{\mathbf{s}} \ . \quad (6.21)
\end{aligned}
$$

The d-dimensional Ricci scalar evaluated on a $(d-1)$-dimensional surface is

$$
{}^dR = {}^{d-1}R + \epsilon(K^2 - K_{ab}K^{ab}) + 2\epsilon\nabla_a(n^b \nabla_b n^a - n^a \nabla_b n^b) \quad (6.22)
$$

where K_{ab} is the extrinsic curvature of the $(d-1)$ surface defined by the normal vector n^a, which is normalized to $n^2 = \epsilon$. In the case of the surfaces Σ and $\mathcal{S}$, the normal vector is

u^a, the extrinsic curvature is $\Theta_{\mathbf{u}ab}$, and $\epsilon = -1$, so we have that

$$\begin{aligned}
{}^3R &= {}^2R - \theta_{\mathbf{u}}^2 + \Theta_{\mathbf{u}ab}\Theta_{\mathbf{u}}^{ab} + D_a(u^a D_b u^b - u^b D_b u^a) \\
&= {}^2R - \tfrac{1}{2}\theta_{\mathbf{u}}^2 + \tilde{\Theta}_{\mathbf{u}ab}\Theta_{\mathbf{u}}^{ab} - 2D_a \mathrm{a}_{\mathbf{u}}^a + 2\dot{\theta}_{\mathbf{u}} + 2\theta_{\mathbf{u}}^2 \\
&= {}^2R + \tfrac{3}{2}\theta_{\mathbf{u}}^2 + \tilde{\Theta}_{\mathbf{u}ab}\Theta_{\mathbf{u}}^{ab} - 2(\mathrm{d}_a + \mathrm{a}_{\mathbf{u}a})\mathrm{a}_{\mathbf{u}}^a + 2\dot{\theta}_{\mathbf{u}}
\end{aligned} \tag{6.23}$$

The constraint equation thus becomes (having reintroduced the factor $8\pi G$):

$$-(16\pi G)T_{\mathbf{ss}} = {}^2R + \tfrac{3}{2}\theta_{\mathbf{u}}^2 + 2\dot{\theta}_{\mathbf{u}} + \tilde{\Theta}_{\mathbf{u}ab}\Theta_{\mathbf{u}}^{ab} + \tilde{\Theta}_{\mathbf{s}ab}\Theta_{\mathbf{s}}^{ab} - 2(\mathrm{d}_a + \mathrm{a}_{\mathbf{u}a})\mathrm{a}_{\mathbf{u}}^a - 2\omega^2 - 2\gamma_{\mathbf{u}}\theta_{\mathbf{s}} - \tfrac{1}{2}\theta_{\mathbf{s}}^2$$

With the gravity equations in hand, we can proceed with discussing conservation of momentum and energy for a relativistic viscous fluid, which we will derive in the next section.

6.2 Relativistic Hydrodynamics

As discussed earlier, there are already a number of contexts in which the geometric features of boundaries within a spacetime can be understood to have fluid-like properties. With the exception of the fluid/gravity correspondence and AdS/CFT, all of those examples draw analogues between gravitational features and *Newtonian* fluids. For example, in the membrane paradigm the conservation equations for the stretched horizon are shown to be in correspondence with the Navier-Stokes equations, a decidedly non-relativistic proxy for the gravitational features of the black hole. This is also the case for earlier work involving gravitational screens themselves. Our main goal here will be to elevate the fluid side of these correspondences to the relativistic regime, placing it on an equal covariant footing with the gravity side. We review some of the essential aspects of relativistic hydrodynamics, and study the covariant conservation laws for a relativistic hydrodynamic system. We refer the reader to a number of texts that give much more substantial treatments of the subjects discussed herein [205–208].

At all times we assume that the time scales of the system's dynamics are large compared to the time scales of the microscopic physics, and that each fluid *element* is small enough to be locally in thermodynamic equilibrium, while at the same time containing a large enough number of particles that microscopic dynamics are averaged out. We denote the rest-mass density of the fluid with ρ, the fluid four-velocity with u^a (which is normalized to $u^a u_a = -1$), and the fluid acceleration with $a^a = u^b \nabla_b u^a$ (which also satisfies $a^a u_a = 0$). Describing the fluid at the statistical level is the Lorentz invariant distribution function $f = f(x, p)$, which gives the particle number density in phase space at time t, and depends on the properties of the microscopic constituents of the fluid. Though we will largely bypass the direct use of the distribution function, it plays an important role in defining various quantities at the statistical level.

Our understanding of relativistic fluid systems is broadly separated into two regimes, equilibrium and non-equilibrium (dynamical, or dissipative) systems. The study of systems at equilibrium is especially appealing because the laws of thermodynamics can be easily formulated, and adiabatic or quasistatic processes allow us to move from one equilibrium state to another in a way that is often physically reasonable. Indeed, a great number of physical systems possess a separation of scales (usually in the temporal sense) that allows for such an equilibrium description. In the context of gravity, equilibrium thermodynamics encompasses the celebrated 'laws of black hole thermodynamics' formulated by Bardeen, Hawking, and Carter, and has led to entire fields of research into the thermodynamic behaviour of black holes [11]. However, where dynamical processes are concerned (such as the formation/evaporation of a black hole) we often find ourselves in a regime where the first law fails to provide an adequate description. From the fluid perspective, such non-equilibrium scenarios fall into the dissipative regime, where viscous effects and heat fluxes lead to entropy production in the fluid. These far from equilibrium scenarios are the ones we seek to eventually understand, and will require the machinery of non-equilibrium hydrodynamics, though we focus mainly on equilibrium phenomena in this chapter.

Our discussion begins with the relativistic conservation laws, which can be constructed from various moments of the distribution function f. The first moment of the distribution function gives the *number density current* N^a and *rest-mass density current* J^a of the fluid, which can also be written in terms of u^a, the rest-mass density ρ, and the number density n as

$$N^a = \int p^a f \frac{d^3p}{p^0} = nu^a \ , \qquad J^a = mN^a = \rho u^a \ . \tag{6.24}$$

The second moment of the distribution function gives the fluid *stress-energy tensor*

$$T^{ab} = \int p^a p^b f \frac{d^3p}{p^0} \ . \tag{6.25}$$

In the absence of sources, the rest-mass density current and stress-energy tensor are both divergence-free, leading to the covariant conservation laws for a *generic* relativistic fluid,

$$\nabla_a T^{ab} = 0 \ , \qquad \nabla_a J^a = 0 \tag{6.26}$$

while conservation of rest-mass is expressed by the continuity equation,

$$\nabla_a N^a = \nabla_a (\rho u^a) = 0 \tag{6.27}$$

These equations may of course be supplemented on their right hand side by source terms if appropriate. In practice the relativistic equilibrium distribution function f is unknown, but we can avoid using it by instead specifying the stress-energy tensor directly, taking the covariant conservation laws as a starting point[3].

Finally, the number density current N^a and entropy density current s^a (we give precise meaning to this quantity in the following section) for the non-perfect fluid can be written

[3]Likewise, (6.26) is easily derived if f is known.

as

$$N^a = nu^a + n^a \ , \tag{6.28}$$

$$s^a = su^a + s^a \ , \tag{6.29}$$

where n^a and s^a are the non-equilibrium contributions to the currents and vanish for a perfect fluid. The picture presented here is valid in both flat and curved spacetime in any dimension.

6.2.1 Thermodynamical Laws

Hydrodynamic systems of the variety described above are of course *thermodynamic* systems, and have well defined behaviour captured by the laws of thermodynamics. The laws of thermodynamics provide information about how the thermodynamic properties of a fluid change when the system evolves in a quasi-static equilibrium. In this section, we derive some useful thermodynamic relations that will be used throughout this chapter.

We begin with first law of thermodynamics, which captures how various physical processes (such as heat exchange with the environment, through work being done on the system, or through the creation/destruction of fluid components) lead to changes in a system's internal energy U. For a relativistic fluid, the first law of thermodynamics in the fluid's rest frame is the same as the first law in flat space, and takes the form

$$dU = TdS - pdV + \mu dN \ , \tag{6.30}$$

where T is the temperature of the system, S is the entropy, p is the pressure, V is the volume, N is the number of fluid particles, and μ is the chemical potential. This is the same form of the first law encountered in Chapter 1, which can easily generalized to include other species of particles (for multi-component fluids) or other thermodynamic potentials. Many useful relations can be extracted directly from (6.30) through scaling arguments. In particular, let us express the internal energy U as a function of V, S and N. Since these are *extensive*[4] quantities, a rescaling of V, S, N corresponds to a rescaling of U as

$$U(\lambda V, \lambda S, \lambda N) = \lambda U(V, S, N) \ . \tag{6.31}$$

Differentiating with respect to λ gives:

$$V\partial_{\lambda V}U(\lambda V, \lambda S, \lambda N) + S\partial_{\lambda S}U(\lambda V, \lambda S, \lambda N) + N\partial_{\lambda N}U(\lambda V, \lambda S, \lambda N) = U(V, S, N) \tag{6.32}$$

Setting $\lambda = 1$ and using (6.30) gives

$$U = TS - pV + \mu N \ . \tag{6.33}$$

[4]Extensive quantities are represented by homogeneous functions of degree 1, satisfying $f(\lambda x) = \lambda f(x)$. Intensive quantities (such as temperature) are homogeneous functions of degree 0, such that $f(\lambda x) = f(x)$.

This is the so-called *Euler relation* which we will use extensively. Dividing through by V we obtain

$$e + p = Ts + \mu n \tag{6.34}$$

which is the Euler relation expressed in terms of the internal energy density $e = U/V$, entropy density $s = S/V$, and number density $n = N/V$. Taking the differential of the Euler relation and using the first law again we arrive at:

$$dp = sdT + nd\mu \ . \tag{6.35}$$

This is the *Gibbs-Duhem relation* which expresses the fact that the intensive variables p, T, μ are not independent. This equation reduces the number of independent thermodynamic degrees of freedom in the system by one[5]. Finally, we can combine the Euler relation and first law to get an expression for the entropy density of the system

$$\frac{ds}{s} = \frac{de}{e + p - \mu n} \tag{6.36}$$

which is valid when the number density is a constant ($dn = 0$).

The Second Law

One of our primary goals is to obtain a useful notion of entropy for gravitating systems through the properties of the holographic fluid. To this end, we require a geometric version of the second law of thermodynamics, which we demand that any physically reasonable fluid system must satisfy. From a kinetic theory point of view, the microscopic origin of the second law is encoded in the so-called *relativistic H-theorem*, which arises from conditions on the relativistic collision integral and states that

$$\frac{\partial H^\mu}{\partial x^\mu} \leq 0 \ , \quad H^\mu \equiv \int p^\mu f \left[\ln\left(f A_H\right) - \left(1 + \frac{1}{f B_H}\right) \ln\left(1 + f B_H\right) \right] \frac{d^3p}{p^0} \tag{6.37}$$

where f is the distribution function. For an equilibrium distribution function f_0, equality is achieved. Away from equilibrium, $\frac{\partial H^\mu}{\partial x^\mu} < 0$, and collisions within the system will drive it back towards $\frac{\partial H^\mu}{\partial x^\mu} = 0$. This is the content of the second law of thermodynamics. Because H^μ is defined in terms of the distribution function we can use it to define the fluid entropy in terms of an *entropy current* four-vector:

$$S^a = -k_B \int p^a f \left[\ln(f A_H) - \left(1 + \frac{1}{f B_H}\right) \ln(1 + f B_H) \right] \frac{d^3p}{p^0} \ . \tag{6.38}$$

A_H and B_H are constant coefficients that capture, respectively, the Newtonian and quantum contributions to the fluid entropy. They are given by

$$A_H = \frac{h_p^3}{g(s)}, \quad B_H = \pm \frac{h_p^3}{g_{\rm s}} \tag{6.39}$$

[5]Thermodynamic degrees of freedom are independent intensive variables/coordinates.

where $g(s) = 2s + 1$ is the degeneracy factor[6] arising from internal spin degrees of freedom and the $\pm$ accounts for Fermi $(+)$ and Bose $(-)$ statistics. The second law of thermodynamics can now be written in terms of the entropy current. Consider integrating S^a over a spacelike hypersurface χ with normal vector field n^a and metric h_{ab} to get the total entropy:

$$S_{\rm tot}(\chi) = \int_\chi \sqrt{h}\, S^a n_a \, d^3x \ . \tag{6.40}$$

This quantity should be non-decreasing for all surfaces χ' in the future of χ, so that

$$S_{\rm tot}(\chi') - S_{\rm tot}(\chi) = \int \sqrt{-g}\left(\nabla_a S^a\right) d^4x \geq 0 \ , \tag{6.41}$$

where the divergence theorem was used. Since the surfaces can be chosen arbitrarily, the second law is the condition that

$$\nabla_a S^a \geq 0 \ . \tag{6.42}$$

One rarely works at the level of the distribution function f, as it is often computationally impossible to track its evolution. Instead, adopting a more macroscopic point of view, it is useful to write the entropy current as

$$S^a = s\rho u^a + \frac{R^a}{T} \tag{6.43}$$

such that for a perfect fluid $R^a = 0$ and equality is achieved in (6.42). Deviations from equality (entropy production) are thus captured by the dissipative part R^a, which should be built from the non-equilibrium parts of the stress-energy tensor. We comment further on this in Section 7.2 after introducing the concept of the perfect and non-perfect fluids.

6.2.2 Perfect Fluids

We first consider the relativistic perfect (sometimes called 'ideal') fluid, seeking the conservation laws that govern its evolution. In the case of a perfect fluid, there are no viscous effects or heat flux, and the pressure tensor is diagonal. As a result, there is no entropy production and the fluid is at equilibrium. For a fluid living on the surface Σ with metric h_{ab} this stress-energy tensor takes the form

$$T^{ab} = (e + p)u^a u^b + p h^{ab} \ , \tag{6.44}$$

where e is the internal energy density of the fluid and p is the isotropic (equilibrium) pressure. For a perfect fluid, the velocity u^a is uniquely defined as the vector parallel to the density flux J^a, and defines a frame that is comoving with the fluid called the Eckart frame. Conservation of number density gives

$$\nabla_a(nu^a) = u^a\nabla_a n + n\nabla_a u^a = \nabla_u n + \theta n = \dot{n} + \theta n = 0 \ . \tag{6.45}$$

[6]For massless constituent particles one should instead use $g(s) = 2s + 1$.

The divergence of the stress-energy tensor is

$$\nabla_a T^{ab} = (e+p)u^a\nabla_a u^b + (e+p)u^b\nabla_a u^a + u^a u^b \nabla_a (e+p) + h^{ab}\nabla_a p \ .$$

Projecting this along the fluid velocity u^a gives the energy conservation equation:

$$\begin{aligned} u_b\nabla_a T^{ab} &= (e+p)u_b u^a\nabla_a u^b + (e+p)u_b u^b\nabla_a u^a + u_b u^a u^b \nabla_a (e+p) + u_b h^{ab}\nabla_a p \\ &= -(e+p)\theta - u^a\nabla_a(e+p) + u^a\nabla_a p \\ &= -(e+p)\theta - \dot{e} = 0 \ , \end{aligned} \tag{6.46}$$

where we have used $u_b u^a \nabla_a u^b = 0$ in the first and second line and defined $\dot{x} \equiv u^a\nabla_a x$. Projecting in the direction orthogonal to u_a (given by the metric $q^{ab} = h^{ab} + u^a u^b$) gives the conservation of momentum equation

$$\begin{aligned} q_{cb}\nabla_a T^{ab} &= (e+p)q_{cb}u^a\nabla_a u^b + (e+p)q_{cb}u^b\nabla_a u^a + q_{cb}u^a u^b\nabla_a(e+p) + q_{cb}h^{ab}\nabla_a p \\ &= (e+p)q_{cb}\dot{u}^b + q_c{}^a\nabla_a p \\ &= (e+p)q_{cb}\dot{u}^b + \mathrm{d}_c p = 0 \ , \end{aligned} \tag{6.47}$$

where we have used that $q_{ab}u^b = 0$ and defined $\mathrm{d}_a x = q_c{}^a\nabla_a x$. The relativistic conservation equations for number density, energy, and momentum are thus:

$$\dot{n} + n\theta = 0 \tag{6.48}$$

$$\dot{e} + (e+p)\theta = 0 \tag{6.49}$$

$$(e+p)q_{cb}\dot{u}^b + \mathrm{d}_c p = 0 \tag{6.50}$$

In $2+1$ dimensions, this is a set of 4 equations for the 5 unknowns representing the fluid. Equations (6.48) and (6.49) are scalar equations while (6.50) is a vector equation with 3 components, one of which is equivalent to the normalization condition $u^a u_a = -1$. The final ingredient needed to close the system is the equation of state. This is a (usually phenomenological) relationship between the state variables that arises from microscopic interactions within the fluid, and is typically cast in the form $p = p(\rho, e)$. The equation of state can in principle be derived from the distribution function if one knows the microscopic physics, though often it suffices to assume a particular equation of state based on the macroscopic features of the system being considered. In Section 7.1, we further clarify the role of the equation of state in the screen formalism.

6.2.3 Non-Perfect Fluids

Let us turn to the case where viscous effects and heat fluxes are present and write the full relativistic conservation equations. In the presence of heat flux and viscous effects, the definition of the local rest frame of the fluid is ambiguous [209]. We adopt the so-called Eckart frame, where u^a is parallel to the density current, so that the continuity equation is the same as for the perfect fluid case. We can decompose the stress tensor, number density,

and entropy density for the non-perfect fluid into equilibrium (perfect) and non-equilibrium (non-perfect) parts as follows:

$$T^{ab} = T^{ab}_{eq} + \Delta T^{ab} \qquad N^a = N^a_{eq} + \Delta N^a \qquad S^a = S^a_{eq} + \Delta S^a \tag{6.51}$$

Here, T^{ab}_{eq} is given by the perfect fluid stress tensor (6.44). The quantities $N^a_{eq} = nu^a$, $S^a_{eq} = su^a$, and T^{ab}_{eq} represent the equilibrium contributions that yield equations (6.48) to (6.50). The non-equilibrium parts are

$$\Delta T^{ab} = \epsilon u^a u^b + \pi \tilde{h}^{ab} + u^a q^b + u^b q^a + \Pi^{ab} \tag{6.52}$$
$$\Delta N^a = \eta u^a + n^a \tag{6.53}$$
$$\Delta S^a = \sigma u^a + s^a \tag{6.54}$$

where ϵ is the internal viscous energy, π is the dynamic pressure (the difference between the total pressure and pressure at equilibrium), Π^{ab} is the anisotropic (or viscous) stress tensor, q^a is the heat (or thermal momentum) flux orthogonal to u^a, n^a is the number density current, η is the non-equilibrium contribution to the number density, and σ is the non-equilibrium contribution to the entropy density. Π^{ab}, q^a, and π are the thermodynamic fluxes that capture the deviations from a perfect fluid, and are given in this case by the following:

$$\begin{aligned} \Pi^{ab} &= q^a{}_c q^b{}_d \, \delta T^{cd} - (p+\pi) q^{ab} \ , \\ q^a &= -q^a{}_c \, \delta T^{cb} u_b \ , \\ p + \pi &= \frac{1}{2} q_{ab} \, \delta T^{ab} \ . \end{aligned} \tag{6.55}$$

The full stress-energy tensor for the non-perfect fluid can be written:

$$T^{ab} = (e+\epsilon) u^a u^b + (p+\pi) q^{ab} + u^a q^b + u^b q^a + \Pi^{ab} \tag{6.56}$$

Conservation of mass gives:

$$\begin{aligned} 0 = \nabla_a N^a &= \nabla_a (N^a_{eq} + \Delta N^a) \\ &= \nabla_a (n u^a) + \nabla_a (\eta u^a + n^a) \\ &= n \nabla_a u^a + u^a \nabla_a n + \eta \nabla_a u^a + u^a \nabla_a \eta + \nabla_a n^a \\ &= \dot{n} + n\theta + \eta\theta + \dot{\eta} + (\mathrm{d}_a + \dot{u}_a) n^a \end{aligned} \tag{6.57}$$

Conservation of stress-energy gives:

$$\begin{aligned} 0 = \nabla_a T^{ab} &= \nabla_a \big[(e+\epsilon) u^a u^b + (p+\pi)(g^{ab} + u^a u^b) + u^a q^b + u^b q^a + \Pi^{ab} \big] \\ &= u^a u^b \nabla_a (e + \epsilon + p + \pi) + (\dot{u}^b + u^b \theta)(e + \epsilon + p + \pi) + g^{ab} \nabla_a (p + \pi) + q^b \theta \\ &\quad + u^a \nabla_a q^b + q^a \nabla_a u^b + u^b \nabla_a q^a + \nabla_a \Pi^{ab} \end{aligned} \tag{6.58}$$

Projected in the direction of u^a, (6.58) gives the conservation of energy equation

$$\begin{aligned} 0 = u_b \nabla_a T^{ab} &= -u^a \nabla_a (e + \epsilon + p + \pi) - (e + \epsilon + p + \pi)\theta + u^a \nabla_a (p + \pi) + u_b q^b \theta \\ &\quad + u_b u^a \nabla_a q^b + u_b q^a \nabla_a u^b - \nabla_a q^a + u_b \nabla_b \Pi^{ab} \\ &= -(\dot{e} + \dot{\epsilon}) - (e + \epsilon + p + \pi)\theta - (\mathrm{d}_a + 2\dot{u}_a) q^a + \Pi^{ab} \sigma_{ab} \end{aligned} \tag{6.59}$$

where we used the fact that $u_a \Pi^{ab} = u_a q^a = u_b q^a \nabla_a u^b = 0$, $\nabla_a q^b = (\mathrm{d}_a + \dot{u}_a) q^b$ and defined $\sigma_{ab} = \mathrm{d}_{<a} u_{b>}$ as the shear tensor. Finally, projecting (6.58) into directions orthogonal to u^a gives the conservation of momentum equation

$$\begin{aligned} 0 = q_{cb} \nabla_a T^{ab} &= q_{cb}(\dot{u}^b + u^b \theta)(e + \epsilon + p + \pi) + q_{cb} g^{ab} \nabla_a (p + \pi) + q_{cb} q^b \theta + q_{cb} u^a \nabla_a q^b \\ &\quad + q_{cb} q^a \nabla_a u^b + q_{cb} \nabla_a \Pi^{ab} \\ &= \dot{u}_c (e + \epsilon + p + \pi) + \mathrm{d}_c (p + \pi) + (\mathrm{d}_a + \dot{u}_a) \Pi^a_c + q_{cb} \dot{q}^b \\ &\quad + q_{cb} q^b \theta + q_{cb} q^a \nabla_a u^b \\ &= \dot{u}_c (e + \epsilon + p + \pi) + \mathrm{d}_c (p + \pi) + (\mathrm{d}_a + \dot{u}_a) \Pi^a{}_c + q_{cb} \dot{q}^b \\ &\quad + q_{cb} q^b \theta + q_{cb} q^a \left(\omega_a{}^b + \sigma_a{}^b + \tfrac{1}{2} \theta q_a{}^b - \dot{u}_a u^b \right) \\ &= \dot{u}_c (e + \epsilon + p + \pi) + \mathrm{d}_c (p + \pi) + (\mathrm{d}_a + \dot{u}_a) \Pi^a{}_c + q_{cb} \dot{q}^b \\ &\quad + \left(\omega_{ac} + \sigma_{ac} + \tfrac{3}{2} \theta q_{ac} \right) q^a \end{aligned} \tag{6.60}$$

where we have used the decomposition $\nabla_a u_b = \omega_{ab} + \sigma_{ab} + \frac{1}{2}\theta q_{ab} - \dot{u}_a u_b$. This decomposition breaks the covariant derivative of the fluid four-velocity into the antisymmetric *twist* or *vorticity* tensor ω_{ab}, the symmetric trace-free *shear* tensor σ_{ab}, and the expansion scalar θ. This decomposition is useful in that the irreducible parts of $\nabla_a u_b$ have straightforward physical interpretations. Consider an ideal spherical fluid element $\mathcal{X}$, which consists of a large number of fluid molecules in equilibrium. The twist ω_{ab} describes rotations of the fluid element about a principal axis in the local frame, the shear σ_{ab} induces volume-preserving deformations of $\mathcal{X}$ that also preserve the principal axes, and the expansion θ describes deformations that change the volume of the fluid element while retaining its shape.

To summarize, the conservation of mass, energy, and momentum equations for the relativistic non-perfect fluid are (respectively):

$$0 = \dot{n} + n\theta + \eta\theta + \dot{\eta} + (\mathrm{d}_a + \dot{u}_a) n^a \tag{6.61}$$

$$0 = -(\dot{e} + \dot{\epsilon}) - (e + \epsilon + p + \pi)\theta - (\mathrm{d}_a + 2\dot{u}_a) q^a + \Pi^{ab} \sigma_{ab} \tag{6.62}$$

$$0 = \dot{u}_c (e + \epsilon + p + \pi) + \mathrm{d}_c (p + \pi) + (\mathrm{d}_a + \dot{u}_a) \Pi^a{}_c + q_{cb} \dot{q}^b \tag{6.63}$$

$$+ \left(\omega_{ac} + \sigma_{ac} + \tfrac{3}{2} \theta q_{ac} \right) q^a \tag{6.64}$$

6.3 The Dictionary

Having derived equations (6.62) and (6.63) representing conservation of energy and momentum for a relativistic fluid, and equations (6.17) and (6.19) representing the same for a gravitational screen, we can now see that they in fact take on the exact same form, with each geometric variable describing the screen possessing a direct analogue in the fluid system. We now show the conservation of momentum and energy equations side by side:

Energy conservation

$$0 = -D_{\mathbf{u}}\theta_{\mathbf{s}} - \theta_{\mathbf{u}}\theta_{\mathbf{s}} + (\gamma_{\mathbf{u}} + \tfrac{1}{2}\theta_{\mathbf{s}})\theta_{\mathbf{u}} + \tilde{\Theta}^{ab}_{\mathbf{s}}\Theta_{\mathbf{u}ab} - (\mathrm{d}_a + 2\mathrm{a}_{\mathbf{u}c})\omega^a - (8\pi G)T_{\mathbf{su}}$$
$$0 = (\dot{e} + \dot{\epsilon}) + (e + \epsilon)\theta + (p + \pi)\theta - \Pi^{ab}\sigma_{ab} + (\mathrm{d}_a + 2\dot{u}_c)q^a$$

Momentum conservation

$$0 = \theta_{\mathbf{s}}\mathrm{a}_{\mathbf{u}c} - (\mathrm{d}_c + \mathrm{a}_{\mathbf{u}c})(\gamma_{\mathbf{u}} + \tfrac{1}{2}\theta_{\mathbf{s}}) + D_b\tilde{\Theta}^b_{\mathbf{s}c} + \mathrm{d}_{\mathbf{u}}\omega_c + (\tfrac{3}{2}\theta_{\mathbf{u}}q_{bc} + \tilde{\Theta}_{\mathbf{u}bc} + \epsilon_{bc})\omega^b - (8\pi G)T_{\mathbf{s}c}$$
$$0 = -(e + \epsilon)\dot{u}_c - (\mathrm{d}_c + \dot{u}_c)(p + \pi) - (\mathrm{d}_a + \dot{u}_a)\Pi^a{}_c - q_{cb}\dot{q}^b - \left(\tfrac{3}{2}\theta q_{ac} + \sigma_{ac} + \omega_{ac}\right)q^a$$

There appears to be a freedom in the choice of sign in the identifications above. This fixed by observing that the terms $T_{\mathbf{su}}$ and $T_{\mathbf{s}c}$, which represent respectively the energy and momentum flux across the screen, appear to be unaccounted for in the fluid description. Indeed, this is because we initially took the hydrodynamic conservation laws (6.26) to be source-free, resulting in the vanishing left hand side of equations (6.62) and (6.63). It is clear now that non-zero $T_{\mathbf{su}}$ or $T_{\mathbf{s}c}$ will manifest themselves as non-zero source terms in (6.26). These terms have a natural interpretation, as any energy-momentum flux into (or out of) the screened region would necessitate a change in the fluid's energy-momentum density, which is achieved by the source (or sink) terms. Consistently matching these source terms to the fluxes above and taking into account the direction chosen for the surface normals fixes the sign of the identifications.

The final step is to introduce a time flow vector t^a with a dual t^*_a describing the choice of time foliation, which will be normal to the sphere $\mathcal{S}$ and normalized to

$$t^2 = -f^2 \ , \quad t^{*2} = f^2 \tag{6.65}$$

where f is the lapse. Choosing[7] a frame such that

$$t^a = fu^a \qquad t^{*a} = fs^a \tag{6.66}$$

allows us to define the rescaled geometric quantities:

$$\gamma_t \equiv f\gamma_{\mathbf{u}} \quad \Theta_t \equiv f\theta_{\mathbf{s}} \quad \Theta_{t^*} \equiv f\theta_{\mathbf{s}} \qquad \theta_t \equiv f\theta_{\mathbf{s}} \qquad \theta_{t^*} \equiv f\theta_{\mathbf{s}} \tag{6.67}$$

[7]Note that in general, u^a may not be parallel to t^a. This *will* be the case whenever u^a is hypersurface orthogonal (the twist vanishes), a choice that will suffice for the examples we consider in Chapter 7.

Multiplying (6.17) and (6.19) by f^2 and rescaling the quantities as defined above, we finally arrive at the correspondence:

$$\boxed{\begin{aligned} e+\epsilon &= -\frac{\theta_{t^*}}{8\pi G} \qquad p+\pi = \frac{\gamma_t + \frac{1}{2}\theta_{t^*}}{8\pi G} \qquad \theta = \theta_t \qquad \omega_{ab} = \epsilon_{ab} \\ \Pi_{ab} &= -\frac{\tilde{\Theta}_{t^*ab}}{8\pi G} \qquad \sigma_{ab} = \Theta_{tab} \qquad q_a = -\frac{f^2\omega_a}{8\pi G} \end{aligned}} \tag{6.68}$$

We now turn to the main features of the dictionary. In this picture, the fluid energy density e is related to the rate of expansion of outgoing radial null geodesics at the boundary. The 2D fluid pressure p is now identified with $\gamma_t + \frac{1}{2}\theta_{t^*}$, in contrast with the membrane paradigm and non-relativistic screen formalism, where it is simply γ_t [189, 196]. The pressure can thus vanish for non-trivial screen geometries leading to complex thermodynamic behaviour. The fluid expansion θ is directly related to the expansion in the time direction of the screen. The intuition is clear: if the screen expands in the spatial direction, the 2D volume available to the fluid increases, and the fluid expands. Neither the number density n nor the fluid particle rest mass m map to a gravitational analogue, so that the rest-mass density $\rho = nm$ of the fluid remains undetermined from the dictionary. This is perhaps expected, as we are working at a classical, macroscopic level. One can understand the ambiguity by considering a distant observer viewing a screened region: their gravitational probe would be unable to distinguish between a fluid with $n = \frac{1}{2}$ and $m = 2$ from one with $n = 2$ and $m = \frac{1}{2}$.

A new feature appearing in our work is the fluid twist or kinematic vorticity ω_{ab} which is equal to the twist ϵ_{ab} of the screen observers. The fluid twist measures rigid rotations of fluid lines with respect to the local inertial rest frame. In contrast to the Newtonian case, the relativistic kinematic vorticity does not fully capture the phenomenon of relativistic vorticity. This is related to the fact that relativistic hydrodynamics does not have a straightforward Newtonian limit [209]. Traditionally, quasi-local approaches to studying gravitational thermodynamics use shell observers whose 4-velocities are hypersurface orthogonal, avoiding the complications introduced by a non-vanishing twist. For the screen constructions we consider in Chapter 7, this will turn out to be sufficient, but it is nice to have incorporated the twist here for applications to rotating screens, where it will certainly play a role. We also note the appearance of the non-equilibrium contributions to the energy and pressure, ϵ and π, to the fluid side of (6.68), which do not appear in the perfect fluid case (6.14). No new contributions that might correspond with ϵ and π appear on the gravity side. Clearly, these are absorbed into the expansion and normal acceleration, but is not clear what the appropriate splitting should be. This can likely be determined by considering a dynamic process such as a null shell collapsing onto an otherwise static screen, where the distinction between equilibrium and dynamic effects is obvious.

Now that we have a precise relationship between the gravitational variables representing the evolution of our screen, and the thermodynamic variables representing the fluid, we can investigate different screen evolutions and background geometries. We are particularly interested in determining which situations allow for the construction of physical screens, how the properties of various screen fluids differ from those encountered in non-gravitational settings, and which thermodynamic considerations should be used as guides in formulating a consistent duality between geometry and hydrodynamics.

6.4 Summary

In this chapter we have given the relativistic completion of the gravitational screen formalism first presented in [196], and constructed the map between geometric variables describing the evolution of the screen Σ and the thermodynamic variables describing a relativistic fluid system. With the formalism in place, we can consider explicit screen constructions and examine the properties of the fluids that arise. We can also assign a geometric interpretation to phenomena appearing in relativistic hydrodynamic systems, with the eventual goal of providing a quasi-local measure of gravitational entropy and energy through the 'holographic' boundary fluid.

Of course much remains to be understood concerning the formalism presented above, especially in the context of time-evolving screens. We have notably omitted the discussion of how one should incorporate non-orthogonal boundaries, and the implications of a non-vanishing twist when deviating from hypersurface orthogonality. Another important task is to make contact with other well-known results from hydrodynamics. Here we have focused on the essentials, conservation of energy and momentum, but in principle with the dictionary in hand, many other gravity equations can be translated into their hydrodynamic counterparts (and vice versa). For example, in the non-relativistic case one can show that the radial constraint appearing in Section 6.1.4 can be mapped to the dynamical Young-Laplace equation that appears in the study of capillary systems [196]. This equation is purely Newtonian, so in our case we should seek the appropriate relativistic generalization. The answer is likely given by the Darmois-Israel formalism [210], though it remains to be seen what fluid interpretation will be given to the screen variables in this relativistic context.

We would also like to examine the extent to which these screens are in fact holographic, namely, are there enough degrees of freedom present in the fluid description to reconstruct uniquely the bulk interior geometry? As Σ is not achronal, it is not obvious how the initial-value problem should be cast. The usual theorem concerning the well-posedness of the initial value problem for Cauchy surfaces (See [56] for example) cannot be extended to null surfaces, much less timelike surfaces. Only recently has the initial value problem for timelike surfaces been explored [211, 212]. Of course, we take the perspective here that the background geometry is known *a priori*, but this is certainly an area that requires more exploration. Finally, as we have mentioned, we will eventually need to consider dynamic processes to fully disentangle the dynamic fluid variables from their equilibrium

parts. With these questions in mind, we will now move on to the direct application of (6.68). In the next chapter, we will concern ourselves with the simplest examples of screen constructions to demonstrate how the formalism can be applied, and comment on some of the salient features of the dictionary.

Chapter 7

Using the Dictionary

In this chapter, we will explore various concrete applications of the dictionary (6.68). We will be particularly interested in the extent to which these screens have fluids with 'sensible' thermodynamic properties, what kinds of geometries can be encoded by physical fluids, and what equations of state they possess. Only single-component fluids will be considered here, and we ignore the internal gravitational interaction. We emphasize that this chapter is largely exploratory in nature, and there are many open questions concerning the interpretation of the screen's fluid properties. We aim to demonstrate how these properties are determined in the most salient examples, discuss the interpretation of the results, and comment on future applications and developments for the screen formalism.

In Section 7.1, we briefly discuss the role of the equation of state in our construction, and its geometric interpretation. In Section 7.2, we construct the gravitational analogue of the second law, and comment on the link between entropy production in the fluid and gravitational wave propagation in the bulk. Finally, in Section 7.3 we apply the gravitational screen formalism to a number of different scenarios, focusing primarily on static, spherically symmetric backgrounds and screen geometries. We explicitly construct the screens and determine their equations of state, along with the temperature and entropy of the screen fluids. We close by highlighting what we have learned and promising directions for future research.

7.1 Equations of State

The system described by (6.26) has more degrees of freedom than equations. To close the system we require an equation of state, which describes the relationship between global thermodynamic variables that arises from microscopic interactions within the fluid, usually in the form $p = p(\rho, e)$. This can be derived from the distribution function if one knows the microscopic physics, though often it suffices to assume a particular equation of state based on the macroscopic features of the system being considered. With the dictionary in hand, we can assign a geometric interpretation to the equation of state for the screen fluid.

Examining (6.68), it is clear that from the gravity point of view the equation of state will be uniquely determined by the expansion $\theta_{\mathbf{s}}$ and normal acceleration $\gamma_{\mathbf{u}}$, which are in turn determined by the screen geometry and evolution (the unit normal and tangent vectors s_a and u_a, along with the 2-metric q_{ab}). This allows for two approaches: we can either fix the screen geometry, and ask what equation of state is required to support that geometry, or fix the equation of state, and determine what screen geometry/evolution arises from it. We will tend towards the former, assuming a given background geometry and determining the extent to which physically reasonable fluids can describe the geometry. Note that non-trivial time evolution for the boundary (such as an expanding screen) generically leads to time-dependent equations of state, as we will see in Section 7.3.2. Though uncommon, such equations of state appear in some attempts at modelling the expansion of the universe, see [213,214] for example. Note that the equation of state for the screen fluid, being completely determined by the chosen geometry/evolution, will not be affected by our prescription for assigning a temperature and entropy to the screen fluid. These variables do not have gravitational analogues in our dictionary, and require additional input to determine.

7.2 Entropy Production

Though we focus primarily on equilibrium scenarios here, it is interesting to discuss the origin of entropy production in non-equilibrium situations. In relativistic fluids this comes from two primary sources, viscous dissipation and heat fluxes, the presence of which lead to deviations from equilibrium. Using the dictionary (6.68), we eventually hope to map these sources of entropy production directly to the geometry of the screen/spacetime.

As discussed in Section 6.2.1, the statement of the second law of thermodynamics is that the total entropy of the fluid never decreases, such that

$$\nabla_a S^a \geq 0 \qquad \text{with} \quad S^a = s\rho u^a + \frac{R^a}{T} \ , \tag{7.1}$$

where R^a has non-zero divergence and is a function of the thermodynamic fluxes π, q^a, and π^{ab}. The equilibrium state of a fluid is characterized by the absence of such transport phenomena, with $\pi = q_a = \pi_{ab} = 0$. In this case $R^a = 0$, leading to strict equality in (7.1) and a perfect fluid description. Though R^a can in principle be determined from the full distribution function, this is generally not done. Instead, the form of R^a depends on which description of non-perfect fluids is used. A common framework for discussing relativistic dissipative fluids is Classical Irreversible Thermodynamics (CIT), in which a linear dependence of R^a on the thermodynamic fluxes is assumed. Upon imposing all the relevant constraints, one can show that the most general form of the entropy current for such "first-order" theories is [215]

$$S^a = s\rho u^a + \frac{q^a}{T} \ . \tag{7.2}$$

The entropy production rate is then

$$\nabla_a S^a \geq \frac{-1}{T}\left(\Pi^{ab}\sigma_{ab} + \pi\theta + q^a(D_a \ln T + \mathrm{a}_a)\right) , \tag{7.3}$$

where we have used the continuity equation and conservation of energy. The first two terms capture the entropy production due to viscous dissipation, while the rest describe entropy changes due to heat fluxes. The simplest possible constraints on the right-hand side that satisfy the inequality are

$$\pi = -\zeta\theta \tag{7.4}$$
$$q_a = -\kappa T\left(D_a \ln T + \mathrm{a}_a\right) \tag{7.5}$$
$$\Pi_{ab} = -2\eta\sigma_{ab} \tag{7.6}$$

These represent the constitutive relations of CIT, where κ is the thermal conductivity, ζ is the bulk viscosity coefficient, and η is the shear viscosity coefficient. When translated to the gravity picture, we have that

$$\nabla_a S^a \geq \frac{1}{T}\left(\tilde{\Theta}^{ab}_{\mathbf{s}}\Theta_{\mathbf{u}ab} + \zeta\theta_t^2 - \omega^a(D_a \ln T + \mathrm{a}_a)\right) . \tag{7.7}$$

The first term suggests that viscous dissipation in the fluid maps to gravitational wave production in the bulk, since this quantity is related to the Weyl tensor C_{abcd} in the null limit. It would be interesting to examine a screen in a gravitational wave background to study precisely how the rate of entropy generation is tied to the wave propagation in the bulk.

The second term in (7.7) expresses dissipation arising from the screen expansion, while the last term is a source term that captures entropy changes due to heat fluxes in the fluid, which come from matter/energy fluxes through the screen. S^a and T can only be identified with a gravitational analogue once the equation of state (i.e. screen evolution) is fixed. As we will see, spherically symmetric screens in static, spherically symmetric spacetimes have screen fluids with no heat flux or viscous dissipation.

CIT represents the simplest dissipative framework, with only linear departures from equilibrium. Inherit to CIT are superluminal diffusion speeds and instabilities, though it has proven extremely useful in Newtonian regimes and reproduces the correct equilibrium behaviour of fluids. One can consider higher-order contributions to the dissipative flux R^a to resolve the issues with CIT, as is done in the Israel-Stewart formalism [216]. Here, contributions to R^a which are second-order in the dissipative fluxes are included, giving enough freedom to cure the causality and stability issues of CIT (though the higher-order terms often lack a simple physical interpretation). In future work, we hope to translate well-known results from these frameworks into the gravity picture, and present a clearer geometric interpretation of the dissipative terms that give rise to entropy production.

7.3 Static, Spherically Symmetric Screens

In the remaining sections, we focus on the application of the formalism described above to explicit screen constructions. We start with the general static, spherically symmetric case in four dimensions. We consider a screen Σ whose spatial sections S are 2-spheres of fixed areal radius r, and a spherically symmetric bulk metric g_{ab} with the general form

$$ds_+^2 = -f(r)^2 dt^2 + \frac{dr^2}{f(r)^2} + r^2\left(d\theta^2 + \sin^2\theta\, d\phi^2\right) \ . \tag{7.8}$$

Let $f = f(r)$. The time evolution of S is represented by the timelike hypersurface Σ, whose metric defined in terms of the spacelike normal vector $s_a = [0, f^{-1}, 0, 0]$ is

$$h_{ab} = g_{ab} - s_a s_b = -f^2 dt^2 + r^2\left(d\theta^2 + \sin^2\theta\, d\phi^2\right) \tag{7.9}$$

with $s_a s^a = 1$. The extrinsic curvature of Σ is given by

$$H_{ab} = h_a{}^c h_b{}^d \nabla_c s_d = \mathrm{diag}\left[-f' f^2, 0, rf, rf\sin^2\theta\right], \qquad H = f' + \frac{2f}{r} \tag{7.10}$$

where $f = f(r)$ and primes denote derivatives with respect to r. Recall from Section 6.1 that the energy-momentum tensor on Σ is

$$\tilde{S}_{ab} = \frac{1}{8\pi G}\big(H h_{ab} - H_{ab}\big) = \frac{1}{8\pi G} S_{ab} \tag{7.11}$$

where H denotes the trace of H_{ab}. The non-zero components of S_{ab} are

$$\begin{aligned} S_{tt} &= -\frac{2f^3}{r} \\ S_{\theta\theta} &= r^2 f' + rf \\ S_{\phi\phi} &= r^2 f' \sin^2\theta + rf\sin^2\theta \end{aligned} \tag{7.12}$$

We now choose $u_a = [-f, 0, 0, 0]$ to be the timelike vector field tangent to Σ normalized to $u_a u^a = -1$. Recall also that the twist vanishes in the spherically symmetric case and that $u_a s^a = 0$. The extrinsic geometry of S is given by

$$\Theta_{\mathbf{u}ab} = 0, \qquad \Theta_{\mathbf{s}ab} = \mathrm{diag}\ [0, 0, rf, rf\sin^2\theta] \tag{7.13}$$

where the trace parts are

$$\theta_{\mathbf{u}} = 0, \qquad \theta_{\mathbf{s}} = -\frac{2f}{r} \ . \tag{7.14}$$

The normal one-form representing the fluid momentum density is

$$\omega_A = q_A{}^a (s_b \nabla_a u^b) = 0 \ , \tag{7.15}$$

and the normal accelerations are

$$\gamma_s \equiv -u_b s^a \nabla_a s^b = 0 \ , \qquad \gamma_{\mathbf{u}} \equiv s_b u^a \nabla_a u^b = f' \ . \tag{7.16}$$

Rescaling the above according to (6.67) and using the dictionary (6.68) it is straightforward to translate these quantities to their fluid counterparts. We summarize the results in the table below.

Fluid Quantity	Gravity Quantity	Value
Energy Density (e)	$\dfrac{-\theta_{t*}}{8\pi G}$	$\dfrac{-f^2}{4\pi G\, r}$
2D Pressure (p)	$\dfrac{\gamma_t + \frac{1}{2}\theta_{t^*}}{8\pi G}$	$\dfrac{1}{8\pi G}\left(f f' + \dfrac{f^2}{r}\right)$
Fluid Expansion (θ)	θ_t	0
Heat Flux (q_a)	$-\dfrac{f^2 \omega_a}{8\pi G}$	0
Viscous Stress (Π_{ab})	$-\Theta_{tab}$	0
Shear (σ_{ab})	$\tilde{\Theta}_{t^* ab}$	$\mathrm{diag}[0, 0, r f^2, r f^2 \sin^2\theta]$

What can be said about the general properties of a fluid described by the table above? From the fluid point of view, entropy production comes from two sources, viscous dissipation and heat flux. As we have seen, the (local) entropy production rate for the fluid in terms of the screen variables is

$$\nabla_a S^a \geq \frac{1}{T}\left(\tilde{\Theta}^{ab}_{\mathbf{s}} \Theta_{\mathbf{u}ab} + \zeta \theta_t^2 - \omega^a (D_a \ln T + \mathrm{a}_a)\right) \ . \tag{7.17}$$

Notice in particular that for static screens in static, spherically symmetric spacetimes, $\Pi_{ab} \sim \Theta_{\mathbf{u}ab}) = 0$, so there is no viscous dissipation, and since there is no heat flux, $q_a \sim \omega_a = 0$, there is no entropy production. A perfect fluid description will therefore arise in all static, spherically symmetric background geometries. Notice also that this means the constitutive relation is $\Theta_{\mathbf{s}}(\Theta_{\mathbf{u}}) = 0$ which is the constitutive relation of a fluid with vanishing shear viscosity. The equation of state may however be highly non-trivial owing to the functional forms of e and p. This will be clear when we specialize to particular background geometries in the following sections.

7.3.1 Static Screens in Minkowski Space

Now let us take the results above and apply them to some explicit examples. We consider first the simplest case of a static screen of fixed areal radius r in Minkowski space. We

work in units where $G = 1$. The bulk metric (outside the screen) is simply

$$ds^2 = -dt^2 + dr^2 + r^2 d\Omega^2 \ . \tag{7.18}$$

The unit vectors tangent and normal to the screen are $s^a = [0, 1, 0, 0]$ and $u^a = [1, 0, 0, 0]$. The screen has the following stress-energy tensor

$$S_{ab} = \text{diag}\,[-2/r, 0, r, r\sin^2\theta] \tag{7.19}$$

and bare geometric quantities

$$\begin{aligned} \tilde{\Theta}_{\mathbf{s}ab} &= 0 & \Theta_{\mathbf{u}ab} &= 0 \\ \theta_{\mathbf{s}} &= \frac{1}{4\pi r} & \theta_{\mathbf{u}} &= 0 \\ \gamma_s &= 0 & \gamma_{\mathbf{u}} &= 0 \ . \end{aligned}$$

Since the fluid expansion θ vanishes (it is mapped to $\theta_{\mathbf{u}}$), equation (6.48) reduces to $\dot{n} = 0$ which implies that $n = $ const. and we are justified in using (6.36). Using the dictionary, the energy density and pressure of the screen fluid are found to be

$$e = -\frac{1}{4\pi r} \qquad p = \frac{1}{8\pi r} \ . \tag{7.20}$$

The equation of state is therefore

$$e(p) = -2p \quad \longleftrightarrow \quad p(e) = -\tfrac{1}{2}e \ , \tag{7.21}$$

which is the equation of state of a *barotropic fluid*[1] This fluid has the familiar equation of state from cosmology, $p(e) = we$ with $w = -\frac{1}{2}$, which appears in some quintessence and k-essence models [208]. The strong and dominant energy conditions are satisfied, though the speed of sound $c_s^2 = \partial p/\partial e$ is imaginary, so classical perturbations are not supported. In Figure 7.1 we plot e, p, and $e + p$ as a function of the screen radius r.

We can now use the Euler relation along with the first law (6.36) to determine the entropy and temperature of the screen fluid. Two very different cases arise depending on whether a chemical potential μ is included[2] in the fluid description. We analyze these separately as the limit $\mu \to 0$ is subtle.

[1] A barotropic fluid is a fluid whose energy density depends on pressure only.

[2] Recall that μ has no gravitational analogue in our dictionary, and is thus unspecified.

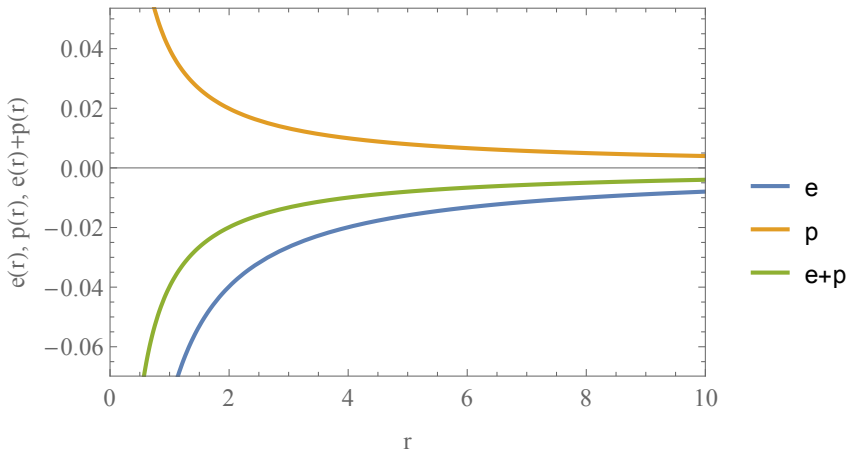

Figure 7.1: Energy density e and pressure p of the static, flat screen.

Vanishing chemical potential ($\mu = 0$)

We begin with the case of vanishing chemical potential. This is reminiscent of a photon fluid or non-interacting Bose-Einstein condensate, though the equations of state of those are rather different than the one we see here. With no chemical potential, it is straightforward to solve (6.36) for the entropy density of the fluid. We have that

$$\int \frac{ds}{s} = \int \frac{de}{e+p} \quad \rightarrow \quad s(e) = Ce^2 \ . \tag{7.22}$$

where C is a positive integration constant which we take to be unity. We can express this in terms of the screen radius r as

$$s(r) = \frac{1}{16\pi^2 r^2} \tag{7.23}$$

The temperature is:

$$T = \left(\frac{ds}{de}\right)^{-1} \quad \rightarrow \quad T(e) = \frac{1}{2e}, \quad T(r) = -2\pi r \tag{7.24}$$

Figure 7.2 shows a plot of the temperature, entropy density, and total entropy of the screen as a function of the screen radius r. The entropy density scales like $\sim r^{-2}$ so the total screen entropy is independent of the size of the enclosed space. This is a reassuring since from the outset we were hoping to somehow attribute the fluid entropy to the curvature of the enclosed region.

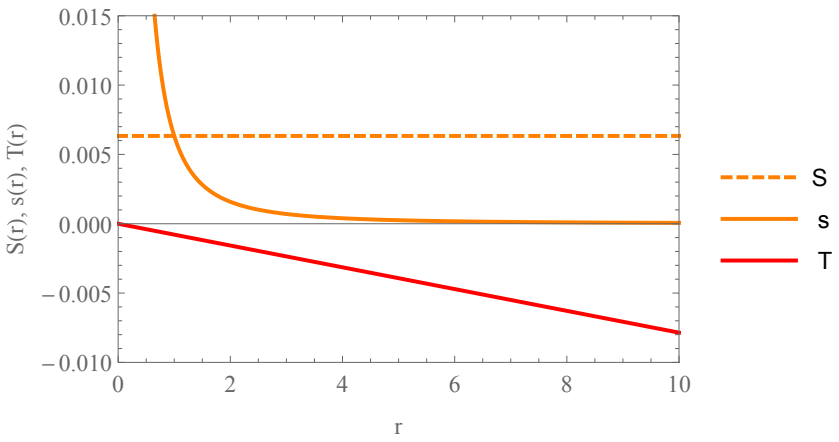

Figure 7.2: Temperature T, entropy density e, and total entropy S as a function of screen radius r for the static, spherically symmetric screen in Minkowski space.

From Section 6.2.2, the conservation of energy and momentum equations for a perfect fluid are

$$\begin{aligned} \dot{e} + (e+p)\theta = 0 \quad &\rightarrow \quad \dot{\theta}_s + (\gamma_{\mathbf{u}} - \tfrac{1}{2}\theta_{\mathbf{s}})\theta_{\mathbf{u}} = 0 \\ (e+p)a_c + D_c p = 0 \quad &\rightarrow \quad (\gamma_{\mathbf{u}} - \tfrac{1}{2}\theta_{\mathbf{s}})\dot{u}_c + D_c(\gamma_{\mathbf{u}} + \tfrac{1}{2}\theta_{\mathbf{s}}) = 0 \end{aligned}$$

Notice that since $\theta_{\mathbf{s}}$ and u^a are constant and $\theta_{\mathbf{u}} = 0$, the conservation equations are trivially satisfied (as they should be). The temperature being negative is not particularly surprising because $e < 0$ for any finite screen. That the fluid energy density is negative is a common feature in such programs (indeed, in the membrane paradigm the identification $e \sim -\theta_{\mathbf{s}}$ is the same), and arises from the binding energy associated with the gravitational field. On the other hand, one can demand that the properties of the fluid resemble those of a traditional one to the greatest extent possible, and explore the consequences of the demand. That the energy density is negative is unavoidable, but perhaps a more sophisticated model can give rise to positive temperature fluids. Next, we will examine whether a non-zero chemical potential can resolve these issues.

Non-zero chemical potential ($\mu \neq 0$)

With a non-zero chemical potential, the geometric properties of the screen are identical to the preceding case; it is only the thermodynamic description that changes. In particular, the Euler relation becomes $e + p = Ts - \mu n$, which combined with the first law gives

$$\int \frac{ds}{s} = \int \frac{de}{e + p - \mu n} \ . \tag{7.25}$$

To solve this integral, we must specify the functional dependence of the chemical potential

on r. Let us assume a constant chemical potential. We then find

$$s(e) = (e - 2\mu n)^2 \quad \leftrightarrow \quad s(r) = \left(\frac{1}{4\pi r} + 2\mu n\right)^2 \tag{7.26}$$

$$T(e) = \frac{1}{2(e - 2\mu n)} \quad \leftrightarrow \quad T(r) = \frac{-2\pi r}{1 + 8\pi r \mu n} \ . \tag{7.27}$$

Positivity of T thus requires choosing a chemical potential such that

$$\mu n < \frac{-1}{8\pi r} \tag{7.28}$$

Since $r > 0$ and $n > 0$, this implies that the fluid must have negative chemical potential, as in most classical gases and in quantum bosonic gases. In Figure 7.3 we plot the entropy density s, total entropy S, and temperature T for fixed r, showing that for a particular choice of chemical potential there is a minimum screen radius that can be supported before the temperature becomes negative, namely when $\mu n = -1/8\pi r$. The entropy density approaches a constant value $4(\mu n)^2$ as $r \to \infty$ and T approaches $-1/4\mu n$. The total screen entropy grows like $\sim r^2$ at large r.

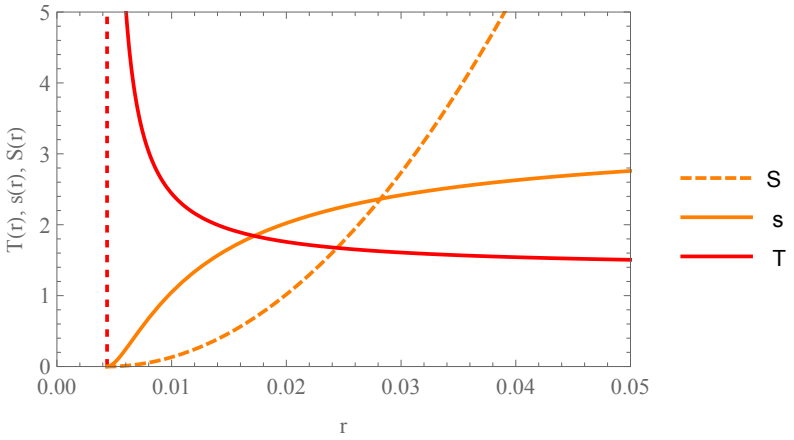

Figure 7.3: Total entropy S, entropy density s, and temperature T of a gravitational screen at fixed radius in flat space with $\mu n = -9$. The dashed line corresponds to the minimum supported screen radius, below which $T < 0$. e and T are rescaled to fit on the graph.

It is clear that even in the absence of curvature, the screen entropy is non-zero and in fact increases with the size of the region bounded by the screen. Of course, flat space is scale-invariant, so it is surprising that there is a dependence at all on the screen radius. In this way the example with $\mu = 0$ is somehow more sensible, though the energy density of the fluid there is still non-zero even though we have assumed a flat, vacuum spacetime.

The lesson appears to be the following: it does not make much sense to speak of gravitational screens with physical boundary stress tensors in the absence of curvature. In some ways this makes perfect sense. We are effectively excising a region of the spacetime

when we impose the membrane-like conditions on the screen's extrinsic curvature ($[H] \to H$), which now acts like a boundary in the spacetime. This necessarily induces a non-trivial surface stress-energy due to the junction conditions, which an external observer would find puzzling as the spacetime is presumed to empty in the first place, having no gravitational content. Only a completely trivial fluid would then match their expectations. That the total screen entropy grows with the size of the screened region indicates that some kind of flat space background contribution is being counted, which one could hope to remove through some renormalization procedure. However, one still has to deal with the issue of scale invariance and the instability that occurs when the screen becomes too small. Perhaps then, one can only assign thermodynamic meaning to the gravitational screen when there is something non-trivial to screen, though certainly more work needs to be done to understand the Minkowski example.

7.3.2 Accelerating Screens in Minkowski Space

In this section we briefly consider a spherically symmetric screen in flat space that is accelerating radially outward with constant acceleration a to illustrate some difficulties that arise for non-static screens. The metric outside the screen is

$$ds^2 = -dt^2 + dr^2 + r^2 d\Omega^2 \tag{7.29}$$

The velocity of an observer on the screen is $u^a = [\cosh(at), \sinh(at), 0, 0]$ and the spacelike unit normal to the screen is $s^a = [\sinh(at), \cosh(at), 0, 0]$. The screen radius is $r(t) = a^{-1}\cosh(at)$ with area $A = 4\pi r(t)^2$. The stress-energy tensor of the screen is

$$S_{ab} = \begin{bmatrix} -2a\cosh^2(at) & -2a\tanh(at) & 0 & 0 \\ -2a\tanh(at) & -2a\sinh^2(at) & 0 & 0 \\ 0 & 0 & -\dfrac{\cosh^2(at)\big(1+\cosh(at)\big)}{a} & 0 \\ 0 & 0 & 0 & -\dfrac{\cosh^2(at)\big(1+\cosh(at)\big)\sin^2(\theta)}{a} \end{bmatrix}$$

and the following bare geometric quantities:

$$\Theta_{\mathbf{s}ab} = \begin{bmatrix} \dfrac{\cosh^2(at)}{a} & 0 \\ 0 & \dfrac{\cosh^2(at)\sin^2(\theta)}{a} \end{bmatrix} \qquad \Theta_{\mathbf{u}ab} = \begin{bmatrix} \dfrac{\tanh(at)}{a} & 0 \\ 0 & \dfrac{\tanh(at)\sin^2(\theta)}{a} \end{bmatrix}$$

$$\begin{aligned} \tilde{\Theta}_{\mathbf{s}ab} &= 0 & \tilde{\Theta}_{\mathbf{u}ab} &= 0 \\ \theta_{\mathbf{s}} &= 2a & \theta_{\mathbf{u}} &= 2a\tanh(at) \\ \gamma_s &= -a\sinh(at) & \gamma_{\mathbf{u}} &= a\cosh(at) \end{aligned}$$

The energy density and pressure are therefore

$$e = 2a, \qquad p = -a\big(1 + \cosh(at)\big) \tag{7.30}$$

giving an equation of state:

$$p(e) = -\frac{1}{2}\left(1 + \cosh\left(\frac{e\,t}{2}\right)\right) \tag{7.31}$$

This satisfies the perfect fluid conservation of energy equation

$$\begin{aligned}\dot{e} + (e+p)\theta &= D_{\mathbf{u}}\theta_{\mathbf{s}} - (\gamma_{\mathbf{u}} - \tfrac{1}{2}\theta_{\mathbf{s}})\theta_{\mathbf{u}} \\ &= 2a^2\tanh(at)\big(\cosh(at) - 1\big) - 2a\tanh(at)\big(a\cosh(at) - a\big) \\ &= 0\end{aligned}$$

as well as conservation of momentum

$$(e+p)q_{cb}\dot{u}^b + \mathrm{d}_c p = -(\gamma_{\mathbf{u}} - \tfrac{1}{2}\theta_{\mathbf{s}})q_{cb}\dot{u}^b - \mathrm{d}_c(\gamma_{\mathbf{u}} + \tfrac{1}{2}\theta_{\mathbf{s}}) = 0$$

however notice that the equation of state $p(e)$ is now time-dependent. Such equations of state, though far less common than their time-independent counterparts, have recently been considered in cosmology where dark energy is modelled as a fluid with an inhomogeneous equation of state [217–219]. We note that constant acceleration is not required for this to occur; a time-dependent equation of state is a generic feature of non-static screens. In the present case, that screen observers experience a local acceleration a means that in principle the screen temperature should be related to the Unruh temperature. We leave the analysis of these types of screens for future work.

7.3.3 Schwarzschild Screens

We now turn to the important case of the Schwarzschild background, considering a gravitational screen Σ with fixed areal radius $r > 2m$ centered at the origin of the Schwarzschild chart. We will focus here on the case of a non-zero chemical potential, and comment briefly on the issues one encounters if $\mu = 0$ is chosen. The background metric is

$$ds^2 = -f^2dt^2 + f^{-2}dr^2 + r^2d\Omega_2^2, \qquad f = f(r) = \sqrt{1 - \frac{2m}{r}} \tag{7.32}$$

where m is the ADM mass of the black hole. The timelike unit vector tangent to the screen is $u^a = [f^{-1}, 0, 0, 0]$ and the spacelike unit normal to the screen is $s^a = [0, f, 0, 0]$. The

non-zero components of the stress-energy tensor on the screen are

$$\begin{aligned} S_{tt} &= -\frac{2f^3}{r} \\ S_{\theta\theta} &= r^2 f' + rf \\ S_{\phi\phi} &= r^2 f' \sin^2\theta + rf\sin^2\theta \end{aligned} \tag{7.33}$$

and the bare geometric variables are

$$\begin{aligned} \tilde{\Theta}_{\mathbf{s}ab} &= 0 & \Theta_{\mathbf{u}ab} &= 0 \\ \theta_{\mathbf{s}} &= \frac{2f}{r} & \theta_{\mathbf{u}} &= 0 \\ \gamma_{\mathbf{s}} &= 0 & \gamma_{\mathbf{u}} &= f' \ . \end{aligned}$$

This represents a fluid with

$$e = -\frac{r-2m}{4\pi r^2} \ , \qquad p = \frac{r-m}{8\pi r^2}, \quad e+p = \frac{r-3m}{8\pi r^2} \ . \tag{7.34}$$

The figure below shows the behaviour of e and p as well as their sum $e+p$ as a function of the screen radius. The Schwarzschild case is rather more complex than the static flat

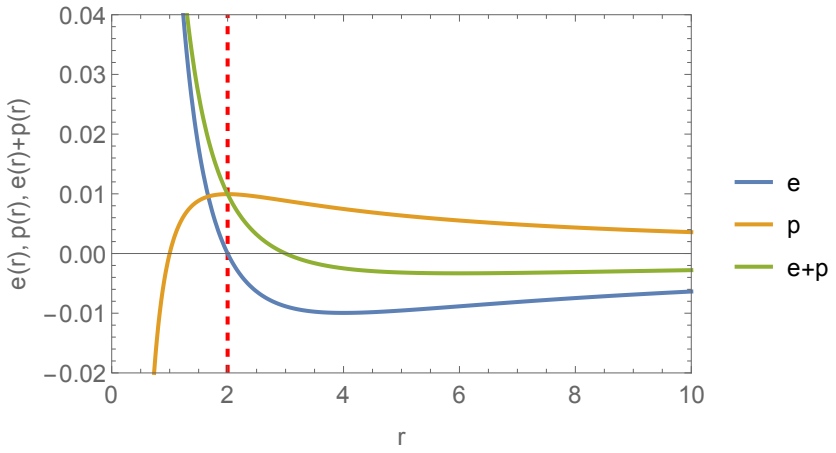

Figure 7.4: Energy density e, pressure p, and enthalpy $e+p$ for a gravitational screen at fixed radius outside of a Schwarzschild black hole of mass $m=1$. The horizon is indicated by a red dashed line.

case, since r(e) is given by the solution to a quadratic now, with solutions

$$r_1(e) = \frac{-1-\sqrt{1+32\pi me}}{8\pi e} \ , \quad r_2(e) = \frac{-1+\sqrt{1+32\pi me}}{8\pi e} \tag{7.35}$$

There are two branches of solutions that must be considered together. Subscripts on quantities label whether they correspond to branch 1 or 2 of (7.35). The resulting equations of state are

$$p_1(e) = \frac{1 - 16\pi me - \sqrt{1 + 32\pi me}}{64\pi m} , \qquad p_2(e) = \frac{1 - 16\pi me + \sqrt{1 + 32\pi me}}{64\pi m} . \tag{7.36}$$

This is the equation of state of a barotropic fluid (as in the flat case) though the dependence of pressure on energy density is no longer linear. Expanding $p(e)$ for small m shows that branch 1 limits to the flat case considered previously:

$$p_1(e) \approx -\tfrac{1}{2}e - 2e^2\pi m + \mathcal{O}(m^2) , \qquad p_2(e) \approx -\frac{1}{32\pi m} + 2\pi e^2 m + \mathcal{O}(m^2) . \tag{7.37}$$

As long as $r > 2m$, classical perturbations are supported by this fluid. At $r = 4m$, $\partial e/\partial p = 0$ and so the sound speed c_s diverges, indicating the fluid has become incompressible. We again determine the entropy density from the first law and Euler relation. For $p_1(e)$ we have

$$\ln(s(e)) = \int \frac{de}{e + p_1(e) - \mu n} = \int \frac{64\pi m \, de}{1 + 48\pi me - \sqrt{1 + 32\pi me} - 64\pi m\mu n} \tag{7.38}$$

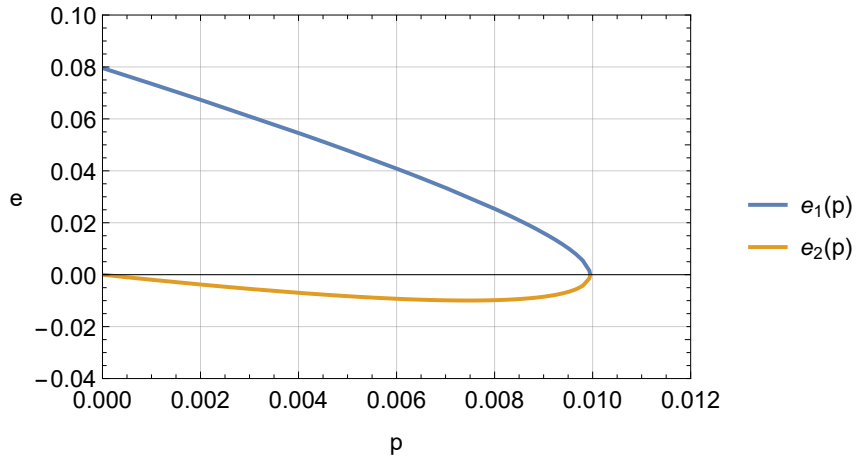

Figure 7.5: Equations of state $e_1(p)$ and $e_2(p)$ for the Schwarzschild screen, with $m = 1$. The first branch has a well-defined $m \to 0$ limit while the second does not.

Evaluating the integral explicitly, the entropy density and temperature can be found as functions of the screen radius and mass parameter:

$$s_1(r,m) = \frac{\left(2r^2(1-32\pi m\mu n)+8m(3m-2r)\right)^{4/3}}{r^{8/3}} \exp\left[\frac{4\tanh^{-1}\left(\frac{2r-6m}{r\sqrt{1+96\pi m\mu n}}\right)}{3\sqrt{1+96\pi m\mu n}}\right] \tag{7.39}$$

$$T_1(r,m) = \frac{r^{2/3}}{128\pi m\big(-m\,(8\,\pi r^2\mu n + r - 3\,m)\,\big)} \exp\left[\frac{4\tanh^{-1}\left(\frac{6m-2r}{r\sqrt{96\pi cm+1}}\right)}{3\sqrt{1+96\pi m\mu n}}\right] \tag{7.40}$$

In Figure 7.6 we plot these as a function of screen radius for fixed mass and μn, along with the total screen entropy $S(r)$ which is just the density integrated over $\mathcal{S}$.

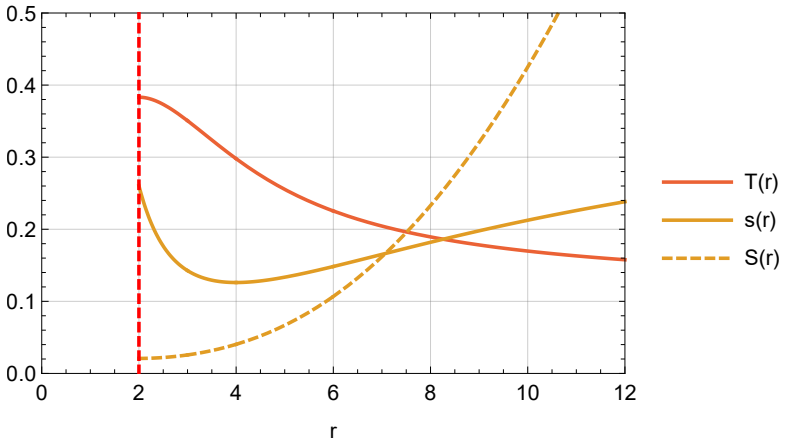

Figure 7.6: Total entropy $S(r)$, entropy density $s(r)$ and temperature T of a gravitational screen at fixed areal radius r in a Schwarzschild background with $m = 1$ and $\mu n = -0.01$. T and S are rescaled to fit on the graph. The dashed red line corresponds to the event horizon $r_h = 2m$.

The temperature and entropy density approach constant values at large-r, while the total entropy increases without bound (as in the flat case). As the screen fluid replaces the *interior* of $\mathcal{S}$, we interpret this entropy as the entropy of the screened region. However, we still need to develop a renormalization/subtraction scheme to correctly remove the 'vacuum' contribution to the entropy arising in Minkowski space. The correct way to account for the flat space contribution remains an open problem in our work. In any case, what will remain true is that the entropy achieves a finite value at the horizon, which can be normalized to give the Bekenstein-Hawking entropy through the integration constant (which we had set equal to unity previously). Let us assume such a normalization, so that $s \approx 1/4$ for a screen very close to the horizon. The limit as $\Sigma \to \partial\mathcal{H}$ is a null limit where $u^a \to s^a$, and $\theta_{\mathbf{u}} \to 0$. Close to the horizon, the expansion will be negligible compared to

the normal acceleration $\gamma_{\mathbf{u}}$. From the Euler relation[3] and the dictionary we have:

$$Ts = e + p = \frac{\gamma_t - \frac{1}{2}\theta_{t^*}}{8\pi} = \frac{1}{8\pi}\left(ff' + \frac{f^2}{r}\right) \tag{7.41}$$

Let $\epsilon = r - 2m$ and perform a near-horizon expansion $\epsilon \to 0$. With the entropy density defined above, this becomes

$$Ts \approx \frac{1}{32\pi m} + \mathcal{O}(\epsilon) \quad \to \quad T \approx \frac{1}{8\pi m} \tag{7.42}$$

which is just the usual Hawking temperature of the Schwarzschild black hole. This is not surprising because in this limit the normal acceleration, which is equal to the surface gravity κ, dominates over the expansion. In the null limit the temperature becomes exactly $T = 1/8\pi m$. This limit coincides with the membrane paradigm, where a near horizon expansion is assumed, while our formulation does not require the screen to be close to the black hole. As the screen is pulled back from the horizon, the temperature defined above receives corrections due to θ_{t^*} becoming non-negligible. It remains an open question as to what meaning to assign to the fluid temperature. Away from the horizon it is not simply equal to the redshifted Hawking temperature, though it is comforting that our formalism can incorporate well-known results from the special case of a horizon-like screen.

7.4 Summary

In this chapter, we have given some explicit examples of screen constructions, focusing on spherically symmetric and static examples. We have shown that for such cases, a perfect fluid resides on the boundary Σ, whose equation of state is sensitive to the background geometry. We have also shown that time-dependent screen evolution generically leads to time-dependent equations of state, leaving the analysis of these situations for future work. Though the interpretation of the Minkowski space screen is difficult, in a Schwarzschild background things become more clear. We are able to consistently derive the equation of state, temperature, and entropy of the screen fluid, noting that since we are working at the purely classical level T and S can only be determined up to a constant. One approach to arrive at an explicit result for these quantities is to take the limit as the screen approaches a surface whose entropy is known. We show this in the case of the event horizon, where the fact that we should obtain $S = A/4G\hbar$ in the limit where the screen approaches the horizon can be used to fix the normalization and determine the fluid temperature, which is found to be the Hawking temperature.

We remark again on the fact that T and S are unspecified in the dictionary (6.68). Though not surprising, this means that determining the entropy and temperature of the screen fluid requires additional input. We appealed to the Euler relation to do so, noting

[3]Note that in the null limit we must have that $\mu \to 0$ otherwise the temperature will receive a (constant) correction $+\mu n$.

that the inclusion of the chemical potential term μn was essential if one demands 'reasonable' fluid properties. Of course, the screen fluid can never fully resemble a traditional fluid; at the very least the energy density is negative owing to the attractive nature of the gravitational interaction. This does not, however, prevent us from using the tools of relativistic hydrodynamics to examine the properties of such a fluid. One apparent subtlety in our application of the Euler relation is important to mention. Recall that it was derived not from the extensivity of S, V, N, but rather the assumption that the internal energy is a homogeneous function of degree one in these variables. There are examples where this is not the case, leaving the possibility of different constructions for T and S. This was the case in Chapter 2, where a black hole in a finite radius cavity was shown to satisfy $e + p = 2\,Ts$ instead, so the energy is a homogeneous function of degree one-half in S. To avoid potential ambiguities in the choice of Euler relation, one can instead appeal to the experience of local screen observers to assign a temperature to the fluid. For example, the motion of fluid observers on the fixed-radius Schwarzschild screen is not geodesic. Near the horizon, they appear to be locally Rinder observers, and in a semi-classical setting can be expected to experience a temperature $T = a/2\pi$ where $a \sim \kappa$. This is also true of the accelerating screen observers, and can perhaps be used as a guide for assigning a temperature to the screen fluid without any assumptions about the Euler relation. We leave this interesting possibility for future exploration.

This concludes our construction and first application of the relativistic gravitational screen formalism. Though we have highlighted many open questions concerning its interpretation and technical construction, we hope to have also demonstrated the potential of the framework in answering fundamental questions about the holographic nature of gravity. We hope to eventually devise, in a consistent way, quasi-local notions of the entropy and energy of arbitrary gravitational systems, and most of all, provide an avenue for understanding geometric phenomena through a completely different lens.

Epilogue

What have we learned?

In Part I of this thesis, we investigated the thermodynamics and phase structure of a number of asymptotically de Sitter black hole solutions. In Chapter 1 we found that in the Einstein-Maxwell case, uncharged black holes exhibit first-order HP transitions with a locally stable supercooled region. Charged black holes showed pressure-dependent compact small-large phase transitions indicated by a 'swallowtube' in $F-T-P$ space, whose coexistence line terminated in the $P-T$ plane at two second-order critical points. This swallowtube is a feature unique to de Sitter, and arises from the presence of the cosmological horizon rather than the cavity. In Chapter 3, we showed that Born-Infeld black holes exhibit this same swallowtube structure, though when the BI parameter b is small, each constant-P slice contains a reentrant (small-large-small) phase transition. We also demonstrated the first example of a radiation-black hole-radiation transition in the grand canonical ensemble. In Chapter 4, we examined Schwarzschild-de Sitter black holes with a conformally coupled scalar field. We found that HP transitions occur generically, though the scalar field introduces a cosmic censorship bound which places restrictions on the choice of cavity location. Finally, in Chapter 5 we investigated Gauss-Bonnet-de Sitter black holes in $D \geq 5$, where we found small-large transitions with a minimum temperature when the GB coupling is positive.

In all cases we derived the various thermodynamic potentials that entered into the appropriate generalizations of the first law, and verified that the Smarr relation can be suitably extended. We also showed that the analogy between HP transitions and liquid-gas van der Waals transitions are not as universal as once believed. Though ubiquitous in AdS spacetimes, they appear to be absent in de Sitter, at least when a cavity is used as the equilibrating mechanism. This is despite the fact that on the surface, the cavity appears to play the same role as the asymptotic structure of AdS. The presence of the cavity necessarily modifies the equation of state in a non-trivial way, such that the oscillations in the $P-V$ plane characteristic of the liquid-gas transition do not appear. More work should be done to understand fully whether such transitions are possible. At the very least, we have shown yet another example in which AdS is a truly unique space.

In Part II, we generalized the gravitational screen formalism by promoting the fluid side to the relativistic, dissipative regime, and incorporated the twist ϵ_{ab} on the gravity side. We constructed the dictionary, relating in a consistent way the geometric and hydrodynamic variables, and discussed the interpretation of the map. We showed how entropy production is linked to gravitational wave generation, and provided an avenue for exploring higher-order dissipative frameworks from a geometric point of view. We examined a number of examples of screens, finding the equation of state of the holographic fluid and determining its entropy and temperature. We found that in the limit as a screen approaches the horizon, we formally recover the membrane paradigm, and can deduce that the temperature of the black hole is approximately equal to the Hawking temperature, with corrections arising from the separation between screen and horizon. We also show that the screen entropy can be tied to the curvature of the exterior Schwarzschild geometry, though the question of how to normalize this quantity remains unanswered. Finally, we demonstrated the critical role the chemical potential plays in the holographic description.

From a broader perspective, I hope to have convinced the reader that the study of the thermodynamic aspects of gravity is worthwhile, interesting, and an essential part of our journey towards a deeper understanding of the fundamental nature of reality. There are three main lessons from the present work that I would like to emphasize.

The first is that in a thermodynamic context black holes possess an extremely rich and interesting phenomenology, especially in their phase structure where many analogies to everyday thermodynamic systems arise. That black holes display behaviour akin to the evaporation of water, supercooling of helium, quark deconfinement, and much more, speaks to the universality of the coarse graining procedure and the power of thermodynamics in physics. We have also seen that gravity in many contexts behaves no differently than these ordinary systems, despite the unique role the gravitational interaction takes on among the fundamental forces. In this work we have shown that despite many technical difficulties, these ideas and phenomena can indeed be extended to asymptotically de Sitter black holes, which display an equally varied and interesting thermodynamic landscape.

The second is that there is much subtlety in even these equilibrium contexts, and one should always be mindful of the physical interpretation of their framework (where possible). My experience is that we are often too easily satisfied with the state of affairs once a notion of equilibrium is available for our system, where it is often thinly disguised behind the first law. In de Sitter, there are a number of ways to formally achieve equilibrium in the sense that one has something resembling the first law, but the interpretation of such a law takes on a dramatically different meaning in each context. Indeed, sometimes one doesn't really have equilibrium at all despite a first law appearing. Our cavity approach has a simple physical interpretation: the black hole is being placed in a reflecting box. One could even imagine some advanced civilization doing this in the laboratory. However, we have seen that in many cases this reflecting box has a profound impact on the phenomenology. Many situations where one might have guessed the thermodynamic behaviour would mirror the AdS case turned out to be strikingly different. The broader lesson here is that one should always be mindful of the assumptions that form the basis of the system at hand, and not be hasty in judging two situations to be similar based on surface-level features.

The third is that much can be learned by looking for connections and relations between disparate systems. Theoretical physics centers around constructing mathematical models to explain observed phenomena, and these models are at some level nothing more than a collection of labels with rules for their manipulation. Often times, when a simple relabelling relates two models describing completely different systems (as was the case in Chapter 7), it reveals profound and deep connections between those systems. This has proven to be the case many times over (in the relationship between supergravity and conformal field theory [4], between asymptotic symmetries and the gravitational memory effect [220], etc.) often revealing an underlying unifying theory which explains both facets, as was the case with electromagnetism. It is not surprising then that the greatest ideas and inspirations often emerge at the intersection of different fields, and we should always strive to integrate the vast pools of knowledge available from others into our own endeavours.

Where do we go?

Though I have touched on many unresolved questions both conceptual and technical throughout this work, there are three avenues of exploration that I would like to highlight as being especially interesting and relevant for future investigation.

Rotating Black Holes

Much of our motivation for studying de Sitter black hole thermodynamics, especially compared to the well-known AdS cases, comes from their astrophysical significance. Astrophysical black holes are almost certainly of the Kerr-de Sitter variety; as nearly all observable stars rotate [221], there is little reason to expect that a black hole would form with zero angular momentum (at least, a vanishingly small probability of doing so). Clearly then, we should extend our analysis to these Kerr-de Sitter black holes, the likes of which have been studied extensively in asymptotically AdS space. Beyond the issues already present in de Sitter, Kerr black holes complicate matters further as there is no real Euclidean metric associated with a rotating black hole. One can consider complex metrics which yield a real thermodynamic action, but the interpretation of such constructions is not entirely clear [95]. The choice of cavity geometry is also more subtle. A natural choice may be a set of zero angular momentum observers (ZAMOs), such that the cavity is axisymmetric and rotating with the black hole. Such observers however do not rotate at the same angular velocity as would be required for a heat bath to be in equilibrium with a Kerr black hole. Exploring these questions will be an important step towards elevating our understanding of thermodynamics in de Sitter space to the same degree that anti-de Sitter space enjoys.

The Dual Description

As we have mentioned, there has been significant interest in the phase structure of AdS black holes owing to their dual interpretation in AdS/CFT, though we stress that the implication these exotic bulk transitions have for their corresponding boundary CFTs is not often explored, and should be. Can we hope to learn something about strongly coupled systems from de Sitter thermodynamics? There has been some work towards realizing a dS/CFT correspondence in analogy with the well-known AdS/CFT examples [39], however the situation is significantly more complicated for de Sitter. This stems from the serious problems one faces when attempting to construct a stable de Sitter vacuum in string theory, about which a number of no-go theorems have been formulated [222, 223]. The issues arise from the fundamental role that boundary correlators play in string theory; in AdS the natural boundary is timelike, while in de Sitter the spatial sections are compact. Still, there is at least one example of such a correspondence between bulk dS_3 and a CFT on the S^2 at null infinity [39], though the precise form of the bulk theory is not known. In any case, it is natural to ask what interpretation these Hawking-Page-like phase transitions have in the context of dS/CFT, if they can at all be realized there (our cavity is at a finite radius after all). This connection certainly warrants more exploration given the wealth of insights we have gained from studying the AdS case.

Unifying Frameworks

The gravitational screen formalism, being quite general in its construction, should be able to realize many interesting limits. We have already shown (though not in explicit detail) how one can recover the results of the membrane paradigm by taking the limit as the gravitational screen approaches the event horizon of the black hole. Already in the membrane paradigm, the first law of thermodynamics as discussed in Part I is manifest, so in this sense the screen formalism can rather trivially recover known results from black hole thermodynamics. In principle, we should be able to consider an appropriate limit where the screen tends towards the boundary of some asymptotically anti-de Sitter space, and in so doing recover the fluid/gravity correspondence as well. It will also be interesting to examine how the screen construction relates to the cavity approach we pursued in Part I, having a similar 'boundary thermodynamics' flavour. The explicit demonstration of these various limits would serve to unify these opposing views on gravitational thermodynamics into one coherent framework, something we hope to eventually achieve.

Non-equilibrium Systems

The study of black hole thermodynamics rests firmly in the realm of *equilibrium* thermodynamics. We operated at all times under the assumption that the timescales involved (evaporation for example) are large compared to the typical equilibration timescale of the system, assumed all evolution was quasi-stationary, and ignored entirely any backreactions that might be present from Hawking radiation. Even in our treatment of gravitational screens and their dual hydrodynamic interpretation, we focused mainly on static cases where a perfect fluid (equilibrium) description arises. This leaves open many questions (some of which we touched on in Chapter 7) about the nature of entropy production and viscous dissipation, which arise from distinctly non-equilibrium processes. It is clear, however, that eventually nonequilibrium processes must be considered if we are to uncover the statistical mechanical nature of gravitational entropy. Consider the example of Hawking radiation, where the result $T_H = (8\pi m)^{-1}$ is really just constraining the asymptotic form of the density matrix at $\mathcal{I}_+$. It says little of the dynamics of the radiative process, yet many of the apparent 'paradoxes' arise due to the equilibrium approximation, and are perhaps resolved by moving away from this regime [224]. In our screen formalism, we saw that there is an ambiguity in the splitting of the viscous and equilibrium parts of the pressure and energy, something which undoubtedly will require us to consider dynamic processes where these can hopefully be separated. The point is, only so much can be done at equilibrium.

Closing Remarks

Above all else, I hope to have conveyed that the subject of black hole and gravitational thermodynamics lies at the center of a dramatically interconnected web. Throughout my work in this area, I have experienced a regular amazement at the frequency with which concepts from different fields find application in unexpected areas. The most impactful ideas often result from a confluence of knowledge from across these areas, while ignoring (or lacking the ability to translate from) other fields has frequently stagnated progress. I hope that my work here contributes in some small way to our collective understanding of black holes and the gravitational interaction, and that I have perhaps added a strand or two to the web of theoretical physics.

Letters of Copyright Permission

American Physical Society
Reuse and Permissions License

26-May-2021

This license agreement between the American Physical Society ("APS") and Fil Simovic ("You") consists of your license details and the terms and conditions provided by the American Physical Society and SciPris.

Licensed Content Information

License Number:	**RNP/21/MAY/040405**
License date:	26-May-2021
DOI:	10.1103/PhysRevD.101.084051
Title:	Thermodynamics of Gauss--Bonnet--de Sitter black holes
Author:	Sumarna Haroon et al.
Publication:	Physical Review D
Publisher:	American Physical Society
Cost:	USD $ 0.00

Request Details

Does your reuse require significant modifications: No

Specify intended distribution locations:	Canada
Reuse Category:	Reuse in a thesis/dissertation
Requestor Type:	Author of requested content
Items for Reuse:	Whole Article
Format for Reuse:	Electronic

Information about New Publication:

University/Publisher:	University of Waterloo
Title of dissertation/thesis:	Gravitational Thermodynamics: From Black Holes to Holography
Author(s):	Fil Simovic
Expected completion date:	May. 2021

License Requestor Information

Name:	Fil Simovic
Affiliation:	Individual
Email Id:	fil.simovic@gmail.com
Country:	Canada

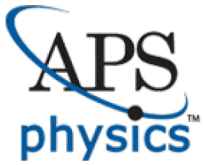

American Physical Society
Reuse and Permissions License

TERMS AND CONDITIONS

The American Physical Society (APS) is pleased to grant the Requestor of this license a non-exclusive, non-transferable permission, limited to Electronic format, provided all criteria outlined below are followed.

1. You must also obtain permission from at least one of the lead authors for each separate work, if you haven't done so already. The author's name and affiliation can be found on the first page of the published Article.
2. For electronic format permissions, Requestor agrees to provide a hyperlink from the reprinted APS material using the source material's DOI on the web page where the work appears. The hyperlink should use the standard DOI resolution URL, http://dx.doi.org/{DOI}. The hyperlink may be embedded in the copyright credit line.
3. For print format permissions, Requestor agrees to print the required copyright credit line on the first page where the material appears: "Reprinted (abstract/excerpt/figure) with permission from [(FULL REFERENCE CITATION) as follows: Author's Names, APS Journal Title, Volume Number, Page Number and Year of Publication.] Copyright (YEAR) by the American Physical Society."
4. Permission granted in this license is for a one-time use and does not include permission for any future editions, updates, databases, formats or other matters. Permission must be sought for any additional use.
5. Use of the material does not and must not imply any endorsement by APS.
6. APS does not imply, purport or intend to grant permission to reuse materials to which it does not hold copyright. It is the requestor's sole responsibility to ensure the licensed material is original to APS and does not contain the copyright of another entity, and that the copyright notice of the figure, photograph, cover or table does not indicate it was reprinted by APS with permission from another source.
7. The permission granted herein is personal to the Requestor for the use specified and is not transferable or assignable without express written permission of APS. This license may not be amended except in writing by APS.
8. You may not alter, edit or modify the material in any manner.
9. You may translate the materials only when translation rights have been granted.
10. APS is not responsible for any errors or omissions due to translation.
11. You may not use the material for promotional, sales, advertising or marketing purposes.
12. The foregoing license shall not take effect unless and until APS or its agent, Aptara, receives payment in full in accordance with Aptara Billing and Payment Terms and Conditions, which are incorporated herein by reference.
13. Should the terms of this license be violated at any time, APS or Aptara may revoke the license with no refund to you and seek relief to the fullest extent of the laws of the USA. Official written notice will be made using the contact information provided with the permission request. Failure to receive such notice will not nullify revocation of the permission.
14. APS reserves all rights not specifically granted herein.
15. This document, including the Aptara Billing and Payment Terms and Conditions, shall be the entire agreement between the parties relating to the subject matter hereof.

References

[1] S. W. Hawking, "Particle Creation by Black Holes," *Commun. Math. Phys.*, vol. 43, pp. 199–220, 1975.

[2] J. D. Bekenstein, "Black holes and entropy," *Phys. Rev.*, vol. D7, pp. 2333–2346, 1973.

[3] L. Susskind, "The World as a Hologram," *Journal of Mathematical Physics*, vol. 36, pp. 6377–6396, Nov. 1995. arXiv: hep-th/9409089.

[4] J. M. Maldacena, "The large N limit of superconformal field theories and supergravity," *Adv. Theor. Math. Phys.*, vol. 2, pp. 231–252, 1998.

[5] D. Harlow, "Jerusalem Lectures on Black Holes and Quantum Information," *Rev. Mod. Phys.*, vol. 88, p. 015002, Feb. 2016. arXiv: 1409.1231.

[6] S. Sachdev, "Condensed matter and AdS/CFT," *arXiv:1002.2947 [cond-mat, physics:hep-th]*, vol. 828, pp. 273–311, 2011. arXiv: 1002.2947.

[7] S. Carlip, "Black Hole Entropy and the Problem of Universality," *J. Phys.: Conf. Ser.*, vol. 67, p. 012022, May 2007. arXiv: gr-qc/0702094.

[8] W. G. Unruh, "Notes on black-hole evaporation," *Phys. Rev. D*, vol. 14, pp. 870–892, 1976.

[9] S. W. Hawking, "Particle creation by black holes," *Commun.Math. Phys.*, vol. 43, pp. 199–220, Aug. 1975.

[10] A. Strominger and A. Zhiboedov, "Gravitational memory, BMS supertranslations and soft theorems," *J. High Energ. Phys.*, vol. 2016, p. 86, Jan. 2016.

[11] J. Bardeen, B. Carter, and S. Hawking, "The Four laws of black hole mechanics," *Commun.Math.Phys.*, vol. 31, pp. 161–170, 1973.

[12] S. W. Hawking and D. N. Page, "Thermodynamics of Black Holes in anti-De Sitter Space," *Commun. Math. Phys.*, vol. 87, p. 577, 1983.

[13] A. Belhaj, M. Chabab, H. El Moumni, and M. Sedra, "On Thermodynamics of AdS Black Holes in Arbitrary Dimensions," *Chin.Phys.Lett.*, vol. 29, p. 100401, 2012.

[14] G. Gibbons, M. Perry, and C. Pope, "The First law of thermodynamics for Kerr-anti-de Sitter black holes," *Class.Quant.Grav.*, vol. 22, pp. 1503–1526, 2005.

[15] R. A. Hennigar, E. Tjoa, and R. B. Mann, "Thermodynamics of hairy black holes in Lovelock gravity," *JHEP*, vol. 02, p. 070, 2017.

[16] A. M. Frassino, D. Kubiznak, R. B. Mann, and F. Simovic, "Multiple Reentrant Phase Transitions and Triple Points in Lovelock Thermodynamics," *JHEP*, vol. 09, p. 080, 2014.

[17] E. Witten, "Anti-de Sitter space, thermal phase transition, and confinement in gauge theories," *Adv. Theor. Math. Phys.*, vol. 2, pp. 505–532, 1998.

[18] D. Harlow, "Jerusalem Lectures on Black Holes and Quantum Information," *Rev. Mod. Phys.*, vol. 88, p. 015002, Feb. 2016. arXiv: 1409.1231.

[19] J. L. Cardy, "Effect of boundary conditions on the operator content of two-dimensional conformally invariant theories," *Nuclear Physics B*, vol. 275, pp. 200–218, Oct. 1986.

[20] H. W. J. Blöte, J. L. Cardy, and M. P. Nightingale, "Conformal invariance, the central charge, and universal finite-size amplitudes at criticality," *Phys. Rev. Lett.*, vol. 56, pp. 742–745, Feb. 1986.

[21] H. E. Camblong and C. R. Ordonez, "Black Hole Thermodynamics from Near-Horizon Conformal Quantum Mechanics," *Phys. Rev. D*, vol. 71, p. 104029, May 2005. arXiv: hep-th/0411008.

[22] D. Kastor, S. Ray, and J. Traschen, "Enthalpy and the Mechanics of AdS Black Holes," *Class.Quant.Grav.*, vol. 26, p. 195011, 2009.

[23] M. Cvetic, G. Gibbons, D. Kubiznak, and C. Pope, "Black Hole Enthalpy and an Entropy Inequality for the Thermodynamic Volume," *Phys.Rev.*, vol. D84, p. 024037, 2011.

[24] C. V. Johnson, "Holographic Heat Engines," *Class.Quant.Grav.*, vol. 31, p. 205002, 2014.

[25] M. Appels, R. Gregory, and D. Kubiznak, "Thermodynamics of Accelerating Black Holes," *Phys. Rev. Lett.*, vol. 117, no. 13, p. 131303, 2016.

[26] A. B. Bordo, F. Gray, R. A. Hennigar, and D. Kubizňák, "Misner Gravitational Charges and Variable String Strengths," *Class. Quant. Grav.*, vol. 36, no. 19, p. 194001, 2019.

[27] S. Andrews, R. A. Hennigar, and H. K. Kunduri, "Chemistry and Complexity for Solitons in AdS," 2019.

[28] A. Karch and B. Robinson, "Holographic Black Hole Chemistry," *JHEP*, vol. 12, p. 073, 2015.

[29] J. Couch, W. Fischler, and P. H. Nguyen, "Noether charge, black hole volume and complexity," 2016.

[30] M. Sinamuli and R. B. Mann, "Higher Order Corrections to Holographic Black Hole Chemistry," *Phys. Rev.*, vol. D96, no. 8, p. 086008, 2017.

[31] D. Kubiznak and R. B. Mann, "P-V criticality of charged AdS black holes," *JHEP*, vol. 1207, p. 033, 2012.

[32] N. Altamirano, D. Kubiznak, and R. B. Mann, "Reentrant phase transitions in rotating anti–de Sitter black holes," *Phys. Rev.*, vol. D88, no. 10, p. 101502, 2013.

[33] R. A. Hennigar, R. B. Mann, and E. Tjoa, "Superfluid Black Holes," *Phys. Rev. Lett.*, vol. 118, no. 2, p. 021301, 2017.

[34] D. Kubiznak and F. Simovic, "Thermodynamics of horizons: de Sitter black holes and reentrant phase transitions," *Class. Quant. Grav.*, vol. 33, no. 24, p. 245001, 2016.

[35] B. P. Dolan, D. Kastor, D. Kubiznak, R. B. Mann, and J. Traschen, "Thermodynamic Volumes and Isoperimetric Inequalities for de Sitter Black Holes," *Phys.Rev.*, vol. D87, p. 104017, 2013.

[36] S. Perlmutter, G. Aldering, G. Goldhaber, R. A. Knop, P. Nugent, P. G. Castro, S. Deustua, S. Fabbro, A. Goobar, D. E. Groom, I. M. Hook, A. G. Kim, M. Y. Kim, J. C. Lee, N. J. Nunes, R. Pain, C. R. Pennypacker, R. Quimby, C. Lidman, R. S. Ellis, M. Irwin, R. G. McMahon, P. Ruiz-Lapuente, N. Walton, B. Schaefer, B. J. Boyle, A. V. Filippenko, T. Matheson, A. S. Fruchter, N. Panagia, H. J. M. Newberg, and W. J. Couch, "Measurements of Omega and Lambda from 42 High-Redshift Supernovae," *ApJ*, vol. 517, pp. 565–586, June 1999. arXiv: astro-ph/9812133.

[37] W. J. Percival, B. A. Reid, D. J. Eisenstein, N. A. Bahcall, T. Budavari, J. A. Frieman, M. Fukugita, J. E. Gunn, Z. Ivezic, G. R. Knapp, R. G. Kron, J. Loveday, R. H. Lupton, T. A. McKay, A. Meiksin, R. C. Nichol, A. C. Pope, D. J. Schlegel, D. P. Schneider, D. N. Spergel, C. Stoughton, M. A. Strauss, A. S. Szalay, M. Tegmark, M. S. Vogeley, D. H. Weinberg, D. G. York, and I. Zehavi, "Baryon Acoustic Oscillations in the Sloan Digital Sky Survey Data Release 7 Galaxy Sample," *Monthly Notices of the Royal Astronomical Society*, vol. 401, pp. 2148–2168, Feb. 2010. arXiv: 0907.1660.

[38] P. Collaboration, N. Aghanim, Y. Akrami, M. Ashdown, J. Aumont, C. Baccigalupi, M. Ballardini, A. J. Banday, R. B. Barreiro, N. Bartolo, S. Basak, R. Battye, K. Benabed, J.-P. Bernard, M. Bersanelli, P. Bielewicz, J. J. Bock, J. R. Bond, J. Borrill, F. R. Bouchet, F. Boulanger, M. Bucher, C. Burigana, R. C. Butler, E. Calabrese, J.-F. Cardoso, J. Carron, A. Challinor, H. C. Chiang, J. Chluba, L. P. L. Colombo, C. Combet, D. Contreras, B. P. Crill, F. Cuttaia, P. de Bernardis, G. de Zotti, J. Delabrouille, J.-M. Delouis, E. Di Valentino, J. M. Diego, O. Doré, M. Douspis, A. Ducout, X. Dupac, S. Dusini, G. Efstathiou, F. Elsner, T. A. Enßlin, H. K.

Eriksen, Y. Fantaye, M. Farhang, J. Fergusson, R. Fernandez-Cobos, F. Finelli, F. Forastieri, M. Frailis, A. A. Fraisse, E. Franceschi, A. Frolov, S. Galeotta, S. Galli, K. Ganga, R. T. Génova-Santos, M. Gerbino, T. Ghosh, J. González-Nuevo, K. M. Górski, S. Gratton, A. Gruppuso, J. E. Gudmundsson, J. Hamann, W. Handley, F. K. Hansen, D. Herranz, S. R. Hildebrandt, E. Hivon, Z. Huang, A. H. Jaffe, W. C. Jones, A. Karakci, E. Keihänen, R. Keskitalo, K. Kiiveri, J. Kim, T. S. Kisner, L. Knox, N. Krachmalnicoff, M. Kunz, H. Kurki-Suonio, G. Lagache, J.-M. Lamarre, A. Lasenby, M. Lattanzi, C. R. Lawrence, M. L. Jeune, P. Lemos, J. Lesgourgues, F. Levrier, A. Lewis, M. Liguori, P. B. Lilje, M. Lilley, V. Lindholm, M. López-Caniego, P. M. Lubin, Y.-Z. Ma, J. F. Macías-Pérez, G. Maggio, D. Maino, N. Mandolesi, A. Mangilli, A. Marcos-Caballero, M. Maris, P. G. Martin, M. Martinelli, E. Martínez-González, S. Matarrese, N. Mauri, J. D. McEwen, P. R. Meinhold, A. Melchiorri, A. Mennella, M. Migliaccio, M. Millea, S. Mitra, M.-A. Miville-Deschênes, D. Molinari, L. Montier, G. Morgante, A. Moss, P. Natoli, H. U. Nørgaard-Nielsen, L. Pagano, D. Paoletti, B. Partridge, G. Patanchon, H. V. Peiris, F. Perrotta, V. Pettorino, F. Piacentini, L. Polastri, G. Polenta, J.-L. Puget, J. P. Rachen, M. Reinecke, M. Remazeilles, A. Renzi, G. Rocha, C. Rosset, G. Roudier, J. A. Rubiño-Martín, B. Ruiz-Granados, L. Salvati, M. Sandri, M. Savelainen, D. Scott, E. P. S. Shellard, C. Sirignano, G. Sirri, L. D. Spencer, R. Sunyaev, A.-S. Suur-Uski, J. A. Tauber, D. Tavagnacco, M. Tenti, L. Toffolatti, M. Tomasi, T. Trombetti, L. Valenziano, J. Valiviita, B. Van Tent, L. Vibert, P. Vielva, F. Villa, N. Vittorio, B. D. Wandelt, I. K. Wehus, M. White, S. D. M. White, A. Zacchei, and A. Zonca, "Planck 2018 results. VI. Cosmological parameters," *arXiv:1807.06209 [astro-ph]*, Sept. 2019. arXiv: 1807.06209.

[39] A. Strominger, "The dS / CFT correspondence," *JHEP*, vol. 10, p. 034, 2001.

[40] R. Bousso, "The holographic principle," *Rev. Mod. Phys.*, vol. 74, pp. 825–874, Aug. 2002.

[41] V. Balasubramanian, J. de Boer, and D. Minic, "Mass, entropy, and holography in asymptotically de Sitter spaces," *Phys. Rev. D*, vol. 65, p. 123508, June 2002.

[42] D. Anninos, G. S. Ng, and A. Strominger, "Asymptotic symmetries and charges in de Sitter space," *Class. Quantum Grav.*, vol. 28, p. 175019, Sept. 2011.

[43] E. Mottola, "Particle creation in de Sitter space," *Phys. Rev. D*, vol. 31, pp. 754–766, Feb. 1985.

[44] B. Allen, "Vacuum states in de Sitter space," *Phys. Rev. D*, vol. 32, pp. 3136–3149, Dec. 1985.

[45] N. Goheer, M. Kleban, and L. Susskind, "The Trouble with de Sitter Space," *J. High Energy Phys.*, vol. 2003, pp. 056–056, July 2003. arXiv: hep-th/0212209.

[46] A. Ashtekar, B. Bonga, and A. Kesavan, "Asymptotics with a positive cosmological constant. II. Linear fields on de Sitter spacetime," *Phys. Rev. D*, vol. 92, p. 044011, Aug. 2015.

[47] M. Urano, A. Tomimatsu, and H. Saida, "Mechanical First Law of Black Hole Spacetimes with Cosmological Constant and Its Application to Schwarzschild-de Sitter Spacetime," *Class.Quant.Grav.*, vol. 26, p. 105010, 2009.

[48] Zhang Li-Chun, L. Huai-Fan, and Z. Ren, "Thermodynamics of the Schwarzchild-de Sitter black hole," *Acta Physica Sinica*, vol. 59, no. 12, 2010.

[49] S. Mbarek and R. B. Mann, "Reverse Hawking-Page Phase Transition in de Sitter Black Holes," *JHEP*, vol. 02, p. 103, 2019.

[50] G. W. Gibbons and S. W. Hawking, "Action Integrals and Partition Functions in Quantum Gravity," *Phys. Rev.*, vol. D15, pp. 2752–2756, 1977.

[51] J. W. York, Jr., "Black hole thermodynamics and the Euclidean Einstein action," *Phys. Rev.*, vol. D33, pp. 2092–2099, 1986.

[52] H. W. Braden, J. D. Brown, B. F. Whiting, and J. W. York, Jr., "Charged black hole in a grand canonical ensemble," *Phys. Rev.*, vol. D42, pp. 3376–3385, 1990.

[53] S. Carlip and S. Vaidya, "Phase transitions and critical behavior for charged black holes," *Class. Quant. Grav.*, vol. 20, pp. 3827–3838, 2003.

[54] R. A. Hennigar, D. Kubizňák, R. B. Mann, and C. Pollack, "On taking the D 4 limit of Gauss-Bonnet gravity: theory and solutions," *J. High Energ. Phys.*, vol. 2020, p. 27, July 2020.

[55] B. F. Schutz, *Geometrical Methods of Mathematical Physics*. Cambridge University Press, 1 ed., Jan. 1980.

[56] R. M. Wald, *General Relativity*. Chicago and London: The University of Chicago Press, 1984.

[57] S. Weinberg, *Gravitation and Cosmology*. New York: John Wiley and Sons, 1972.

[58] S. M. Carroll, *Spacetime and geometry: An introduction to general relativity*. 2004.

[59] E. Poisson, *A Relativist's Toolkit: The Mathematics of Black-Hole Mechanics*. Cambridge: Cambridge University Press, 2004.

[60] V. P. Frolov and I. D. Novikov, *Black hole physics: basic concepts and new developments*. No. v. 96 in Fundamental theories of physics, Dordrecht ; Boston: Kluwer, 1998.

[61] C. M. Will, *Theory and experiment in gravitational physics*. Cambridge [England] ; New York, NY, USA: Cambridge University Press, rev. ed ed., 1993.

[62] E. Poisson and C. M. Will, *Gravity: Newtonian, post-Newtonian, relativistic*. Cambridge ; New York: Cambridge University Press, 2014.

[63] G. Goldhaber, "The Acceleration of the Expansion of the Universe: A Brief Early History of the Supernova Cosmology Project (SCP)," *AIP Conference Proceedings*, pp. 53–72, 2009. arXiv: 0907.3526.

[64] P. M. Garnavich, R. P. Kirshner, P. Challis, J. Tonry, R. L. Gilliland, R. C. Smith, A. Clocchiatti, A. Diercks, A. V. Filippenko, M. Hamuy, C. J. Hogan, B. Leibundgut, M. M. Phillips, D. Reiss, A. G. Riess, B. P. Schmidt, J. Spyromilio, C. Stubbs, N. B. Suntzeff, and L. Wells, "Constraints on Cosmological Models from Hubble Space Telescope Observations of High-z Supernovae," *arXiv:astro-ph/9710123*, Oct. 1997. arXiv: astro-ph/9710123.

[65] D. N. Spergel, R. Bean, O. Dore, M. R. Nolta, C. L. Bennett, J. Dunkley, G. Hinshaw, N. Jarosik, E. Komatsu, L. Page, H. V. Peiris, L. Verde, M. Halpern, R. S. Hill, A. Kogut, M. Limon, S. S. Meyer, N. Odegard, G. S. Tucker, J. L. Weiland, E. Wollack, and E. L. Wright, "Three-Year *Wilkinson Microwave Anisotropy Probe* (*WMAP*) Observations: Implications for Cosmology," *ASTROPHYS J SUPPL S*, vol. 170, pp. 377–408, June 2007.

[66] A. Blanchard, M. Douspis, M. Rowan-Robinson, and S. Sarkar, "Large-scale galaxy correlations as a test for dark energy," *A&A*, vol. 449, pp. 925–928, Apr. 2006.

[67] J. Frieman, M. Turner, and D. Huterer, "Dark Energy and the Accelerating Universe," *Annu. Rev. Astron. Astrophys.*, vol. 46, pp. 385–432, Sept. 2008. arXiv: 0803.0982.

[68] S. W. Hawking, "Quantum gravity and path integrals," *Phys. Rev. D*, vol. 18, pp. 1747–1753, Sept. 1978.

[69] H. W. Hamber, *Quantum gravitation: the Feynman path integral approach*. Berlin: Springer, 2009. OCLC: ocn248994165.

[70] G. W. Gibbons and S. W. Hawking, "Action integrals and partition functions in quantum gravity," *Phys. Rev. D*, vol. 15, pp. 2752–2756, May 1977.

[71] S. W. Hawking, "Gravitational Radiation from Colliding Black Holes," *Phys. Rev. Lett.*, vol. 26, pp. 1344–1346, May 1971.

[72] J. D. Bekenstein, "Generalized second law of thermodynamics in black hole physics," *Phys. Rev.*, vol. D9, pp. 3292–3300, 1974.

[73] T. Jacobson, G. Kang, and R. C. Myers, "On Black Hole Entropy," *Phys. Rev. D*, vol. 49, pp. 6587–6598, June 1994. arXiv: gr-qc/9312023.

[74] D. Youm, "Black Holes and Solitons in String Theory," *Physics Reports*, vol. 316, pp. 1–232, Aug. 1999. arXiv: hep-th/9710046.

[75] A. Ashtekar, J. Baez, A. Corichi, and K. Krasnov, "Quantum Geometry and Black Hole Entropy," *Phys. Rev. Lett.*, vol. 80, pp. 904–907, Feb. 1998.

[76] S. Carlip, "Black Hole Entropy from Horizon Conformal Field Theory," *Nuclear Physics B - Proceedings Supplements*, vol. 88, pp. 10–16, June 2000. arXiv: gr-qc/9912118.

[77] S. N. Solodukhin, "Entanglement Entropy of Black Holes," *Living Rev. Relativ.*, vol. 14, p. 8, Dec. 2011.

[78] E. Bianchi, "Black hole entropy from graviton entanglement," *arXiv:1211.0522 [physics:hep-th]*, Jan. 2013. arXiv: 1211.0522.

[79] V. Iyer and R. M. Wald, "Some Properties of Noether Charge and a Proposal for Dynamical Black Hole Entropy," *Physical Review D*, vol. 50, pp. 846–864, July 1994. arXiv: gr-qc/9403028.

[80] J. Polchinski, "The Black Hole Information Problem," *New Frontiers in Fields and Strings*, pp. 353–397, Jan. 2017. arXiv: 1609.04036.

[81] G. W. Gibbons and S. W. Hawking, "Cosmological event horizons, thermodynamics, and particle creation," *Phys. Rev. D*, vol. 15, pp. 2738–2751, 1977.

[82] D. N. Page, "Average entropy of a subsystem," *Phys. Rev. Lett.*, vol. 71, pp. 1291–1294, Aug. 1993.

[83] R. A. Janik, "AdS/CFT and applications," *arXiv:1311.3966 [gr-qc, physics:hep-ph, physics:hep-th, physics:nucl-th]*, Nov. 2013. arXiv: 1311.3966.

[84] C. Teitelboim, "The cosmological constant as a thermodynamic black hole parameter," *Physics Letters B*, vol. 158, pp. 293–297, Aug. 1985.

[85] J. D. Brown, J. Creighton, and R. B. Mann, "Temperature, Energy, and Heat Capacity of Asymptotically Anti-De Sitter Black Holes," *Phys. Rev. D*, vol. 50, pp. 6394–6403, Nov. 1994. arXiv: gr-qc/9405007.

[86] M. M. Caldarelli, G. Cognola, and D. Klemm, "Thermodynamics of Kerr-Newman-AdS Black Holes and Conformal Field Theories," *Class. Quantum Grav.*, vol. 17, pp. 399–420, Jan. 2000. arXiv: hep-th/9908022.

[87] W. Shuang, W. Shuang-Qing, X. Fei, and D. Lin, "The first laws of thermodynamics of the (2+1)-dimensional BTZ black holes and Kerr-de Sitter spacetimes," *arXiv:hep-th/0601147*, Feb. 2006. arXiv: hep-th/0601147.

[88] N. Altamirano, D. Kubiznak, R. B. Mann, and Z. Sherkatghanad, "Kerr-AdS analogue of triple point and solid/liquid/gas phase transition," *Class. Quant. Grav.*, vol. 31, p. 042001, 2014.

[89] W.-Y. Wen, "Note on deconfinement temperature with chemical potential from AdS/CFT," *arXiv:0707.4116 [hep-th]*, Aug. 2007. arXiv: 0707.4116.

[90] D. Kubiznak and R. B. Mann, "Black Hole Chemistry," 2014.

[91] D. Kubiznak, R. B. Mann, and M. Teo, "Black hole chemistry: thermodynamics with Lambda," *Class. Quant. Grav.*, vol. 34, no. 6, p. 063001, 2017.

[92] J. Dinsmore, P. Draper, D. Kastor, Y. Qiu, and J. Traschen, "Schottky Anomaly of deSitter Black Holes," 2019.

[93] C. V. Johnson, "de Sitter Black Holes, Schottky Peaks, and Continuous Heat Engines," 2019.

[94] G. W. Gibbons and S. Hawking, eds., *Euclidean quantum gravity.* Singapore ; River Edge, NJ: World Scientific, 1993.

[95] J. D. Brown, E. A. Martinez, and J. W. York, "Complex Kerr-Newman geometry and black-hole thermodynamics," *Phys. Rev. Lett.*, vol. 66, pp. 2281–2284, May 1991.

[96] M. K. Parikh, "New Coordinates for de Sitter Space and de Sitter Radiation," *Physics Letters B*, vol. 546, pp. 189–195, Oct. 2002. arXiv: hep-th/0204107.

[97] L. Smarr, "Mass Formula for Kerr Black Holes," *Phys. Rev. Lett.*, vol. 30, pp. 71–73, Jan. 1973.

[98] A. Bravetti, C. Gruber, C. S. Lopez-Monsalvo, and F. Nettel, "The zeroth law in quasi-homogeneous thermodynamics and black holes," *arXiv:1702.03360 [cond-mat, physics:gr-qc, physics:hep-th]*, Jan. 2018. arXiv: 1702.03360.

[99] M. Born and L. Infeld, "Foundations of the New Field Theory," *Proc. Roy. Soc.*, vol. A144, p. 425, 1934.

[100] G. Boillat, "Nonlinear Electrodynamics: Lagrangians and Equations of Motion," *Journal of Mathematical Physics*, vol. 11, pp. 941–951, Mar. 1970.

[101] C. A. M. de Melo, L. G. Medeiros, and P. J. Pompeia, "Causal structure and birefringence in nonlinear electrodynamics," *Mod. Phys. Lett. A*, vol. 30, p. 1550025, Feb. 2015.

[102] E. Fradkin and A. Tseytlin, "Non-linear electrodynamics from quantized strings," *Physics Letters B*, vol. 163, pp. 123–130, Nov. 1985.

[103] A. A. Tseytlin, "Born-Infeld action, supersymmetry and string theory," *arXiv:hep-th/9908105*, pp. 417–452, July 2000. arXiv: hep-th/9908105.

[104] J. Callan and J. M. Maldacena, "Brane Dynamics From the Born-Infeld Action," *Nuclear Physics B*, vol. 513, pp. 198–212, Mar. 1998. arXiv: hep-th/9708147.

[105] G. W. Gibbons and C. A. R. Herdeiro, "The Melvin universe in Born-Infeld theory and other theories of non-linear electrodynamics," *Class. Quantum Grav.*, vol. 18, pp. 1677–1690, 2001.

[106] P. N. Akmansoy and L. G. Medeiros, "Constraining Born-Infeld-like Nonlinear Electrodynamics Using Hydrogen's Ionization Energy," *arXiv:1712.05486 [hep-ph, physics:hep-th]*, Dec. 2017. arXiv: 1712.05486.

[107] J. Ellis, N. E. Mavromatos, and T. You, "Light-by-Light Scattering Constraint on Born-Infeld Theory," *Phys. Rev. Lett.*, vol. 118, p. 261802, June 2017.

[108] S. Gunasekaran, R. B. Mann, and D. Kubiznak, "Extended phase space thermodynamics for charged and rotating black holes and Born-Infeld vacuum polarization," *JHEP*, vol. 1211, p. 110, 2012.

[109] P. G. Ferreira and M. Joyce, "Cosmology with a Primordial Scaling Field," *Phys. Rev. D*, vol. 58, p. 023503, June 1998. arXiv: astro-ph/9711102.

[110] S. Tsujikawa, "Introductory review of cosmic inflation," *arXiv:hep-ph/0304257*, Apr. 2003. arXiv: hep-ph/0304257.

[111] S. L. Liebling and C. Palenzuela, "Dynamical Boson Stars," *Living Rev Relativ*, vol. 20, p. 5, Dec. 2017. arXiv: 1202.5809.

[112] A. S. Arapoğlu, K. Y. Ekşi, and A. E. Yükselci, "Neutron Star Structure in the Presence of Nonminimally Coupled Scalar Fields," *Phys. Rev. D*, vol. 99, p. 064055, Mar. 2019. arXiv: 1903.00391.

[113] J. D. Barrow, "Slow-roll inflation in scalar-tensor theories," *Phys. Rev. D*, vol. 51, pp. 2729–2732, Mar. 1995.

[114] J. A. Vázquez, L. E. Padilla, and T. Matos, "Inflationary Cosmology: From Theory to Observations," *Rev. Mex. Fis. E*, vol. 17, p. 73, Jan. 2020. arXiv: 1810.09934.

[115] N Bocharova, K Bronnikov, and V Melnikov, "The first MP-type solution with a conformal scalar field," *Moscow Univ. Phys. Bull.*, vol. 25, no. 80, 1970.

[116] J. D. Bekenstein, "Exact solutions of Einstein-conformal scalar equations," *Annals of Physics*, vol. 82, pp. 535–547, Feb. 1974.

[117] C. Martinez, R. Troncoso, and J. Zanelli, "de Sitter black hole with a conformally coupled scalar field in four dimensions," *Phys. Rev. D*, vol. 67, p. 024008, Jan. 2003. arXiv: hep-th/0205319.

[118] A. Achucarro, R. Gregory, and K. Kuijken, "Abelian Higgs Hair for Black Holes," *Phys. Rev. D*, vol. 52, pp. 5729–5742, Nov. 1995. arXiv: gr-qc/9505039.

[119] A. E. Mayo and J. D. Bekenstein, "No hair for spherical black holes: charged and nonminimally coupled scalar field with self–interaction," *Phys. Rev. D*, vol. 54, pp. 5059–5069, Oct. 1996. arXiv: gr-qc/9602057.

[120] C. A. R. Herdeiro and E. Radu, "Asymptotically flat black holes with scalar hair: a review," *arXiv:1504.08209 [astro-ph, physics:gr-qc, physics:hep-th]*, Dec. 2018. arXiv: 1504.08209.

[121] O. B. Zaslavskii, "Thermodynamics of black holes with an infinite effective area of a horizon," *Classical and Quantum Gravity*, vol. 19, pp. 3783–3797, July 2002. tex.publisher: IOP Publishing.

[122] E. Winstanley, "Classical and thermodynamical aspects of black holes with conformally coupled scalar field hair," *arXiv:gr-qc/0408046*, Aug. 2004. arXiv: gr-qc/0408046.

[123] E. Radu and E. Winstanley, "Conformally coupled scalar solitons and black holes with negative cosmological constant," *Phys. Rev. D*, vol. 72, p. 024017, July 2005. arXiv: gr-qc/0503095.

[124] I. Quiros, "Selected topics in scalar-tensor theories and beyond," *Int. J. Mod. Phys. D*, vol. 28, p. 1930012, May 2019. arXiv: 1901.08690.

[125] A. De Felice and S. Tsujikawa, "f(R) theories," *Living Rev. Relativ.*, vol. 13, p. 3, Dec. 2010. arXiv: 1002.4928.

[126] A. Anabalon and A. Cisterna, "Asymptotically (anti) de Sitter Black Holes and Wormholes with a Self Interacting Scalar Field in Four Dimensions," *Phys. Rev. D*, vol. 85, p. 084035, Apr. 2012. arXiv: 1201.2008.

[127] M. P. Hertzberg, "On Inflation with Non-minimal Coupling," *J. High Energ. Phys.*, vol. 2010, p. 23, Nov. 2010. arXiv: 1002.2995.

[128] O. Hrycyna and M. Szydlowski, "Cosmological dynamics with non-minimally coupled scalar field and a constant potential function," *J. Cosmol. Astropart. Phys.*, vol. 2015, pp. 013–013, Nov. 2015. arXiv: 1506.03429.

[129] L. H. Ford, "Gravitational particle creation and inflation," *Phys. Rev. D*, vol. 35, pp. 2955–2960, May 1987.

[130] J. D. Bekenstein, "Novel "no-scalar-hair" theorem for black holes," *Phys. Rev. D*, vol. 51, pp. R6608–R6611, June 1995.

[131] V. Faraoni, "Nonminimal coupling of the scalar field and inflation," *Phys. Rev. D*, vol. 53, pp. 6813–6821, June 1996.

[132] P. D. Prester, "Field redefinitions, Weyl invariance, and nature of mavericks," *Class. Quantum Grav.*, vol. 31, p. 155006, Aug. 2014. arXiv: 1405.1941.

[133] K. C. K. Chan, J. D. E. Creighton, and R. B. Mann, "Conserved masses in GHS Einstein and string black holes and consistent thermodynamics," *Phys. Rev. D*, vol. 54, pp. 3892–3899, Sept. 1996.

[134] J. Cruz, A. Fabbri, and J. Navarro-Salas, "Can conformal transformations change the fate of 2D black holes?," *Physics Letters B*, vol. 449, pp. 30–38, Mar. 1999.

[135] A. Anabalon and H. Maeda, "New Charged Black Holes with Conformal Scalar Hair," 2009.

[136] E. Dyer and K. Hinterbichler, "Boundary Terms, Variational Principles and Higher Derivative Modified Gravity," *Phys. Rev. D*, vol. 79, p. 024028, Jan. 2009. arXiv: 0809.4033.

[137] A.-M. Barlow, D. Doherty, and E. Winstanley, "Thermodynamics of de Sitter black holes with a conformally coupled scalar field," *Phys. Rev. D*, vol. 72, p. 024008, July 2005. arXiv: gr-qc/0504087.

[138] G. Gibbons, R. Kallosh, and B. Kol, "Moduli, Scalar Charges, and the First Law of Black Hole Thermodynamics," *Phys. Rev. Lett.*, vol. 77, pp. 4992–4995, Dec. 1996. arXiv: hep-th/9607108.

[139] K. Hajian and M. M. Sheikh-Jabbari, "Redundant and Physical Black Hole Parameters: Is there an independent physical dilaton charge?," *Physics Letters B*, vol. 768, pp. 228–234, May 2017. arXiv: 1612.09279.

[140] D. Astefanesei, R. Ballesteros, D. Choque, and R. Rojas, "Scalar charges and the first law of black hole thermodynamics," *Physics Letters B*, vol. 782, pp. 47–54, July 2018. arXiv: 1803.11317.

[141] L. J. Romans, "Supersymmetric, cold and lukewarm black holes in cosmological Einstein-Maxwell theory," *Nuclear Physics B*, vol. 383, pp. 395–415, Sept. 1992. arXiv: hep-th/9203018.

[142] R. B. Mann and S. F. Ross, "Cosmological production of charged black holes pairs," *Phys. Rev. D*, vol. 52, p. 2254, 1995.

[143] U. Le Verrier, "Lettre de M. Le Verrier à M. Faye sur la théorie de Mercure et sur le mouvement du périhélie de cette planète," *Comptes rendus hebdomadaires des séances de l'Académie des sciences*, vol. 49, pp. 379–383, 1859.

[144] D. M. Popper, "Red Shift in the Spectrum of 40 Eridani B.," *ApJ*, vol. 120, p. 316, Sept. 1954.

[145] R. V. Pound and G. A. Rebka, "Apparent Weight of Photons," *Phys. Rev. Lett.*, vol. 4, pp. 337–341, Apr. 1960.

[146] F. W. Dyson, A. S. Eddington, and C. Davidson, "A determination of the deflection of light by the sun's gravitational field, from observations made at the total eclipse of May 29, 1919," *Phil. Trans. R. Soc. Lond. A*, vol. 220, pp. 291–333, Jan. 1920.

[147] A. N. Whitehead, "The principle of relativity with applications to physical science," *Cambridge University Press*, 1922.

[148] l. Cartan, "Sur une généralisation de la notion de courbure de Riemann et les espaces à torsion," *Comptes Rendus Hebdomadaires des Séances de l'Académie des Sciences*, vol. 174, pp. 1104–1108, 1922.

[149] M. Fierz and W. Pauli, "On relativistic wave equations for particles of arbitrary spin in an electromagnetic field," *Proc. R. Soc. Lond. A*, vol. 173, pp. 211–232, Nov. 1939.

[150] K. Yagi and T. Tanaka, "Constraining alternative theories of gravity by gravitational waves from precessing eccentric compact binaries with LISA," *Phys. Rev. D*, vol. 81, p. 109902, May 2010. arXiv: 0906.4269.

[151] N. Yunes and X. Siemens, "Gravitational-Wave Tests of General Relativity with Ground-Based Detectors and Pulsar-Timing Arrays," *Living Rev. Relativ.*, vol. 16, p. 9, Dec. 2013.

[152] Y. Gong, E. Papantonopoulos, and Z. Yi, "Constraints on scalar-tensor theory of gravity by the recent observational results on gravitational waves," *Eur. Phys. J. C*, vol. 78, p. 738, Sept. 2018. arXiv: 1711.04102.

[153] J. C. Fabris, P. L. C. de Oliveira, D. C. Rodrigues, I. L. Shapiro, and A. M. Velasquez-Toribio, "Quantum corrections to gravity and their implications for cosmology and astrophysics," *Int. J. Mod. Phys. A*, vol. 27, p. 1260006, June 2012. arXiv: 1203.2695.

[154] D. Lovelock, "The Einstein tensor and its generalizations," *J. Math. Phys.*, vol. 12, pp. 498–501, 1971.

[155] R. C. Myers, "Higher Derivative Gravity, Surface Terms and String Theory," *Phys. Rev.*, vol. D36, p. 392, 1987.

[156] C. Teitelboim and J. Zanelli, "Dimensionally continued topological gravitation theory in Hamiltonian form," *Class. Quant. Grav.*, vol. 4, p. L125, 1987.

[157] S. C. Davis, "Generalized Israel junction conditions for a Gauss-Bonnet brane world," *Phys. Rev.*, vol. D67, p. 024030, 2003.

[158] H. Lu and Y. Pang, "Horndeski Gravity as $D\rightarrow4$ Limit of Gauss-Bonnet," *Physics Letters B*, vol. 809, p. 135717, Oct. 2020. arXiv: 2003.11552.

[159] S.-W. Wei and Y.-X. Liu, "Critical phenomena and thermodynamic geometry of charged Gauss-Bonnet AdS black holes," *Phys.Rev.*, vol. D87, no. 4, p. 044014, 2013.

[160] R.-G. Cai, L.-M. Cao, L. Li, and R.-Q. Yang, "P-V criticality in the extended phase space of Gauss-Bonnet black holes in AdS space," *JHEP*, vol. 1309, p. 005, 2013.

[161] J.-X. Mo and W.-B. Liu, "$P-V$ criticality of topological black holes in Lovelock-Born-Infeld gravity," *Eur.Phys.J.*, vol. C74, p. 2836, 2014.

[162] S.-W. Wei and Y.-X. Liu, "Triple points and phase diagrams in the extended phase space of charged Gauss-Bonnet black holes in AdS space," *Phys. Rev.*, vol. D90, no. 4, p. 044057, 2014.

[163] D.-C. Zou, Y. Liu, and B. Wang, "Critical behavior of charged Gauss-Bonnet AdS black holes in the grand canonical ensemble," 2014.

[164] A. Belhaj, M. Chabab, H. EL Moumni, K. Masmar, and M. B. Sedra, "Ehrenfest scheme of higher dimensional AdS black holes in the third-order Lovelock–Born–Infeld gravity," *Int. J. Geom. Meth. Mod. Phys.*, vol. 12, no. 10, p. 1550115, 2015.

[165] H. Xu, W. Xu, and L. Zhao, "Extended phase space thermodynamics for third order Lovelock black holes in diverse dimensions," 2014.

[166] B. Dolan, "Black holes and Boyle's law – the thermodynamics of the cosmological constant," 2014.

[167] S. H. Hendi and A. Dehghani, "Thermodynamics of third-order Lovelock-AdS black holes in the presence of Born-Infeld type nonlinear electrodynamics," *Phys. Rev.*, vol. D91, no. 6, p. 064045, 2015.

[168] R. A. Hennigar, W. G. Brenna, and R. B. Mann, "P–v criticality in quasitopological gravity," *JHEP*, vol. 07, p. 077, 2015.

[169] Z.-Y. Nie and H. Zeng, "P-T phase diagram of a holographic s+p model from Gauss-Bonnet gravity," *JHEP*, vol. 10, p. 047, 2015.

[170] S. He, L.-F. Li, and X.-X. Zeng, "Holographic Van der Waals-like phase transition in the Gauss–Bonnet gravity," *Nucl. Phys.*, vol. B915, pp. 243–261, 2017.

[171] E. Caceres, P. H. Nguyen, and J. F. Pedraza, "Holographic entanglement entropy and the extended phase structure of STU black holes," *JHEP*, vol. 09, p. 184, 2015.

[172] B. P. Dolan, "Pressure and compressibility of conformal field theories from the AdS/CFT correspondence," *Entropy*, vol. 18, p. 169, 2016.

[173] Y.-Z. Li, H.-S. Liu, and H. Lu, "Quasi-Topological Ricci Polynomial Gravities," 2017.

[174] A. Dehyadegari, B. R. Majhi, A. Sheykhi, and A. Montakhab, "Universality class of alternative phase space and Van der Waals criticality," 2018.

[175] S. H. Hendi and A. Dehghani, "Criticality and extended phase space thermodynamics of AdS black holes in higher curvature massive gravity," 2018.

[176] J. Louko, J. Z. Simon, and S. N. Winters-Hilt, "Hamiltonian thermodynamics of a Lovelock black hole," *Phys. Rev. D*, vol. 55, pp. 3525–3535, Mar. 1997. arXiv: gr-qc/9610071.

[177] P. Wang, H. Yang, and S. Ying, "Thermodynamics and Phase Transition of a Gauss-Bonnet Black Hole in a Cavity," *Phys. Rev. D*, vol. 101, p. 064045, Mar. 2020. arXiv: 1909.01275.

[178] S. Deser and A. V. Ryzhov, "Curvature invariants of static spherically symmetric geometries," *Class. Quant. Grav.*, vol. 22, pp. 3315–3324, 2005.

[179] D. G. Boulware and S. Deser, "String Generated Gravity Models," *Phys.Rev.Lett.*, vol. 55, p. 2656, 1985.

[180] A. Buchel and R. C. Myers, "Causality of Holographic Hydrodynamics," *JHEP*, vol. 08, p. 016, 2009.

[181] M. A. Cuyubamba, R. A. Konoplya, and A. Zhidenko, "Quasinormal modes and a new instability of Einstein-Gauss-Bonnet black holes in the de Sitter world," *Phys. Rev. D*, vol. 93, p. 104053, May 2016. arXiv: 1604.03604.

[182] R. A. Konoplya and A. Zhidenko, "Instability of Higher-Dimensional Charged Black Holes in the de Sitter World," *Phys. Rev. Lett.*, vol. 103, p. 161101, Oct. 2009.

[183] D. Glavan and C. Lin, "Einstein-Gauss-Bonnet gravity in 4-dimensional space-time," *Phys. Rev. Lett.*, vol. 124, p. 081301, Feb. 2020. arXiv: 1905.03601.

[184] C. Rovelli, "Notes for a brief history of quantum gravity," *arXiv:gr-qc/0006061*, Jan. 2001. arXiv: gr-qc/0006061.

[185] C. B. Thorn, "Reformulating String Theory with the \$1/N\$ Expansion," *arXiv:hep-th/9405069*, May 1994. arXiv: hep-th/9405069.

[186] G. t. Hooft, "Dimensional Reduction in Quantum Gravity," *arXiv:gr-qc/9310026*, Mar. 2009. arXiv: gr-qc/9310026.

[187] J. D. Bekenstein, "Universal upper bound on the entropy-to-energy ratio for bounded systems," *Phys. Rev. D*, vol. 23, pp. 287–298, Jan. 1981.

[188] J. M. Maldacena, "The Large N Limit of Superconformal Field Theories and Supergravity," *International Journal of Theoretical Physics*, vol. 38, no. 4, pp. 1113–1133, 1999. arXiv: hep-th/9711200.

[189] R. H. Price and K. S. Thorne, "Membrane Viewpoint on Black Holes: Properties and Evolution of the Stretched Horizon," *Physical Review D*, vol. 33, pp. 915–941, Feb. 1986.

[190] V. E. Hubeny, S. Minwalla, and M. Rangamani, "The Fluid/Gravity Correspondence," *arXiv:1107.5780 [gr-qc, physics:hep-th, physics:physics]*, July 2011. arXiv: 1107.5780.

[191] A. P. Balachandran, G. Bimonte, K. S. Gupta, and A. Stern, "Conformal Edge Currents in Chern-Simons Theories," *Int. J. Mod. Phys. A*, vol. 07, pp. 4655–4670, July 1992. arXiv: hep-th/9110072.

[192] A. P. Balachandran, L. Chandar, and E. Ercolessi, "Edge States in Gauge Theories: Theory, Interpretations and Predictions," *Int. J. Mod. Phys. A*, vol. 10, pp. 1969–1993, May 1995. arXiv: hep-th/9411164.

[193] L. Freidel, M. Geiller, and D. Pranzetti, "Edge modes of gravity – I: Corner potentials and charges," *arXiv:2006.12527 [gr-qc, physics:hep-th]*, June 2020. arXiv: 2006.12527.

[194] A. Bagchi, R. Basu, A. Kakkar, and A. Mehra, "Flat holography: aspects of the dual field theory," *J. High Energ. Phys.*, vol. 2016, p. 147, Dec. 2016.

[195] H. Afshar, H. A. González, D. Grumiller, and D. Vassilevich, "Flat space holography and the complex Sachdev-Ye-Kitaev model," *Phys. Rev. D*, vol. 101, p. 086024, Apr. 2020.

[196] L. Freidel and Y. Yokokura, "Non-Equilibrium Thermodynamics of Gravitational Screens," *Classical and Quantum Gravity*, vol. 32, p. 215002, Nov. 2015. arXiv: 1405.4881.

[197] L. Freidel, "Gravitational Energy, Local Holography and Non-equilibrium Thermodynamics," *Class. Quantum Grav.*, vol. 32, p. 055005, Mar. 2015. arXiv: 1312.1538.

[198] J. D. Brown and J. W. York, "Quasilocal Energy and Conserved Charges Derived from the Gravitational Action," *Physical Review D*, vol. 47, pp. 1407–1419, Feb. 1993. arXiv: gr-qc/9209012.

[199] R. J. Epp, R. B. Mann, and P. L. McGrath, "On the Existence and Utility of Rigid Quasilocal Frames," *arXiv:1307.1914 [gr-qc]*, July 2013. arXiv: 1307.1914.

[200] S. A. Hayward, "Quasilocal gravitational energy," *Phys. Rev. D*, vol. 49, pp. 831–839, Jan. 1994.

[201] I. S. Booth and R. B. Mann, "Moving observers, nonorthogonal boundaries, and quasilocal energy," *Phys. Rev. D*, vol. 59, p. 064021, Feb. 1999.

[202] M. Francaviglia and M. Raiteri, "Hamiltonian, energy and entropy in general relativity with non-orthogonal boundaries," *Class. Quantum Grav.*, vol. 19, pp. 237–258, Jan. 2002.

[203] W. Israel, "Singular Hypersurfaces and Thin Shells in General Relativity," *Il Nuovo Cimento B Series 10*, vol. 48, pp. 463–463, Apr. 1967.

[204] L. Susskind and L. Thorlacius, "Gedanken Experiments involving Black Holes," *Phys. Rev. D*, vol. 49, pp. 966–974, Jan. 1994. arXiv: hep-th/9308100.

[205] L. D. Landau and E. M. Lifshitz, *Fluid Mechanics: Landau and Lifshitz: Course of Theoretical Physics, Volume 6.* Cambridge: Elsevier Science, 1987. OCLC: 1048397862.

[206] J. R. Wilson and G. J. Mathews, *Relativistic Numerical Hydrodynamics*. Cambridge University Press, 1 ed., Nov. 2003.

[207] E. Gourgoulhon, "An introduction to relativistic hydrodynamics," *EAS Publications Series*, vol. 21, pp. 43–79, 2006. arXiv: gr-qc/0603009.

[208] L. Rezzolla and O. Zanotti, *Relativistic Hydrodynamics*. Oxford University Press, Sept. 2013.

[209] E. Gourgoulhon, "An introduction to relativistic hydrodynamics," *EAS Publications Series*, vol. 21, pp. 43–79, 2006. arXiv: gr-qc/0603009.

[210] J. P. Pereira, J. G. Coelho, and J. A. Rueda, "Stability of thin-shell interfaces inside compact stars," *Phys. Rev. D*, vol. 90, p. 123011, Dec. 2014. arXiv: 1412.1848.

[211] P. Allen, L. Andersson, and J. Isenberg, "Timelike Minimal Submanifolds of General Co-dimension in Minkowski SpaceTime," *arXiv:math/0512036*, Dec. 2005. arXiv: math/0512036.

[212] J. Liu and Y. Zhou, "Initial-boundary value problem for the equation of timelike extremal surfaces in Minkowski space," *Journal of Mathematical Physics*, vol. 49, p. 043507, Apr. 2008.

[213] O. G. Gorbunova and A. V. Timoshkin, "Dark energy with time-dependent equation of state," *arXiv:0903.1339 [gr-qc]*, Mar. 2009. arXiv: 0903.1339.

[214] S. Roy, "A Model of Time Dependent Equation-of-State Parameter in the Framework of Brans-Dicke Theory," *IJCRR*, vol. 08, June 2017.

[215] I. Prigogine, *Introduction to thermodynamics of irreversible processes*. New York: Interscience Publ, 3. ed ed., 1967. OCLC: 34099422.

[216] W. Israel and J. Stewart, "Transient relativistic thermodynamics and kinetic theory," *Annals of Physics*, vol. 118, pp. 341–372, Apr. 1979.

[217] S. Nojiri and S. D. Odintsov, "Inhomogeneous equation of state of the universe: Phantom era, future singularity, and crossing the phantom barrier," *Phys. Rev. D*, vol. 72, p. 023003, July 2005.

[218] A. K. Yadav, F. Rahaman, and S. Ray, "Dark Energy Models with Variable Equation of State Parameter," *Int J Theor Phys*, vol. 50, pp. 871–881, Mar. 2011.

[219] A. Pradhan, "Accelerating dark energy models with anisotropic fluid in Bianchi type VI $_0$ space-time," *Res. Astron. Astrophys.*, vol. 13, pp. 139–158, Feb. 2013.

[220] A. Strominger and A. Zhiboedov, "Gravitational Memory, BMS Supertranslations and Soft Theorems," *arXiv:1411.5745 [gr-qc, physics:hep-th]*, Nov. 2014. arXiv: 1411.5745.

[221] M. B. Nielsen, L. Gizon, H. Schunker, and C. Karoff, "Rotation periods of 12 000 main-sequence Kepler stars: Dependence on stellar spectral type and comparison with v sin i observations," *A&A*, vol. 557, p. L10, Sept. 2013. arXiv: 1305.5721.

[222] G. Obied, H. Ooguri, L. Spodyneiko, and C. Vafa, "De Sitter Space and the Swampland," *arXiv:1806.08362 [hep-th]*, July 2018. arXiv: 1806.08362.

[223] M. Dine, J. A. P. Law-Smith, S. Sun, D. Wood, and Y. Yu, "Obstacles to Constructing de Sitter Space in String Theory," *J. High Energ. Phys.*, vol. 2021, p. 50, Feb. 2021. arXiv: 2008.12399.

[224] C. Anastopoulos and N. Savvidou, "Multi-Time Measurements in Hawking Radiation: Information at Higher-Order Correlations," *Class. Quantum Grav.*, vol. 37, p. 025015, Jan. 2020. arXiv: 1909.00438.

APPENDICES

Appendix A

The Reduced Action

Here we demonstrate the evaluation of the reduced action I_r for Einstein-Hilbert-Maxwell gravity using an alternative method where the action is written as a total derivative, rather than being explicitly integrated. We begin with the action

$$I = -\frac{1}{16\pi}\int_{\mathcal{M}} d^4x\sqrt{g}\left(R - 2\Lambda + F^2\right) + \frac{1}{8\pi}\int_{\partial\mathcal{M}} d^3x\sqrt{k}\left(K - K_0\right) \tag{A.1}$$

and the following ansatz for the metric in terms of the radial coordinate $y \in [0,1]$:

$$ds^2 = f(y)^2 d\tau^2 + \alpha(y)^2 dy^2 + r(y)^2 d\Omega^2 \tag{A.2}$$

The horizon is located at $r_h = r(0)$, and has topology S^2. The boundary has topology $S^1 \times S^2$, is located at $y = 1$, and has an S^2 component (the cavity) with area $4\pi r_c^2$, where $r_c = r(1)$. The temperature of the boundary is given by the proper length of the circle S^1:

$$T^{-1} = \beta = \int_0^{2\pi} f(1)d\tau = 2\pi f(1) \tag{A.3}$$

The requirement that the horizon be $\mathcal{S}^2$ immediately implies that $f(0) = 0$. This requires further that

$$\left.\frac{f'}{\alpha}\right|_{y=0} = 0 \tag{A.4}$$

in order for the near-horizon geometry to be flat. With the constraints in place we first examine the bulk part of the action:

$$I_{\mathcal{M}} = -\frac{1}{16\pi}\int_{\mathcal{M}} d^4x\,\sqrt{g}\left(R - 2\Lambda + F^2\right) \tag{A.5}$$

The Ricci scalar can be evaluated for the metric (A.2), giving

$$R = \frac{2f'\alpha'}{f\alpha^3} - \frac{2f''}{f\alpha^2} - \frac{4r'f'}{rf\alpha^2} + \frac{4r'\alpha'}{r\alpha^3} + \frac{2}{r^2} - \frac{2(r')^2}{r^2\alpha^2} \tag{A.6}$$

where primes indicate derivatives with respect to y. The field strength tensor is $F_{ab} = \partial_a A_b - \partial_b A_a$. For a static, spherically symmetric spacetime, the gauge freedom allows us to write $A_a = A_\tau(y)$ with all other components vanishing. The boundedness of A_a at $y = 0$ and $y = 1$ requires

$$A_\tau(0) = 0, \qquad A_\tau(1) = \frac{k\beta\phi}{2\pi} \tag{A.7}$$

where $\phi \equiv \phi(0) - \phi(1)$ and k is a constant. With this, the Maxwell part of the action reduces to:

$$F^2 = F_{ab}F^{ab} = \frac{2(A')^2}{\alpha^2 f^2} \tag{A.8}$$

Substituting (A.6) and (A.8) into (A.5) and performing the integrations over θ and ϕ gives:

$$I_{\mathcal{M}} = \int dy\, d\tau \left[\frac{r^2 f''}{2\alpha} + \frac{rr'f'}{\alpha} + \frac{rr''f}{\alpha} - \frac{\alpha f}{2} + \frac{(r')^2 f}{\alpha} + \frac{r^2\alpha f\Lambda}{2} - \frac{r^2(A')^2}{2\alpha f}\right] \tag{A.9}$$

Next we solve the Hamiltonian constraint $G^\tau{}_\tau + \Lambda g^\tau{}_\tau - 8\pi T^\tau{}_\tau = 0$ for Λ and insert it into (A.9). The electromagnetic contributions cancel and we are left with:

$$I_{\mathcal{M}} = \int dy\, d\tau \left[\frac{r^2 f''}{2\alpha} + \frac{rr'f'}{\alpha} + \frac{rr'f\alpha'}{\alpha^2}\right] \tag{A.10}$$

Now we turn to the boundary action. The electromagnetic boundary term makes no contribution, with the charge-dependence entering only through the metric function. We are left with:

$$I_{\partial\mathcal{M}} = \frac{1}{8\pi}\int_{\partial\mathcal{M}} d^3x\, \sqrt{k}\,\big(K - K_0\big) \tag{A.11}$$

K is the trace of the extrinsic curvature of the boundary surface, k is the metric on that surface, and the subtraction term K_0 is chosen such that $I = 0$ when $m = 0$. K is defined in terms of the radial spacelike unit normal vector to the boundary $s^a = s^y = \alpha^{-1}(y)$ which gives

$$K = K_{ab}K^{ab} = -\frac{rf' + 2r'f}{r\alpha f} \tag{A.12}$$

where $K_{ab} = k_a{}^c k_b{}^d \nabla_c s_d$ and $k_{ab} = g_{ab} - s_a s_b$ is the metric on the boundary. Using (A.12) in (A.11) and integrating over ϕ and θ gives:

$$I_{\partial\mathcal{M}} = -\int d\tau \left[\frac{r^2 f'}{2\alpha} + \frac{rr'f}{\alpha} + \frac{r^2 f K_0}{2}\right]\Bigg|_{y=1} \tag{A.13}$$

The full action is therefore:

$$I = \int dy\, d\tau \left[\frac{r^2 f''}{2\alpha} + \frac{rr'f'}{\alpha} + \frac{rr'f\alpha'}{\alpha^2}\right] - \int d\tau \left[\frac{r^2 f'}{2\alpha} + \frac{rr'f}{\alpha} + \frac{r^2 f K_0}{2}\right]\Bigg|_{y=1} \tag{A.14}$$

Before proceeding further, we return to the Hamiltonian constraint, rewriting it as a total

derivative with respect to y:

$$\begin{aligned} G^{\tau}{}_{\tau} + \Lambda g^{\tau}{}_{\tau} - 8\pi T^{\tau}{}_{\tau} = 0 &= \frac{(r')^2}{r^2\alpha^2} - \frac{1}{r^2} + \frac{2r''}{r\alpha^2} - \frac{2r'\alpha'}{r\alpha^3} + \Lambda + \frac{q^2}{r^4} \\ 0 &= \frac{\left(\frac{r'}{\alpha}\right)^2 - 1}{r^2} + \frac{2}{r\alpha}\left(\frac{r''\alpha - r'\alpha'}{\alpha^2}\right) + \Lambda + \frac{q^2}{r^4} \\ 0 &= \frac{1}{r^2 r'}\left[r\left(\left(\frac{r'}{\alpha}\right)^2 - 1\right)\right]' + \Lambda + \frac{q^2}{r^4} \\ 0 &= \left[r\left(\left(\frac{r'}{\alpha}\right)^2 - 1\right)\right]' + \frac{\Lambda}{3}[r^3]' - q^2\left[\frac{1}{r}\right]' \end{aligned} \tag{A.15}$$

This is then integrated to obtain

$$\left(\frac{r'}{\alpha}\right)^2 = 1 + \frac{C}{r} + \frac{q^2}{r^2} - \frac{\Lambda r^2}{3} \tag{A.16}$$

The integration constant is found by requiring that the near-horizon geometry (the $y - \tau$ plane near $y = 0$) be isometric to $\mathcal{R}^2$, and that the Euler number be $\chi = 2$. With the given metric, these conditions imply that

$$\left.\frac{f'}{\alpha}\right|_{y=0} = 1 \ , \qquad \left(\frac{r'}{\alpha}\right)^2_{y=0} = 0 \tag{A.17}$$

The second condition, along with (A.9) and the fact that $r(0) = r_h$ gives that

$$C = -r_h - \frac{q^2}{r_h} + \frac{\Lambda r_h^3}{3} \tag{A.18}$$

which leads to

$$\begin{aligned} \left(\frac{r'}{\alpha}\right)^2 &= 1 - \frac{r_h}{r} - \frac{q^2}{r_h r} + \frac{\Lambda r_h^3}{3r} + \frac{q^2}{r^2} - \frac{\Lambda r^2}{3} \\ &= \left(1 - \frac{r_h}{r}\right)\left(1 - \frac{q^2}{r_h r} - \frac{\Lambda}{3}\left(r^2 + r r_h + r_h^2\right)\right) \end{aligned} \tag{A.19}$$

We now use the conditions (A.17) along with integration by parts and the product rule multiple times to rewrite the action (A.14) as a total derivative in y:

$$I = \int dy\, d\tau \left[\left(\frac{K_0\, r^2 f}{2}\right)' - \left(\frac{r r' f}{\alpha}\right)'\right] = \int_0^{2\pi} d\tau \left[\frac{K_0\, r^2 f}{2} - \frac{r r' f}{\alpha}\right] \Bigg|_{y=0}^{y=1} \tag{A.20}$$

Finally, we use the fact that $f(0) = 0$, $r(1) = r_c$, $\beta = 2\pi f(1)$, and (A.19) to arrive at:

$$\begin{aligned} I &= \int_0^{2\pi} d\tau \left[\frac{K_0\, r^2 f}{2} - \frac{r r' f}{\alpha}\right] \Bigg|_{y=0}^{y=1} - \int_0^{2\pi} d\tau \left[\frac{r^2}{2}\right] \Bigg|_{y=0} \\ &= 2\pi \left[\frac{K_0\, r(1)^2 f(1)}{2} - r(1) f(1) \left(\frac{r'}{\alpha}\right)\right] - \pi r(0)^2 \\ &= \beta\, r_c \left[\frac{K_0\, r_c}{2} - \sqrt{\left(1 - \frac{r_h}{r_c}\right)\left(1 - \frac{q^2}{r_h r_c} - \frac{\Lambda}{3}\left(r_c^2 + r_c r_h + r_h^2\right)\right)}\,\right] - \pi r_h^2 \end{aligned} \tag{A.21}$$

As noted in the main text, we choose K_0 such that the action vanishes when $m = 0$ (which implies $q = 0$ and $r_h = 0$). This requires

$$K_0 = \frac{2}{r_c}\sqrt{1 - \frac{\Lambda r_c^2}{3}} \tag{A.22}$$

which is easily verified to be the trace of the extrinsic curvature of the boundary when $m = 0$. With this choice we arrive at the reduced action:

$$I = \beta\, r_c \left[\sqrt{1 - \frac{\Lambda r_c^2}{2}} - \sqrt{\left(1 - \frac{r_h}{r_c}\right)\left(1 - \frac{q^2}{r_h r_c} - \frac{\Lambda}{3}\left(r_c^2 + r_c r_h + r_h^2\right)\right)}\,\right] - \pi r_h^2 \tag{A.23}$$

In this way, we avoid direct radial integration of the bulk action, which may be very difficult to do analytically. However, it may not always be possible to write the action as a total derivative.

Appendix B

Replacing Spacetime with Screens

Here we review the junction conditions that lead to boundary stress tensors in the presence of metric discontinuities. We also clarify the difference between merely positing a surface within a spacetime, and treating the surface as a boundary of that spacetime.

Consider a hypersurface Σ with normal vector field n^a which separates two regions $\mathcal{V}_+$ and $\mathcal{V}_-$ of spacetime, with respective metrics g^+_{ab} and g^-_{ab}. We can write the full metric as a distribution-valued tensor

$$g_{ab} = \Theta(l) g^+_{ab} + \Theta(-l) g^-_{ab} \ , \tag{B.1}$$

where $\Theta(l)$ is the Heaviside distribution and l is an affine parameter along congruence of geodesics which orthogonally pierce the boundary, chosen such that $l = 0$ at Σ. Then, using (B.1) one can evaluate the Riemann tensor, finding that

$$R^a{}_{bcd} = \Theta(l) R^a_{+bcd} + \Theta(-l) R^a_{-bcd} + \delta(l) A^a{}_{bcd} \tag{B.2}$$

where

$$A^a{}_{bcd} = [\Gamma^a{}_{bd}]\, n_c - [\Gamma^a{}_{bc}]\, n_d \tag{B.3}$$

and square brackets indicate the discontinuity of the quantity across Σ. There is an apparent curvature singularity (the third term) at the boundary Σ. Inserting the above into the field equations, one can absorb the delta function part of the singularity into a contribution to the stress-energy tensor as

$$T_{ab} = \Theta(l) T^+_{ab} + \Theta(-l) T^-_{ab} + \delta(l) S_{ab} \ . \tag{B.4}$$

The last term has the interpretation of the stress-energy of a thin shell on the boundary Σ. Some algebra allows one to write S_{ab} in terms of the induced metric h_{ab} and extrinsic curvature H_{ab} of Σ. One finds that

$$S_{ab} \equiv [H] h_{ab} - [H_{ab}] \ . \tag{B.5}$$

The result is intuitive if one imagines a surface Σ whose spatial section is an S^2 with

radius R. Suppose one had a thin shell of matter evenly distributed across Σ with total mass m. Already from Newtonian physics one realizes that the interior metric g^-_{ab} must be Minkowski, while the exterior metric g^+_{ab} will be the Schwarzschild metric, so there is clearly a discontinuity

$$[H_{ab}] = H_{ab}|_{\mathcal{V}^+} - H_{ab}|_{\mathcal{V}^-} \tag{B.6}$$

in the extrinsic curvature between the two sides, which contributes to the stress-energy tensor (B.5). In our work, as in the membrane paradigm, Σ is treated as the boundary of the spacetime. This is significantly different from the situation above, as the stress-energy tensor only receives a contribution from the extrinsic curvature in the exterior region. To accomplish this, one imposes a Z_2 symmetry at the boundary, such that the interior is a mirror copy of the exterior. One then has

$$[H_{ab}] = 2H_{ab}|_{\mathcal{V}^+} \ . \tag{B.7}$$

The resulting surface stress-energy tensor is markedly different. In particular, assuming an exterior metric of the form

$$ds^2 = -f(r)^2 dt^2 + \frac{dr^2}{f(r)^2} + r^2 d\theta^2 + r^2 \sin(\theta)^2 d\phi^2 \tag{B.8}$$

the stress-energy tensor using (B.7) is

$$S_{tt} = -\frac{4f^3}{r}, \qquad S_{\theta\theta} = 2(r^2 f' + rf), \qquad S_{\phi\phi} = 2r\sin^2(\theta)(rf' + f) \tag{B.9}$$

while the stress-energy tensor resulting from (B.6) is

$$S_{tt} = -\frac{2f^2(f-1)}{r}, \qquad S_{\theta\theta} = r^2 f' + r(f-1), \qquad S_{\phi\phi} = r\sin^2(\theta)(rf' + f - 1) \tag{B.10}$$

These are clearly very different.